Universidade do Minho
Escola de Engenharia

Hassan Abdolpour

Development of prefabricated modular
houses in pure composite sandwich panels

Universidade do Minho
Escola de Engenharia

Hassan Abdolpour

Development of prefabricated modular
houses in pure composite sandwich panels
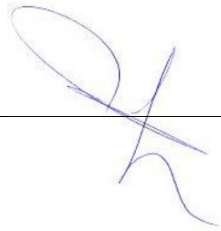
April 2017

STATEMENT OF INTEGRITY

I hereby declare having conducted my thesis with integrity. I confirm that I have not used plagiarism or any form of falsification of results in the process of the thesis elaboration.
I further declare that I have fully acknowledged the Code of Ethical Conduct of the University of Minho.

University of Minho,   School of Engineering

Full name: Hassan Abdolpour

Signature:

Abstract

In the scope of the ClickHouse R&D Project, a residential modular temporary building was proposed and developed to accommodate, in urgent situations, dislocated families due to e.g. the occurrence of natural disasters. Proposed building is composed of a frame structure, panels and a tailored connection system. The frame structure and connection are composed of glass fibre reinforced polymer (GFRP) pultruded tubular profiles. While for the panels, composite sandwich panels made of polyurethane foam (PU) core and GFRP skins, are utilized. A new connection system is defined for connecting adjacent members. This modular construction of temporary housing, should be capable of being prefabricated according to the pultrusion technology (for the case of frame and connection components), transported at low cost to the area of installation (due to the reduced weight and being packed), and being easily and quickly assembled.

In the ambit of the present thesis, the following research programs, which contributed for the ClickHouse outcomes, were developed: (I) material testing program; (II) development/ characterization of a connection system for jointing composite panels, (III) evaluation of the mechanical performance of single panel, two jointed panels and three jointed panels under flexural loading; (IV) assessment of single and two jointed wall panel's behaviour under axial loading; (I) performance/characterization of two floor modular prototypes.

Phase I is comprising comprehensive material testing program for establishing constitutive relation of the constituent materials of the sandwich panel, namely the PU foam core, GFRP skins and the bond between these two materials. Furthermore, bearing strength behaviour of GFRP skin and pultruded profiles is subjected to study in this phase.

In the phase II, a connection system is proposed for connecting floor and wall sandwich panels. Proposed connection is composed of two main parts namely as end integrated U-shape GFRP profile and two connected tubular square GFRP profiles. The end former working as a connector by interlocking inside the U-shape profiles. Two approaches are used to study mechanical behaviour of jointed panels: friction technique and hybrid technique. An experimental program is performed to study the mechanical response of this connection system in the longitudinal and transversal directions.

Phase III is included a series of experimental tests are carried out on a single panel, on two and three jointed panels. Flexural responses of the panels, in short term, is analysed, including evaluation of the failure mechanism and the efficiency of the proposed connection system between panels in jointing sandwich panels. Additionally, the creep behaviour of the panels, which is a limiting factor for their serviceability design, is investigated. Numerical and analytical models are proposed and verified including capturing the local failure of the panel using experimental program. The proposed models are used to go further in-depth to understand capability of connection in jointing panels and influence of U-shape GFRP profiles in increasing flexural stiffness of the panels. Additionally, contribution of single sandwich panels components in total shear deflection is investigated.

In the phase IV, the structural performances of the sandwich wall panels under axial loading condition are experimentally tested and thereafter analytically assessed in two cases: (i) single wall panels; (ii) two jointed wall panels. The influence of the proposed connection system on the axial load capacity of the jointed panels is analytically evaluated.

In phase V, performances of the two floor prototypes to support typical load conditions of residential houses are also assessed. The experimental program is complemented with an extensive finite element modelling and analytical study to verify the experiments results and to obtain connection flexibility, load distribution factor and stress distribution within the floor modular components. Additionally, several parametric studies are developed using FEM models developed and validated by varying geometric aspect ratios and numbers of U-shape GFRP profiles to show potentiality of this structure to have more housing space and consequently to extend this concept for other markets.

Keywords: Floor and wall sandwich panel; Connection system; GFRP profiles; modular prototype; prefabricated emergency house; experimental research; FEM-modelling.

Resumo

No âmbito do Projeto I&D ClickHouse, uma habitação modular temporária foi proposta e desenvolvida para acomodar, em situações de urgência, famílias deslocadas, devido à ocorrência de e.g. desastres naturais. A habitação proposta é composta por uma estrutura porticada, painéis sanduíche e um sistema de conexão. A estrutura porticada e ligações são em perfis tubulares pultrudidos em polímeros reforçados com fibra de vidro (GFRP). Por sua vez, os painéis de sanduíche compósitos são constituídos por uma espuma de poliuretano (PU) no núcleo e lâminas de GFRP nas extremidades. Um novo sistema de conexão é proposto para a ligação de elementos adjacentes. Esta construção modular de alojamento temporário, pré-fabricada de acordo com a tecnologia de pultrusão (no caso da estrutura porticada e conexões), pode transportada a baixo custo para a área da instalação (devido ao peso reduzido e sistema embalamento), e ser fácil e rapidamente montada.

No âmbito da presente tese, os seguintes programas de investigação, que contribuíram para os resultados do ClickHouse, foram desenvolvidos: (I) programa experimental de caracterização dos materiais; (II) o desenvolvimento/caracterização do sistema de conexão, (III) a avaliação do comportamento mecânico de um painel isolado, dois painéis e três painéis ligados entre si sob cargas de flexão; (IV) a avaliação do comportamento mecânico de um painel isolado e dois painéis ligados entre si sob carga axial; (I) performance/caracterização de dois protótipos de piso modular.

A fase I é composta por amplo programa de ensaios dos materiais para o estabelecimento de relações constitutivas dos materiais constituintes do painel de sanduíche, ou seja, o núcleo de espuma PU, as lâminas de GFRP e a aderência entre estes dois materiais. Além disso, a resistência ao esmagamento das lâminas e perfis de GFRP para o caso de ligações mecânicas é também estudada nesta fase.

Na fase II, um sistema de ligação é proposto para ligar painéis sanduíche de piso e de parede. O sistema de conexão proposto é composto de duas partes principais, nomeadamente (i) perfis GFRP em "U" integrados no contorno dos painéis e (ii) perfis retangulares em GFRP. A ligação entre painéis é por encaixe, sendo que os elementos (ii) realizam a respetiva

Resumo

ligação. Duas abordagens são usadas para estudar o comportamento mecânico dos painéis ligados: encaixe (apenas por atrito) e técnica híbrida (atrito e mecânica). Um programa experimental é realizado para estudar a resposta mecânica deste sistema de ligação nas direções longitudinais e transversais

Na fase III inclui-se série de ensaios experimentais realizados num painel isolado, em dois e três painéis ligados entre si. A resposta à flexão dos painéis, a curto prazo, é analisada, incluindo a avaliação dos mecanismos de rotura e a eficiência do sistema de ligação. Além disso, o comportamento de fluência dos painéis, o que é um aspeto condicionante no dimensionamento deste tipo de painéis, é investigada. Modelos numéricos e analíticos são propostos e validados com recursos aos resultados experimentais obtidos. Os modelos propostos são posteriormente usados na compreensão da capacidade da ligação entre painéis no aumento da rigidez à flexão dos painéis. Além disso, a contribuição da deformação por corte na deformação dos painéis sanduíche é também investigada.

Na fase IV, o desempenho estrutural dos painéis sanduíche de parede é testado experimentalmente, sob condições de carga axial, e posteriormente avaliados analiticamente, em dois casos: (i) painéis de parede isolados; (ii) dois painéis de parede ligados entre si. A influência do sistema de ligação proposto na capacidade de carga axial dos painéis é avaliada analiticamente.

Na fase V, o desempenho de dois protótipos modulares é avaliada para as condições de carga típicas de habitações residenciais. O programa experimental é complementado com uma extensa simulação numérica e analítica para verificar os resultados experimentais e obter a flexibilidade de ligação, o fator de distribuição de carga e a distribuição de tensões nos componentes modulares do piso. Além disso, vários estudos paramétricos foram desenvolvidos utilizando modelos FEM para mostrar a potencialidade do sistema ser aplicável a estruturas de vãos superiores e, consequentemente, estender este conceito para outros mercados.

Palavras-chave: painel de sanduíche de piso e parede; sistema de conexão; perfis GFRP; protótipo modular; habitação de emergência pré-fabricada; investigação experimental; simulação FEM.

Acknowledgements

After an intensive period of years, today is the day to write this note of thanks for finishing of my thesis. Writing this thesis had a big impact on me. I would like to reflect on the people who have supported and helped me so much throughout this period.

Foremost, I would like to express my sincere gratitude to my supervisor Prof. Joaquim Barros for the continuous support of my Ph.D. study and research, for his patience, motivation, enthusiasm, and immense knowledge. His guidance helped me in all the time of research and writing of this thesis. I could not have imagined having a better advisor and mentor for my Ph.D. study. Besides my advisor, I would like to thank my co-supervisor Prof. Jose Sena-Cruz for his kindly encouragement, insightful comments, and hard questions.

I am also deeply thankful to the technical staff of the Laboratory of the Structural Division of the Civil Engineering of Minho University (LEST). Their names cannot be disclosed, but I want to acknowledge and appreciate their help and transparency during my research. Their helping supported me to perform all of my experimental tests in the laboratory.

I would like to express my full thanks to Instituto Superior Técnico and FEDER through the Operational Program for Competitiveness Factors – COMPETE and the Portuguese National Agency of Innovation (ADI). Special thanks are given to company ALTO - Perfis Pultrudidos, Lda., who manufactured all the elements (GFRP profiles and sandwich panels) involved in this work. The author also wants to express their gratitude to Engineers Mário Alvim and Tomé Santos, for their invaluable collaboration, help and support in this research.

Dozens of people have helped and taught me immensely during my Ph.D. Ali Bahrami, Julio Rocco, Carlos Martins thank you so much for supporting and helping me. I did not find any word except than thank you Dr. Bahmani. You were always a source of love and energy ever since by your words and guides.

I cannot finish without thanking my family. I warmly thank and appreciate my parents, my sisters and brother for their material and spiritual support in all aspects of my life. Their support has been unconditional all these years; they have given up many things for me to be at Minho; they have cherished with me every great moment and supported me whenever I needed it.

The highest education is that which does not
merely give us information but makes our
life is harmony with all existence

Rabindranath Tagore

Table of Contents

List of Figures

List of figures

List of Tables

CHAPTER 1: Introduction

1.1   Context and motivation

In the field of temporary shelters and emergency management, a great deal of time is placed in the act of responding to disasters. After any event, the main priority is to re-establish normality for the affected populace. This return to normalcy is first brought about by clearing away the aftermath of the event and rehousing affected people whom have lost their homes. A home is a source of pride and cultural identity linking the livelihoods of those that inhabit it and acts as the social centre of a family. The ability to quickly return a populace to their daily activities allows communities to not only continue their daily efforts but also contribute to the effort of reconstruction.

Currently, temporary houses vary widely in quality and performance and are typically directly correlated with the displaced community's means. Low performance solutions use materials such as sand, earth bags, and tents. In most circumstances, these solutions are not capable of handling the standardized design loads required for use. In contrast, high performance solutions are available with materials such as: wood, steel, or concrete. However, these high performance solutions have the detriment of requiring highly skilled labour for installation, long installation times - as materials are not always readily available - and high capital cost.

In this thesis, a temporary modular dwelling system is proposed in the scope of the ClickHouse R & D project and studied in the ambient of the present thesis. Although the main target of this project is developing an emergency house for displaced communities, the methods and results of this study have the ability to serve other potential applications. The main tenants that were considered in designing this system were: material selection, ease of transportation and constructability, potential for reuse, and a code compliant design. Additionally, utilizing modular structures was considered to reduce building cost and to improve the quality of the manufacturing [1-3].

The proposed building types included in this study comprise the study of wall panels, floor panels, roof panels and connections between them and with the framed-structure composing of the house. Accordingly, pultruded GFRP material was used for the frame structure while the remaining elements, mainly panels, were materialized using a sandwich wall concept. Pultruded GFRP composite profiles display promising advantages including: low production costs, low maintenance, high durability, immunity to corrosion, and high strength [4-7]. Likewise, sandwich panels have been increasingly used in structural applications due to their high strength, stiffness to weight ratio, immunity to corrosion, and low thermal and acoustic conductivity [8-12]. The proposed sandwich panels, consist of two thin and stiff GFRP skins separated by a relatively thick and lightweight PU foam core.

Feasibility and cost of the system was key factor in constructing and designing this structure. The proposed modular system in this study is expected to be quickly and effortlessly assembled on a site with a handful of unskilled labourers. This easy of construction is possible due to the low weight components and simple assemblage. Additionally, the low weight component of the system allows for faster and lower costs of transportation and assists in transporting the material to areas that have limited accessibility.

1.2 Research objectives and methodology

The research in this thesis is intended to demonstrate an in-depth understanding and a critical evaluation of the proposed residential modular system. Additionally, outcomes from this research have the potential to be used in the several alternative structural applications including flooring, decking, cladding, and roofs.

The specific objectives of this study were set as follows:

1- Establishing the constitutive relationship of the individual materials of the residential modular system;
2- Developing a connection system for jointing composite panels;
3- Evaluating mechanical performances of single, double, and triple jointed panels under flexural loading;
4- Assessing axial behaviour of single and jointed wall panels;
5- Evaluating the floor modular prototypes.

For the first task, an extensive experimental procedure was conducted to obtain mechanical performance of the dwelling materials. This testing included: characterization of the GFRP

pultruded profiles and GFRP laminates under tensile testing, evaluation of the PU foam core under different loading conditions (tensile, compression and shear), assessing tensile bond strength between GFRP skin and PU foam core by performing a pull-off test, and characterization of the polyester resin under tensile test.

The second objective consisted of developing a connection system to joint composite panels; thus, a connection system between adjacent sandwich panels was proposed and studied. The panel to panel connection was accomplished using interlocking tubular U-shaped GFRP profiles as the main connection between integrated end U-shaped GFRP profiles. This module was tested under four-point and three-point bending tests configuration to assess the connection behaviour on overall mechanical response of the jointed panels. The behaviour of the jointed panels was studied along the longitudinal and transverse directions with respect to two different methods of connection namely friction techniques and a hybrid technique.

The third objective consisted of the following tasks:

1- Assessing flexural performance of the single sandwich panels;
2- Characterization of the flexural behaviour of single and jointed sandwich panels.

The first task consisted of an experiment research to study flexural performance of the single composite sandwich panels under service load state (SLS), ultimate load state (ULS) and failure. To satisfy the ULS loading condition, the structure must not collapse when subjected to the peak design load for which it was designed. Meanwhile, a structure was deemed to satisfy the SLS loading condition when the structure do not deflect by more than certain limits laid down in the building code. To accomplish this, full scale sandwich panels were tested in four-point and three-point bending test to analyse the flexural behaviours in SLS and ULS loading. Thereafter, failure mechanisms and long-term behaviour (creep) were investigated on small scale specimens. Next, ultimate capacity of a full scale single floor panel and its corresponding failure mechanisms were experimentally assessed. Finally, analytical and FE assessments were executed to further understand the failure mode of the sandwich panels as well as the influence of the ribs placed inside the panels.

The second task involved experiments to evaluate flexural behaviour of the jointed panels under SLS and ULS conditions. Several analytical and FE simulations were developed to test these conditions. The FE models simulated and predicted the experimentally observed responses by analysing the efficacy and contribution of the connection between panels. By

studying the transference of loads from one panel to another, the effects of the proposed connection system in increasing flexural stiffness of the jointed panel were quantified.

The fourth objective aimed to assess the axial behaviour of single and jointed wall panels in two parts:

1- Axial performance of single sandwich wall panels;
2- Axial performance of two jointed wall panels.

The first and second task involved assessing the structural behaviour of both the single and double sandwich panels under concentric axial loading. Aspects related to assembly and disassembly as well as ease of integration in the production line was also evaluated. Finally, an analytical investigation was performed to determine the axial capacity and stresses associated with various failure modes, both in the single and double jointed panel.

Finally, the fifth objective was to develop a modular floor prototype for the temporary building. Functionality of this system was assessed experimentally by assembling/disassembling and fulfilling the requirements established in the engineering standards. Analytical and numerical models were created and validated using the experimental results. The research aimed at simulating and predicting the response, analysing the efficiency, and measuring the contribution of the connection between panels. By studying the transference of loads from one panel to another, the load distribution factor and connection flexibility in the floor modular prototype was attained. Finally, parametric studies were carried out on the modular floor systems to explore differences in the used materials in order to achieve higher span to length ratios.

1.3 Thesis outline

This thesis is organized in nine chapters. The following paragraphs give a brief summary of the contents of each chapter.

Chapter 1 presents the main subject of this thesis. In this chapter a general overview and motivation behind this research is included. Furthermore, the methodology is established in order to provide a rational underpinning.

Chapter 2 presents literature review, including the historical background, fundamental characterization of the sandwich panel's materials, and potential application areas for the sandwich panels. Composite sandwich panels are categorized according to their configuration and current research of the subject is summarized.

Chapter 3 describes the architectural design of the proposed temporary building. The typology of each structural element is described in terms of geometry, functionality, and layout.

Chapter 4 provides the experimental program carried out to evaluate mechanical performance of the composite sandwich panel's constituent materials including the GFRP pultruded profile, GFRP skin, PU foam core, polyester resin, GFRP skin-PU foam core bond strength, bearing strength of the GFRP skin, and pultruded profiles.

Chapter 5 of this thesis presents the experimental programs for characterizing the efficiency of the proposed connection techniques in jointing composite sandwich panels. Flexural characterization of the jointed panels in transferring the imposed load in longitudinal and transverse direction was investigated by using friction and hybrid techniques.

Chapter 6 explores a series of experimental programs carried out to evaluate flexural performance of single, double, and triple jointed panels subjected to the vertical loading conditions under serviceability and failure behaviour. Analytical and FE simulations are also provided. Analytical simulations enabled the research to dive deeper in evaluating the effects of each component on the global behaviour of the structures.

Chapter 7 provides a system for connecting composite sandwich wall panels. The structural performance of full scale wall panels including maximum axial load, failure modes, lateral deflections, axial deflection and strains were evaluated in two cases. An analytical investigation was created to determine the axial capacity and stresses associated with various failure modes, both in the single and double jointed panels.

Chapter 8 provides information about two modular prototypes proposed for the flooring system of the temporary building. Since the floor panels were studied independently of the GFRP framed structures, this chapter focuses on the feasibility of assemblage/disassembling and the responses of the prototypes under uniform loading (SLS). The experimental results were used to validate the theoretical and numerical models and verified the effects of connection in terms of stiffness and flexibility on the behaviour of the systems. Furthermore, the validated models were used for parametric study to explore the potential of the used materials as well as structural behaviour for pavements with different typology.

Chapter 2: Literature overview

2.1   Introduction

One of the major concerns after a natural disaster is settling down surviving communities in shelters or temporary houses. This issue remains difficult to manage despite decades of experience. Availability of temporary housing is crucial since it allows people to quickly commence their daily activities such as school, working and cooking [13-15]. Even though there are different sorts of temporary buildings made of steel, wood and plastic [16-18], many of these temporary dwellings do not offer a basic level of security and protection for its occupants, and/or result in very complex and expensive solutions. Nowadays, a clear trend is observed in the industrial manufacturing and prefabrication of temporary building towards. This modern method of construction leads to achive tangible benefits in terms of faster construction, improved quality and reduced wasting resource material [19].

Lightness is a key factor when proposing a material/structural system for a temporary building because, after a natural disaster, accessibility to roads is usually limited. Thus, low weight prefabricated components are very convenient for packing, shipping, unpacking and assembling [20]. Taking this into account, sandwich panels made fundamentally by GFRP pultruded profiles and sandwich panels may constitute excellent options in the field of temporary buildings. Sandwich panels and pultruded profiles are lightweight elements with very good mechanical performance, being able to be manufactured and rapidly assembled in modular sections.

In this chapter, the main principle of sandwich elements is presented to obtain a better vision about the composite sandwich structures. Furthermore, the fabrication processes are described and the potential applications of sandwich panels are presented.

2.2   Definition of Sandwich Structures

A sandwich structure is a special type of laminated composite structure. Generally, sandwich structures follow the same pattern of two face sheets (also called skins) separated by a thick

layer (called the core). To transfer the load between the separate components, the skins are adhesively bonded to the core material (**Fig. 2.1**).
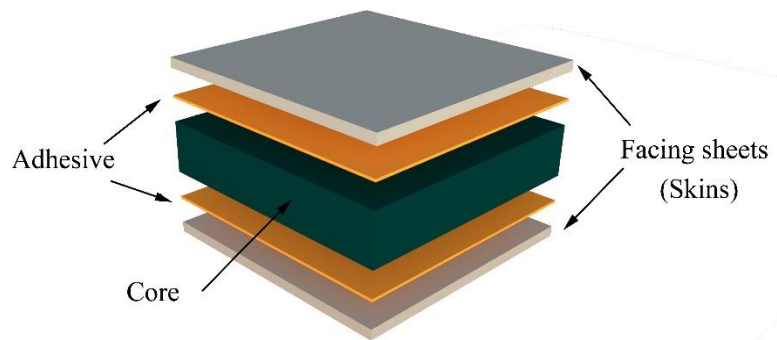
Fig. 2.1. Definition of sandwich structure.

External faces are normally thin, and composed of stiff and high strength material. In contrast, core material is relatively thick yet light with sufficient stiffness in a direction normal to the face of the panel [21]. Structural component material properties must be selected according to the specific application and design criteria [22]. There are two kinds of sandwich structure namely symmetric and asymmetric. In the symmetric structure, the skins material and thickness are identical. In contrast, in the asymmetric type, the skin may differ in thickness or material because of different loading conditions or environmental factors [23].

2.3 Principle of Sandwich Structures

The main concept of sandwich structure can be explained as such: bending loads are to imposed on the skins and the shear loads are transferred through the core [24]. Furthermore, the core material must stabilize the skins against buckling or wrinkling. The bond between skins and core must have sufficient strength to withstand the shear and tensile stresses introduced between them.

A sandwich structure acts similar to an I-beam with two flanges and narrow web [22]. Flanges resist tensile and compression stresses while the web that connects the two flanges carries mostly shear forces [25]. The main difference between the sandwich structure and the traditional I-beam is that in the case of the sandwich structure materials for the core and skins are different. Additionally, instead of connecting the skins by a narrow web, the core of sandwich structure provides continuous supports for the skin (**Fig. 2.2**).

In these structures, placing two skins apart from each other leads to an increase in section modulus [26].

(a)   (b)
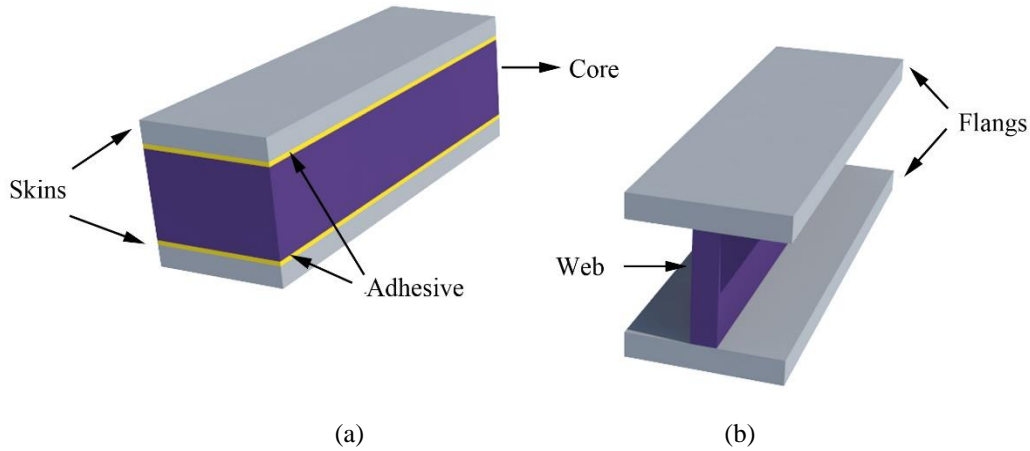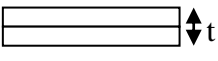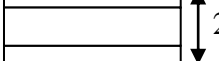
Fig. 2.2. Comparison between sandwich structure and I beam: (a) sandwich structure; (b) I beam.

The main advantages of using sandwich panel are that, the flexural strength and flexural rigidity can be improved in comparison with a homogeneous plate of material without increasing weight Considering a single skin structure (see **Table 2.1**) one can apply bending to this beam and calculate weight, bending stiffness, and bending strength and set them into unity. Now one can cut the beam from the middle and separate parts with insulation (core), and one more time calculate weight, bending stiffness, and bending strength. The more the distance between the two parts is increased, the bigger value for flexural strength and flexural rigidity will be obtained [27]. The relative properties of each beam are provided in **Table 2.1**.

The resulting sandwich structure's advantages can be summarized as: high stiffness and strength to weight ratio, excellent thermal insulation, rapid constructability without requiring lifting equipment of high capacity, and easy repair in the case of damage [22, 23, 25].

Table 2.1. Sandwich structural efficiency [23].

	t	$2t$	$4t$
Relative bending stiffness	1	7	39
Relative bending strength	1	3.5	9.2
Relative weight	1	1.03	1.06

2.4 Historical Background of Sandwich Structure Application

Engineers, designers, artists, and inventors have used sandwich structure concepts at various times in the history. The earliest sandwich structure drawings can be found in the works of

Leonardo da Vinci [28]. However, the first person to describe the sandwich structure principle (using two cooperating skins separated by a thick core) on the record appears to be done by the Frenchman, Duleau, in 1820 [8]. A bridge was built in Wales by two plates separated by a wooden egg crate core in 1845 [29]. The use of sandwich structure in aeronautics began in 1919 when the pontoons of a seaplanes were primarily constructed of a mahogany skins and a balsa wood cores. Thereafter, in 1945 the first aluminium sandwich panel was constructed. The proposed panel was composed of two aluminium skins and aluminium honeycomb core. Numerous small, aluminium hexagon cells were bonded to form the honeycomb core. It should be mentioned that at this stage, adhesives were being utilized for bonding the skins and core, and presented low viscosity, which could not properly bond the skins to the core [30].

The first major structures to incorporate sandwich panels were created during the Second World War. Sandwich panels were used in airframes such as the case of the ''Mosquito'' bomber aircrafts [21, 28].

In 1969, the successful application of sandwich panels in various new technological fields, such as rocket engineering and computers assisted to the successful landing of Apolo 11 on the moon. The spaceship was constructed by using sandwich technology in order to be light yet have adequate strength to withstand the induced stress from acceleration and landing. (see **Fig. 2.3**).
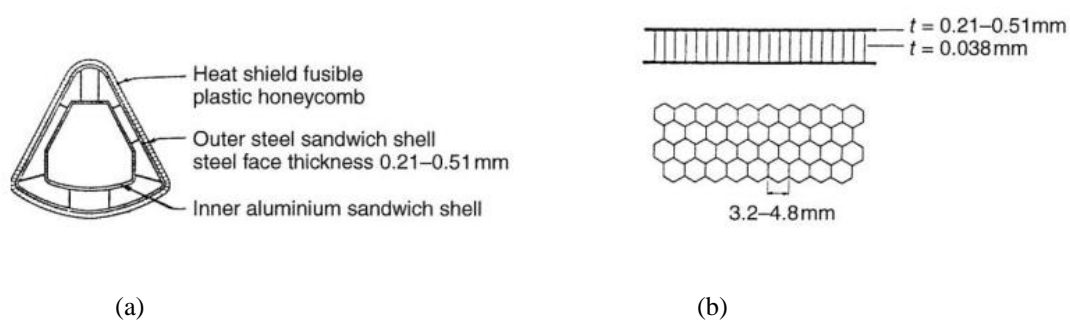
Fig. 2.3. Details of Apollo 11 capsule: (a) Sandwich construction details; (b) Cellular sandwich forming the outer shell [21].

2.5   Constituent of Sandwich Panels

Composite sandwich panels can be manufactured by choosing different materials for skins and cores. In the last decade, introduction of fibre composites robustly increased the choices of face sheets and core materials [8]. However, component material properties still must be

selected to fulfil the design criteria needs of the structure. The following section describes the basic functions and material properties for different components of sandwich structures.

2.5.1 Face Skin Materials

In general, the primary purpose of face sheets supports bending loads [9, 31]. In sandwich structures, both face sheets are usually identical in materials and thickness [9]. Hence face sheets must have specific mechanical characteristics such as: high tensile and compressive strength, high stiffness, as well as high resistance impact loading and to the environmental conditions[8, 9, 21].

A proper guide towards the selection of face sheet materials is presented by Ashby [32]. Zenkert divided face materials into two main groups namely metallic and non-metallic [8]. Metallic materials include steel, aluminium, and titanium, while non-metallic materials can be composed of wood, concrete, and fibre composite materials. Mechanical properties of some typical face sheets are tabulated in **Table 2.2** and **Table 2.3** . It must be mentioned that the listed mechanical properties represent short-term conditions according to standard testing methods. In reality, mechanical properties may vary depending on the temperature and humidity [31].

Table 2.2. Metallic Face Sheet Mechanical Properties [33, 34] .

Metallic material	ρ (kg/m^3)	E(GPa)	σ_T(MPa)
Aluminium (2024-T3)	2800	73	414
Steel (AISI 1025)	7800	207	394
Titanium	4400	108	550

ρ =density, E =Young's modulus, σ_T = Ultimate tensile strength

2.5.2 Core Material

The other component of the sandwich structure, is the core material. The core material has several main functions which must be considered when designing a sandwich structure. Separating the face sheets at a set distance from one another is the main function of core material. In order to ensure that the core thickness is maintained during the loading, this material must have adequate stiffness perpendicular to the face sheet [28]. Decreasing core thickness, led to loss of flexural rigidity in the structure [8]. In addition, in order to minimize the weight of the structure, core material requires a low density material. In sandwich structures, the core is mainly subjected to shear forces. Thus, in order to prevent the sliding of

skins during the loading, core material must have adequate shear stiffness, otherwise, face sheets will act as two independent beams or panels without interaction [28].

Table 2.3. Non-Metallic Face Sheet Mechanical Properties [8] .

Non-Metallic Material		ρ (kg/m$^{3)}$)	E (GPa)	σ_T (MPa)
Wood	Pine	520	12	47.7
	Plywood	580	12.4	21
Unidirectional Fibre Composite ($v_f \approx 0.6$-0.7)	Carbon/Epoxy	1600	180/10	1500/40
	Glass/Epoxy	1800	39/8	1060/30
	Kevlar/Epoxy	1300	76/6	1400/12
Bi-directional Fibre Composite ($v_f \approx 0.3$-0.4)	Kevlar/Polyester	1300	17.5	375
	Glass weave/ Polyester	1700	16	250
	Glass WR (woven roving)/Polyester	1600	12	215
Random Fibres ($v_f \approx 0.15$-0.25)	Glass CSM (chopped stand mat)	1500	6.5	85
	SMC (sheet moulding compound)	1800	9	60

v_f: fibre volume fraction

Core material could be classified to structural and cellular according to **Fig. 2.4**. The structural core material is formed by a corrugated, continuous web made by of solid elements. However, cellular core material has a number of voids inside to increase the insulation properties. These voids in the material are to be referred as cells. Cellular core comprising, cellular foam, honeycomb and balsa wood. Cellular foam contains polyurethane (PU), polystyrene (PS), Polyvinyl-chloride (PVC), polymethacrylimide (PMI)
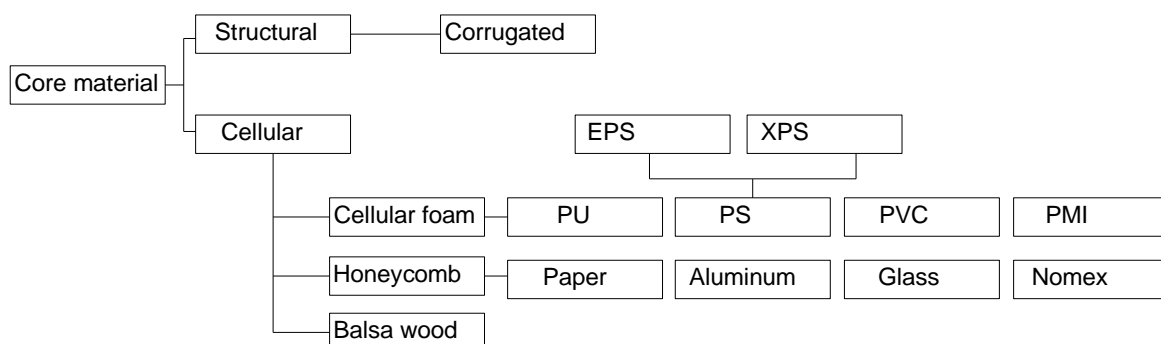
Fig. 2.4. Core material classifications.

In addition to that, **Fig. 2.5** shows ranges of the mechanical properties for PU foam core.

(a)   (b)
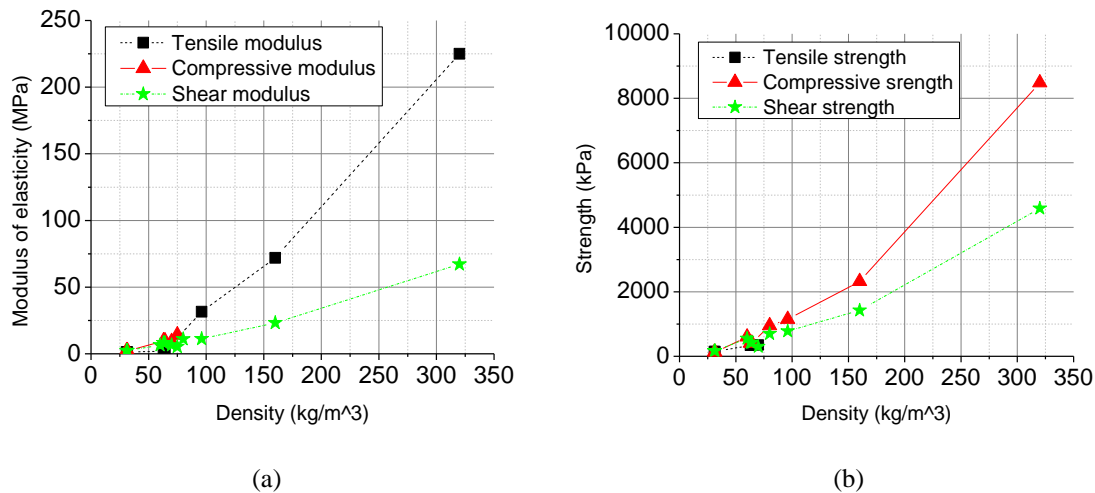
Fig. 2.5. Ranges of the mechanical properties of PU foam core: (a) modulus of elasticity *versus*. density; (b) strength *versus*. density.

2.6   Application areas of sandwich panels

This pat tends to classify application of sandwich panels. Accordingly, sandwich panels are classified into: industrial applications and civil engineering applications and structure members.

2.6.1   Industrial applications

In recent years, sandwich structures have been widely used in the aerospace industry due to their high strength to weight ratio that leads to lower total weight and enhanced fatigue resistance. Usually sandwich structures are composed of smooth metal skins or fibre reinforced polymer (FRP) materials with an aluminium honeycomb, corrugated core, balsa wood, or aramid paper core due to the excellent fatigue characteristics exhibited. [8, 28, 29, 35]. The combination of the materials used is dependent on the application. For instance, aluminium skins with honeycomb cores used for military transport aircraft where concentrated loading is expected. FRP skins and aramid honeycomb, predominately utilised in a passenger aircraft. In the aerospace industry different sandwich panels can be used for each part of the plan: fuselage, flooring, wings, speed brakes, seats, doors, doors frame, tail boom, horizontal stabilizers, and flap segments.

The successful application of composites in the aerospace industry led researchers to utilize these composite systems in the marine industry including naval vessels [36]. Sandwich structures can be used in applications such as: bulkheads, sail boats, hulls, and decks. When designing marine applications, lowering the centre of gravity reduces the weight above the water line and is one of the several important aspects the designer face. In the field of marine

engineering, FRPs material are prevalently used for the skins due to the high corrosion resistance. Foam core materials are primarily used due to the low rate of water absorption.

Finally, sandwich panels have been used in many land based vehicles to lower fuel consumption. By implementing lighter components less energy is required to propel the vehicle forward. Differing variations of sandwich panels are used throughout vehicles to replace ordinarily heavy parts. In recent history, sandwich structures have been used in parts of the vehicle including the roof, hood, and doors. Additionally, sound insulation characteristics of sandwich structure make them optimal for use as walls and floors in vans, trucks, and trailers. Some of the applications of sandwich panels in the industrial filed are presented in the **Fig. 2.6**.

(a)	(b)	(c)
(d)	(e)	(f)
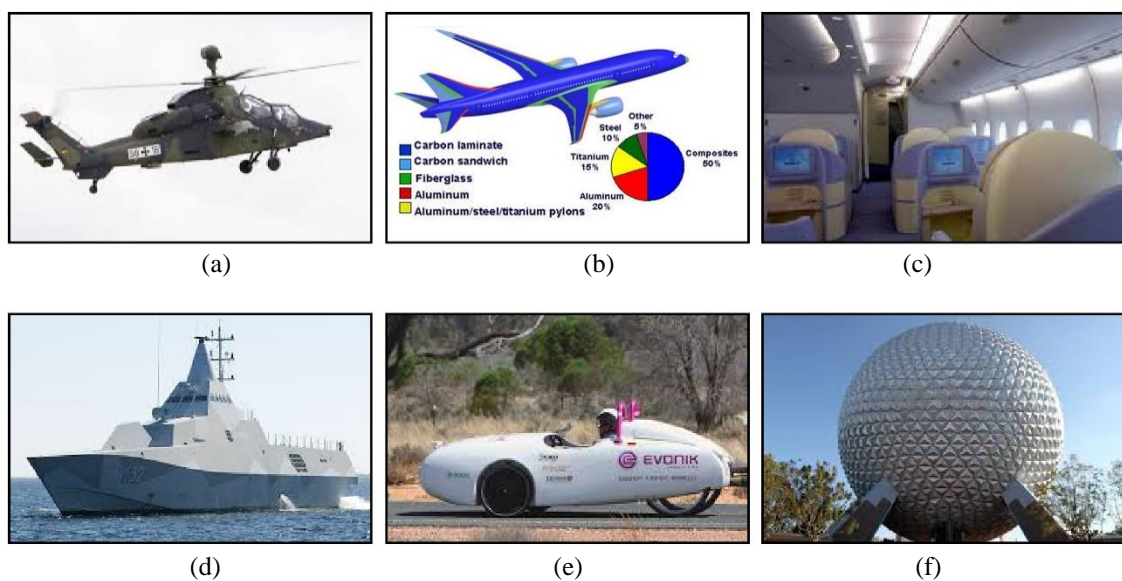
Fig. 2.6. Industrial application of sandwich panels: (a) Sandwich structure used in Eurocopter EC 665 German's helicopter parts such as fuselage, flooring and tail boom; (b) Boing 787 details made of sandwich structure; (c) First class seating system for Airbus 318 made of sandwich panel; (d) Corvette Viby; (e) Evonik electric car; (f) Epcot's spaceship building.

A sandwich panel has several different failure modes, which may condition its load-bearing capacity. Such load-bearing capacity depends on the sandwich materials, the panel dimensions and the structural geometry itself. **Fig. 2.7** presents the most common failure modes and their corresponding design equations.

(a)   (b)   (c)   (d)   (e)   (f)   (g)   (h)
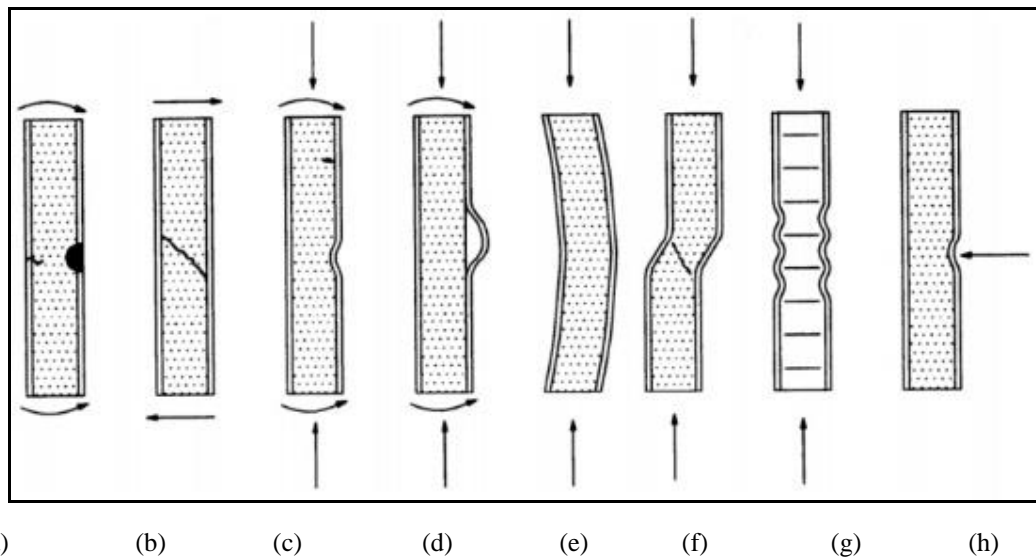
Fig. 2.7. Failure modes in sandwich panel: (a) face/core yielding; (b) core shear; (c) buckling-face wrinkling; (d) debonding; (e) general buckling; (f) buckling-shear crimping; (g) buckling-face dimpling; (h) core indentation-core yield.

2.6.2 Civil engineering applications

Civil structures typically involve the use of traditional materials such as concrete, steel, timber and masonry. Usage of these materials is time-consuming and prone to errors during construction. Implementing composite materials in buildings would provide a more beneficial such as: frugal, designed oriented properties, higher quality control, lightweight, non-susceptibility to corrosion, easier and faster application in case of using pre-fabricated elements, etc. Further, sandwich panels can exhibit a variety of architectural flourishes such as freeform shapes, ranges of colours, and transparencies. In addition, sandwich structures have superior acoustic and sound insulation qualities. In this section, material characterization for the face skins and core is tabulated in the **Table 2.4** and **Table 2.5**, respectively. Additionally, the results of the experimental analysis are shown in **Table 2.6** and **Table 2.7**

2.6.2.1 Floor and roof applications

In this part, sandwich panels applications for the floor and roof are classified as: panels without internal ribs, panels with internal ribs and Hybrid panels.

Sandwich panels without internal ribs

In 2001, Kim and Swanson investigated composite beams that were manufactured with a polyurethane foam core and Carbon Fibre Reinforced Polymer (CFRP) skins. The relevant results obtained for the mechanical behaviour are displayed in **Table 2.4** and **Table 2.5**. The

beams were evaluated under three-point bending test to understand the behaviour of the sandwich panel in localized loading region, such is the case of accidental impact. In order to investigate the failure modes in this composite sandwich panels, the authors used different densities and thickness for the foam core material. In this study, the densities of 96.1 kg/m^3, 160 kg/m^3, and 320 kg/m^3 were selected for the polyurethane foam core.

Different types of failure modes including shear failure (**Fig. 2.8**a), compression and delamination failure in the CFRP skin (**Fig. 2.8**b), as well as fibre failure on the skins (**Fig. 2.8**c) were observed. The authors reported that, in the low density solution, the shear failure mode occurred in the core. By increasing the thickness and density of the core, the failure began to occur on the compression CFRP face of the specimen.

(a)   (b)   (c)
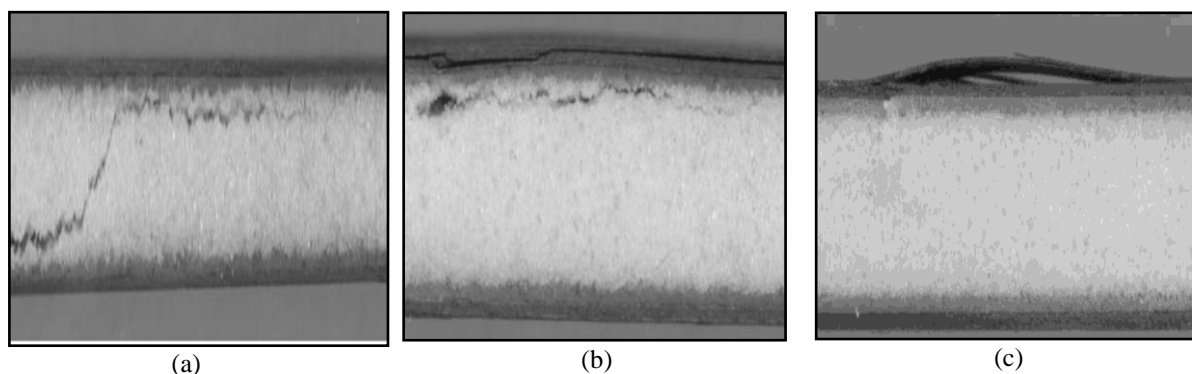
Fig. 2.8. Failure modes in sandwich panels of a core thickness of 6.35mm: (a) Shear failure in sandwich beam with 96 kg/m^3 polyurethane core of thickness 6.35 mm; (b) debonding failure in sandwich beam with 160 kg/m^3 polyurethane core of thickness 6.35 mm; (c) failure of the carbon/epoxy face in sandwich beam with 320 kg/m^3 polyurethane core of thickness 6.35 mm [37].

As can be seen in **Fig. 2.9**, it was observed that, for this type of sandwich structure, the load carrying capacity of the structure has increased with the core density of composite sandwich panel[37]. The additional results of three-point bending tests are indicated in **Table 2.6** and **Table 2.7 .**

(a)   (b)   (c)
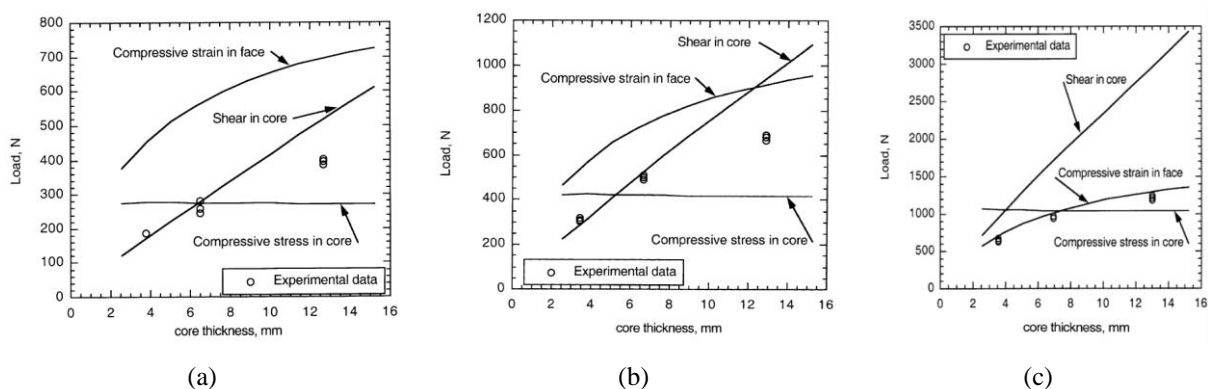
Fig. 2.9. Comparison of experimental failure load for sandwich beam with predicted competing failure modes: a) 96 kg/m3 polyurethane core of thickness 6.35 mm; b) 160 kg/m3 polyurethane core of thickness 6.35 mm; c) 320 kg/m3 polyurethane core of thickness 6.35 mm [37].

In 2010, Sharaf et al. studied the performance of composite sandwich panels as wall panel cladding that consisted of GFRP laminate skins and polyurethane foam core with the dimensions of 9000×2400×76 mm^3 (see **Fig. 2.10**). Densities of 31 kg/m^3 Kgm3 and 63 kg/m^3 for the polyurethane foam core were selected. **Table 2.4** and **Table 2.5** summarizes the effective mechanical properties of the skins and the core materials determined from testing.

Fig. 2.10. Typical full-scale sandwich composite cladding Wall [38].

Panels with dimensions of 1500×300×70 mm^3 were manufactured and one-way bending, three-point bending, four-point bending, and uniform load tests were carried out. The corresponding results are indicated in **Table 2.6** and **Table 2.7**. The results indicated that flexural strength and stiffness of the panels increased by doubling the core density. The dominate failure mode was the shear failure in both of the soft and hard foam cores. In the soft core, very large deflections were associated with excessive shear deformation of the core, which led to nonlinear behaviour in the panel; The authors suggested utilizing GFRP ribs inside the foam in order to connect the faces and increase the shear capacity of the core material [38].

In 2010, Manalo et al. studied flexural strength and failure modes of composite sandwich beam under four-point bending test (4PBT) in flatwise and edgewise directions. The proposed sandwich beams were comprised of phenolic core material and GFRP skins. The mechanical properties of the proposed sandwich panel components are indicated in **Table 2.4** and **Table 2.5**. The load-deflection behaviour, stress-strain behaviour, failure loads, and failure mechanisms of the utilized beam were evaluated under four-point static bending tests in flatwise (normal orientation) and edgewise direction (perpendicular orientation). **Fig. 2.11**

illustrates the scheme of flexural test of composite sandwich beams in two different directions.

<div align="center">(a)   (b)</div>
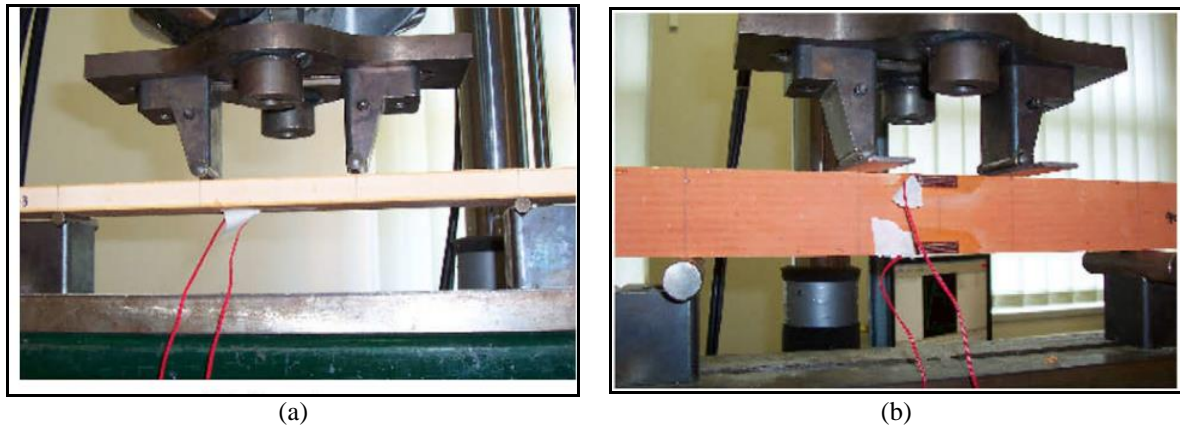
Fig. 2.11. Test Setup for 4PBT in two different positions: (a) flatwise; (b) edgewise position[39].

In this study, the analytical simulation was carried out by considering the linear elastic behaviour of GFRP laminate and the non-linear behaviour of the core material which acted linearly in tension and bi-linearly in compression.

Table 2.4. Summary of experimental study on the mechanical properties of Fibre Reinforced Polymer in sandwich panel.

Reference	Fibre orientation (°)		Type of FRP material	Average thickness (mm)	Component of composite sandwich panel		Mechanical properties of FRP material		
					Skin	Ribs	Tensile modulus (GPa)	Tensile strength (MPa)	Shear modulus (GPa)
[38]	0/90	0	GFRP	1.6	×		25.0	272	2.1
		90					22.5		
[40]	0/90	0	CFRP	1.5	×		19.1	NA	2.9
		90							1.6
[41]	0/90	0	GFRP	2.1	×	×	68.3	NA	NA
		90							
[39]	0/90	0	GFRP	1.8	×		15.4	246.8	2.5
		90							
[42]	0/90	0	GFRP	1.6	×	×	25.0	272	3.5
		90							
[43]	0/90	0	GFRP	5.5	×	×	24.0	NA	16
		90							8.7
[44]	0/90	0	GFRP	6		×	20.5	228	NA
		90							
[44]	0/90	0	GFRP	8	×		12.2	132	NA
		90							
[39]	0/90	0	GFRP	1.6	×		15.0	247	2.5
		90					13.0	208	
[45]	0/90	0	GFRP	1.5	×		14.7	267	NA
		90					13.1	187	

Table 2.5. Summary of experimental study on the mechanical properties of foam in sandwich panels.

Reference	Type of foam	Density (kg/m³)	Tensile properties		Compressive properties		Shear properties	
			Ultimate Tensile Strength (kPa)	Tensile modulus (MPa)	Ultimate Compressive Strength (kPa)	Compressive modulus (MPa)	Ultimate shear strength	Shear modulus (MPa)
[38]	PU	31	150	1.24	125	2.15	172	2.3
	PU	63	340	2.1	412	9.5	426	8.2
[40]	PU	60			600		550	6.5
	PU	80			950		700	11
	HDPE	80			800		600	13
	HDPE	100			1300		900	17
	PET	80			1000		600	20
	PMI	52			900		800	19
	PVC	60			900		760	20
	PVC	80			1400		1150	27
[40]	PU	75				14		5.4
[37]	PU	96		31.6	1145		779	11.22
	PU	160		72	2320		1427	23.2
	PU	320		225	8480		4590	67.2
[42]	PU	31	150	1.24	125	2.15	172	2.3
	PU	64	340	2.1	412	9.5	426	8.2
[44]	PU	70	350		300	9	300	6.5
	PP	110	760		2400	93.6	600	9
[39]	PF	850	5950	980	21350	2571	4250	746.88
[39, 46]	SF	550	15600	2200	28200	1600		

PU=:polyurethane; HDPE: High density polyethylene; PET: Polymethyl-therephalate; PMI: Polymethyl-methacrylate; PVC: Polyvinyl-chloride; PP: Polypropylene; PF: Modified phenolic core; SF: Syntactic foam

The results from experimental investigation revealed that the composite sandwich panels in flatwise orientation failed in a brittle manner due to either shear failure of the core or compressive failure of the skin followed by debonding between the skin and the core. In contrast, edgewise position specimens, failed due to progressive failure of the skin. **Fig. 2.12** illustrates load-deflection behaviour of the specimen under the four-point bending test. According to this figure, under the same level of loading, the deflection in the specimens tested in the flatwise position, experienced twice as much deflection as that of in the edgewise position. The composite sandwich panel in the edgewise position failed in the higher load than flatwise position. The final results of the investigation displayed the potential for use of this composite sandwich panel in structural laminated beam [46]. The corresponding results of the four point bending test (4PBT) in different positions is indicated in **Table 2.6** and **Table 2.7**.

(a)   (b)
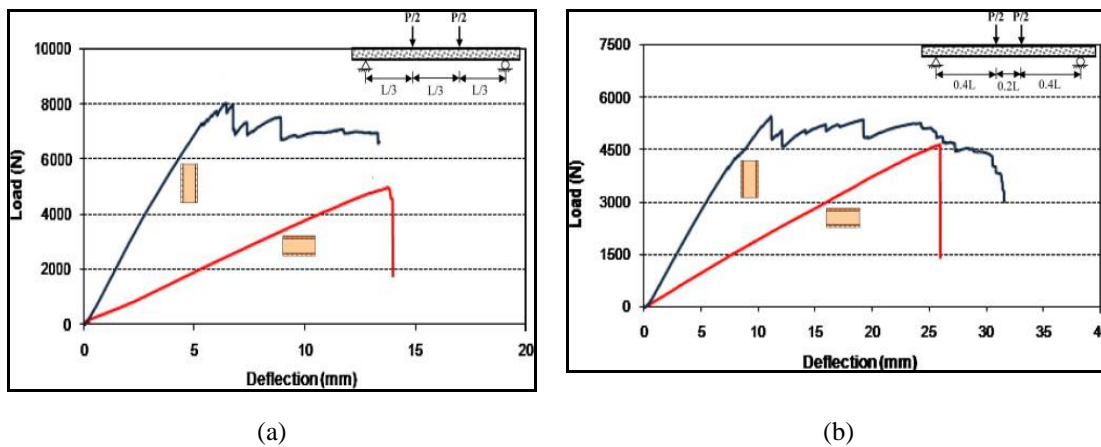
Fig. 2.12. Load-midspan deflection relation of specimen in flatwise and edgewise direction: (a) 4PBT with 100 mm shear span; (b) 4PBT with 160 mm shear span [46].

Sandwich panels with internal ribs

Reis and Rizkalla in 2008 [47] for avoiding delamination problems which typically occurred in traditional sandwich panels, proposed sandwich panels containing 3-D fibre reinforced polymer ribs. In this system, the top and bottom skins were connected together by using GFRP fibres, which were inserted in the foam core. **Fig. 2.13** illustrates the scheme of this system.
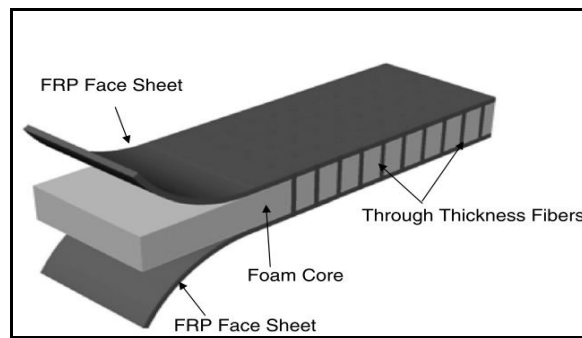
Fig. 2.13. Schematic Illustration of new 3-D Sandwich Panel [47].

Two different patterns for the through-thickness fibres were investigated in this study namely as regular array (**Fig. 2.14**a) and continuous wall (**Fig. 2.14**b). In the first pattern, the through-thickness fibres were evenly spaced in each direction. While in the second pattern the through-thickness fibres were arranged in semi-solid rows, like in a closely spaced picket fence, in one direction forming a rigid web.

(a)

(b)
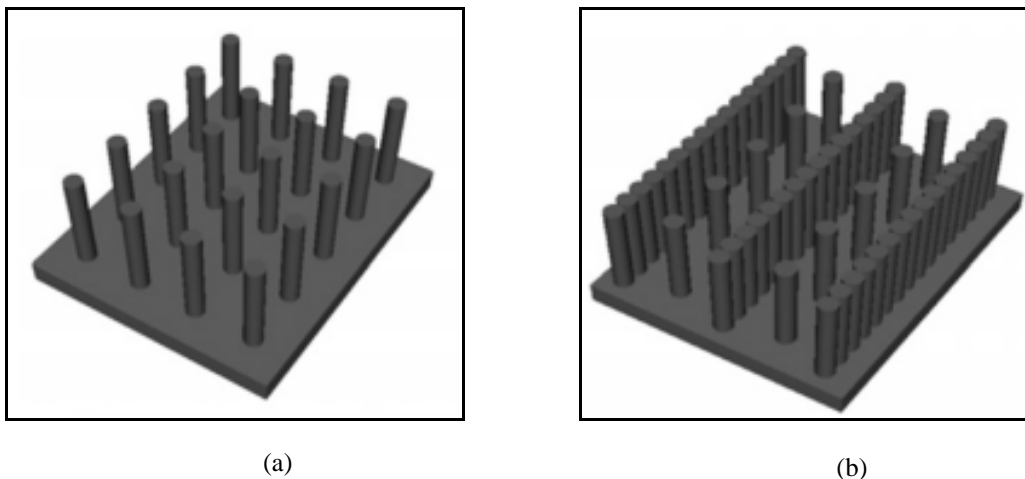
Fig. 2.14. Different arrangements of through-thickness fibres: (a) regular array; (b) continuous wall [47].

The mechanical properties of the face sheets were evaluated using in-plane tensile tests. A total of 33 tension coupons with different number of plies and different configuration of fibres were tested. It was observed that increasing the densities of fibres resulted in decreasing elastic modulus as well as the tensile strength of face sheets. This explained by the fact that by increasing the densities of the fibres creates zones of imperfection and waviness among the fibres. Influences of the through-thickness fibres on the proposed sandwich panels were evaluated using shear, compression and flexural tests.

In the shear test, the results indicated linear behaviour up to the initiation of the shear crack in the foam core followed by a nonlinear behaviour with significantly low shear modulus up to failure. The shear tests results showed that the density and configuration of 3-D fibres affect

the core shear modulus. Additionally, tests results suggested that increasing the thickness of the sandwich panels did not have significant effect on the shear modulus of the sandwich panel. **Fig. 2.15**a shows shear cracks in the shear test.

Compression test results showed that, increasing the quantity of 3-D fibres increased the compressive strength of the tested panels. The increase in the compressive strength was linearly proportion to the increase in density of the through-thickness. Additionally, test results revealed that decreasing the thickness of the panel, increasing the buckling load of the through-thickness fibres, resulting in the increase of the compressive strength of the panel significantly. The buckling of the through-thickness fibres at compression test is shown in **Fig. 2.15**b.

(a)   (b)
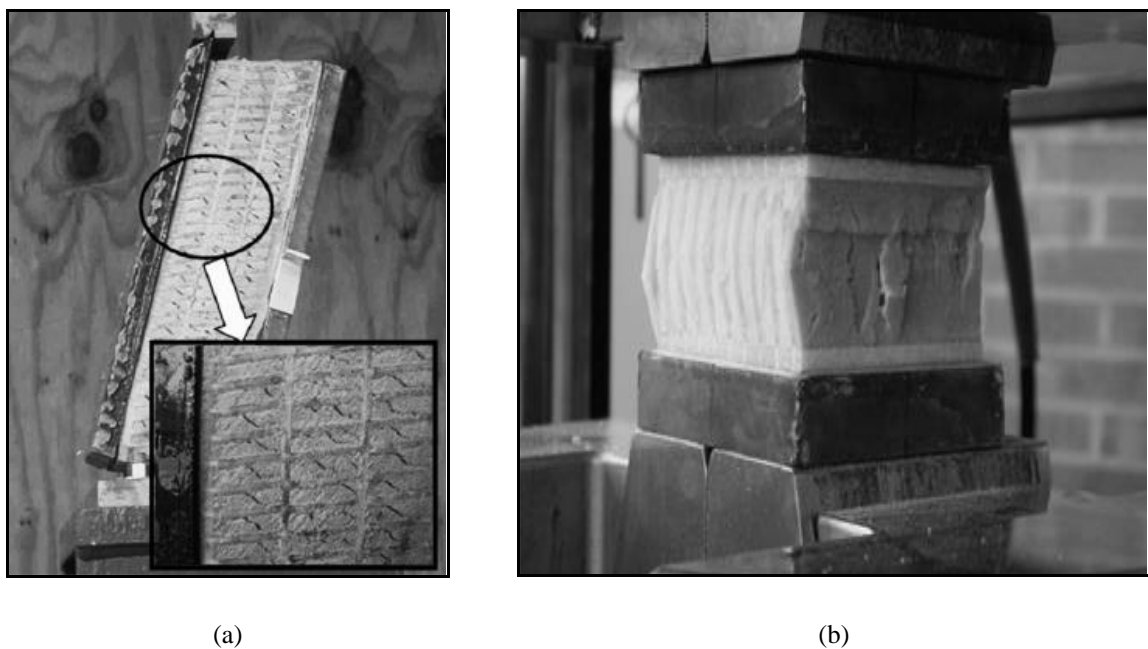
Fig. 2.15.Failure of the tested sandwich specimens: (a) shear cracks in shear test; (b) buckling of through-thickness fibres at failure

Fam and Sharaf studied the composite sandwich panels composed of polyurethane foam cores with the densities of 31.6 kg/m^3 and 64.6 kg/m^3 and GFRP skins. The main mechanical properties of the constituents are shown in **Table 2.1** and **Table 2.2**. In this research, six sandwich panels (P1-P6) with different rib configurations and dimensions were fabricated. Configurations of the test panels and the fabrication process are shown in **Fig. 2.16**a and **Fig. 2.16**b, respectively. In this study, the internal and external ribs consisted of two back to back C-shape GFRP profiles (see **Fig. 2.16**a- detail B). While for the external ribs only one C-

shape profile (see **Fig. 2.16**a- detail C) was utilised. The fabrication method using Vacuum Assisted Resin Transfer Moulding (VARTM) process is depicted in **Fig. 2.16**b.

(a)

(b)
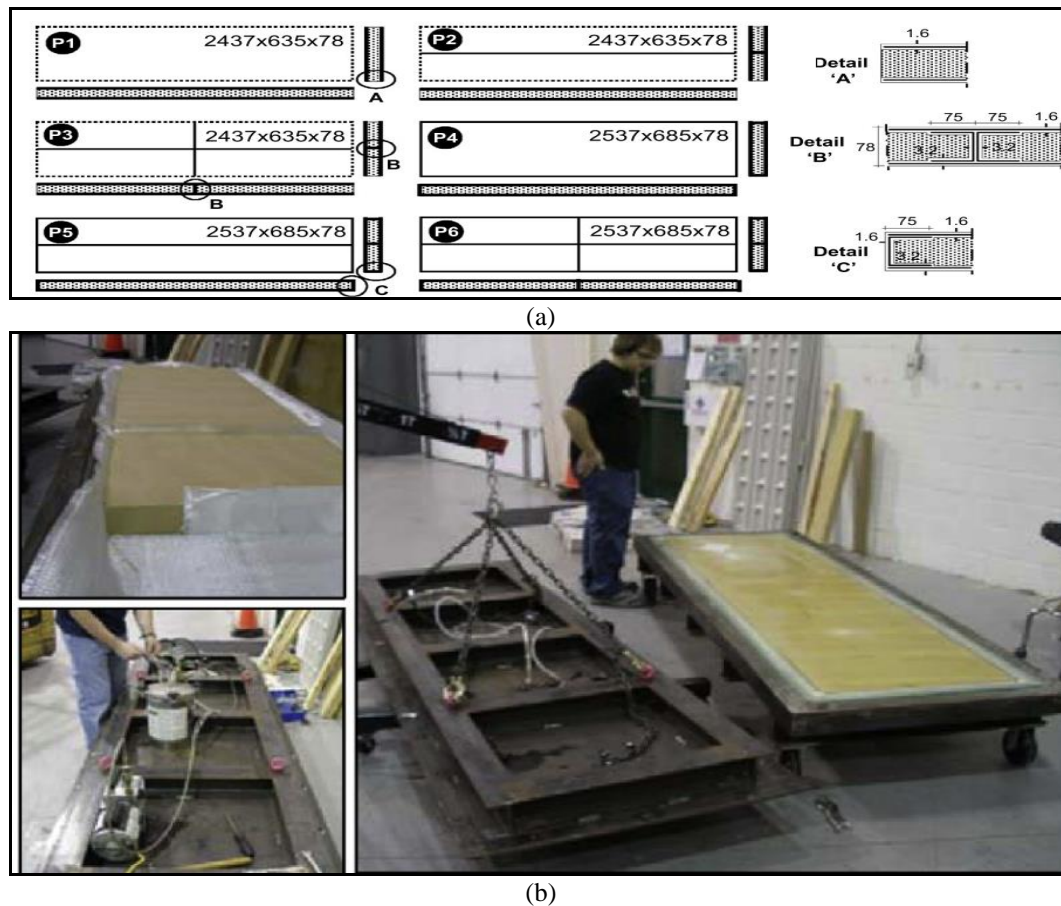
Fig. 2.16. Proposed Composite Sandwich Panel: (a) configurations of tested panels; (b) fabrication process [42].

The specimens were tested in one-way bending with a span of 2300 mm, under a uniform load. The results indicated that the flexural strength and stiffness of a composite sandwich panel increased by adding GFRP interior ribs. From the preformed experimental works the importance of using internal and external GFRP ribs in increasing flexural stiffness and stiffness of the panels was observed. Accordingly, a single internal and external rib influence in increasing flexural strength and stiffness was obtained by a value of 95% and 50% respectively. However, in the panel with both internal and external rib, increase for the flexural strength and stiffness was obtained by a value of 140%.

Furthermore, it was observed that, in the sandwich panel without any internal GFRP ribs, shear contributed to over 50% of midspan deflection. By adding GFRP ribs, flexural became more dominate and shear deformations of the ribs contributed 15-20% of the total deflection (see **Fig. 2.17**).
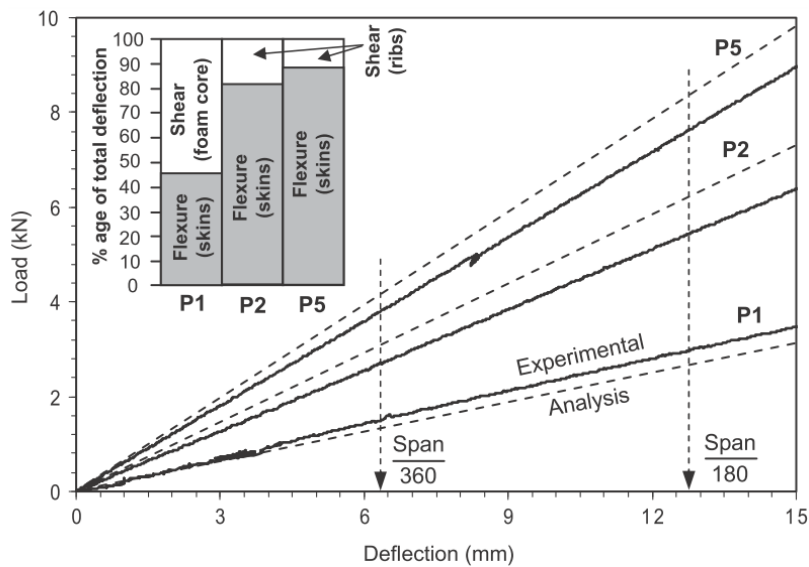
Fig. 2.17. Load- Deflection response for the different composite sandwich panel [42].

Regarding to the failure modes. Two types of failure were noticed namely as wrinkling and crushing of GFRP skin (see **Fig. 2.18**). Accordingly, in the sandwich panels without any ribs and in the panels with only longitudinal ribs the outward wrinkling of the GFRP skin in the compression side was reported as a failure mode. Additionally, in the panels with both longitudinal and external ribs wrinkling and crushing of the GFRP skin in the compression side was reported as failure modes.

(a)

(b)

(c)   (d)   (e)
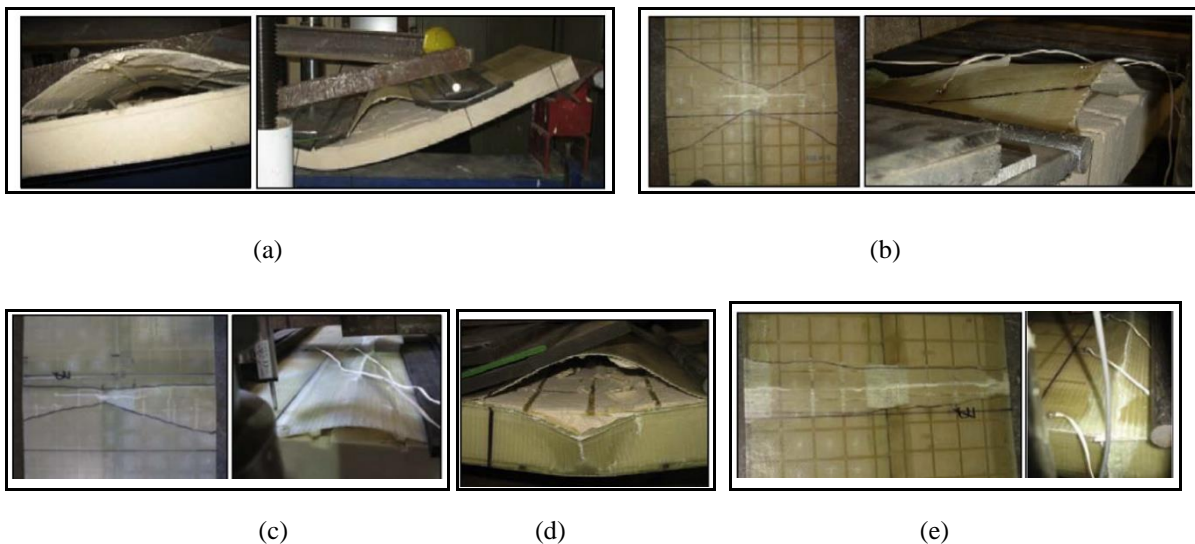
Fig. 2.18. Failure modes of sandwich panels: (a) cylindrical wrinkling of compression skin in specimen P1; (b) conical wrinkling of compression skin in specimen P2; (c) Conical wrinkling of compression skin in specimen P3; (d) delamination of corner in specimen P4; (e) crushing of compression skin in specimens P5 and P6 [42].

In 2012, Correia et al. investigated composite sandwich panels, which were composed of polyurethane (PU) and polypropylene (PP) foam core, with GFRP laminate skins and internal

GFRP ribs for civil engineering applications. The results for the mechanical properties of materials in this study are indicated in **Table 2.4** and **Table 2.5**.

The following four types of composite sandwich panels made of GFRP skins were produced and studied: (i) two standard sandwich panels without lateral reinforcement (see **Fig. 2.19**a), formed by a core of either PU or PP (panels PU-U and PP-U, respectively) and (ii) two sandwich panels (see **Fig. 2.19**b) comprising GFRP ribs, each one with the aforementioned core materials (panels PU-R and PP-R, respectively).

(a)   (b)
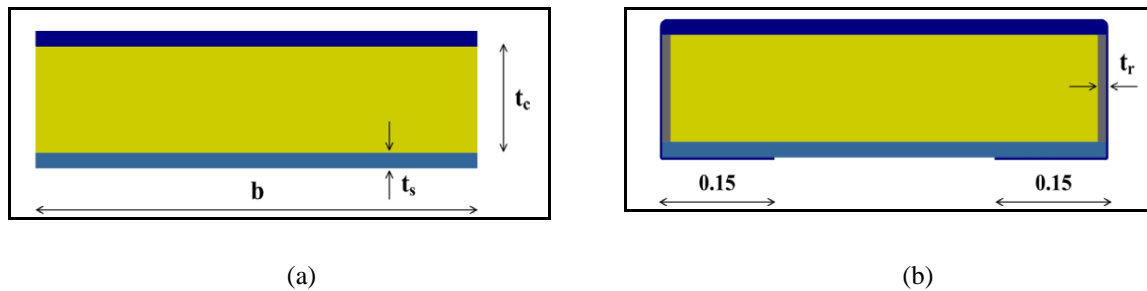
Fig. 2.19. Configurations of Test Panels: (a) Unconfined Panels; (b) Confined Test Panels [44].

In the proposed sandwich panels, the nominal dimensions were: core thickness=90 mm, skin thickness= 7 mm, and ribs thickness= 6 mm. For the large scale panels, four-point bending tests were carried out. The relevant results for the static flexural test are indicated in **Table 2.6**and **Table 2.7**.

The results indicated that specimen's response was linear up to failure with a slight stiffness reduction prior to collapse. The unconfined sandwich panels with PP foam core were stiffer than panels with PU foam core. GFRP ribs in the confined panels led to a change of the failure mode from shear failure in the unconfined panel to wrinkling and delamination failure mode in the skins. **Fig. 2.20** illustrates the different kinds of failure modes in composite sandwich panels in this study [44].

(a)   (b)

(c)   (d)
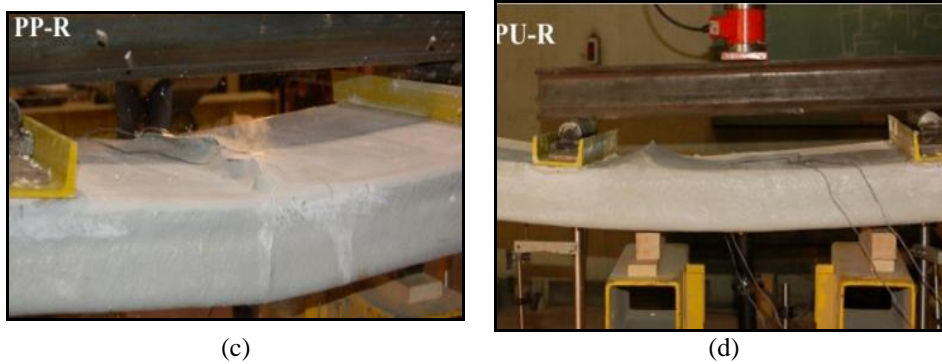
Fig. 2.20. Failure modes in static flexural tests in different panels: (a) Shear failure mode in PP-U panel; (b) Shear failure mode in PU-U panel; (c) Wrinkling failure mode in PP-R panel; (d) Delamination failure mode in PU-R panel [44].

Hybrid concrete sandwich panel

In 2004, Norton worked on a new sandwich panel with the aim of using it in bridge decks. This panel consists of basalt core material and GFRP corrugated internal ribs. In this system, concrete was used as skin in the compression side of the sandwich panel (see **Fig. 2.21**).
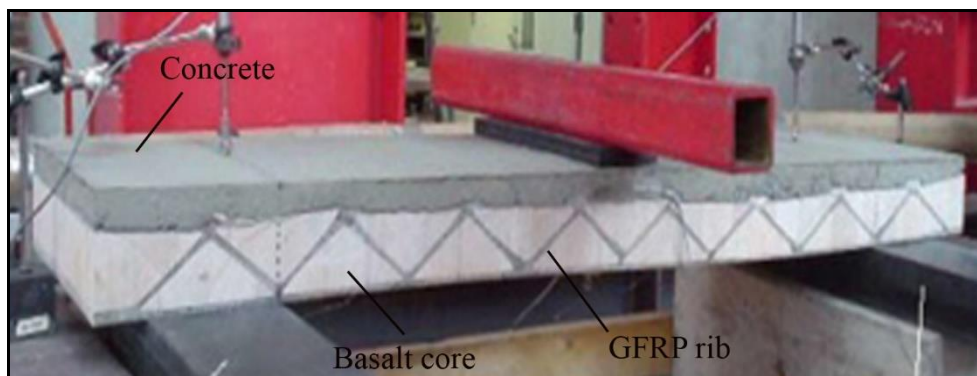
Fig. 2.21. Photo of the hybrid concrete sandwich panel being tested [48].

In order to prepare adequate surface for bonding concrete to the sandwich panel, two kinds of shear connectors, namely metal shear connectors and composite shear connectors, were utilized in this system before casting the concrete. After installing the metal and composite shear connector to the top of the specimen, concrete was cast on the panels (see **Fig. 2.22**). To evaluate the effects of through-thickness internal corrugated GFRP, three kinds of decks were produced. In Deck 1 the metal shear connector was utilized with corrugated GFRP ribs, whereas in Deck 2, the basalt core was used without corrugated GFRP; in Deck 3 the composite shear connector was used with corrugated GFRP ribs.

(a)   (b)   (c)
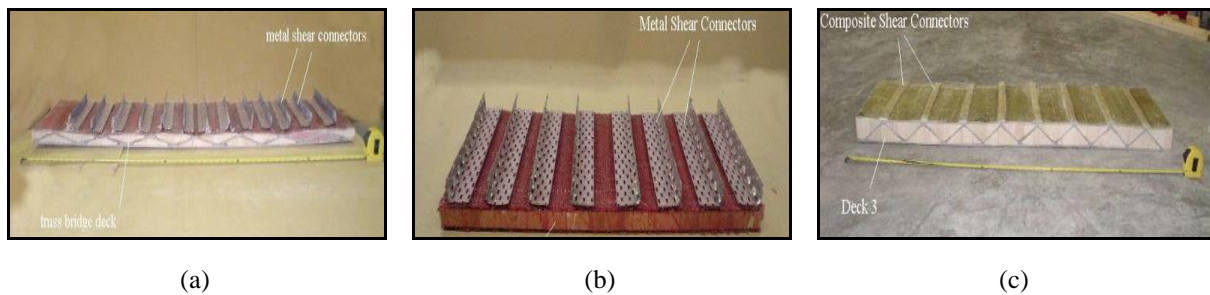
Fig. 2.22. Sandwich panels with different configuration of shear connectors: (a) sandwich panel with metal shear connectors and corrugated ribs (Deck 1); (b) sandwich panel with composite shear connectors and without corrugated ribs (Deck 2); (c) sandwich panel with composite shear connectors and corrugated ribs [48].

Three-point bending tests were carried out on the proposed specimens. **Fig. 2.23** shows different the type of failure modes registered in the tested specimens. As can be seen, Deck 1 failed due to concrete crushing and buckling of the top concrete skin. In Deck 2 the failure was due to shear failure in the concrete, while Deck 3 failed by the concrete delamination of the top skin.

Results for the different decks revealed that shear connectors led to an increase in the load carrying capacity for all of the specimens. When comparing the metal and composite shear connectors, metal shear connectors were found to be useful, but the installation of these connectors on the top surface was very difficult. Furthermore, it was suggested that shear bolts be used by drilling them into the top surface [48].

(a)   (b)   (c)
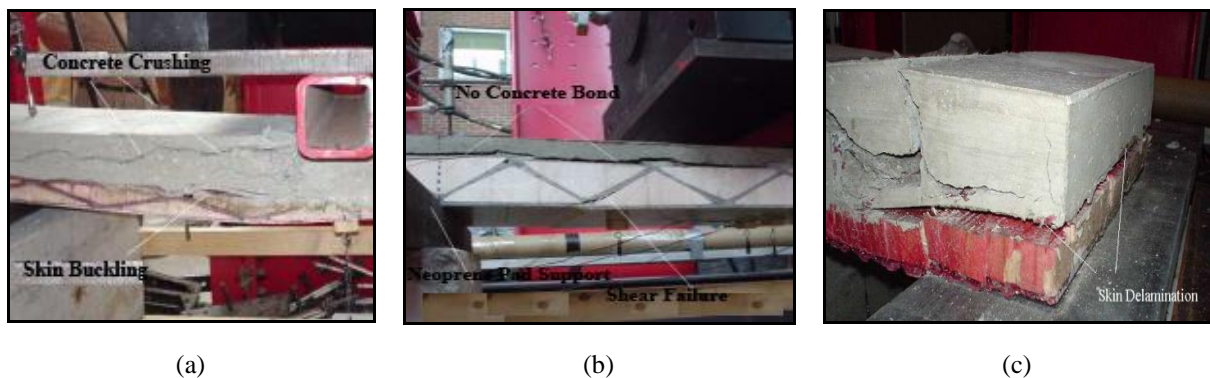
Fig. 2.23. Failure modes in the proposed specimens: (a) concrete crushing and skin buckling in deck 1; (b) concrete shear failure in deck 2 ; (c) concrete delamination in deck 3 [48].

2.6.2.2 Building Façade

Several experimental and theoretical investigations have been carried out by different researchers to evaluate the behaviour of composite sandwich wall panels and their failure modes under eccentric or concentric axial loads.

Recently, Mathieson and Fam [49] performed an in-depth study to investigate the influence of the slenderness ratio on the concentric axial behaviour of sandwich wall panels. The study examined the effects of cross-sectional configurations and slenderness ratio (KL_e:r) ranging from 15 to 70 on the axial behaviour. Where L_e is the length between the two end pins, K=1 for pinned-pinned condition and r=(I/A)$^{1/2}$, where I and A are the moment of inertia and cross-sectional area of GFRP component including skin and ribs and neglecting the core.

A total of 45 specimens were manufactured using GFRP skins and PU foam core with a cross section of 150×75 mm^2. Details of tested specimens is indicated in **Fig. 2.24**. A self-reacting axial loading frame was designed consisting of two heavy reaction beams connected together using high-strength DYWIDAG bars (see **Fig. 2.25**).

(a)   (b)   (c)
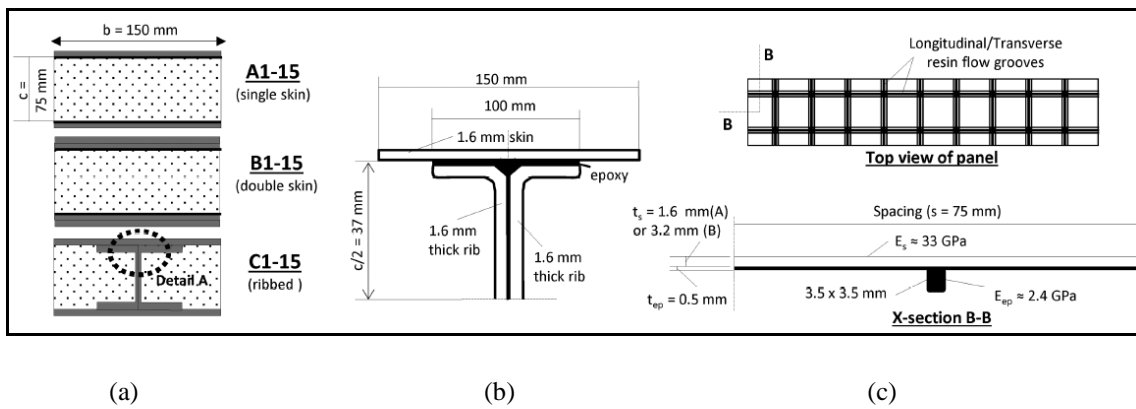
Fig. 2.24. Details of test specimens: (a) cross-section configuration; (b) detail A; (c) core-skin interface.
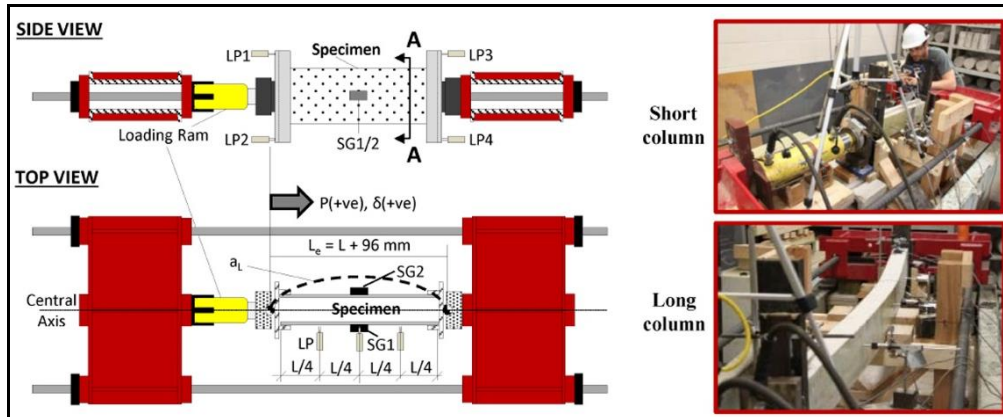
Fig. 2.25. Test setup [49].

The failure modes in this research were categorized in three groups based on the slenderness ratios of the panels as: (i) panels with a slenderness ratio of 15-17 experienced local failure in non-ribbed panels or skin crushing in ribbed panels; (ii) panels with a slenderness ratio of 41-70 experienced global buckling followed by skin wrinkling and core shear failure, as well as

skin crushing in the ribbed panels; (iii) panels with a slenderness ration of 17-41 presented mixed failure modes.

It was found that by increasing the skin thickness by a factor of four, panels with a slenderness ratio of 15 and 75 increased their ultimate axial load by 32% and 86%, respectively. By increasing the core four times resulted in an increase of ultimate axial load of 264% and 52% for the panels with the slenderness ratios of 15 and 75, respectively. Hence, increasing skin thickness of panels with higher slenderness ratios was recommended as more effective when global buckling is the predominant failure mode. Similarly, in panels with a low slenderness ratio, by increasing the shear modulus of the core was indicated as the most effective method when local skin wrinkling is the governing failure mode.

Mousa and Uddin [50, 51] studied the structural behaviour of sandwich wall panels under eccentric loading. The dominant failure mode was described as an abrupt debonding between the GFRP skin and the foam core on the compression side due to out-of-plane interfacial tensile stresses that attained the ultimate tensile strength of the foam core material. This kind of failure is known as wrinkling failure or local buckling. An analytical model was developed to justify the wrinkling failure by considering two kinds of stresses associated to it: (i) interfacial tensile strength between GFRP skin and foam core; and, (ii) the critical wrinkling stress in the compressive GFRP skin.

Different theoretical approaches can be used to analyse the instability that occurs in composite sandwich wall panels. The basic approach was proposed by Euler using the well-known Euler-Bernoulli assumption, where the global buckling load is predicted under various support conditions and slenderness ratios. It was observed that the effect of transversal shear (out-of-plane shear components) can significantly reduce the Euler critical load. Based on that, Engesser [52] and Haringx [53] proposed to include shear deformation in the analysis of axially loaded composite panels. The nonlinear geometrical behaviour of sandwich panels using high-order theory was further developed under various boundary conditions [54, 55].

2.7   Conclusions

The literature review illustrates that sandwich panels are emerging as potential members in light structural application after a long history of successful application in different industrial field. Compared to other traditional construction technologies, composite sandwich panels present higher thermal-acoustic performance and strength-to-weight ratios, making them suitable for applications in the field of civil engineering.

It was observed that GFRP skins combined with PVC or PU foam cores can provide a significant reduction in sectional mass of the sandwich panel. However, the optimization of the composite action in sandwich panels was found to be dependent on the mechanical performance of sandwich panel's components, as well as on the production quality of the structure. In the un-ribbed sandwich panels, the shear stiffness of foam material was verified to be an effective parameter in the design process. Almost all of the performed experiments demonstrated shear failure localized in the foam core. However, in ribbed panels, the debonding and skin wrinkling were the main modes of failure; thus, the quality of the bond between skin and foam, as well as the strength of the skin materials were the driving characteristics throughout the design process.

Potential exists for employing composite sandwich panels as a modular system in a temporary building. Modular construction provides faster and easier assembly with less labour due to the lighter and stronger sandwich panel materials. However, this topic still requires further investigation to achieve appropriate fruition and fulfil the design requirements of temporary houses.

Table 2.6. Summary of excising experimental works on the flexural behaviour of sandwich panel compose of FRP skins and foam core.

Ref.	Skin material Properties			Foam material Properties			Specimen dimension			Static flexural test results		
	Type of material	Tensile modulus (GPa)	Thickness (mm)	Type of material	Density (kg/m^3)	Thickness (mm)	Length (mm)	Width (mm)	Thickness (mm)	Loading type	Maximum deflection (mm)	Maximum load (N)
[37]	GFRP	68.3	0.5	PU	9.10	6.35	203	25.4	6.87	3PBT	10.4	261.33
					160						6.6	501
					320						4.7	1215.66
[40]	GFRP	19.10	1.5	PMI	52	20	560		26	4PBT	26.1	1600
				PET	80						48.2	2100
				HDPE	100						64.1	2300
[38]	GFRP	25	1.6	PU	31	72.8	1500	300	76	3PBT	27.8	2542
					31					4PBT	31	4560
					31					Uniform	64	7174
					63					Uniform	62.03	18243
[46]	GFRP	1.5	1.8	PF		64.4	300	50	50	4PBT	13.7	4657
								18	18		NA	8150
							400	50	20		25.6	4880
							400	20	50		10.6	5250
[42]	GFRP	25	1.6	PU	850	74.8	2437	635	78	Uniform	67.78	13980
					31							
[44]	GFRP	20.5	7	PP	110	90	2500	500	104	4PBT	51.57	28260
				PU	70						72.54	31740

PU=:polyurethane; HDPE: High density polyethylene; PET: Polymethyl-therephalate; PMI: Polymethyl-methacrylate; PVC: Polyvinyl-chloride; PP: Polypropylene; PF: Modified phenolic core; SF: Syntactic foam

Table 2.7. Summary of excising experimental works on the flexural behaviour of sandwich panel compose of FRP skins, foam core and strengthening FRP ribs.

Ref.	FRP material Properties			Foam material Properties		Specimen dimension			Static flexural tests results		
	Type of material	Tensile modulus (GPa)	Component	Type of material	Density (kg/m³)	Length (mm)	Width (mm)	Thickness (mm)	Loading type	Maximum deflection (mm)	Maximum load (N)
[45]	GFRP	14.7	Skin/Ribs	SF	550	110	30	16	3PBT	4.35	8400
			Skin/Ribs (Longitudinal direction)						4PBT	1.32	9450
										68.78	
			Skin/Ribs (Longitudinal and transfer directions)			2437	635			63.75	26720
[42]	GFRP	25	Skin/ Exterior ribs & longitudinal direction ribs	PU	31.6	2537	685	78	Uniform	64.52	33640
			Skin/ Exterior ribs/longitudinal and transfer direction ribs							66.01	
[44]	GFRP	20.5	Skin/ Exterior ribs	PP	110	2500	500	104	4PBT	72.3	72830
				PU	70					89.16	86130

SF: Syntactic foam, PU: Polyurethane, PP: Polypropylene

Chapter 3: Temporary Residential Housing

3.1   Introduction

The timely establishment of emergency structures after natural disasters is an important step in returning an affected community to normality. By quickly providing shelters, risk of death from exposure and illness is diminished, restoration efforts can be undertaken, and communities can begin the process or rebuilding. [14, 56-58].

Existing temporary shelters are categorized into two main categories: (i) shelters made of plastic, earth bags, and tents; (ii) shelters made of woods, metal, or prefabricated materials. The main concern of the first group of temporary structures is that they are not capable of providing the means by which a family can return to daily life. Hence, it is impracticable to call these structures a suitable replacement by which a community can regrow. In the other group of temporary shelters, while the structures are safer, they have the disadvantage of requiring skilled laborers for assembly and install in addition to their large upfront cost. [59].

In this context, the team composed of members of University of Minho (UMinho), Instituto Superior Técnico (IST) from University of Lisbon and the company ALTO - Perfis Pultrudidos, Lda., developed a R&D proposal, named "ClickHouse", for developing a new system of prefabricated temporary buildings into the emergency shelter market. The proposal was accepted and founded by the Portuguese National Agency of Innovation (ANI – "Agência Nacional de Inovação") – project no. 38967. The structure designed uses GFRP pultruded profiles and composite sandwich panels, both made by ALTO - Perfis Pultrudidos, Lda.

The main assumptions when designing 'ClickHouse' included: (i) ease of transport and assembly; (ii) international design code compliance (iii) structural safety and thermal

performance; (iv) self-sufficiency with regard to energy supply and water; and (v) competitive cost against current solutions.

3.2   Architectural Design

The designed temporary structure composed of a single-story building with a rectangular plan of 6.12×3.12 m^2, formed by connecting two units of 3.12×3.12 m^2 with a height of 3.12 m capable of accommodating a family of 4 to 5 members.

All of the house's components including walls, floors, and roof were designed to incorporate water supply, drainage, sewage, and electricity. These disciplines were further developed in the Clickhouse's infrastructure task [60]. **Fig. 3.1** illustrates the plan and elevation view of this temporary housing system. It is important to note that the capability of connecting units with each other provided the possibility of erecting a pre-selected number of buildings by joining them. Comprehensive information about the architectural aspects can be found in [59]. A photo of the single-story built prototype is represented in **Fig. 3.2**.

(a)
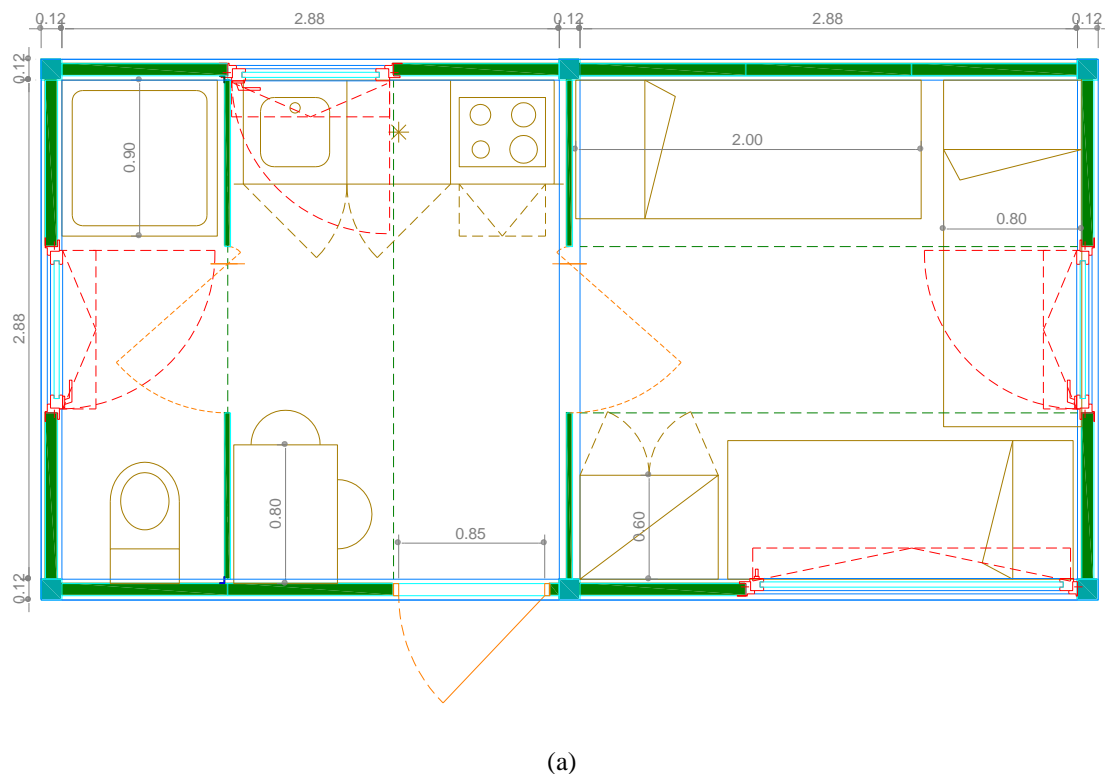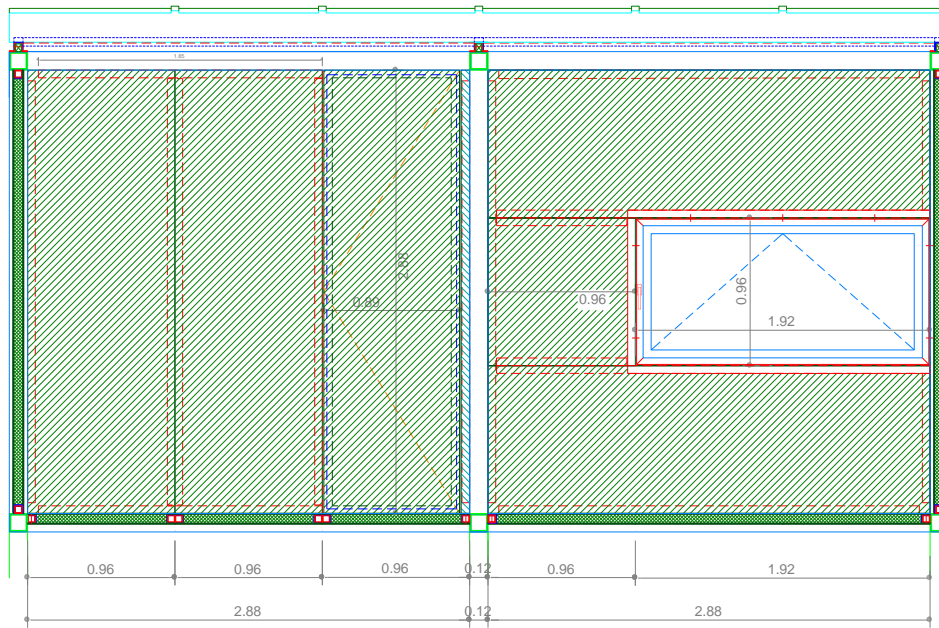
(b)
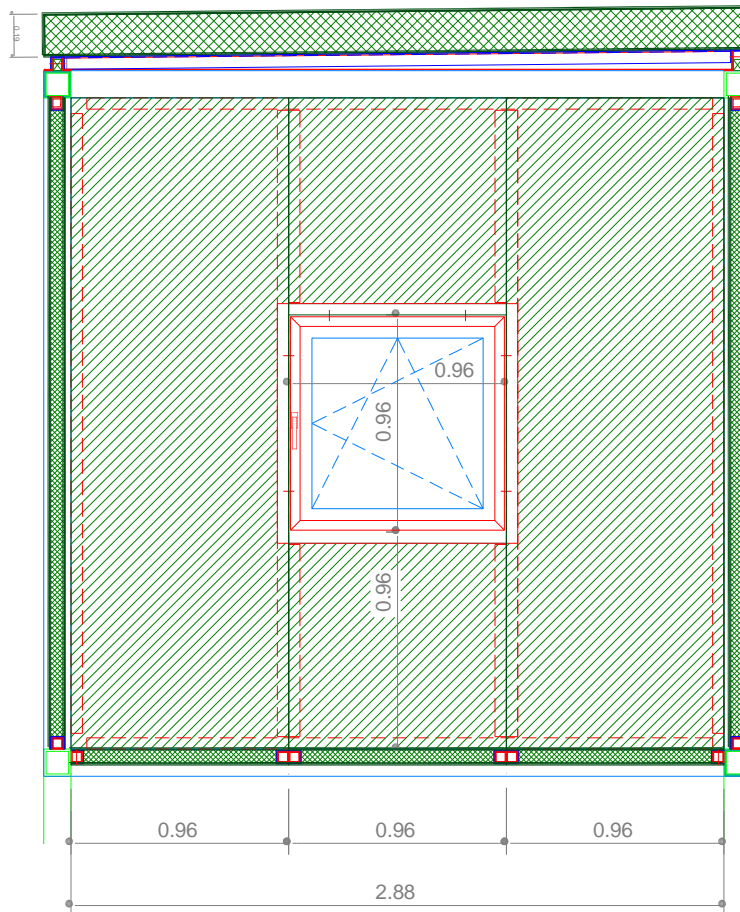
(c)

Fig. 3.1. Modular system plan and elevation views: (a) plan view; (b) south view; (c) east view (all units in millimeters) [59].

Fig. 3.2. Temporary single-story prototype.

3.3 Structural Components

The proposed temporary dwelling was composed of three main components: (i) a framed structure composed of columns and beams, (ii) sandwich panels forming the floor, wall, and roof, and (iii) the connectors. The team of IST designed the framed structure whereas the team of UMinho designed the sandwich panels. Both teams designed the different existing connectors.

3.3.1 Columns and Beams

The framed components of the house were made of tubular GFRP pultruded profiles with a cross section of $120{\times}120$ mm^2 and a wall thickness of 8 mm. For the sake of decreasing segment variation in the manufacturing process, this profile was used in both beams and columns (see **Fig. 3.3**).
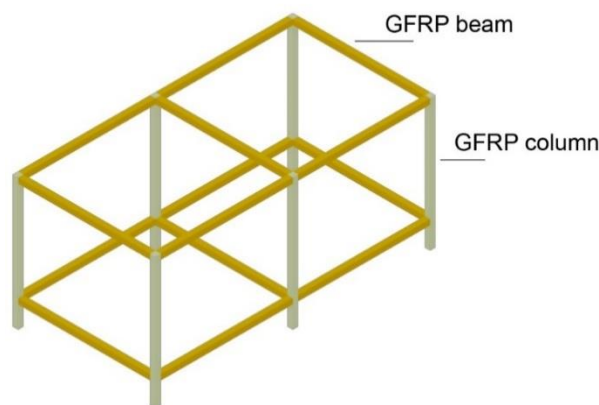
Fig. 3.3. GFRP framed structure.

3.3.2 Floor, Roof, and Façade Panels

3.3.2.1 Floor Sandwich Panels

A common sandwich panel made of two outer skins and an interior core was adopted in this project. Prior investigations indicated that using high strength material such as Carbon Fibre Reinforced Polymer (CFRP) for the skin was not necessary and Glass Fibre Reinforced Polymer (GFRP) was recommended [61]. Additionally, it was found that PU foam material with a minimal internal ribs exhibited satisfactory insulation characteristics [38]. Consequently, GFRP and PU foam were chosen to form the main structure of the wall panels in the study.

The connection between panels and other elements was accomplished using a U-shape GFRP pultruded profile with a cross section of 60×55 mm^2 and a wall thickness of 5 mm (U60$\times$55$\times$5) externally adhered to the PU foam core during a manufacturing process. Two possible geometric profiles for the slab sandwich panels were designed and proposed for use in the ClickHouse' project, as depicted in **Fig. 3.4**:

a) Panel FSP-L2.4_W1.2_t70 consisted of a sandwich panel 2.4 m long, 1.2 m wide, and 0.07 m thick, and with thicknesses of the GFRP skins and foam core equal to 5 mm and 60 mm, respectively. The panel's weight was approximately 65 kg;

b) Panel FSP-L3.0_W1.0_t70 consisted of a sandwich panel 3.0 m long, 1.0 m wide, and 0.07 m thick, with thicknesses of the GFRP skins and foam core equal to 5 mm and 60 mm, respectively, and two interior GFRP ribs made from the same profiles used on each panel side (U60$\times$55$\times$5). The panel weighted around 70 kg.

FSP_L2.4_W1.2_t70   FSP_L3.0_W1.0_t70

Sec. A-A   Sec. B-B

Sec. C-C   Sec. D-D

Detail 1
Scale: 1/10

Detail 2
Scale: 1/10
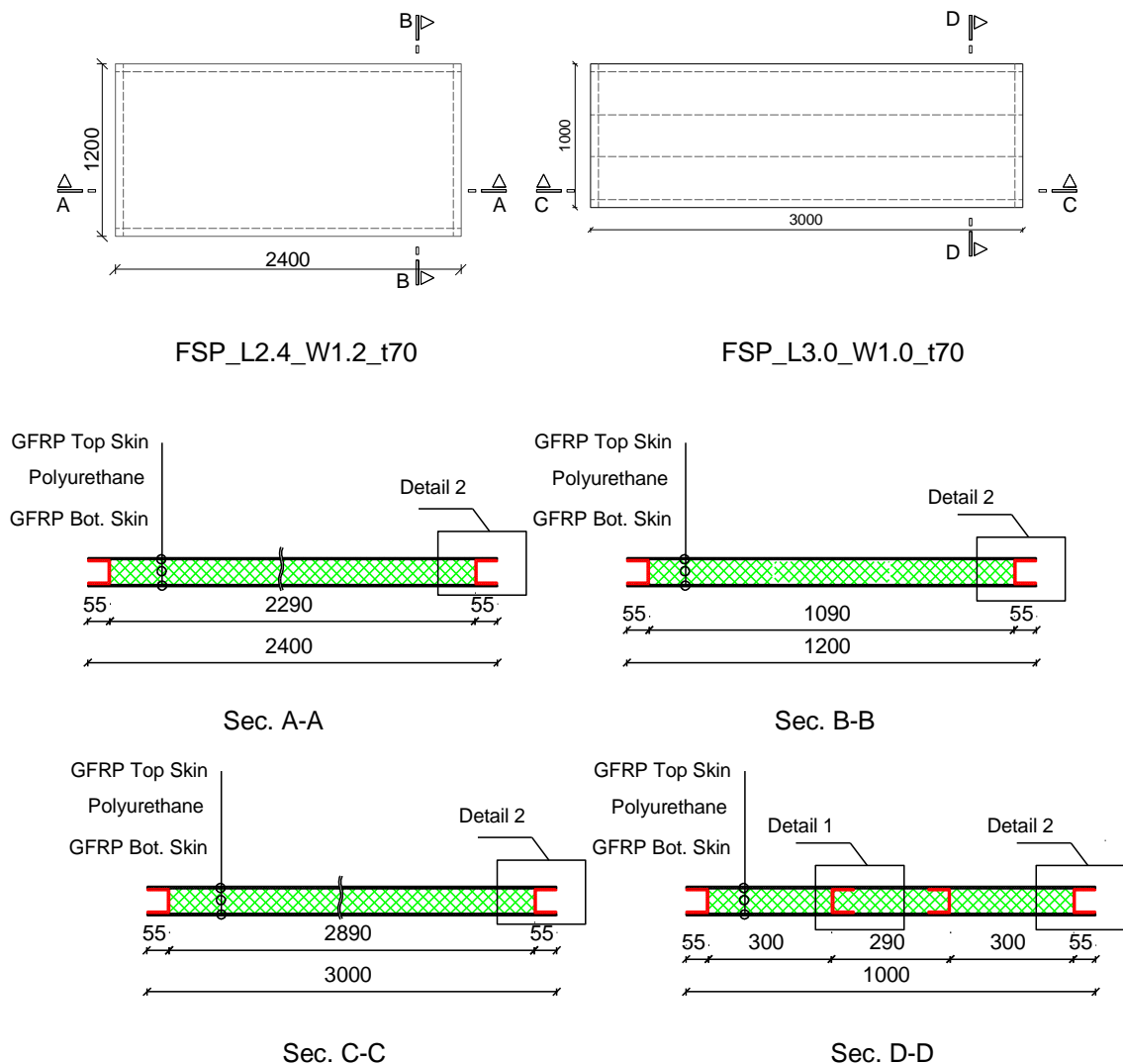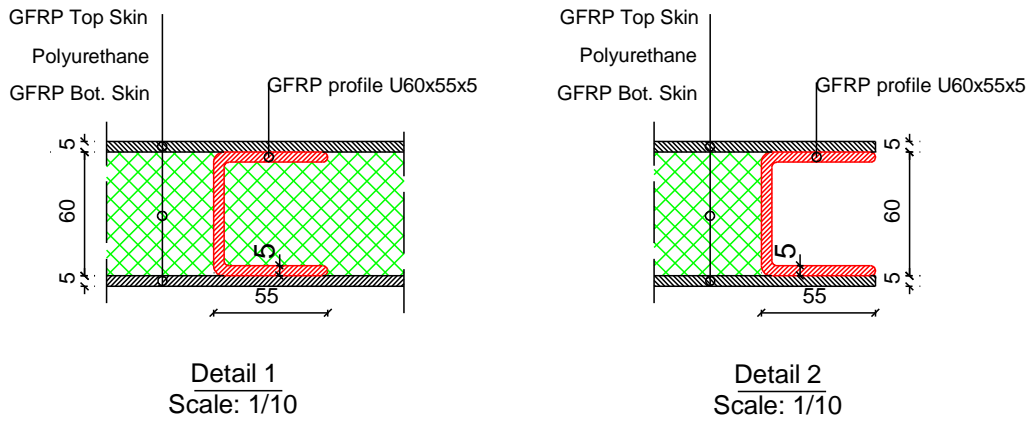
Fig. 3.4. Geometry of proposed floor slab sandwich panels (all units in millimeters).

3.3.2.2 Roof Sandwich Panels

Fig. 3.5 depicts the geometry of the sandwich panels used for the roof slabs. As can be seen, panels are 3.0 m long, 1.0 m wide, and 0.19 m thick, with GFRP skins of 5 mm thickness, and a PU foam core of 180 mm. To allow the connection of panels with other panels, three U-shape GFRP pultruded profiles of dimensions $60\times55\times5$ mm^3 (profile U60$\times$55$\times$5) were placed and adhesively bonded to each of the longitudinal outer faces of the sandwich panel. The roof panel weighted around 100 kg. The thermal requirements stated at the design objectives yielded to this thickness value of the PU foam core.
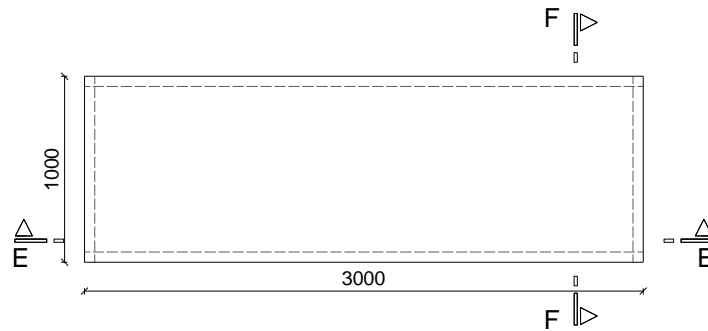
RSP_L3.0_W1.0_t70
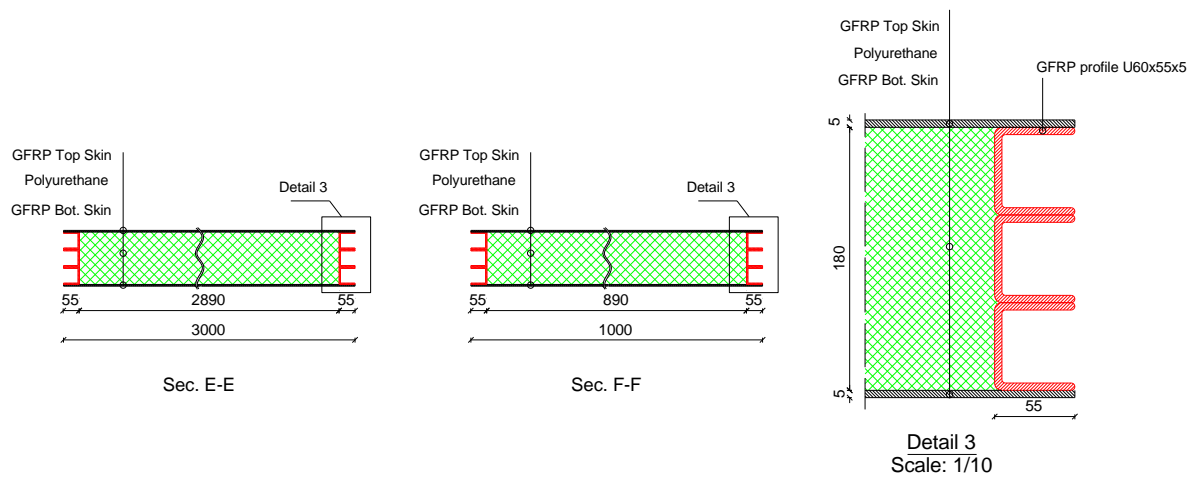
Fig. 3.5. Geometry of the roof sandwich panels (all units in millimeters)

3.3.2.3 Wall Sandwich Panels

The geometry for the sandwich wall panels is depicted in **Fig. 3.6**. Proposed composite sandwich panels for the wall elements have a dimension of 2.88 m of height, 0.96 m of width and 0.64 m of thickness, with GFRP skins of 2 mm thickness, and a PU foam core of 60 mm.

WSP_L2.8_W0.96_t64
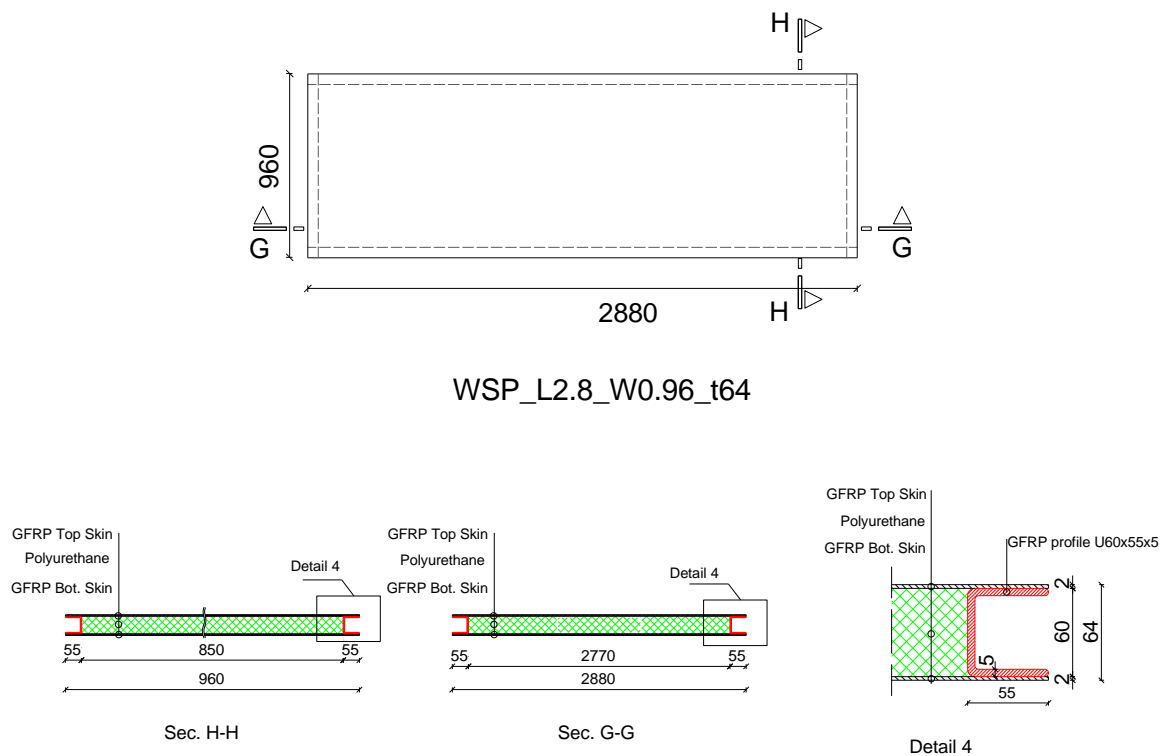
Fig. 3.6. Geometry of the wall sandwich panels (all units in millimeters)

GFRP U-shape profiles, with dimensions of $60\times55\times5$ mm^3, were adhesively bonded to sandwich panel around the edges during the manufacturing process in order to facilitate the

connections of walls to the GFRP beams and GFRP columns. Each panel weighed approximately 42 kg, making them easy to transport and install on-site.

3.3.3 Connections

This study also involved the development of a connection system for joining adjacent ClickHouse' components. Connections were designed with the objective of maximizing the advantage of the inherent elements strength, keeping the integrity of the floor module, and enabling an easy, fast assembly / disassembly of the prototype.

Three types of the connections were developed in the study (see **Fig. 3.7**): (i) beam-column, (ii) beam/column-panel and (iii) panel-panel.

Beam-column connections were formed by tightening GFRP beams to GFRP columns with a series of M8 bolts, and using short steel tubular profiles, (steel class of S235) with a cross section of $120\times120\times3$ mm^3, to ensure a satisfactory transfer of loads between both components (see **Fig. 3.7**a). For beam/column to panel connections, the before mentioned U-shape GFRP profiles were adhered to the edges of the sandwich panels. Next, a 50 mm square tubular GFRP profile with a 5 mm thickness was bonded to the GFRP beam. These two elements were then mechanically and adhesively bonded to form a singular unit as seen in **Fig. 3.7**b and **Fig. 3.7**c. Finally, for the panel to panel connection, a similar approach as the beam to panel connection was used, the U-shape profile was fit into two square tubular profiles (also of 50 mm edge and 5 mm of thickness) attached to a GFRP beam and mechanically and adhesively connected together (**Fig. 3.7**d).

(a)   (b)

(c)   (d)
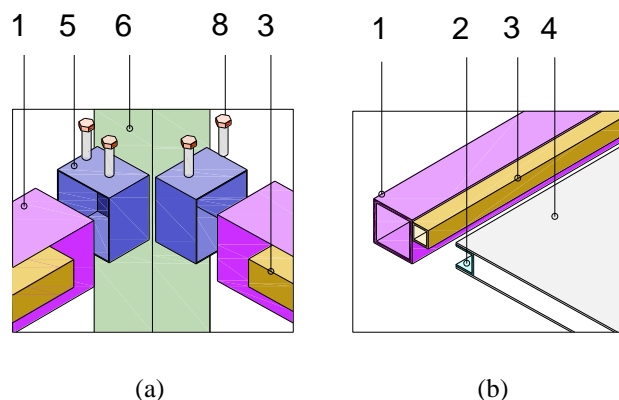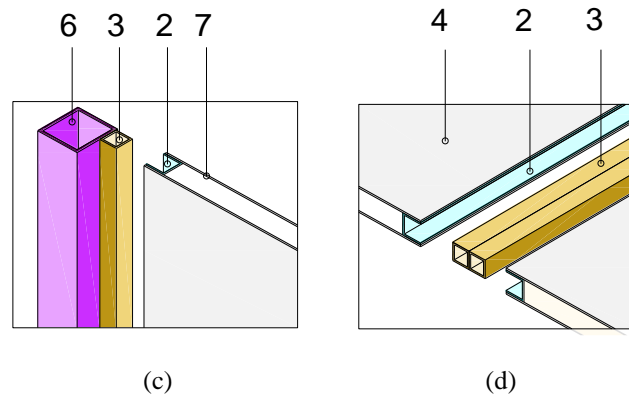
Legend: (1) GFRP beam; (2) GFRP U-shape profile; (3) GFRP square profile; (4) floor sandwich panel; (5) steel profile; (6) GFRP column; (7) sandwich wall panel; (8) M8 bolts

Fig. 3.7. Schematic Presentation of the Connections: (a) Beam-column, (b) Beam-panel; (c) Column-panel; (d) Panel-panel.

3.4   The Manufacturing Process

Pultrusion is a continuous manufacturing process by which a material is coated in resin and then carefully pulled through a heated die to produce consistent pultruded profiles.

The production process of the pultruded profiles using ALTO's technology is illustrated in **Fig. 3.8**. Rolls of GFRP fibres (1 and 2) were employed to keep the strength across the profiles. The pultrusion process begins when fibres are fed from spools into the tension roller. Fibbers are then guided and saturated in resin (4). Thereafter, the saturated GFRP fibres (1 and 2) are then coated with a glass fibre (3) and pulled through a metal preform shape that became the profile. The function of the coating layer was not to add extra strength to the profile but to add colour and enhance the product's appearances as well as protect the final product from corrosion and impact.

Finally, the product entered a hot steel frame to create the final shape of the material. The final cured profile (5) was cut in the appropriate length according to the specifications required.
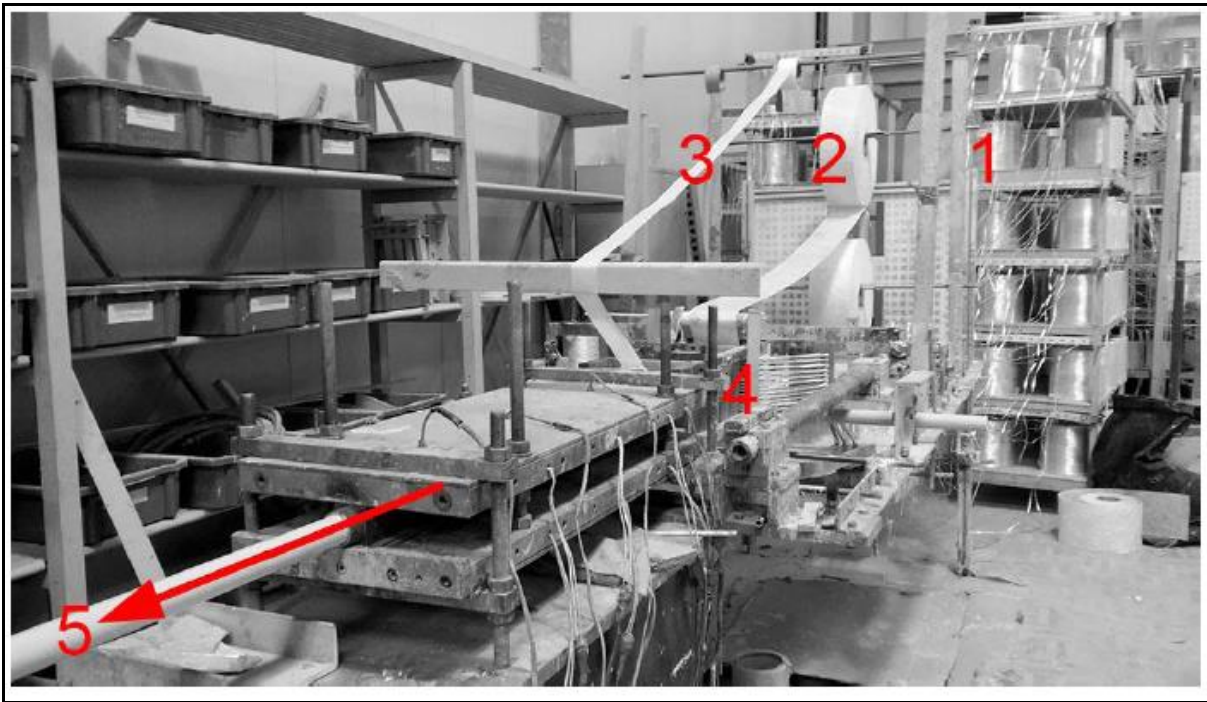
Fig. 3.8. Manufacturing process of pultruded profiles [59].

For the case of the sandwich panels, as an example, a description about the manufacturing of the panel FSP-L3.0_W1.0_t70 was provided to explain the different stages involved.

Manufacturing began with the creation of a structure composed of U60×55×5 GFRP profiles (**Fig. 3.9**a). These profiles were placed at each side of the panels, and were also used as ribs in panel FSP-L3.0_W1.0_t70_ribs. The second step consisted of the producing the GFRP skins using hand-layup technique with dry fibres saturated with an isophthalic polyester resin (**Fig. 3.9**b). In essence, this technique consisted of positioning a glass mat fabric in an open mold, pouring resin, placing a new glass mat fabric layer and continuing the process until finished. Before putting a new layer, entrapped air was removed manually with squeegees or rollers. Curing was initiated by a catalyst in the resin system, which hardens the fibre reinforced resin composite without external heat. Multiple plies of GFRP fabrics were used, employing two different types of mats, chopped strand mat (CSM) and bidirectional woven fabric mats (WFM). Skins had faces of five symmetric layers of epoxy saturated isotropic glass fibre, with total fibre volume ranging from 30% to 40%. Composition of each skin followed the sequence:

- Layer 1: CSM-300 gr/m^2
- Layer 2: CSM-450 gr/m^2
- Layer 3: CSM-450 gr/m^2 + WFM 500 gr/m^2

- Layer 4: CSM-450 gr/m^2
- Layer 5: CSM-300 gr/m^2

Once skins were produced, sandwich panels were mounted (**Fig. 3.9**c and **Fig. 3.9**d). The first skin was placed under the GFRP (both side profiles and ribs) and PU blocks. Then, the upper skin was installed. To glue the skins to the GFRP profiles and the PU blocks, a polyurethane resin was used.
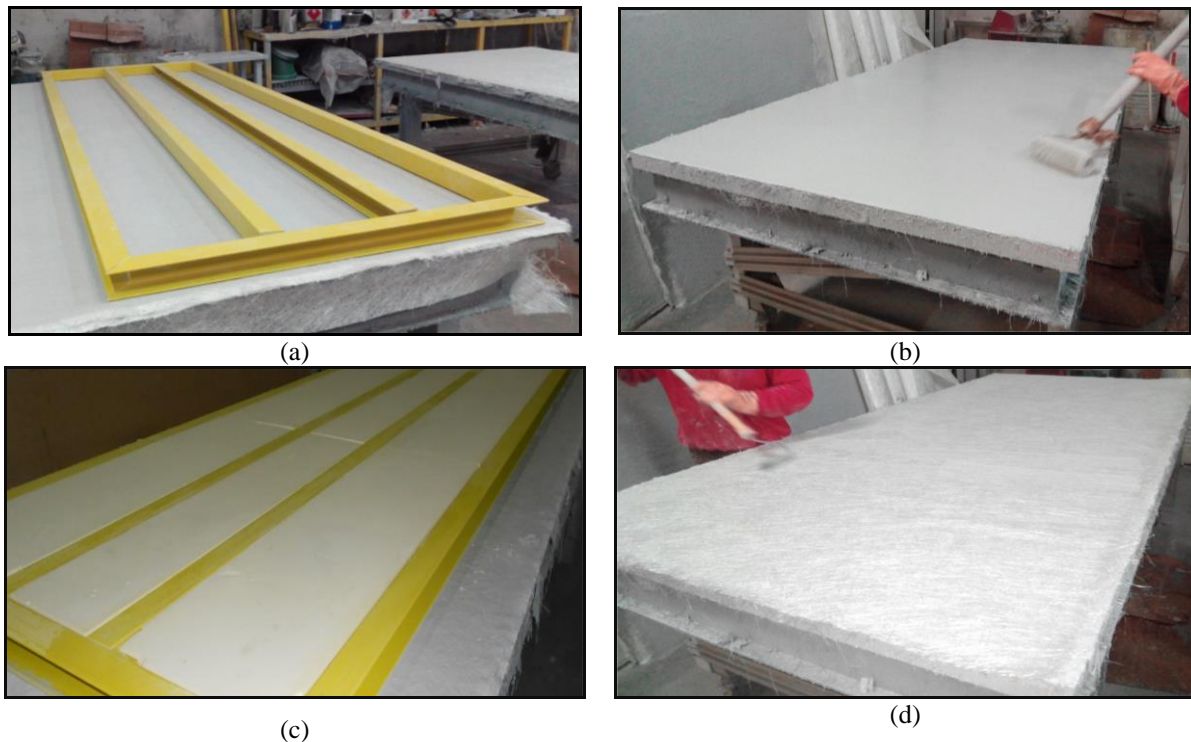
Fig. 3.9. Manufacturing process of the sandwich panels: (a) U60×55×5 GFRP profiles; (b) production of the GFRP skins; (c) placing the GFRP profiles and the foam to the first skin; (d) mounting the second skin.

3.5 Conclusions

In this chapter, a description about the prefabricated emergency housing system developed in the scope of the ClickHouse R&D project for the purpose of relocating families after natural disasters was performed. Throughout the design process, the ability to quickly return affected communities to their lives was the driving factor. Additionally, indoor air-quality and thermal insulation were considered to be important factors in the design process.

Lightweight composite sandwich panels and pultruted profiles were integrated into the ClickHouse prototype. This integration of parts allowed the prefabricated materials to be easily transported to the site and rapidly installed due to reduced weight of the structure. The frame structure (beams and column) consisted of GFRP pultruded profiles. On the other

hand, the floors, roofs, and walls elements consisted of composite sandwich panels utilizing a polyurethane foam core (PU) enclosed by two GFRP skins produced by hand-layup technique. The overall thickness of the floor, roof, and wall panels were considered to be 70 mm, 190 mm, and 64 mm, respectively.

Three kinds of the connections were designed namely: beam-column; panel-panel; beam/column-panel. In the connection design, complexity was avoided to allow assembly of the temporary building to continue without the need for special equipment and expert labourers. Additionally, the connections were designed to be capable of transferring the imposed loads to the different structural components.

Chapter 4: Material characterization

4.1 Introduction

The investigated composite sandwich panels in this research consists of two thin and relatively stiff GFRP skins connected by a polyurethane (PU) foam core with a low density of 48 kg/m^3, along with U-shape GFRP pultruded profiles with a cross section of 60$\times$55 mm^2 and a wall thickness of 5 mm (U60$\times$55$\times$5).

Given the unconventional nature of these materials, performing comprehensive material testing program to evaluate mechanical behaviour on composite sandwich panel's constituent seems to be essential. The main scope of this study was to obtain mechanical material properties of GFRP skins, U-shape GFRP profiles as well as the PU foam core under different loading conditions, namely tension, compression and shear. For these purposes ASTM standards were used to determine the material properties as well as statistical stated methods for analysing the results. It should be mention that all GFRP, PU foam core and pultruded U-shape coupons were extracted from the skins, foam core and pultruded U-shape GFRP profiles of the manufactured sandwich panels.

To assure composite action between composite sandwich panel's constituents, the bond stiffness and strength between skins and core material plays always critical rule, especially when the manufacturing is the hand-layup technique. The use of proper adhesive ensures load transfer between GFRP skins and the core and is a key in achieving the desired strength of the sandwich panel. This bond must have sufficient stiffness and strength to withstand the shear and tensile stresses introduced between them. Accordingly bond strength of the adhesive joint between GFRP skin and PU foam core was measured using pull-off test. Additionally, mechanical properties of the polyester resin (adhesive material used to glue GFRP skin to PU foam core) was assessed under direct tensile tests.

The mechanical fasted joints are gaining interest over adhesive bonded joints, because they present some advantage such as being able to be removed without destroying the connection components – a comprehensive explanation will be discussed in Chapter 5. Hence, some experimental tests were conducted to investigate the mechanical behaviour of bolted joints in

GFRP skins as well as GFRP pultruded profiles. For this aim a procedure was set up to measure bearing stiffness of GFRP laminates as well as GFRP pultruded profiles in single-bolt double lap joint.

4.2 GFRP skins and pultruded profiles

Both GFRP profiles and sandwich panel GFRP skins were characterized by performing tensile tests according to ASTM D3039 [62]. The rectangular-shape coupons were cut out from a panel using a diamond saw in two different directions, namely longitudinal (along the specimen) and transverse (perpendicular to the length of the specimen) directions.

Five coupons were prepared in both longitudinal and transverse directions with the width of 25 mm and length of 250 mm. Thickness of the specimens were measured with a calliper in various positions and average value was determined. Four aluminium tabs with a geometry of $25 \times 50 \times 2$ mm^3 were glued at the end of the coupons. The tabs distribute gripping stresses and prevent premature specimen failure caused by grip jaws. A minimum of 24 hours curing time was allowed for the bonding agent of the tabs to fully cure before testing the samples. Schematic representation of tension test specimen is shown in **Fig. 4.1**

(a)   (b)
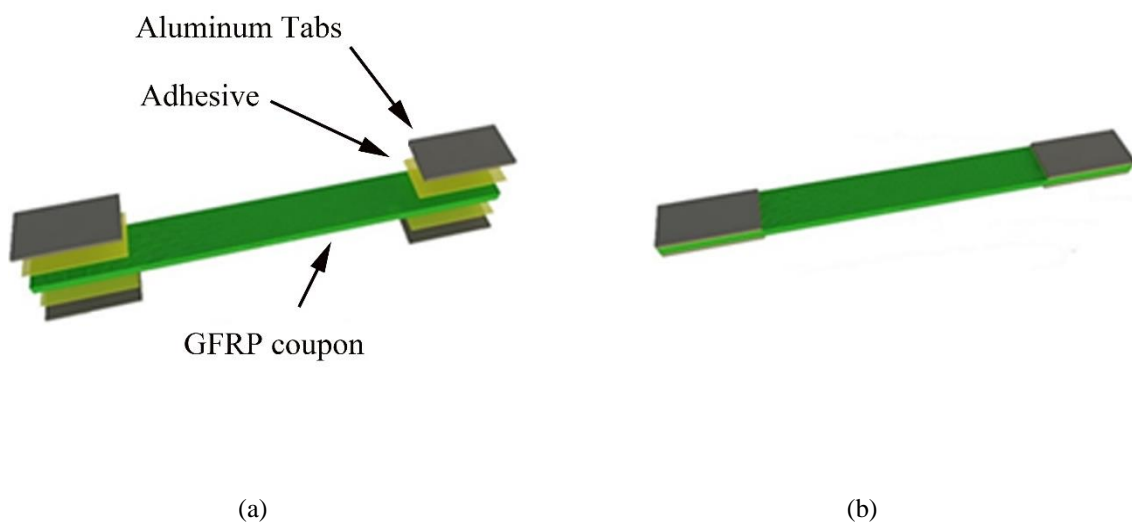
Fig. 4.1. Tension specimens: (a) Preparing coupon for tension test; (b) Tension coupon ready to be tested.

Specimens were mounted in the universal testing machine comprising a fixed and movable member as well as grips for holding the coupons with a grip distance of 150 mm, and monotonically loaded with a head displacement rate of 2 mm/min up to failure. **Fig. 4.2** shows a specimen been tested.

The typical stress-strain curves obtained from the tensile tests are presented in **Fig. 4.3**. The strains given in these curves are engineering strains, this means they are calculated as the extension given by the testing machine divided by the original length of the specimens between the grips. The tensile stress is computed by dividing the applied load by the average original cross-sectional area in the gauge length region.

Fig. 4.2. GFRP tension test.

The tests carried out on GFRP profiles coupons show a linear-elastic behaviour until failure. The typical failure of a specimen started by the quiet sound of crunching followed by a big crack corresponding to the breaking of the surfacing veil and finally the peak load was reached when the glass fibres had lost their strength.

(a)   (b)
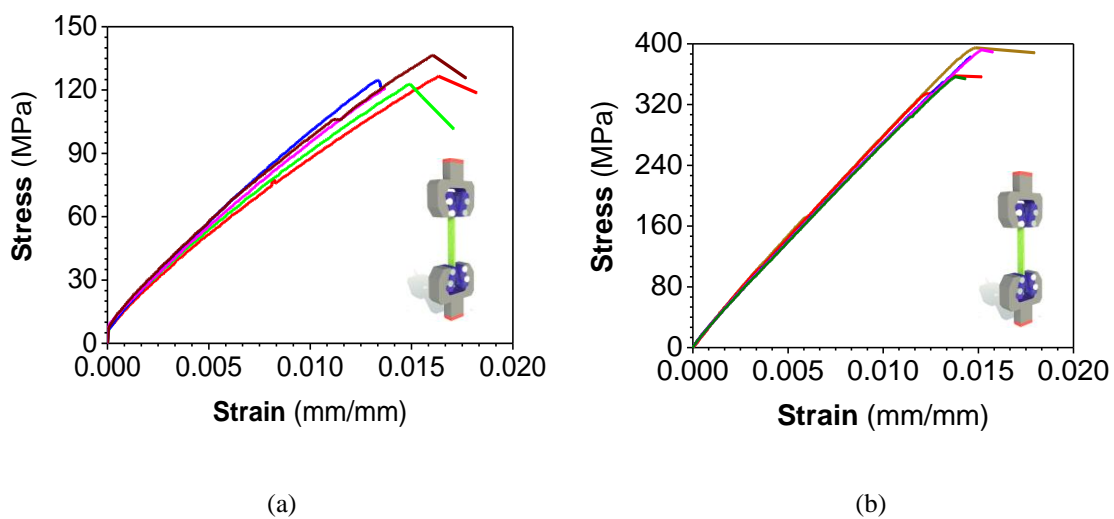
Fig. 4.3. Tensile stress-strain response in the longitudinal direction: (a) GFRP skin; (b) GFRP pultruded profile.

Table 4.1 summarizes the results of the material characterization tests conducted on the different components of the floor prototype, listing the values obtained for maximum stresses (σ), strains (ε), elastic modulus (E) and shear modulus (G).

<div align="center">**Table 4.1.** Mechanical properties of GFRP skin and profiles.</div>

	$\sigma_{max,L}$		$\sigma_{max,T}$		E_L		E_T	
	Mean (MPa)	CoV (%)	Mean (MPa)	CoV (%)	Mean (GPa)	CoV (%)	Mean (GPa)	CoV (%)
GFRP profiles	327.1	8.6	230.1	7.6	32.0	6.8	16.1	8.9
GFRP skin	117.0	10.4	116.9	24.7	9.6	7.4	10.3	8.0

L: longitudinal direction, *T*: transverse direction, CoV: coefficient of variation

4.3 Polyurethane foam core

4.3.1 Tension tests

In order to determine the tensile properties of PU foam core, five coupons were prepared and tested according to ASTM C297/C 297 M-04 [63]. The prism-shape coupons were cut with a cross section of 70×70 mm^2 and thickness of 60 mm. Since this material has low stiffness, in order to assist gripping in the testing machine, the specimens were bonded using adhesive to the T-shape steel profiles. The tests were performed using universal testing machine at a displacement rate of 0.50 mm/min (see **Fig. 4.4**).
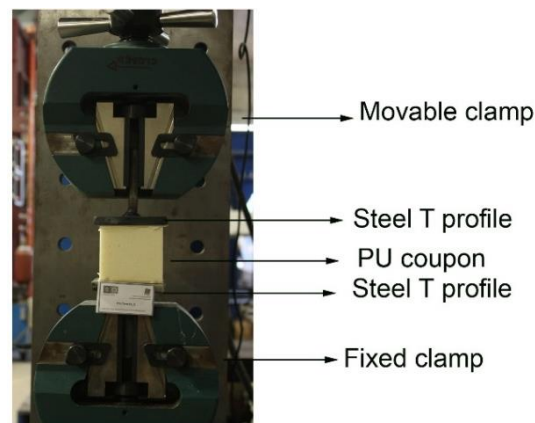
<div align="center">**Fig. 4.4.** PU foam tensile test setup.</div>

The stress-strain curves obtained from the experimental tests, is presented in **Fig. 4.5**a. As can be seen, almost linear behaviour was observed until failure occurred by a rupture close to the T-steel section profile (**Fig. 4.5**b). The results are tabulated in **Table 4.2**.

(a)   (b)
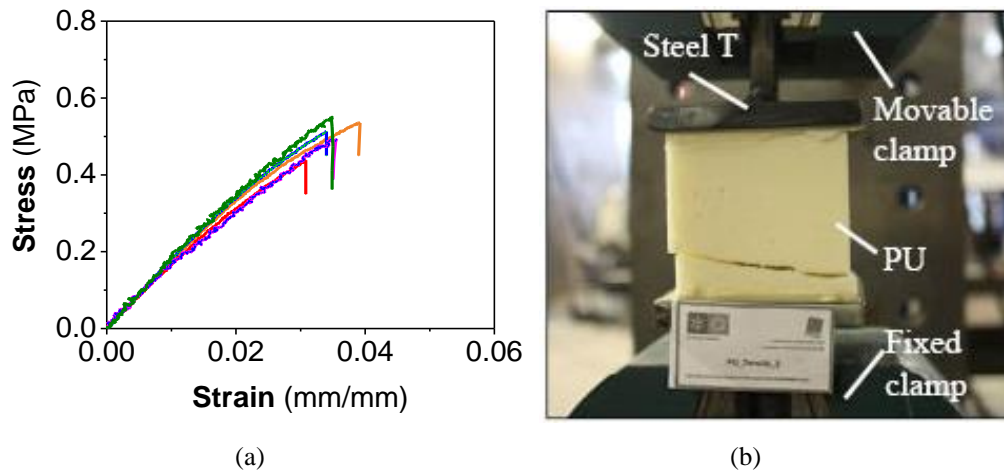
Fig. 4.5. PU foam core tensile test result: (a) stress-strain relation; (b) failure mode.

4.3.2 Compression tests

Mechanical properties of PU foam core subjected to compressive loading was evaluated according to ASTM C365-03 [64] a cross-section of 70×70 mm^2 and thickness of 60 mm. A universal testing was used to test the five prism-shape coupons at the displacement rate of 0.5 mm/min (see **Fig. 4.6**a).

PU foam under compression showed the typical nonlinearity exhibited in this kind of materials (see **Fig. 4.6**b), with a linear elastic branch followed by a plastic plateau with nearly constant stress, and a strain-hardening part at large strains, with large compressive deformation [42, 65].

(a)   (b)
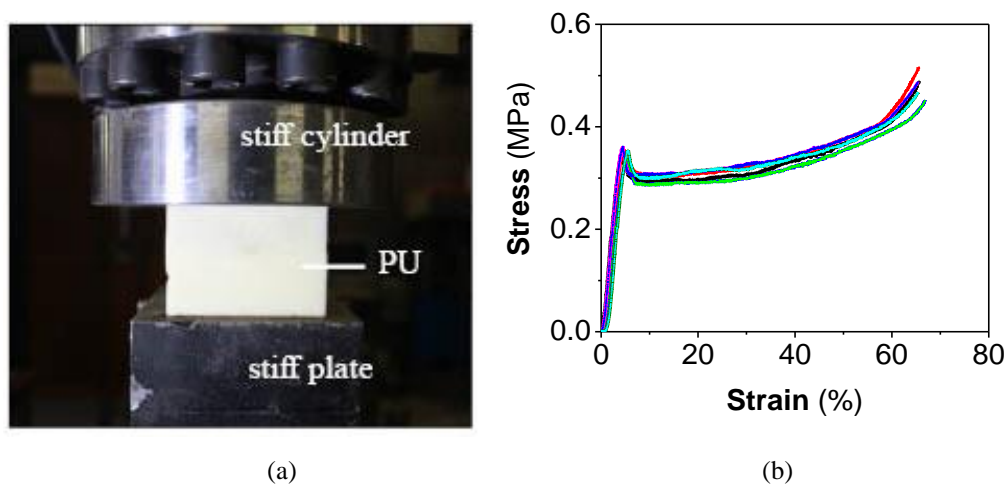
Fig. 4.6. PU foam core compression test: (a) test setup; (b) stress-strain relation.

4.3.3   Shear tests

For the testing the PU under shear loading, five cubic specimens with a dimension of $120 \times 120 \times 120$ mm^3 were prepared. The specimens were bonded to four metallic plates and mounted in the universal testing machine where a tension load was applied along one side of the setup (see **Fig. 4.7**). The applied load was transferred into the plates that were encasing the specimen, by introducing a governing shear stress field in the specimens. Comprehensive information about this test setup can be found elsewhere [66].
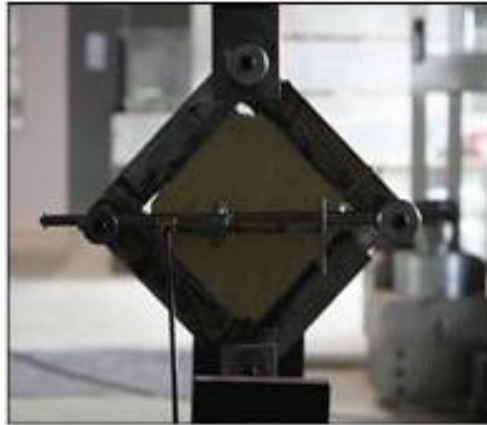
Fig. 4.7. PU foam core shear test setup.

The shear-strain curves obtained from shear test is represented in the **Fig. 4.8**a and the summary of the results are tabulated in **Table 4.2**. Shear behaviour was almost linear-elastic until failure, which occurred in a brittle manner and with the formation of failure surfaces at an angle of nearly 45°.The failure occurred in a brittle manner and with the the formation of failure surfaces along the horizontal diagonal at an angle of nearly 45°off-axis direction relative to the specimens' edges (see **Fig. 4.8**b).
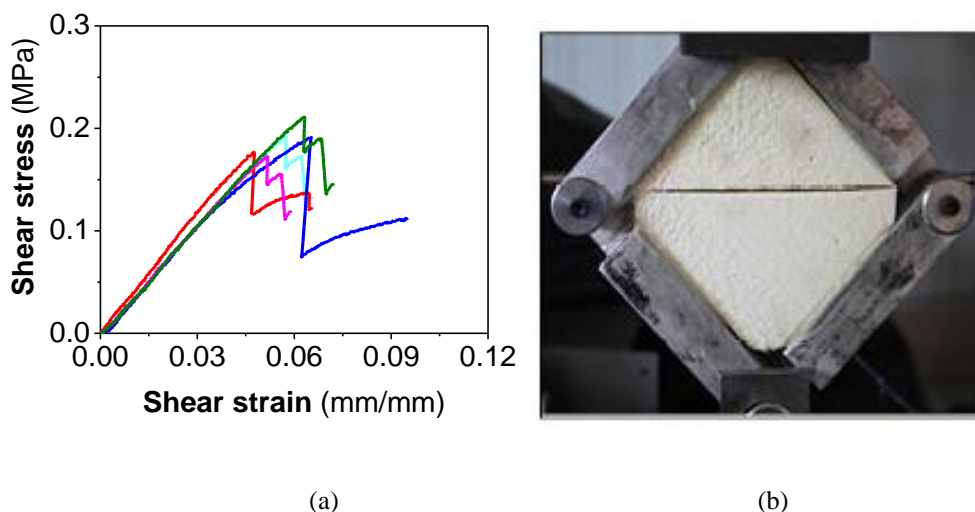
(a)   (b)
Fig. 4.8. PU foam core shear test result: (a) stress-strain relation; (b) failure mode.

Table 4.2. Mechanical properties of PU foam core.

Foam	σ_{max}		E		G	
	Mean (MPa)	CoV (%)	Mean (MPa)	CoV (%)	Mean (MPa)	CoV (%)
Compression test	0.30	10.0	6.3	9.0	---	---
Tensile test	0.49	8.9	---	---	---	---
Shear test	0.15	10.2	---	---	3.15	12.1

CoV: coefficient of variation

4.4 Polyester resin

Mechanical properties of the polyester resin (adhesive material used to glue GFRP skin to PU foam core) was assessed under direct tensile tests, according to ASTM D638 [67].

The polyester resin coupons were casted in a teflon mould in which the mixed epoxy was filled in. The coupons had a length of 170 mm, 4 mm thickness, 10 mm width at the middle and 20 mm width in a dogbone shape. The geometry of the coupons was measured using a digital calliper for accurately estimate the normal stress. Direct tensile tests were performed using the universal testing machine at the displacement rate of 1 mm/min. A load cell with the maximum capacity of 20 kN was used to measure the applied load. A strain gauge was glued at the middle height of each coupon for measuring the axial strain (see **Fig. 4.9**a).

The polyester resin subjected to the direct tensile test exhibited an ultimate tensile strength, ultimate tensile strain and Young's modulus of 40.40 MPa (CoV = 7.87%), 0.0258 m/m (CoV = 3.07%) and 1568 MPa (CoV=9.3%), respectively. All of the coupons failed nearly at the middle of them with the failure surface perpendicular to the length of the specimens (see **Fig. 4.9**b).
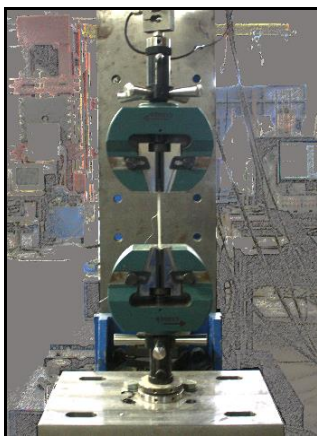
(a)   (b)

Fig. 4.9. Test setup for direct tensile of polyester resin: (a) test setup; (b) failure modes.

4.5 Bond strength of the joint skin/core

Tensile bond strength of the adhesive joint between GFRP skin and PU foam core was measured by pull-off tests based on ASTM 1583-04 [68].

Five cores were drilled on GFRP skins with a diameter of 50 mm and a core depth of around 10 mm (**Fig. 4.10**a). Aluminium disks with a diameter of 50 mm were adhesively glued to the GFRP skin (**Fig. 4.10**b). The prepared specimens after curing, were mounted in the universal testing machine and tensile force was applied to the disks with a head displacement rate of 0.2 mm/min (see **Fig. 4.10**).
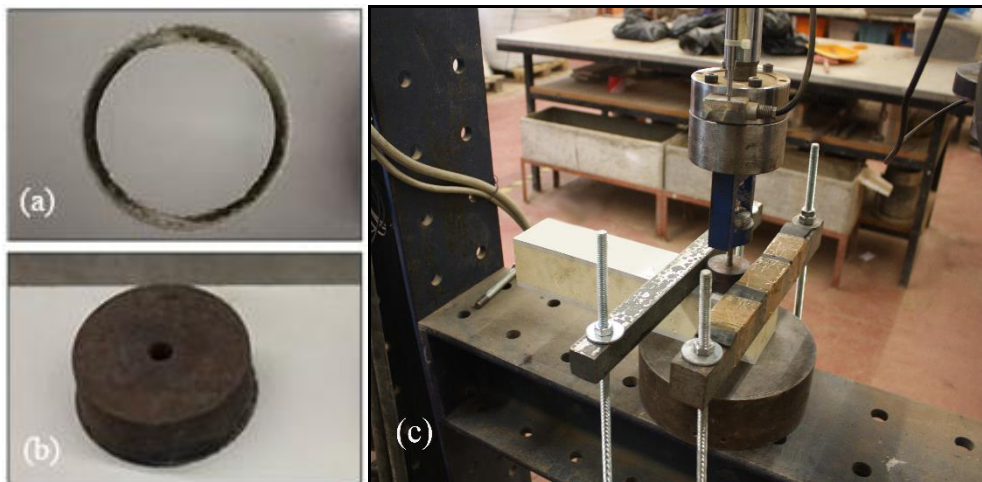
Fig. 4.10. Bond strength assessment of the joint skin/core: (a) a cutting off in sandwich panel; (b) bonded the aluminum disk; (c) pull-off test.

In the pull-off tests, an ultimate tensile strength of 0.50 MPa (CoV = 18.7%) was obtained. The failure occurred in the PU foam core. No failure was detected in the interface between GFRP and the PU foam core. In **Fig. 4.11**a and **Fig. 4.11**b, the failure of sandwich panel foam core and aluminum disk are presented respectively. Comparing the ultimate tensile strength obtained for epoxy (40.40 MPa) with the tensile strength value registered in the pull-off test (0.50 MPa), it is confirmed that the polyester resin had the capability of creating sufficient bond between GFRP skin and PU foam core. On the other hand, the values of ultimate tensile strength of PU foam core and tensile strength obtained by pull-off test were close, so the PU tensile failure occurred due to excessive out-of-plane tensile stress [69].

4.6 Bearing strength of GFRP skin and pultruded profiles

The bearing strength of GFRP skin and pultruded profiles was assessed in the scope of the present work. In the case of GFRP skin, a diamond saw was used to obtain rectangular shape coupons of length 220 mm and width 70 mm, with a thickness of 5 mm. Five coupons were

prepared and a 5-mm-radius hole was drilled in each piece 20 mm far from one of the edges. Two square aluminum tabs with dimensions of $70\times70\times3$ mm^3 were bonded at the opposite end of coupons using epoxy. **Fig. 4.12**a schematically shows the prepared specimens.

(a)   (b)

Fig. 4.11. Pull-off test failure: (a) failure in the PU foam core of sandwich panel; (b) aluminum disk.

In the case of U-shape and square-shape GFRP pultruded profiles, 10 coupons per profile had prepared. It is worth reminding that, U-shape profiles had a length of 100 mm and a cross section of $60\times55\times5$ mm^3 while squared-profiles had a length of 100 mm and cross section of $50\times50\times5$ mm^3. Thereafter 5-mm-radius hole was drilled in each coupon at the middle length of the flange, 20 mm far from the edge. **Fig. 4.12**b depicts schematics of the prepared specimens for evaluating bearing strength.

(a)   (b)
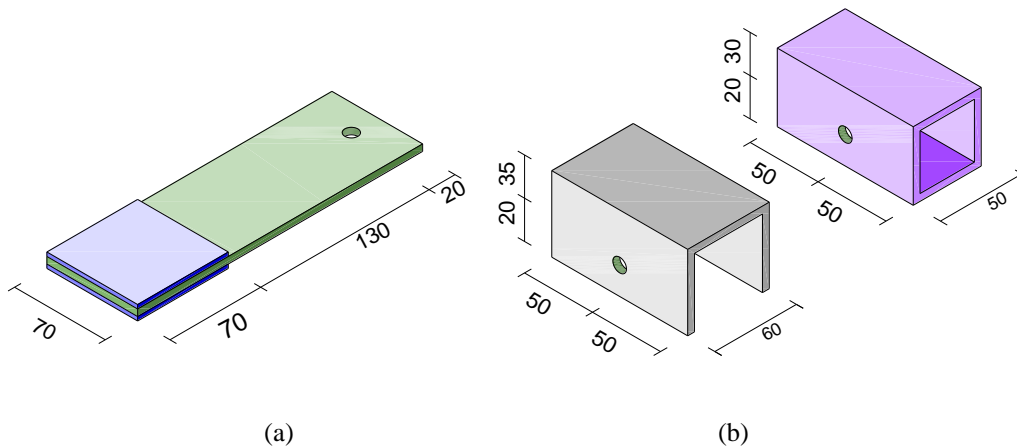
Fig. 4.12. Specimens prepared for evaluating bearing strength: (a) GFRP coupon; (b) pultruded profiles.

Experimental procedures were performed according to ASTM D 953-95 [70]. The GFRP skin coupons were placed in the universal testing machine, taking care to align the longitudinal axis of the specimen. The load was applied through stiff steel pins and lugs (**Fig. 4.13**a). Two steel plates clamped the side without the hole with aluminium tabs. A M10 bolt was inserted in the opposite side, in the 5-mm-radius hole and connected to the fixed part of the test setup

thought two stiff plates and a pin. Two LVDTs with a stroke up to 10 mm were installed vertically along the length of the coupons in order to measure the movement of both sides. An incrementally monotonic load was applied by a hydraulic jack with a maximum capacity of 50 kN until failure.

For U-shape and square-shape profiles testing, the same perception as in the case of GFRP laminate was used. In this case, five coupons were selected and placed in the universal testing machine. Five coupons of each one were tested individually. The rest were tested working together (i.e. attaching a U-shape to a square-shape profile). A T-shape stiff steel profile was placed inside the coupons and gripped to a movable clamp (**Fig. 4.13**b). A M10 bolt was inserted in the 5-mm-radius hole and connected to the fixed part of the test setup thought two stiff plates and a steel pin, in a similar way as in the case of GFP skin coupons. Two LVDTs with a stroke up to 10 mm were installed vertically in order to measure the movement of the pin in both sides.

(a)   (b)
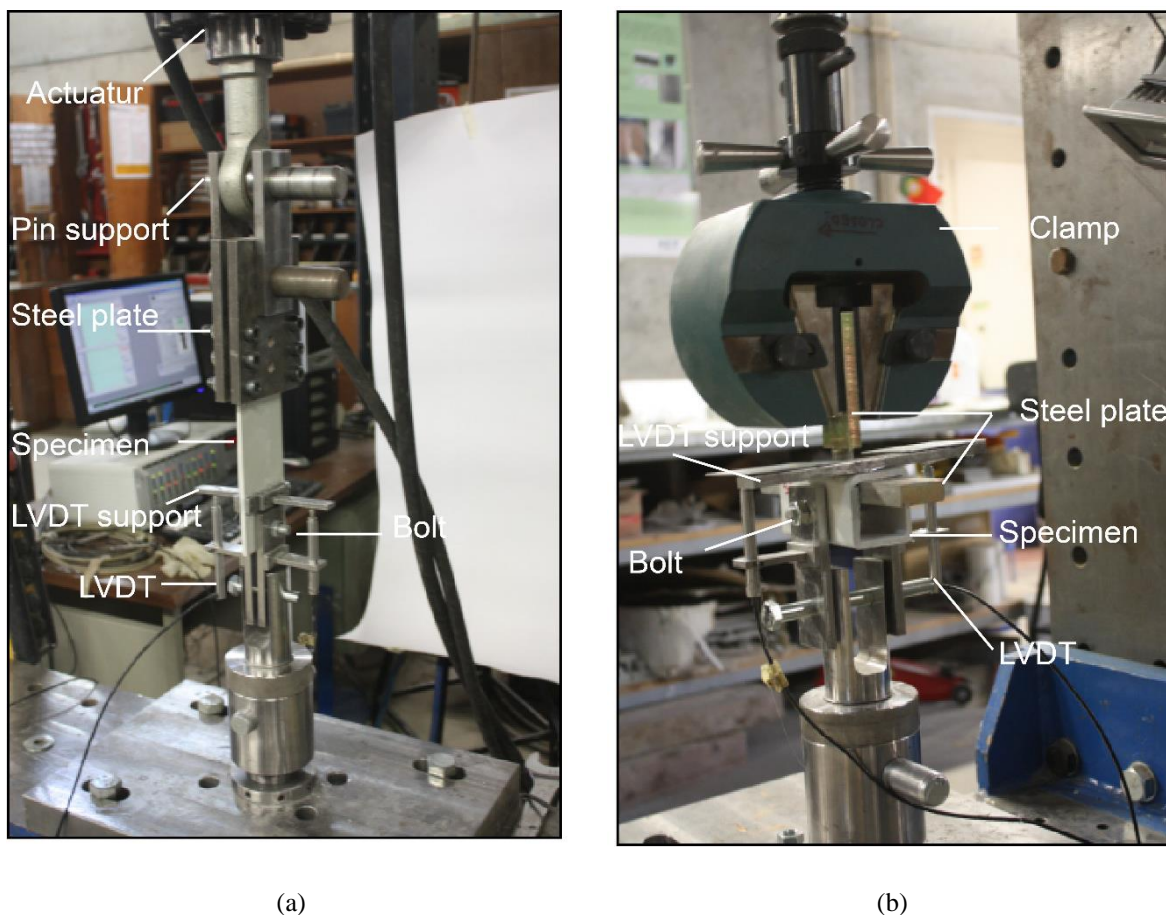
Fig. 4.13. Bearing tests: (a) GFRP laminate; (b) square-shape profile; (c) U-shape and square-shape profiles.

Fig. 4.14 shows the load-pin displacement recorded for all tested coupons. The relation between load and pin displacement in all tested coupons was sensibly linear up to the

maximum force. At that point, a sudden drop was observed. This drop indicated of substantial failure phenomena occurring in the coupons.
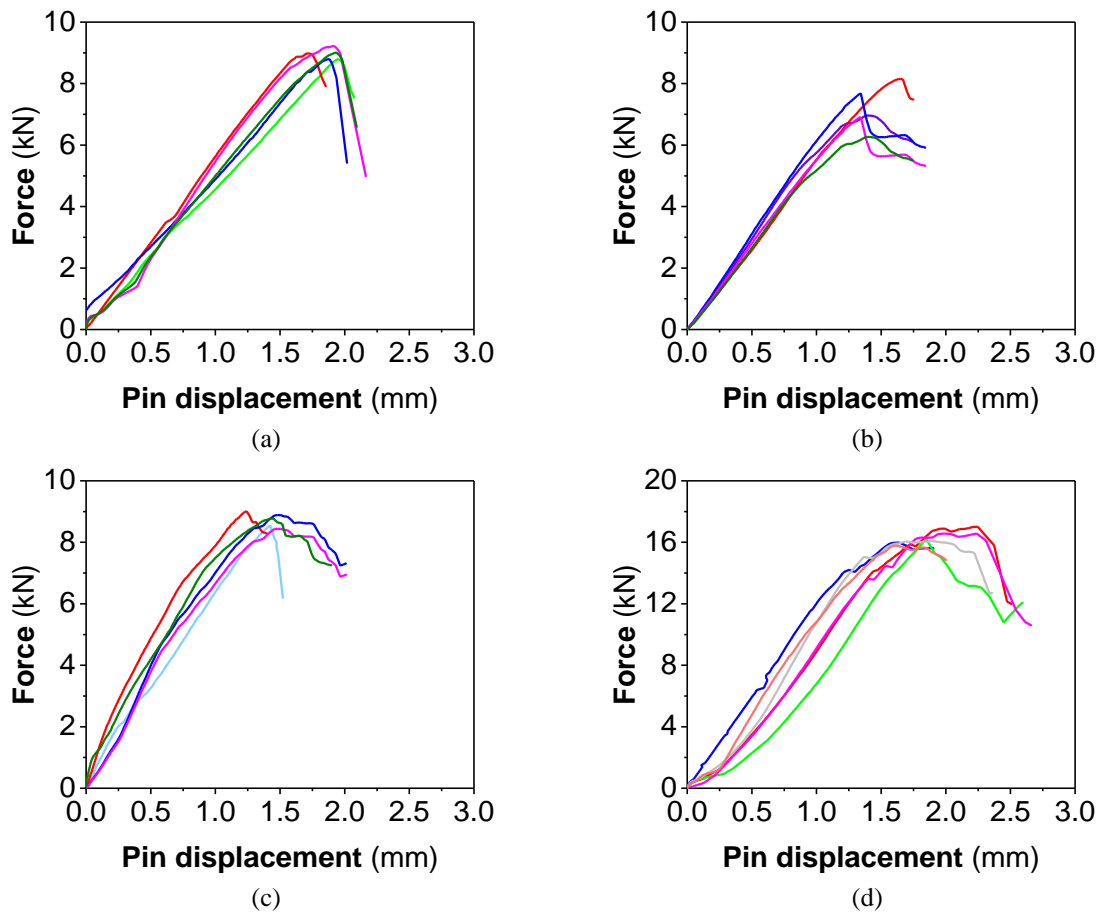
Fig. 4.14. Load-pin displacement curves: (a) GFRP laminate; (b) U-shape profile; (c) square-shape profile; (d) U-shape and squared profiles.

Inspection of **Fig. 4.14** showed that the maximum applied load and pin-displacement in the case of GFRP laminate, U-shape profile and square-shape profile were nearly 8kN and 1.5 mm respectively. However, the maximum applied load and pin-displacement increased to be equal to 16 kN and 2 mm respectively when both U-shape and square-profile worked together. The pin-bearing strength, σ_b, for the all coupons was calculated as the ratio of the maximum load to the hole diameter times the specimen thickness. That resulted to obtain this value for the GFRP laminate as 100 MPa and 50 MPa for the GFRP profiles.

In the experimental study, the progression of the failure was observed visually. Cleavage and net-tension failure modes were the dominate failure modes in the GFRP coupons and pultruded profiles respectively (see **Fig. 4.15**). It is noteworthy reminding that, cleavage failure mode is a mixed net-tension and shear-out failure modes. Net-tension failure is characterized by a sudden transversally crack propagation to the direction of the connecting force, due to a relatively small area of the plate-section. Shear net is caused by shear stresses

and happened along shear-out planes on the hole boundary in the principal bolt load direction [71].
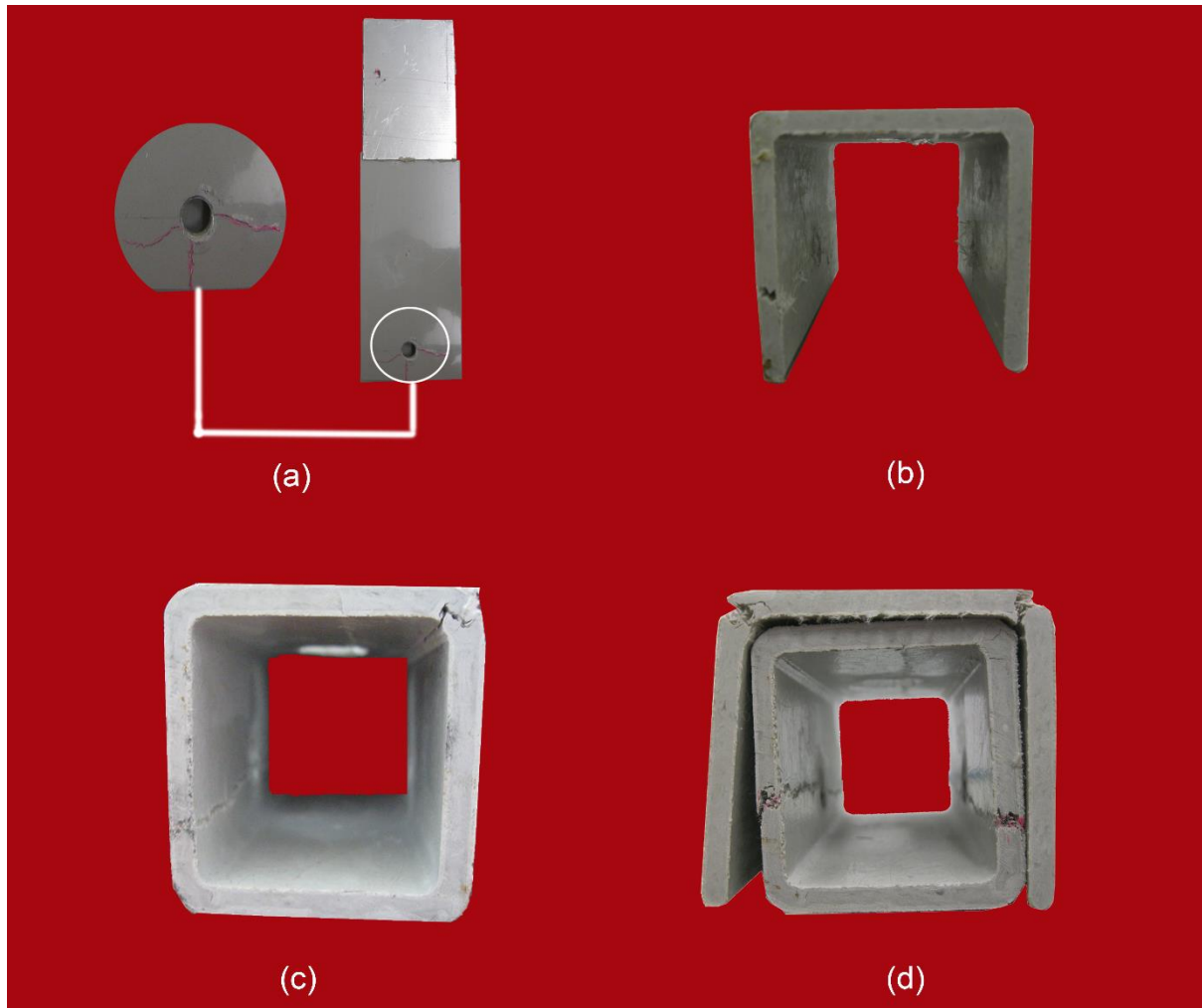
Fig. 4.15. Failure modes: (a) GFRP laminate; (b) U-shape profile; (c) square-shape profile; (d) U-shape and squared profiles.

4.7   Conclusion

A comprehensive mechanical characterization of the sandwich panel constituents was carried out. The study included performing tensile tests of the GFRP skins and pultruded profiles in two different directions namely longitudinal (along the fibre) and transversal (perpendicular to the fibre). In addition to that, mechanical performance of the PU foam core was evaluated under tensile, compressive and shear tests. Since bond between GFRP skin and PU plays a critical action in transferring the load, the bond strength was evaluated using epoxy direct tensile test and pull-off test. Finally, bearing tests were carried out pertaining to the GFRP laminate as well as pultuded GFRP profiles for obtaining maximum bearing load and failure loads using the developed test setup. The following conclusion are drawn:

- Both GFRP laminate skins and pultruded profiles exhibited almost linear-elastic performance during tensile testing regarding to both longitudinal and transversal directions;

- The GFRP laminate skins presented nearly the same elastic modulus in both directions (9.6 GPa). In contrast, GFRP pultruded profiles showed two times of elastic modulus in longitudinal direction (32 GPa) higher than transversal direction (16 GPa);

- PU foam core in compression test exhibited three stages of loading: linear-elastic, plastic and strain hardening. The compressive elastic modulus was calculated from the linear part as 6.3 MPa. In the tensile and shear tests of the PU foam coupons, a linear-elastic behaviour until failure was noticed and consequently the elastic modulus and shear modulus were calculated to be 15 MPa and 3.5 MPa, respectively;

- An ultimate strength of 0.50 MPa was obtained in the pull-off tests of bond strength between GFRP skin and foam core. The failure occurred in the PU foam core. Comparing this value with the ultimate tensile strength of epoxy (40.40 MPa) it was confirmed that the utilized polyester resin had the capability of creating sufficient bond between GFRP skin and PU foam core.

- Regarding to the bearing tests, a bearing strength of 100 MPa was obtained for the GFRP laminate. However, this value decreased to 50% in the case of pultruded profiles. Cleavage and net-tension failure modes were reported as the dominate failure modes in the GFRP laminate and pultruded profiles respectively.

Chapter 5: Connection system for jointing sandwich panels

5.1   Introduction

One of the critical challenge in the application of using composite sandwich panels in the sector of civil engineering is the development of the panel-panel connection. Nowadays, there is a growing interest in finding cost-effective and durable technology for connecting composite sandwich panels.

In general, jointed composite sandwich panels shall be designed for quick assembling on-site and to achieve the objectives of safety, serviceability and constructability [72]. However, this aim is highly dependent on the connection detailing system. Proposed connection system needs to be designed and detailed to facilitate a quick and secure installation procedures [73].

Based on the levels of connection, the design requirements for jointed composite sandwich panels might be different. For this aim, two main levels are defined as component level and panel level. In the component level, preparing adequate integrity between jointed components for ensuring load transfer efficiency is the main objective. In the panel level, the major aspect is the capability of transferring the loads [72].

5.2   Problem statement and technical considerations

Different techniques for connecting FRP panels in modular housing system applications are documented in the literature. Some of these techniques are depicted in **Fig. 5.1**. For instance, 'Z'-shape adhesively connected techniques (**Fig. 5.1**a) have been employed for connecting sandwich panels in the rehabilitation of building floors [74] and in bridge decks [75]. The main drawback of this connection in modular systems is the need of adhesive for integrating the two components. Using adhesive requires time for curing and specific treatment, which increases the time of construction and requires suitable temperatures for the curing process. Additionally, it is fairly difficult to only replace one panel because all the panels are

adhesively jointed. In this case, it might be necessary to replace the entire jointed panel, which can be a relatively expensive process. Scarfed and stepped overlap joints (**Fig. 5.1**b) present the best performance among bonded joints [76]. However, this type of connection results in higher complexity in the production lines and, consequently, increases the price of the produced panels. Male-female connections (**Fig. 5.1**c) have been used in bridge applications [72, 77, 78]. In spite of providing integrity between panels and loading-transfer efficiency of the formed deck, these panels needs to be placed horizontally by employing specific instruments, such as hydraulic jacks, which is a time consuming and expensive process. The use of this technique in building applications seems to be a more demanding procedure due to spatial limitation [74]. Tongue and groove mechanisms (**Fig. 5.1**d) are used in bridge deck applications [73]. The transportation of these panels must be undertaken very carefully. If a small part is damaged, the entire panel needs to be replaced. In addition, the integration of this system in production lines appears to be a major challenge.
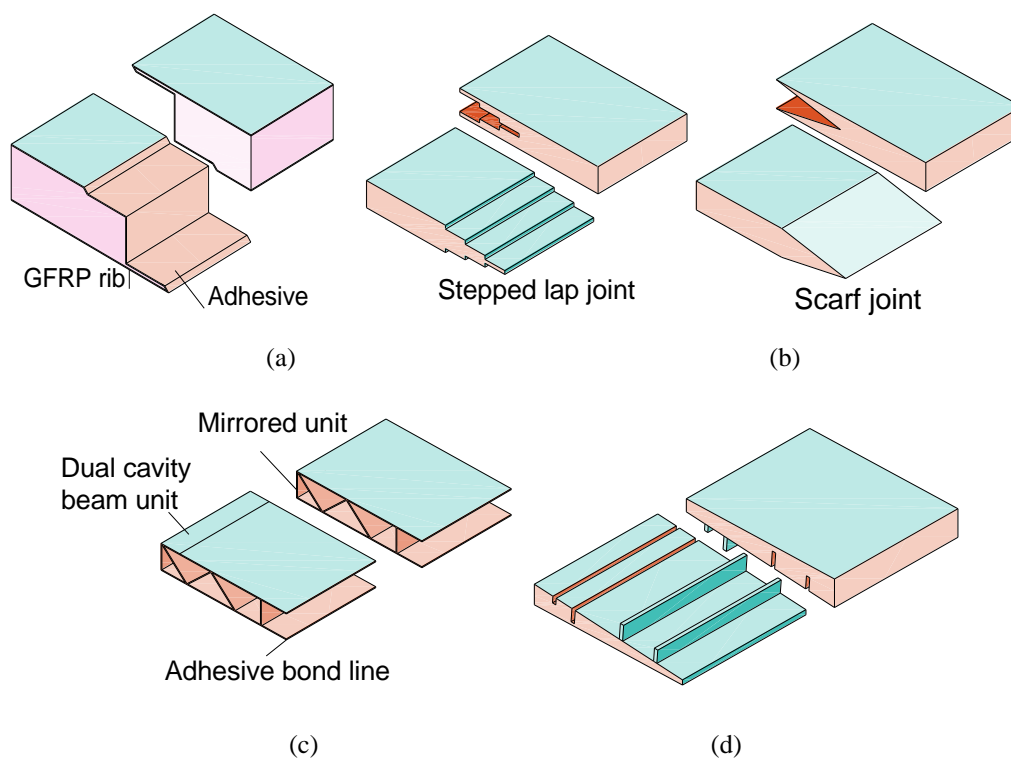
Fig. 5.1. Various types of the jointing sandwich panels techniques: (a) Z-shape; (b) stepped and scarf; (c) male-female; (d) tongue and groove.

For connecting sandwich panels, a fitting system was used to efficiently transfer bending moments and shear forces between jointed panels. Panel-panel connection was composed of two main parts (see **Fig. 5.2**): (i) end integrated "U" cross section pultruted profile ($60 \times 55 \times 5$ mm^3) and (ii) two tubular pultruted GFRP square profiles ($50 \times 50 \times 5$ mm^3). The former works as a connector by interlocking inside the U profiles during the assembling process. Two

approaches were used to connect floor sandwich panels, namely without mechanical fastening (Friction technique) and with mechanical fastening (Hybrid technique). Their mechanical behaviour was studied in this research.

The following objectives were targeted in this study: (i) analyse the connection ability to efficiently distribute stresses and strains between jointed panels; (ii) evaluate the contribution of the connection for the flexural stiffness and shear stiffness of the panels; (iii) analyse the flexural responses of the jointed panels; (iv) understand the failure mechanism of the proposed connections.

5.3 Flexural tests on jointed composite sandwich panels

5.3.1 Description of test specimens

A total of 28 specimens were tested as described in **Table 5.1**, which shows the test matrix. For the longitudinal direction, the specimens were prepared with the dimensions of 850 (length) $\times$ 200 (width) $\times$ 70 (thickness) mm^3. Subsequently, for transverse direction, specimens were prepared with the dimension of 200 (length) $\times$ 100 (width) $\times$ 70 (thickness) mm^3. Two different techniques for connecting the specimens were used. In the first one, a connector is placed inside the U-shape GFRP profile in the sandwich panel (**Fig. 5.2**). The friction introduced between connector and U-shape GFRP profile was used to accomplish the integrity of the structure during loading. In the second approach the floor panels are connected by using hybrid technique composed by connector that is placed into the U-shape GFRP profile of sandwich panels by Friction technique, and then mechanical fastenings were used to stich this connector to the floor sandwich panel.

Table 5.1. Summary of test matrix and parameters.

Specimen ID	Number of specimen	Connecting technique		Loading configuration	
		Friction	Hybrid	3PBT	4PBT
PLF1-PLF3	3	✓	-	-	✓
PLH1-PLH3	3	-	✓	-	✓
PTF1-PTF2	2	✓	-	✓	-
PTF3-PTF4	2	✓	-	-	✓
PTH1-PTH2	2	-	✓	✓	-
PTH3-PTH4	2	-	✓	-	✓

Before assembling

After assembling

Connector

Sandwich specimen

Sandwich specimen

Connector

Longitudinal connection-Friction technique

Bolt (M10)

Bolt (M10)

Sandwich specimen

Connector

Sandwich specimen

Connector

Longitudinal connection-Hybrid technique

Connector

Sandwich specimen

Sandwich specimen

Connector

Sandwich specimen

Transverse connection-Friction technique

Bolt (M10)

Bolt (M10)

Connector

Connector

Sandwich specimen

Sandwich specimen

Transverse connection-Hybrid technique

Fig. 5.2. Details of Friction and Hybrid technique for connecting sandwich panels in longitudinal and transversal directions.

5.3.2   Test setup and instrumentation

Flexural performance of the connected sandwich panels up to failure was studied according to ASTM C393 standard [79]. Longitudinal connected panels were tested in 4PBT under a clear span of 750 mm (**Fig. 5.3**a). Supports were materialized by steel rollers of 50 mm of diameter placed under the specimens at both ends, with one of them allowing a free sliding of the structure (roller support), and the other one representing a pinned support. The load was monotonically applied at one-third and two-third of span by a hydraulic jack of 200 kN of bearing capacity, being monitored using a load cell of 200 kN with a precision of 0.05%. A steel spreader beam plate (300 mm length $\times$ 50 mm width $\times$ 100 mm thickness) and steel rollers of 50 mm of diameter were used to transfer the load to the panels (**Fig. 5.3**a).

Vertical displacements were recorded by eight LVDTs with a stroke ranging from 25 mm to 50 mm, placed at the mid-span and under loaded sections. Moreover, specimens were instrumented in tension skins with TML PFL-30-11-3L strain gauges, placed at the midspan along the centre lines of the specimens.

Transverse connected panels were tested in 3PBT and 4PBT under the clear span of 350 mm. The supports were used in a similar way as to the longitudinal connected panels. The load was monotonically applied by a hydraulic jack of 50 kN of bearing capacity, being monitored using a load cell of 50 kN with a precision of 0.05%. In the case of 3PBT (**Fig. 5.3**b), the load was applied at the middle of span by using a half steel cylinder with the diameter of 40 mm. In the 4PBT (**Fig. 5.3**c), the specimens had a shear span of 90 mm and the load applied by the actuator was distributed by means of a steel spreader beam plate (180 mm length $\times$ 50 mm width $\times$ 100 mm thickness) that includes half steel cylinder with a diameter of 40 mm. Vertical displacements were recorded by two LVDTs with a stroke 25 mm placed at the mid-span of each specimen.
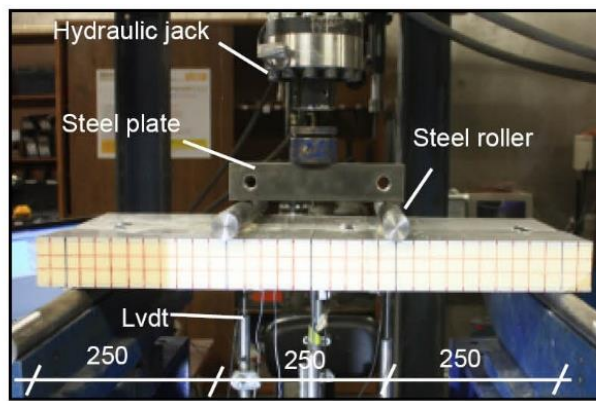
(a)
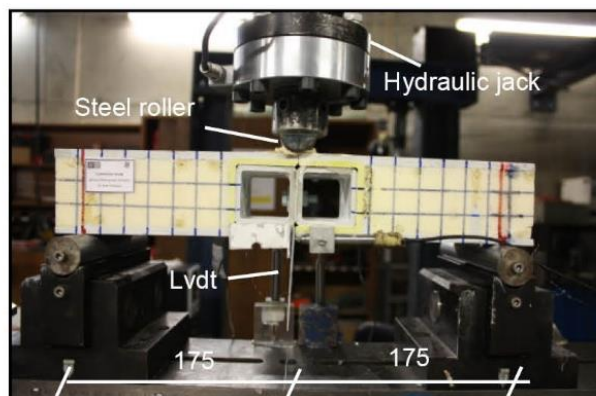
(b)
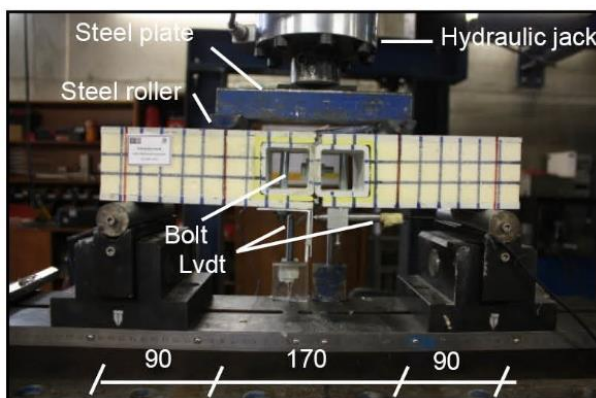
(c)

Fig. 5.3.Test setup: (a) four-point bending test in longitudinal connection; (b) three-point bending test in transversal connection; (c) four-point bending test in transversal connection

5.3.3   Flexural test results

The behaviour of the different connections type is discussed for each of the panel configuration in the following sections.

5.3.3.1 Longitudinal direction connection

The load *versus* midspan deflection curves obtained in the longitudinal jointed specimens submitted to monotonic loading up to failure are presented in **Fig. 5.4**. The results include both techniques of jointing panels namely as friction (**Fig. 5.4**a) and hybrid (**Fig. 5.4**b).

(a)   (b)
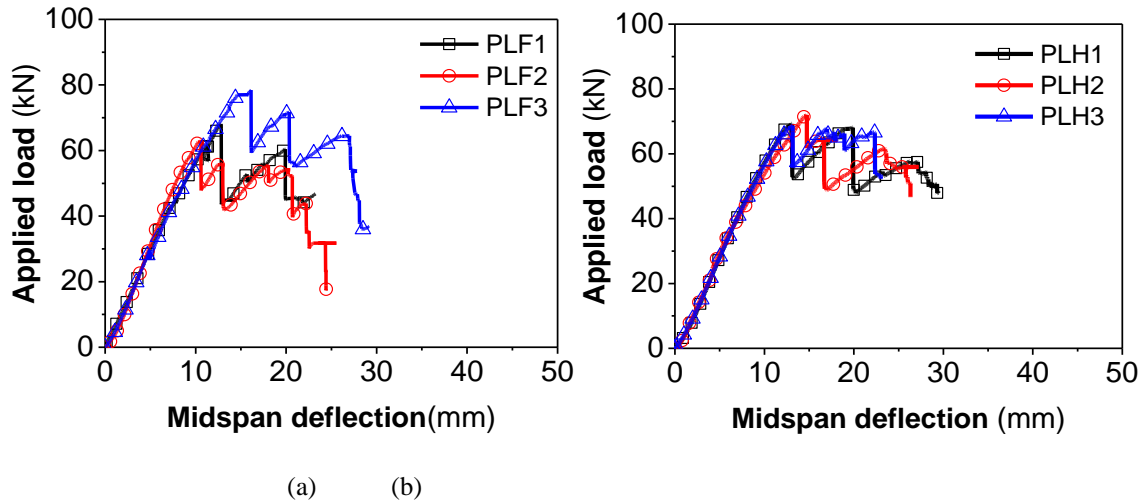
Fig. 5.4. Load *versus* midspan deflection in the longitudinal connected specimens: (a) friction technique; (b) hybrid technique

The results indicated that in both connection techniques, the relation between load and midspan deflection was almost linear up to failure. Load capacity of the tested specimens increased almost linearly until reaching the load and deflection of around 70 kN and 13 mm, respectively. At this stage, a significant, a significant drop in load was observed due to the debonding of the GFRP skin in the bottom side (tension side). Increasing the load, resulted in propagation of debonding toward the U-shape GFRP profile and led to PU foam core detached from U-shape GFRP profile. Debonging of PU foam core from GFRP bottom skin and U-shape GFRP profile resulted in loosing composite action between sandwich panel components. Accordingly, the applied load transferred to the U-shape GFRP profile. In the continuous of loading operation, the specimen continued to sustain load but never exceed the previous peak load as only U-shape GFRP profile and connector were carrying the load. The specimen then failed due to the tensile failure of the U-shape GFRP profile and connector.

The relation between bending stresses and strains at the bottom GFRP skin for the specimens tested is depicted in **Fig. 5.6**. The strain values were those registered in the strain gauges mounted on the bottom surfaces of the specimens, while the stresses were calculated based on the equilibrium of tension and compression forces [31] on the GFRP skin:

$$\sigma = \frac{M}{b \cdot d \cdot h_f} \tag{5.1}$$

where d is the distance between the centroids of the skins ($d = h_c + h_f$, being h_c and h_f the core and skin thickness, respectively), and b is the width of the panel.
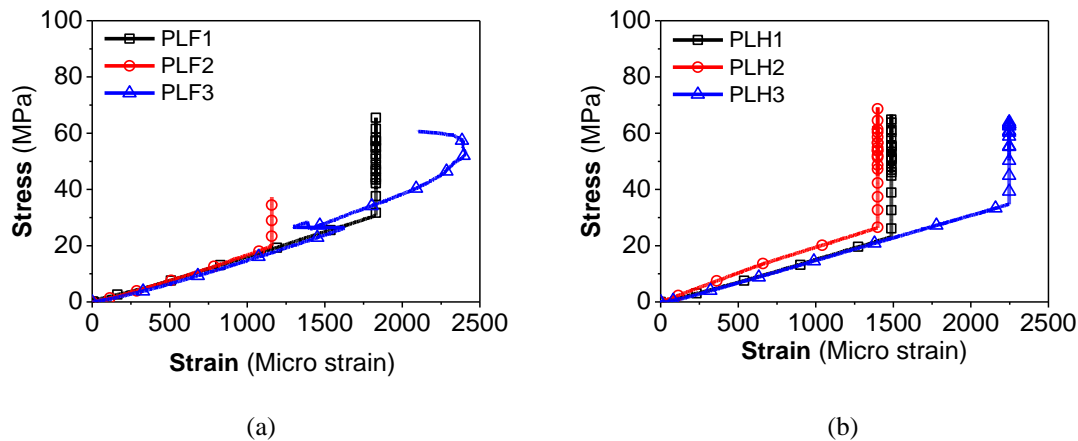
Fig. 5.5. Stress *versus* strain: (a) friction technique; (b) hybrid technique

A quite linear behaviour for strain-stress can be observed, being a consequence of the linear strains measured in the GFRP skins, which at the same time is a reflection of the linear behaviour exhibited by this material. It was observed that after exceeding the tensile stress of 20 (MPa) and corresponding strain of 1500 (με), strain gauges were unable to record properly. It could be explained that, after this level of strain, the strain gauges were damaged due to wire connection problem.

5.3.4   Transverse direction connection

Fig. 5.6 shows the load midspan deflection curves obtained in the transverse jointed specimens subjected to a monotonic loading 3PBT configuration up to failure. Jointed specimens with friction technique presented some nonlinearity. Load capacity of these specimens increased linearly until a load and a displacement of 0.27 kN and 3 mm, respectively (**Fig. 5.6**a). At this point some nonlinearity in the load-deflection response was observed due to stiffness degradation. However, the specimens were capable of supporting extra load until a maximum load and displacement of 0.6 kN and 10 mm, respectively. At this load level, a drops of load was observed due to the failure of the U-shape GFRP profile. This failure led to the degradation of integrity between connector and U-shape profiles due to the decrease level of friction effectiveness. This effect consequently resulted in reduction of stiffness in the jointed specimens. However, in the case of panels with hybrid connections, it was noticed that the relation between load and midspan deflection was nearly linear. A

maximum load and displacement of 0.8 kN and 8.5 mm, respectively, were registered before failure of the specimens. The dominate connector failure mode was observed. Above the deflection corresponding to peak load, the specimens entered in a softening stage with a decrease of load carrying capacity (**Fig. 5.6**b).

(a)   (b)
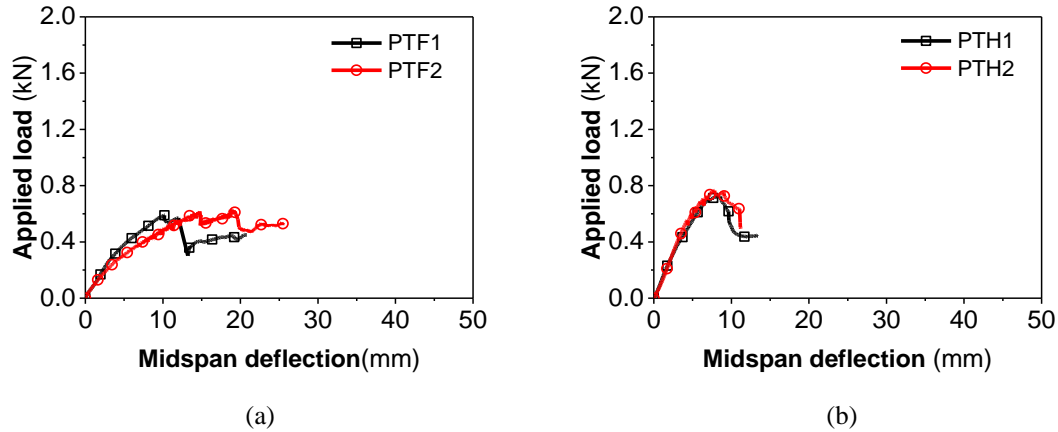
Fig. 5.6. Load *versus* midspan deflection in three-point bending test: (a) friction technique; (b) hybrid technique.

Fig. 5.7 presents the relation between load and midspan deflection of the tested panels in four-point bending tests. The behaviour of the tested specimens in this test was similar to the previous test (3PBT). In the specimens jointed with friction technique (**Fig. 5.7**a) failure of the specimens was noticed due to failure of U-shape GFRP profile at a load and a displacement of 0.45 kN and 5.5 mm, respectively. Just after peak load the specimens presented an abrupt load decay, followed by a stage of pseudo-ductility due to losing integrity of the structure because of decreasing the friction effectiveness between connector and U-shape GFRP profile. On the contrary, linear relation between load and displacement was observed for the specimens with hybrid connections (**Fig. 5.7**b). After reaching a maximum load and displacement of around 1.5 kN and 9.6mmspecimens presented an abrupt load decay due to initiation of a crack in the GFRP square connector. Such as previous specimens in three-point bending test, after reaching this pick load specimen were not able to withstand extra load due to the degradation of the integrity between specimens and connection.

Table 5.2 includes the values for the ultimate moment (M_u), ultimate load (P_u), midspan deflection corresponding to P_u (δ_u), initial stiffness (K) as the slope of the force and deflection in the linear part, maximum longitudinal strain on bottom skin (ε_{ub},) and maximum flexural stress (σ_u).

(a)   (b)
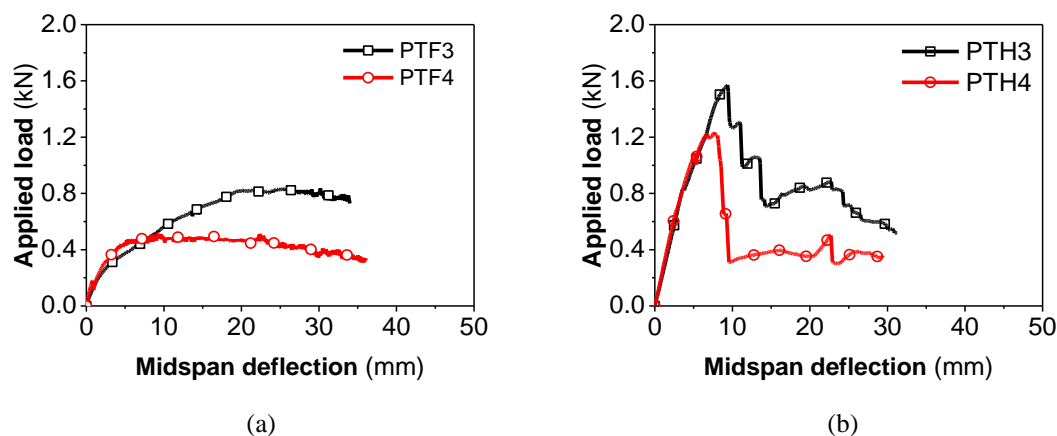
Fig. 5.7. Load *versus* midspan deflection in four-point bending test: (a) friction technique; (b) hybrid technique.

Table 5.2. Main summary results from flexural test in jointed specimens.

Connection Direction	Test Type	Specimen IDE	M_u (kN·m)	P_u (kN)	δ_u (mm)	ε_u (µstrain)	σ_u (MPa)	K (kN/mm)
Longitudinal	4PBT	PLF1	8.516	68.130	12.830	1829.319	65.510	5.310
		PLF2	7.881	63.050	10.568	1157.835	60.625	5.966
		PLF3	9.803	78.420	16.121	2411.513	75.404	5.215
		PLH1	8.659	69.270	13.063	1487.524	66.606	5.302
		PLH2	8.996	71.970	14.693	1398.876	69.202	4.916
		PLH3	8.593	68.740	13.143	2247.221	66.096	5.230
Transverse	3PBT	PTF1	0.051	0.573	10.336		1.542	0.085
		PTF2	0.053	0.617	14.751	-	1.661	0.087
		PTH1	0.063	0.723	8.265		1.946	0.122
		PTH2	0.066	0.765	8.111		2.059	0.124
	4PBT	PTF3	0.104	0.832	11.275		3.200	0.134
		PTF4	0.063	0.509	9.387	-	1.957	0.136
		PTH3	0.196	1.571	9.388		6.042	0.223
		PTH4	0.154	1.234	7.939		4.746	0.224

5.3.5   Failure mechanism

Failure mechanisms of all tested panels are depicted in **Fig. 5.8**. In the case of the longitudinal connected specimens, the same failure modes were noticed for both type of connections (friction and hybrid). The failure for these specimens started with the occurrence of debonding of the GFRP skin in the bottom side (tension side). After that, debonding propagate toward to the U-shape GFRP profile and consequently damage in the U-shape GFRP profile and connector occurred. For the transverse connected specimens, different types of failures were observed for friction and hybrid connections. In the friction connection, the dominant failure was due to creation of damage in the GFRP U profile. Naked eyes inspection of GFRP square connection showed that there were no any cracks or failure in this component. On the contrary, in the hybrid connection the main failure mode was due to damage in the GFRP square connector.
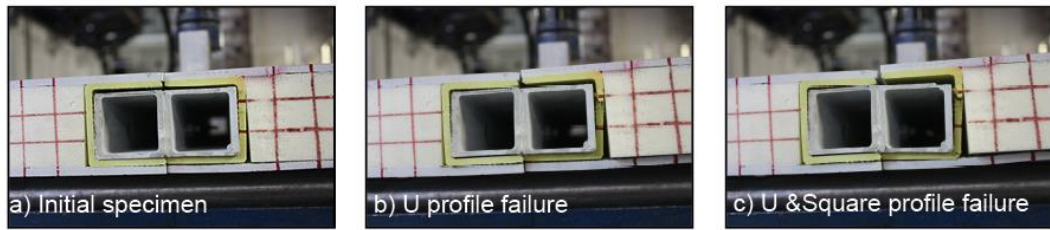
Four-point bending test-Longitudinal connection-Friction
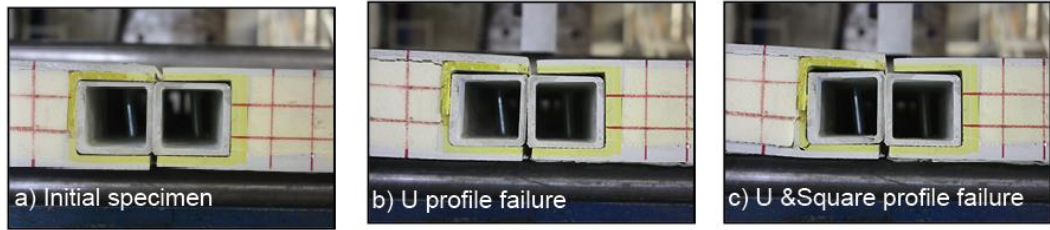
Four-point bending test-Longitudinal connection-Hybrid
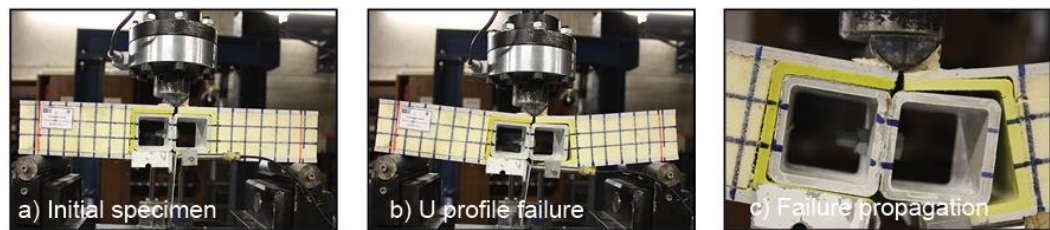
Three-point bending test-Transversal connection-Friction
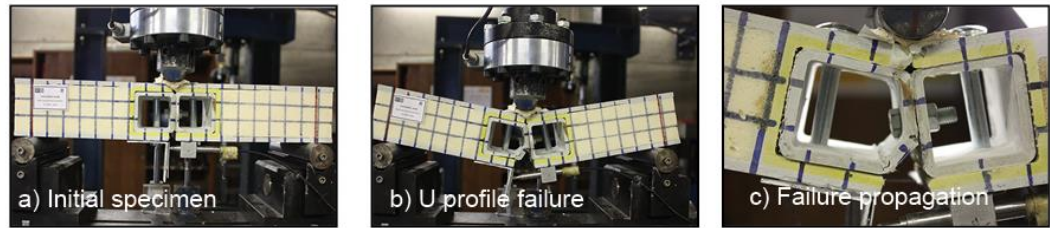
Three-point bending test-Transversal connection-Hybrid
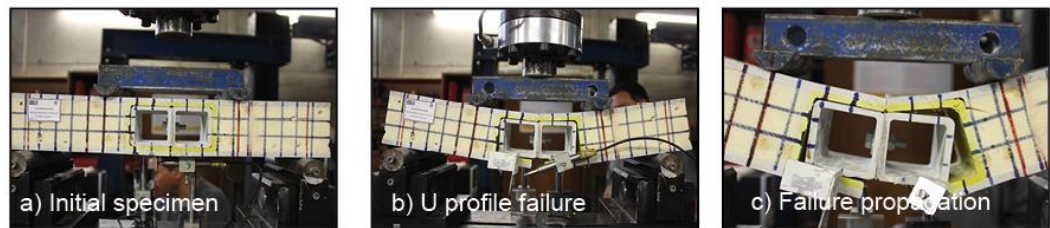
Four-point bending test-Transversal connection-Friction
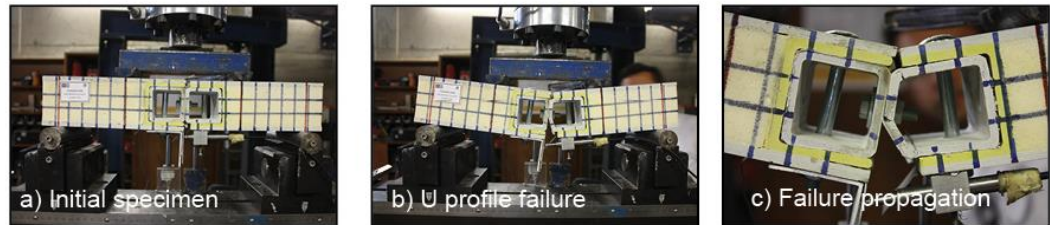
Four-point bending test-Transversal connection-Hybrid

Fig. 5.8. Failure mechanism of tested panels

5.4   Conclusion

This chapter presented a fitting jointing methodology to connect two sandwich panels. The connection is composed of integrated U-shape GFRP profile and interlocked GFRP square profile. Behaviour of the jointed sandwich panels were evaluated in longitudinal and transversal directions. Two approaches were used to connect floor sandwich panels, namely without mechanical fastening (Friction technique) and with mechanical fastening (Hybrid technique). Their mechanical behaviour was studied in this research.

The main concluding remarks drawn from the tests carried out can be listed as:

- Regarding to the longitudinally connected specimens, in both friction and hybrid techniques, the failure started due to debonding of lower GFRP skin and propagate toward the U-shape GFRP profile. By increasing the load, due to degradation of composite action between sandwich panel's component, the applied load transferred to the U-shape GFRP profile and connector. Increasing the load resulted to failure of U-shape GFRP profile happened at the middle of web due to excessive longitudinal tensile stresses. Linear elastic behaviour was observed for the load-deflection in both friction and hybrid techniques. In both techniques, the same amount of ultimate load was obtained. This fact representing that employing mechanical fasteners did not have any influence in increasing flexural capacity of the jointed specimens.

- In the transverse direction specimens, comparing the failure mechanism in specimens connected using friction and hybrid techniques illustrated that, in the specimens jointed by friction technique the failure happened in the U-shape GFRP profile. However, by using hybrid technique failure occurred in the GFRP square connector. Regarding to the load carrying capacity of connected panels, in both three-point and four-point bending tests, connected panels with hybrid techniques represented higher load than friction technique.

- The efficiency of using fitting technique in transferring produced bending moments between jointed modular panels without effecting in flexural stiffness was observed in this system.

Chapter 6: Single and jointed sandwich panels

6.1 Introduction

The composite sandwich panels studied in this chapter can be categorized into two main groups namely as single sandwich panels and jointed sandwich panels. The flexural performances of these two groups of sandwich panels were subjected to study in this chapter.

Single sandwich panels are comprising into small scale panels and full scale panels. Two different types of tests were carried out in the single sandwich panels: (i) static tests up to service load and ultimate load, and (ii) static tests up to failure. The main aims of performing static tests in short-term were evaluating the flexural performance of composite sandwich panels, designed to support serviceability limit state (SLS) and ultimate limit state (ULS) load conditions of residential houses. Furthermore, the long-term static flexural tests had the objective of evaluating the viscoelastic behaviour of the proposed sandwich panels during service life with two kinds of support conditions: (i) with the end U-shape GFRP profiles and (ii) without that profiles. The static flexural tests up to failure aim to assess the ultimate capacity of floor panels and their failure mechanisms.

In a second stage, the flexural behaviour of two and three jointed panels are experimentally assessed under both SLS and ULS conditions. In this stage, capability of the panels in fulfilling the requirements by the standard [80] is assessed. Additionally, the efficacy and contribution of the connection between panels, by studying the transference of loads from one panel to the adjacent ones is studied

Finally, some analytical and numerical studies are performed for: (i) assessing the flexural behaviour of the panels in SLS and ULS conditions, (ii) predicting long-term performance of the panels, (iii) capturing the failure mode of sandwich panels, (iv) evaluating the influence

of the GFRP ribs placed inside the panels, and (v) assessing the performance of the connection system in jointing panels.

6.2 Flexural response of single floor composite sandwich panels

6.2.1 Small scale single composite sandwich panels

Small scale specimens were manufactured with the purpose of conducting a series of flexural and creep tests. The following subsections provide details of test specimens, setup and procedure.

6.2.1.1 Flexural test up to failure

Experimental program

One-way static behaviour of sandwich panels up to failure was investigated according to ASTM C393 standard [79]. Four-point bending tests were carried out with the following two groups of specimens (see **Fig. 6.1**): (i) with an end U-shape GFRP profile (PUi), and (ii) without that profile (Pi).

(a)   (b)
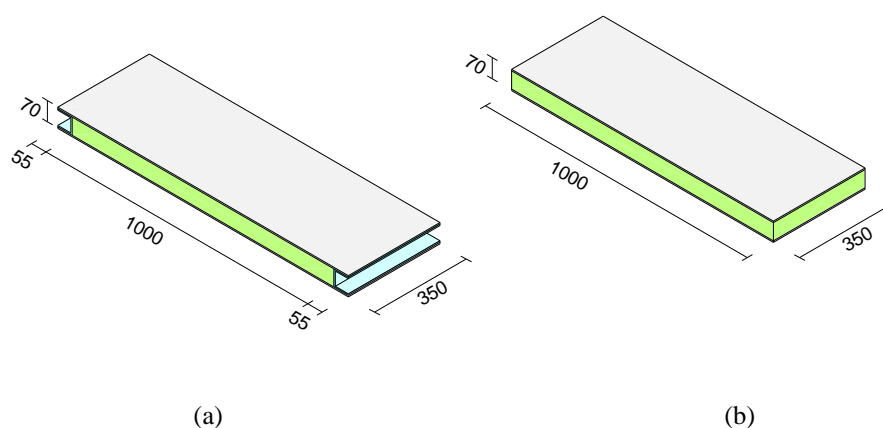
Fig. 6.1. Small scale sandwich specimens: (a) with U-shape GFRP profiles in their supporting extremities (PUi); (b) without U-shape GFRP profiles (Pi) (dimensions in millimeter, i=1,2)

The first group of specimens (PU1 and PU2) were tested under a shear span of 300 mm, with a clear span of 1150 mm and a width of 350 mm (**Fig. 6.2**a). Regarding the panel's support conditions, one of the supports allowed free sliding of the panel, while the other introduced pinned support conditions. A tubular steel profile of $50 \times 50 \times 5$ mm^3 cross section was fixed at each ends of the sandwich panels, and a steel roller with a diameter of 32 mm was placed inside that tubular profile in order to allow free rotation of the panel ends.

For the second group of specimens (P1 and P2), shear span and the width of the tested panels were the same of the PUi, but the clear span was limited to 900 mm. For these specimens the supports were materialized by steel rollers and one of the supports allowed free sliding of the panel, while the other introduced pinned support conditions (**Fig. 6.1**b).

Loads were applied by a hydraulic jack and were monitored using a load cell of 200 kN with a precision of 0.05%. A steel spreader IPE beam profile and steel rollers were used to transfer the load to the panels. Additionally, rubber pads were placed between the specimens and the steel rollers to avoid any indentation failure [81-84]. Vertical displacements were recorded by five LVDTs with a stroke ranging from 25 mm to 50 mm, placed on the supports, midspan and under loaded sections. Moreover, the tension and compression skins of the specimens were instrumented with strain gauges, placed at the intersection of the midspan section of the specimen with its longitudinal axis.

(a)   (b)
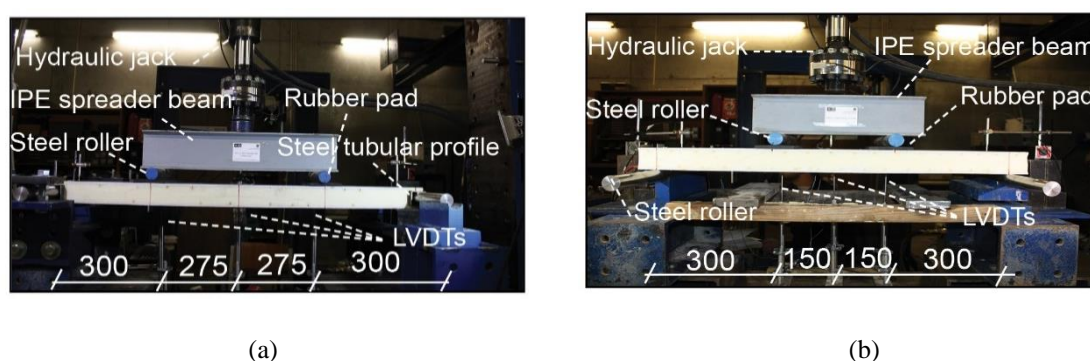
Fig. 6.2. Test setup for four-point bending tests up to failure of specimens: (a) with U-shape GFRP profile (PUi); (b) without U-shape GFRP profile (Pi) (all units in mm).

Results

The load-deflection curves of PUi and Pi are presented in **Fig. 6.3**. For the case of Pi, results show that, the relation between load and midspan deflection was fairly linear up to failure (**Fig. 6.3a**). The load capacity of these specimens increased linearly and continuously until reaching an average load of 7 kN, and an average deflection of 14 mm. At this moment, specimens failed abruptly due to shear rupture of the core. Conversely, as **Fig. 6.3**b shows, for the case of PUi sandwich panels the relation between load and displacement was linear until a load of about 4 kN (which is nearly 60% of the maximum load). Once reached that load, a small reduction in the stiffness was observed due to delamination of the bottom GFRP skin in the maximum flexural zone. However, the specimens were capable of supporting higher load, registering a slightly drop at a load of 5 kN also due to delamination of the

bottom skin. Above this load stage, the stiffness of these panels has gradually decreasing up to the sudden brittle failure that occurred at a load of about 7 kN, caused by the rupture of the core material in the vicinity of the support.

(a)   (b)
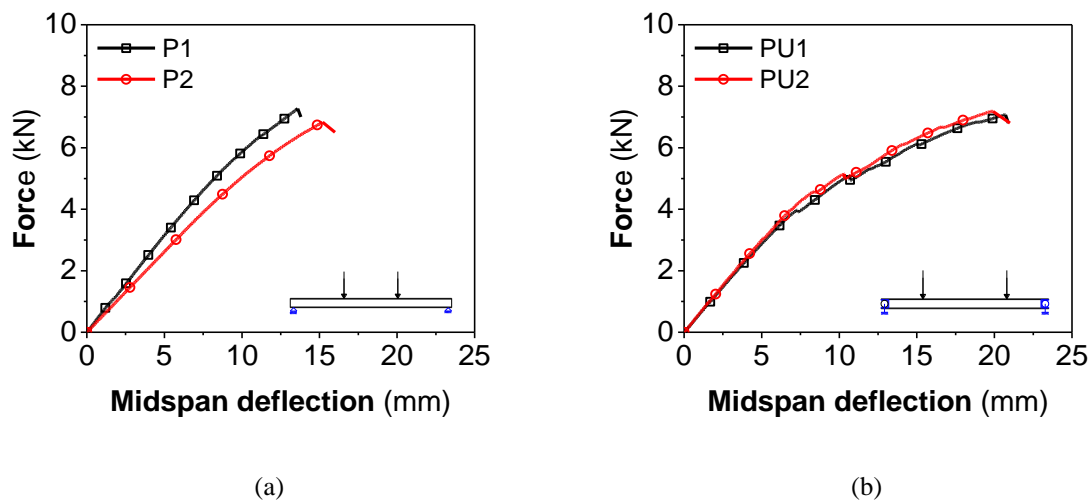
Fig. 6.3. Load-midspan defection curves for tested specimens: (a) without end U-shape GFRP profiles (P) and ; (b) with end U-shape GFRP profiles (PU).

The obtained results show that, both Pi specimens attained nearly the same ultimate load. **Fig. 6.4** shows the moment-curvature diagram at the midspan cross-section for four-point bending tests load configuration, where the curvature was calculated using the information given by the strain gauges placed at the midspan cross-section (top and bottom skins).
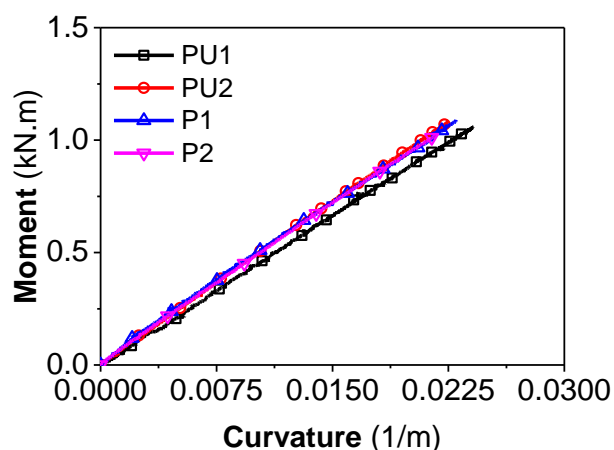
Fig. 6.4. Moment-curvature diagrams for tested specimens without end U-shape GFRP profiles (Pi); with end U-shape GFRP profile (PUi).

Both types of specimens presented a linear behaviour response before failure, being their flexural stiffness (defined as the slope of the moment-curvature diagram) very similar in all

the tested specimens. This confirms that introducing the end U-shape GFRP profiles for providing connection system in the panels did not have any significant effect in terms of flexural stiffness.

Table 6.1 includes the values for the ultimate moment (M_u), the ultimate load (P_u), the maximum deflection (δ_u), the initial stiffness (K) defined as the slope of the force and deflection in the linear part, the maximum longitudinal strain on the top and bottom skins (ε_{ut} and ε_{ub}, respectively), the maximum flexural stress (σ_u), and the maximum average shear stress in the core (τ_u) obtained according to Eq. (6.1) and (6.2), based on equilibrium analysis [31].

$$\sigma = \frac{M}{b \cdot d \cdot h_f} \tag{6.1}$$

$$\tau = \frac{\partial M}{\partial x} \frac{1}{b \cdot d} \tag{6.2}$$

where d is the distance between the centroids of the skins, $d = h_c + h_f$, h_c and h_f are the core and skin thicknesses, respectively, and b is the width of the panel.

Table 6.1. Main summary results from the tests up to the failure.

Specimen	M_u (kN·m)	P_u (kN)	δ_u (mm)	ε_u (µstrain)		σ_u (MPa)	K (kN/mm)	τ_u (kPa)
				ε_{ut}	ε_{ub}			
P1	1.09	7.27	13.59	-807	804	9.58	47.45	159.80
P2	1.02	6.83	15.20	-590	941	9.00	47.14	150.11
PU1	1.06	7.06	20.67	-838	854	9.31	43.91	155.16
PU2	1.07	7.18	20.01	-714	859	9.47	47.93	157.80

Failure modes are presented in **Fig. 6.5**. Shear failure of the core was the mechanism governing the behaviour of the Pi specimens. This failure can be explained by the fact that the registered foam core shear stress in the specimens (see **Table 6.1**) exceeded maximum shear strength obtained in material characterization (see chapter 4, **Table 4.1**). Shear failure occurred in the shear span, with a crack angle of 45 degrees. The propagation of these shear cracks followed toward the skins causing core-skin debonding.

In the case of PUi specimens, the failure was governed by the debonding between the bottom face of the U-shape GFRP profile and the GFRP bottom skin, followed by an abrupt formation of a tensile fracture surface on the core materials due to its residual tensile strength, and propagation of the failure surface at the core-top GFRP skin. Hence, the detachment

process between U-shape GFRP and GFRP bottom skin is eminently a nonlinear phenomenon, which justify the nonlinear response of these panels.
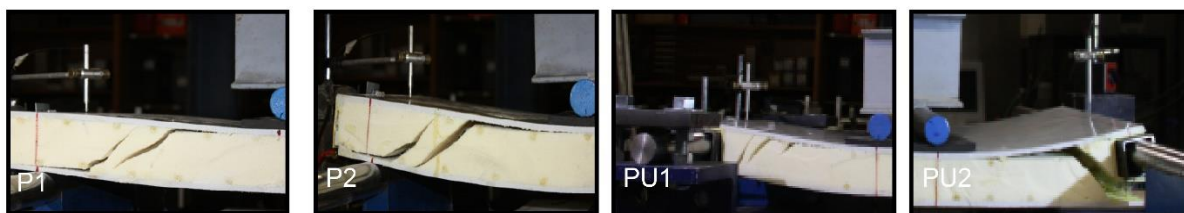
Fig. 6.5. Failure modes.

The strain-stress relation at top and bottom skins for the specimens tested is depicted in **Fig. 6.6**. The strain values were those registered in the strain gauges applied on the top and bottom surfaces of the panels, while the stresses were calculated based on the equilibrium of tension and compression forces on the skins, according to Eq. (6.1) [31]. A quite linear behaviour for strain-stress in both specimens before any failure can be observed, being a consequence of the linear behaviour of the panel, which before the damage initiation is governed by the two outer layers of GFRP that have linear-elastic behaviour.

Moreover, when calculating the elastic modulus, the average elasticity modulus obtained in the GFRP material characterization (around 9.5 GPa) is reached. It is interesting to mention that all the specimens failed at a stress and a strain of approximately 9 MPa and 850 mm/m, respectively. These levels of stress and strain are only 7% of the ultimate stress and strain of the GFRP material obtained from the direct tensile tests.

(a) (b)
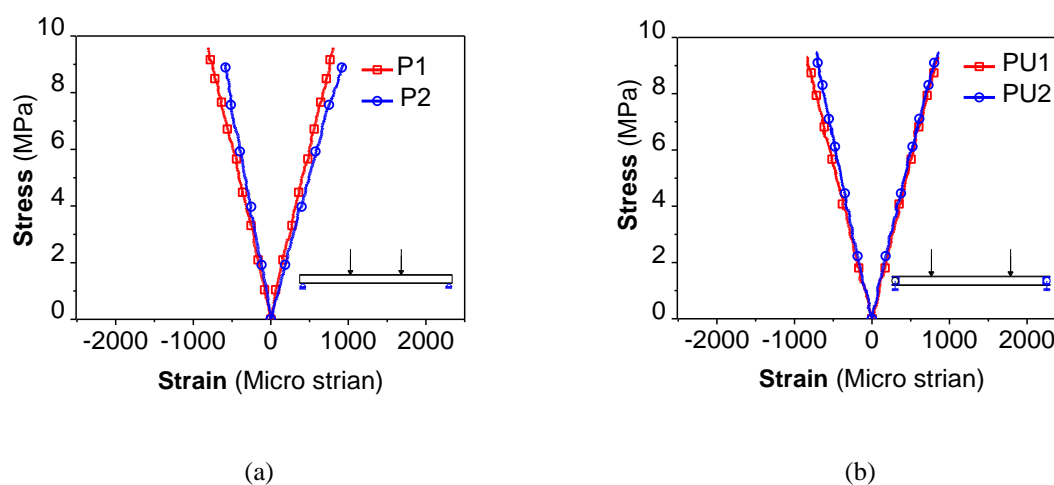
Fig. 6.6. Stress-strain curves: (a) without end U-shape GFRP profiles (Pi) and ; (b) with end U-shape GFRP profiles (PUi).

6.2.1.2 Creep tests

Experimental program

Two panels with and without end U-shape GFRP profiles, PU3 and P3, respectively, were prepared to study the creep behaviour of sandwich panels. Specimens were tested in bending for a period of 263 days (6312 h) to assess long term viscoelastic flexural behaviour of sandwich panel. Four-point bending tests were carried out with the same test setup configurations described in the previous subsection, except the loading conditions (see **Fig. 6.7**). A total load of 1.7 kN was applied, which corresponds to 24% of its ultimate strength. Vertical displacements were measured by using three mechanical dial gauge displacement indicators, with 0.01 mm of precision. These dial gauges were placed underneath of GFRP.

| (a) | (b) |
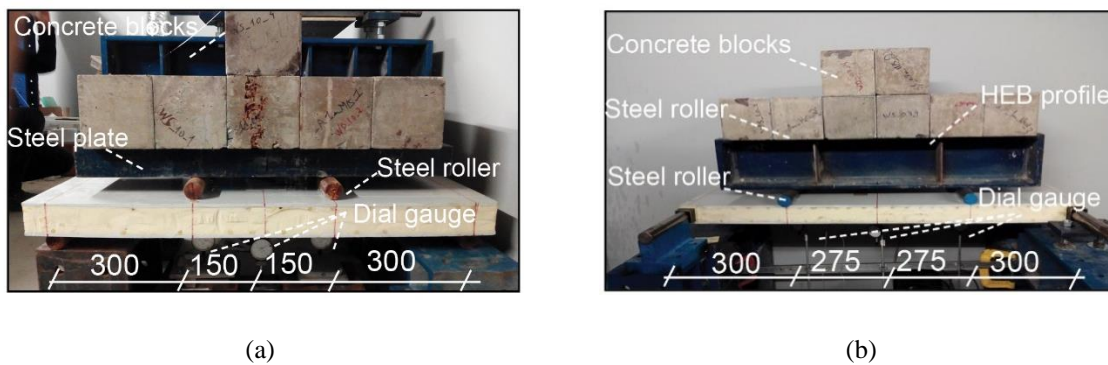
Fig. 6.7. Test setup for creep test: (a) without end U-shape GFRP profiles (P3); (b) with end U-shape GFRP profiles (PU3) (all units in millimeters).

Results

Load *versu*s midspan deflection relationship for the panels P3 and PU3 are illustrated in the **Fig. 6.8**. The applied load of 1.7 kN induced an immediate elastic deformation of 3.33 mm and 3.5 mm for panels P3 and PU3, respectively. Keeping that load constant during almost nine months, the midspan deflection in both P3 and PU3 increased to around a 116% of the elastic deflection. Clearly, it was noted that at the end of this period the creep deflection is still quite active. This evidences the importance of considering long term deformation in composite sandwich panels. Moreover, it was observed that support condition did not have any major effects in long term behaviour of the panels.
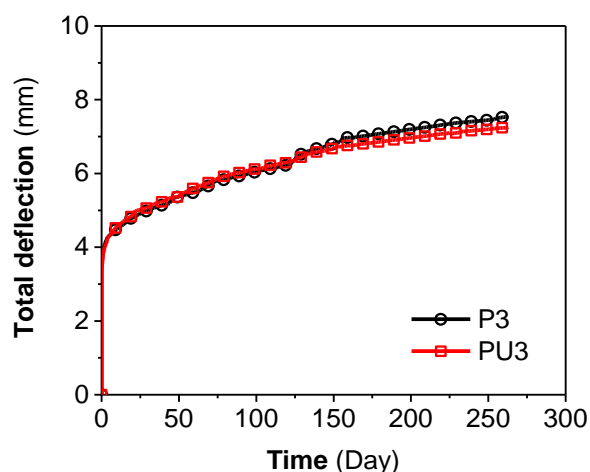
Fig. 6.8. Time-midspan deflection in the panel without end U-shape GFRP profiles (P3) and with end U-shape GFRP profiles (PU3).

6.2.2   Full scale single composite sandwich panels

The full scale panels comprised two distinct configurations, as depicted in **Fig. 3.3** of CHAPTER-3 namely: FSP-L2.4_W1.2_t70 and FSP-L3.0_W1.0_t70. Two different types of tests were carried out: (i) static tests under SLS and ULS loading conditions, and (ii) static tests up to failure. The following subsections provide details of test specimens, setup and procedure.

6.2.2.1 Flexural behaviour at service load, ultimate load and failure

Experimental program

Two FSP-L2.4_W1.2_t70 composite sandwich panels with the dimension of 2400 mm×1200 mm× 70 mm with two internal GFRP U-shape profiles, were manufactured (hereafter FP′1-FP′2). The panels were subjected to a flexural testing as schematically is illustrated in **Fig. 6.9**. The tests were conducted in accordance with ASTM C393 [30], following two load schemes: (i) four-point bending test, and (ii) three-point bending test.

The tests were designed in order to introduce a maximum bending moment in the sandwich panel equivalent to a uniform distributed load, representing a characteristic live load of 2 kN/m^2 in accordance with Eurocode 1 [85], which was assured by submitting the panels to a load of 2.75 kN and 5.5 kN for three-point and four-point bending tests, respectively.
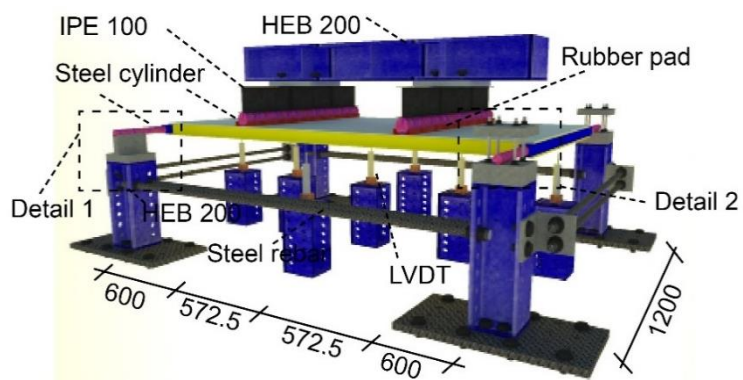
(a)
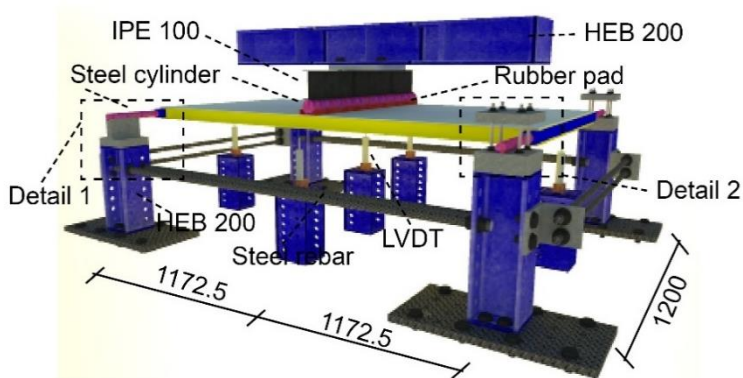
(b)

Detail 1   Detail 2

Fig. 6.9. Schematic representation of the FP′ sandwich panel flexural test under service loads: (a) four-point bending test; (b) three-point bending test (dimensions in mm).

Regarding the panel's support conditions, the same system was used as aforementioned in the case of small scale testing panels (PUi). The monotonic load was applied by a hydraulic jack, and transferred to the panels by means of longitudinal IPE 100 profiles with steel rollers of 20 mm of diameter welded at their bottom flange. A load cell of 300 kN with a precision of

0.05% was used to measure the load, while deflections in the panels were monitored under supports, midspan and in the loaded sections by LVDTs with a measuring stroke of 100 mm.

In the case of FSP-L3.0_W1.0_t70 panels, four full scale floor sandwich panels with a dimension of 3000 mm×1000 mm× 70 mm and four internal U-shape GFRP profiles (designated by FP1 to FP4) were tested under a uniform load to evaluate their structural performance as a single panel. Additionally, after uniform testing, one of the panel tested (FP4) was selected and flexural behaviour of this panel was studied until failure. The panels were tested with a clear span of 2700 mm, and supports were materialized by two steel rollers with a diameter of 50 mm placed under both panel ends. Both supports allowed free rotation and one of them also allowed for longitudinal sliding (roller support), while the other was fixed in the longitudinal direction (pinned support).

Regarding to the uniform loading, based on the UNHCR recommendation [86] for an emergency house, a uniform load of 1.6 kN/m^2 was selected to be load in SLS. That load was increased 1.5 times to evaluate ultimate limit state (ULS) of panels as traditionally defined in the Eurocodes. The load was manually applied by using cement bags of 20 kg each. In a first step (SLS loading configuration), 16 cement bags were disposed in two layers, representing a uniform distributed load of 1.6 kN/m^2 (see **Fig. 6.10**a). In a second step, eight extra bags were added to attain a loading level corresponding to ULS conditions (see **Fig. 6.10**b). Loading operations were performed fast as fast as possible to avoid any potential creep effect. Cement bags completely covered the surface of the panels, and gaps between bags were assured to avoid any arch effect.

Vertical displacement was measured by means of a LVDT placed at the intersection of the specimen's midspan section with its longitudinal axis. The panels were also instrumented in the tension skin (bottom skin) with a strain gauge bonded at a distance of 10 mm from the centre of the panel to avoid any interference with the LVDT.

The static behaviour of one-way full scale sandwich panel up to its failure was investigated by executing a four-point bending test according to the ASTM C393 recommendations [87]. The panel was tested with a shear span of 850 mm, and supports were materialized as already described for the single panels submitted to a uniformly distributed load. Hydraulic jack was used to apply a monotonic load up to the failure of the specimen. The load was transferred to the panel by means of a longitudinal spreader HEB 200 with a length of 2000 mm, and two

IPE 100 profiles with steel rollers of 20 mm of diameter welded at their bottom flange. A load cell of 300 kN (with a precision of 0.05%) was used to register the load applied. Rubber pads were placed between the panel and the steel rollers to avoid any indentation failure[81-84].
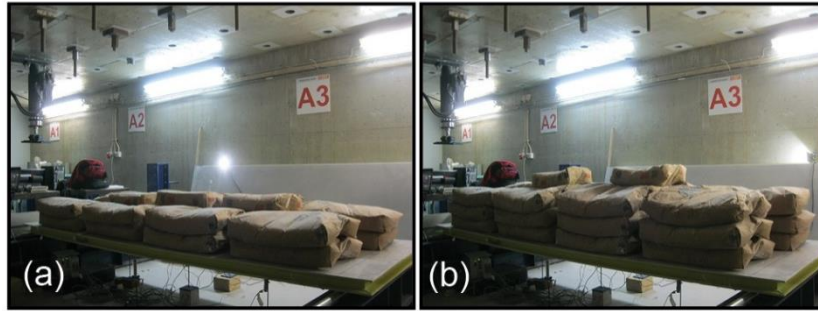
Fig. 6.10. Different phases of uniform single panels loading corresponding to: (a) SLS conditions (1.6 kN/m^2) and (b) ULS conditions (2.4 kN/m^2, 1.5 times SLS load).

Fig. 6.11a shows the test setup configuration. Vertical displacements were recorded by five LVDTs with a stroke ranging from 25 mm to 50 mm, placed under loaded sections (D4-D5) and at midspan (D1-D3). Moreover, six strain gauges were bonded on the bottom skin (S1-S3) and on the top skin (S4-S6) at the midspan section of the specimen (see **Fig. 6.11**b).
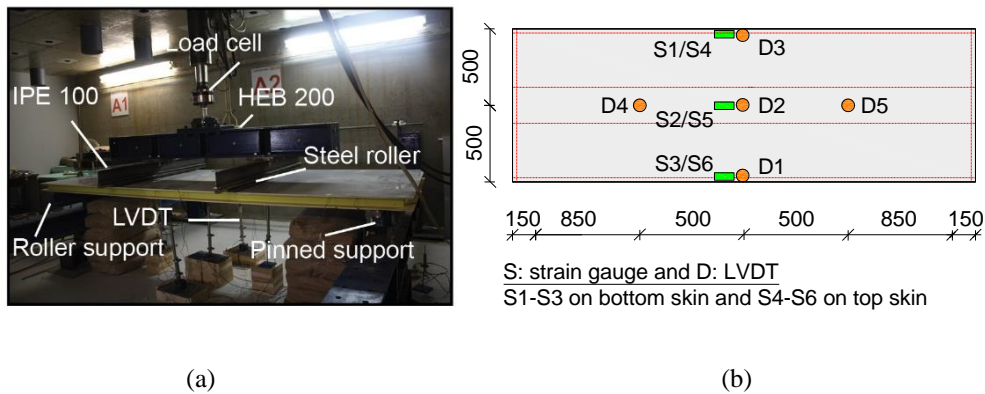
Fig. 6.11. FP4 four-point bending test: (a) test setup; (b) instrumentation (all units in mm).

Results

Load *versus* midspan deflection for the FP$'$ sandwich panels in SLS under three point and four-point bending tests are plotted in **Fig. 6.12**. Both tests presented a very similar response, which is an indicator of the elastic behaviour of the composite sandwich panels under characteristic live loads.
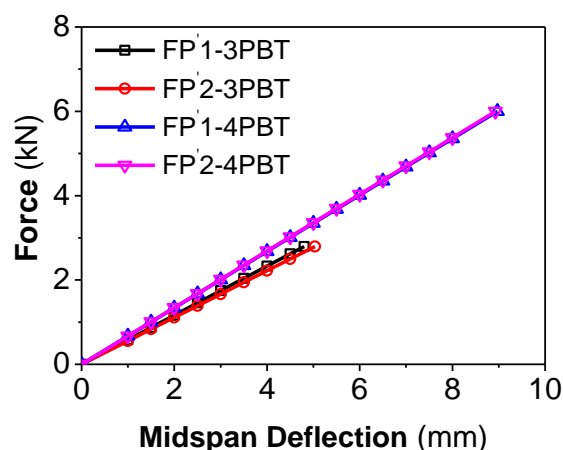
Fig. 6.12. Load-midspan deflection of FP′ sandwich panels under service loads subjected to three-point bending test and four-point bending tests.

The flexural stiffness (K), defined as the ratio between the maximum applied load and its corresponding midspan deflection (δ_{max}), was quite similar in both testing configurations (**Table 6.2**), confirming the same flexural behaviour of both floor panels under serviceability loads.

Table 6.2. Three-point and four-point bending tests results for sandwich panels under service loads.

Panel	Three-point bending test		Four-point bending test	
	δ_{max} (mm)	K (kN/mm)	δ_{max} (mm)	K (kN/mm)
FP′1	4.80	583	8.96	669
FP′2	5.03	556	8.92	672

The registered midspan deflections and midspan strains for the tested panels FP1-FP4 under a uniformly distributed load are shown in **Fig. 6.13**a and **Fig. 6.13**b, respectively. The application of the load in two steps, corresponding to SLS (1.6 kN/m^2) and ULS (2.4 kN/m^2) load conditions is fully recognizable in the graphs by an abrupt increase of midspan deflection and strain after the stabilization stage at the end of the SLS (SLS_L) and ULS (ULS_L) loading processes. As can be seen, a full recovery of the deflections and strains took place after the unloading phase, which evidences that, for the considered load levels the panels have presented an elastic behaviour. Moreover, **Fig. 6.13** shows that, the values for both deflections and strains registered were very similar in the four tested panels, revealing a manufacturing process of high repeatability.

(a)   (b)
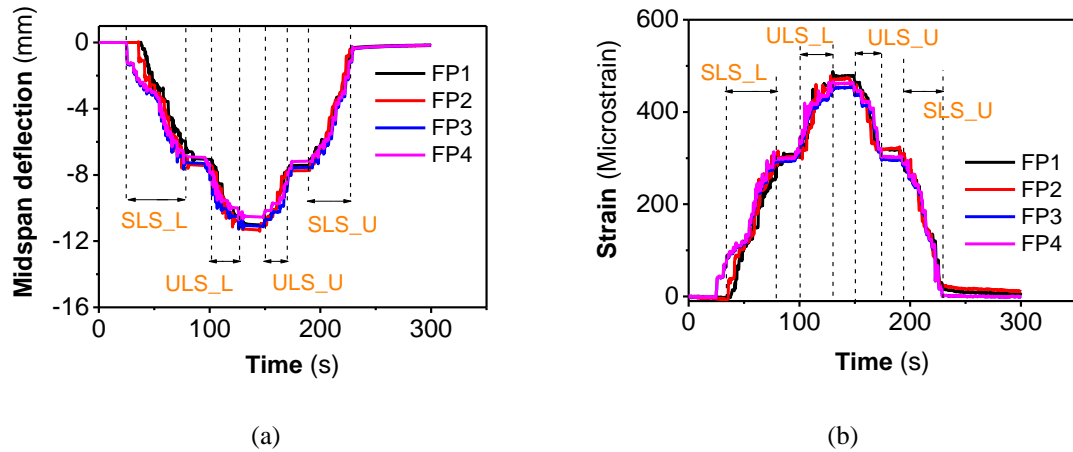
Fig. 6.13. Results of single composite sandwich floor panel testing under uniform loading test in terms of: (a) time *versus* midspan deflection; (b) time *versus* strain.

Under ULS loading conditions, the average of the maximum tensile strain recorded in the bottom GFRP skin at midspan was 491 micro strain (µε),which is significantly lower than the ultimate tensile strain of GFRP skins obtained experimentally (12188 µε).

The load-deflection relationship of the single panel tested up to failure under a four- point bending configuration is depicted in **Fig. 6.14**a. The panel failed at a maximum load of 28.47 kN, at which the midspan deflection was 61.02 mm. The panel exhibited a linear behaviour up to failure, which was also attested by the strain gauges measurements plotted in **Fig. 6.14**b. The maximum tensile strain measured at midspan in both bottom and top skins was around 2600 micro strain.

(a)   (b)
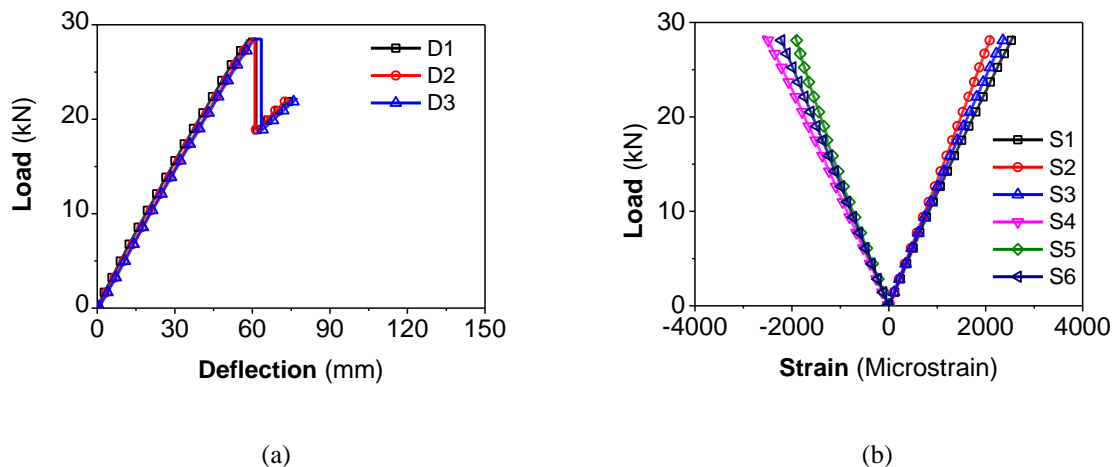
Fig. 6.14. Single panel up to failure test result: (a) load *versus.* deflection and (b) load *versus.* strain.

Fig. 6.15 depicts the failure mode evolution observed on the tested panel at different loading stages. Localized debonding between GFRP compression skin (top skin) and PU foam core was the predominant failure mode of the panel. This failure occurred in the region of pure bending moment, between the two lines of loading, and was caused by a very high out-ward tensile stress between skin and core, as a result of attaining the maximum PU tensile stress [50].

This phenomenon, known as local instability or wrinkling failure mode of a sandwich panel, leads to a sudden outward buckling of the GFRP skin in the compression side where the buckling wavelength is short. The initiation of wrinkling failure mode is schematically shown in **Fig. 6.15**a. It was experimentally observed that, at the beginning, the length of the debonded part was equal to the PU thickness. This observation confirmed previous information mentioned by other authors about the debonded length, referring that it could be equal to the PU thickness [28, 31, 88]. Thereafter, debonded part propagated to the centre of the panel (**Fig. 6.15**b), and finally the sandwich panel presented an overall instability (**Fig. 6.15**c).
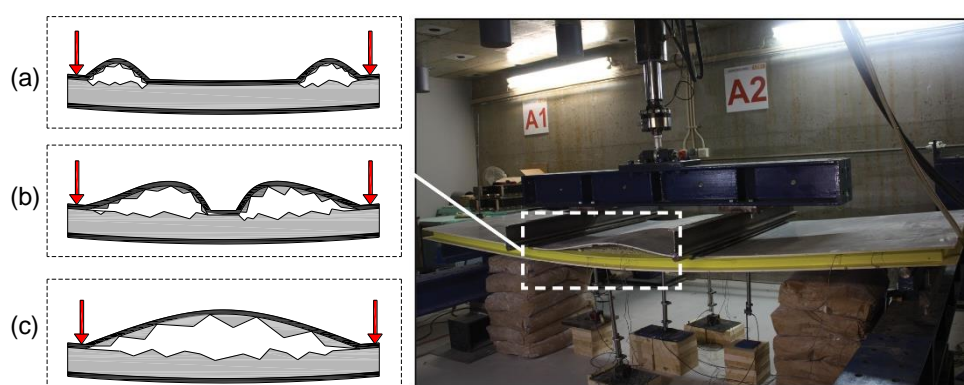
Fig. 6.15. Local instability failure mode stages in single panel up to failure: (a, b) failure mode evolution; (c) final failure mode.

A failure load of 28.47 kN was reached in the tested panel, which is much higher than the ULS load, 5.14 kN. These load levels correspond, in terms of load (maximum bending moment), to an equivalent uniform load for ULS (2.4 kN/m^2) in a four-point bending test configuration. This result is totally in accordance with the behaviour of typical sandwich panels [38, 42], which are commonly designed for mainly fulfilling service loads, being their failing state usually far from the theoretical ultimate state.

6.3 Flexural response of jointed floor composite sandwich panels

6.3.1 Experimental program

After have been submitted to uniformly distributed load, the three floor panels (FP) described in section 6.2 (FP1 to FP3) were also tested (**Fig. 6.16**a) in a two-by-two connection configuration (FP1 with FP2 and FP2 with FP3). Each pair was jointed together by two GFRP tubular profiles of $50 \times 50 \times 5$ mm^3 cross section. A test with the three panels (**Fig. 6.16**b) jointed together (FP1, FP2 and FP3) was also carried out. All these tests were undertaken under a four-point bending configuration with a shear span, a flexural span and a clear span of 850 mm, 1000 mm and 2700 mm, respectively, and according to ASTM C393 recommendations [87]. The support conditions were similar to those adopted previously in the single panel tests.

The load was transferred to the panels by means of a frame formed by a 2000 mm longitudinal metallic HEB 200 profile, to which was attached (welded) two transverse HEB 200 profiles with a length equal to the width of the jointed panels (i.e. 2000 mm for the case of two panels and 3000 mm for the case of three panels). Two-cylinder steel bars of 50 mm diameter were placed between the panel and the load transfer frame in order to apply a line load. A monotonically increase load was applied by a hydraulic jack on the panels until reaching a magnitude of 10.29 kN and 15.43 kN for the case of two and three jointed panels, respectively. These load levels correspond, in terms of load (maximum bending moment), to an equivalent uniform load for ULS (2.4 kN/m^2) in a four-point bending test configuration. A load cell of 300 kN with a precision of 0.05% was used to measure the load.

To assess the effectiveness of the connection in distributing the load amongst the jointed panels, an additional test with three jointed panels was conducted by applying the load only on the central panel (see **Fig. 6.16**c). This test configuration followed exactly the setup previously indicated. But in this case, the length of the steel cylinder placed under the HEB profiles was only 1000 mm, therefore the load is exclusively applied on the central panel.

The instrumentation used for monitoring these tests is depicted in **Fig. 6.16**d and **Fig. 6.16**e. Ten and fifteen LVDTs (with a stroke ranging from 25 mm to 50 mm) were used in the two and three jointed panels, respectively, for measuring the vertical deflection of the panels in their loaded and midspan sections. Strain gauges positioned on both skins (top and bottom),

at the midspan of the specimen were used to measure the strains developed in the GFRP skins.

Two jointed panels
Note: S1-S4 on bottom skin- S5-S6 on top skin

Three jointed panels
Note: S1-S7 on bottom skin- S8-S10 on top skin

(d)   (e)
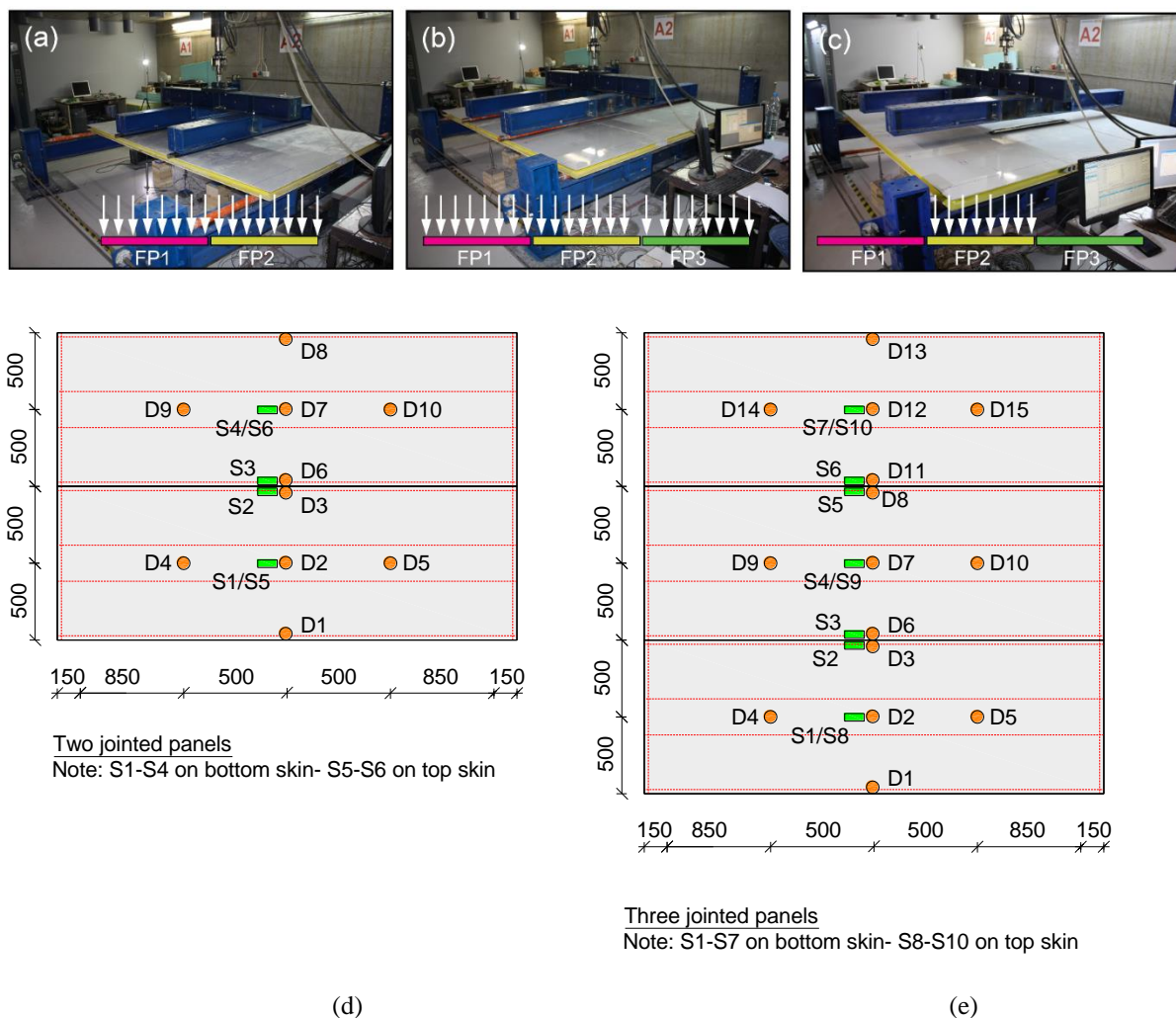
Fig. 6.16. Jointed panel flexural test: (a) two jointed panels; (b) three jointed panels; (c) connection study; (d) instrumentation for two jointed panels; (e) instrumentation for three jointed panels.

6.3.2 Results

The load *versus* midspan deflection in two and three jointed floor sandwich panels is depicted in **Fig. 6.17**a, while the load *versus* strains measured on the bottom skin is depicted in **Fig. 6.17**b. In the system formed by two jointed panels (FP1-FP2 and FP2-FP3), the plotted midspan deflection and strain were computed as the average deflection/strain of the D2, D7/S1, S4 (**Fig. 6.17**d) placed at the center of each panel. In the system formed by three jointed panels, the plotted midspan deflection and strain directly correspond to the measured deflection/strain of the D7/ S4 (**Fig. 6.16**e) placed at the center of the middle panel. The midspan deflection measured for the considered loads level was 10.58 mm and 10.40 mm for

two and three jointed panels, respectively, being the corresponding maximum load 10.29 kN and 15.43 kN, respectively.
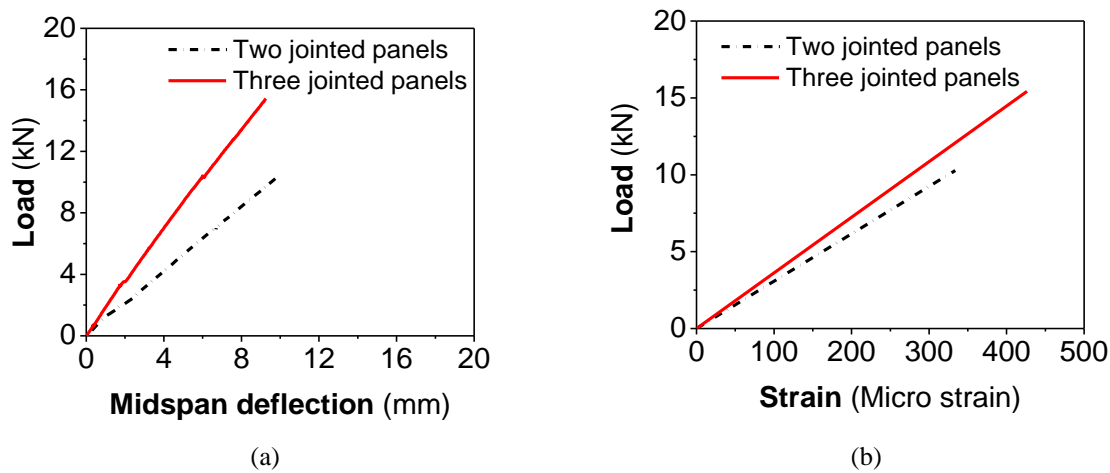
Fig. 6.17. Flexural response of jointed panels: (a) load *versus* midspan deflection; (b) load *versus* strain.

Fig. 6.18a and **Fig. 6.18**b present the deflection along the transverse direction of the midspan section of the systems formed by two and three jointed panels. As can be observed, deflection at center of the jointed panels was smaller than other points, having the highest deflection been measured in the free edges of the system formed by the jointed panels. In the case of two jointed panels, this fact can be justified by the presence of the connection profile at the middle of the panels, which considerably increases the stiffness of this zone. Similarly, in the case of three jointed panels, the connection profiles used for joining the panels are internal stiffeners, leading the middle panel has less deflection.

Moreover, the maximum strain recorded in two and three jointed panels for the ULS load was 334 με and 426 με, respectively, which are significantly lower than the ultimate tensile strain measured in the GFRP skins at material characterization (12188 με).

The effectivity of using the proposed connection system for distributing flexural loads is well demonstrated in **Fig. 6.18**c. This figure shows the deflection along the transversae direction of the midspan section of the systems formed by the three jointed panels when only the central panel is loaded. The obtained results reveal that, as expected, the highest deflection occurred in the central panel since it was the loaded one. However, the lateral panels have also deflected significantly, even their free edge, which evidences that the proposed connection system has the ability to appropriately transfer flexural loads.
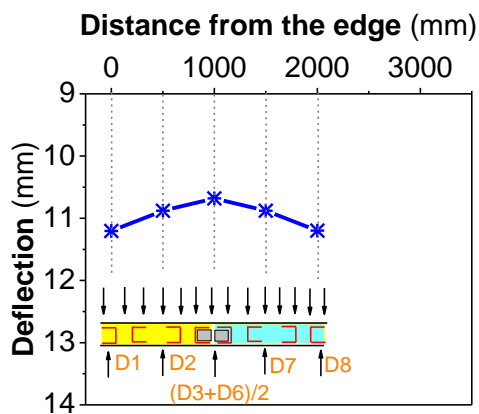
(a)
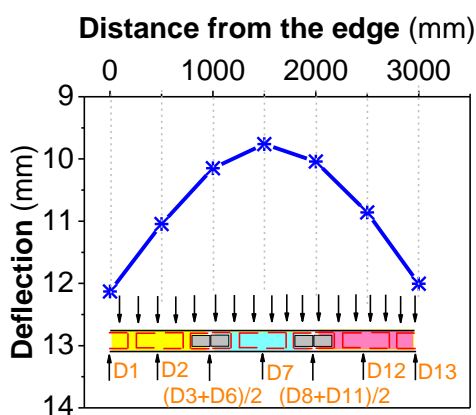
(b)
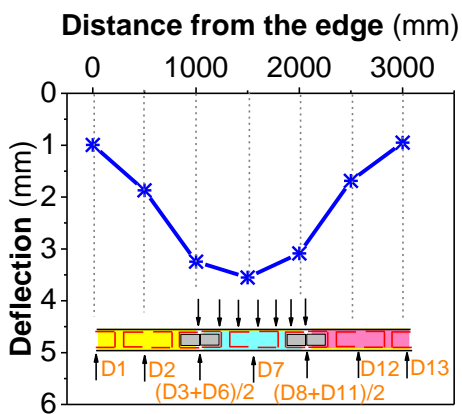
(c)

Fig. 6.18. Measured deflection in jointed panels: (a) two jointed panels; (b) three jointed panels; (c) three panels with load only in the middle panel.

6.4 Analytical assessment

The following subsections provides some theoretical prediction to permit a deeper investigation about flexural behaviour of single sandwich panels and jointed sandwich panels. The mechanical properties of the sandwich panels components established form coupon testing were employed in this investigation.

6.4.1 Service life deflection prediction

Findley power law was used to estimate viscoelastic deformation of the panel by the time, following Eq. (6.3):

$$\delta = \delta_0 + m \times t^n \tag{6.3}$$

where δ is the time dependent deflection (in mm), δ_0 is the instantaneous deflection (in mm), m is the creep amplitude, t is the time after application of load (in days), and n is the time exponent.

Power law has fitted the experimental results by using a creep amplitude of $m=0.41$ and a time exponent of $n=0.41$ in both types of the panels as depicted in **Fig. 6.19**. These parameters were obtained with a coefficient of determination (R^2) of 99%. By using Eq. (6.3) with these values for its parameters, and considering a service life of 5 years for the type of emergency applications that the prototype is designed for, a viscoelastic deformation 252% higher than the initial elastic deflection is estimated at the end of this period.

(a)   (b)
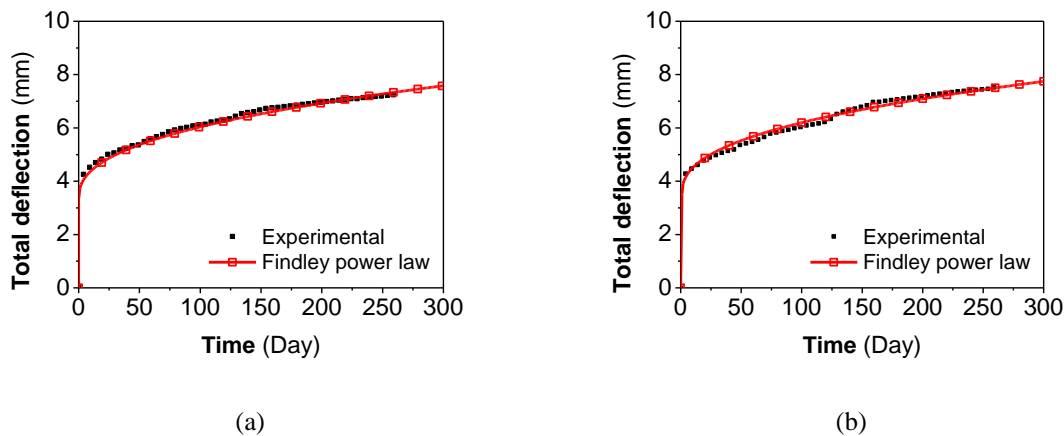
Fig. 6.19. Time-midspan deflection: (a) without end U-shape GFRP profiles (P3); (b) with end U-shape GFRP profiles (PU3).

6.4.2   Long-term deflection in single sandwich panels and jointed sandwich panels

Italian standard CNR [80] is commonly used to verify the performance of composite sandwich panels under SLS conditions. According to this code, the maximum long-term deflection (δ_{LT}) for the quasi-permanent load (equal to 30% of the service load) should be less than *L/250*. Based on this, Eq. (6.4) was proposed:

$$\delta_{LT} = \alpha \times \delta_{SLS} \times \gamma_{Creep} \tag{6.4}$$

where δ_{SLS} is the instantaneous deflection in service limit state (SLS), α is the proportion of quasi-permanent load in respect to the SLS load (i.e. 30%), and γ_{Creep} is the creep coefficient; based on the creep tests value for that coefficient was set to 2.52 (this value takes into account a service life of 5 years).

In the single panel, considering the average experimental deflection value obtained under SLS conditions (7.48 mm), Eq. (6.4) gives a value of 5.70 mm for the maximum deflection expected to be registered in 5 years. This value is lower than that required by CNR code [80] (L/250 = 2700/250 = 10.8 mm), and therefore, panels fulfil the deflection serviceability requirements.

Regarding to the jointed panels, long-term deflections of jointed panels (δ_{LT}) were also estimated with Eq. (6.4), having been obtained for the two and three panels a value of δ_{Quasi} equal to 5.37 mm and 5.28 mm, respectively. Therefore, the computed deflection fulfils the serviceability limit requirement imposed by CNR code [80] (2700/250 = 10.8 mm).

6.4.3   Failure mode of the full scale composite sandwich floor panel tested up to the failure

Interaction between GFRP skin and PU foam core can be treated using Allen's formula by invoking the concept of Winkler hypothesis [28]. In that model, the GFRP skin is modelled as infinitely long strut supported on an elastic medium (the core of the panel). Two kinds of stresses can be developed: interfacial stress (σ_{in}), and critical wrinkling stress (σ_{cr}) [31, 50, 69]. Interfacial stress is defined as:

$$\sigma_{in} = 0.07\pi^2 f(\theta)E_c \tag{6.5}$$

where θ depends of the core thickness (t_c) and half-wave length of l given by $\theta = \dfrac{\pi t_c}{l}$, E_c is the elastic modulus of the PU foam. $f(\theta)$ is a function of the core Poisson's ratio (v_c) and θ. The value of $f(\theta)$ depends on skin wrinkling mode. Three cases of skin wrinkling modes were defined [28]. Case I, represents a sandwich panel in which wrinkling occurred in the compression skin. Case II, deals with antisymmetric wrinkling and Case III, considered symmetric wrinkling. In this research Case I was considered the most appropriate since only one face skin was debonded. Accordingly, Eq. (6.6) was proposed for this purpose as:

$$f(\theta) = (\frac{2}{\theta}) \times \left(\frac{(3 - v_c) \times \sinh\theta \times \cosh\theta + (1 + v_c) \times \theta}{(1 + v_c) \times (3 - v_c)^2 \times \sinh^2\theta - (1 + v_c)^3 \times \theta^2} \right) \qquad (6.6)$$

Debonding occurs when the interfacial tensile strength (σ_{in}) exceeds the tensile strength of the PU foam core. Regarding to the critical wrinkling stress, it is determined by the following equation:

$$\sigma_{cr} = \left(\frac{E_c}{t_f} \right) \times t_c \times f(\theta) + \frac{E_f}{12} \times \left(\frac{\theta}{t_c} \right)^2 \times t_f^2 \qquad (6.7)$$

where t_f and E_f are the thickness and the elastic modulus of the GFRP skin, respectively.

In the experimental program it was observed that, the length of the debonded part was equal to the PU thickness. Based on this, interfacial tensile stress, σ_{in}, was obtained by a value of 0.77 MPa using Eqs. (6.5) and (6.6). A comparison of this value with the maximum tensile strength of PU foam core (σ_{ct}) experimentally determined of 0.49 MPa reveals that the separation between PU foam core and GFRP skin was caused by the attainment of the tensile capacity of the PU.

From Eq. (6.7) a critical wrinkling stress (σ_{cr}) of 62.64 MPa was determined for the GFRP skin. Based on strain values measured in S5 (Fig. 5b), a compressive stress value of 25.07 MPa was calculated on the GFRP skin (the value was computed assuming the modulus of elasticity experimentally recorded). Comparing the experimental and the theoretical values for the critical wrinkling stress, it can be observed that, these two values differ by a factor of nearly 2.5. This stress relation was also found in the previously performed tests [50, 89, 90].

Due to lack of predictive performance of Eq. (6.7), an empirical expression was proposed as expressed by Eq. (6.8):

$$\sigma_{cr} = 0.42 \times E_f^{1/3} E_c^{2/3} \tag{6.8}$$

By applying this equation, a critical wrinkling stress of 25.54 MPa was obtained, which is a value quite close to the one obtained experimentally (25.07 MPa), demonstrating the good predictive performance of Eq. (6.8).

6.4.4   Effects of the U-shape GFRP profiles in the sandwich panels under uniform loading

First-order Shear Deformation Theory (FSDT) may be employed to evaluate flexural performance of a single sandwich panel. In this theory, some hypotheses are assumed, such as considering the panel components are formed by isotropic materials, and assuming perfect bond between constituent components. Besides, the total deflection of the sandwich panel (δ_{Total}) can be estimated by considering the simultaneous contribution of bending and shear deformation:

$$\delta_{Total} = \delta_b + \delta_s \tag{6.9}$$

where δ_b and δ_s are the deflections due to the bending and shear, respectively. Eq. (6.9) could be expressed in the following form:

$$\delta_{Total} = \int_0^L \frac{M_u M_L}{EI} dx + \int_0^L \frac{V_u V_L}{kGA} \tag{6.10}$$

where the first and second terms of the right part of this equation provide the deflection due to bending and shear, respectively. In Eq. (6.10) the M_u (V_u) and M_L (V_L) are the bending moments (shear forces) due to a unit load and the actual load, respectively.

By developing Eq. (6.10) in terms of providing the midspan deflection of a sandwich panel subjected to a uniform loading, it is obtained:

$$\delta_{Total} = \frac{5qL_s^4}{384(EI)_{eq}} + \frac{qL_s^2}{8K(GA)} \tag{6.11}$$

where q, L_s, $(EI)_{eq}$, (GA) and K are the uniform distributed load, span length, equivalent flexural stiffness, shear stiffness and shear correlation factor, respectively. The coefficient K was assumed equal to 1.0 in this study [91]. For the present sandwich panel, the equivalent flexural stiffness is obtained by the following equation:

$$(EI)_{eq} = bE_f \left[\frac{t_f^3}{6} + 2t_f \left(\frac{t_f}{2} + \frac{t_c}{2} \right)^2 \right] + \frac{nE_U}{12} \left[b_u t_c^3 - (b_u - t_u)(t_c - 2t_u)^3 \right] \qquad (6.12)$$

where b is the width of the panel, n is the number of the U-shape GFRP profiles (both located in the interior of the panel and at the edges), and E_U, t_u, b_u are the Young's modulus, thickness and width of those profiles, respectively.

The midspan deflection obtained from Eq. (6.11) and measured experimentally is compared in **Table 6.3**. A very good agreement between experimental and analytical values is observed, showing an adequate precision of FSDT in estimating the total deflection of the sandwich panels.

Table 6.3. Results obtained in the flexural test performed on single composite sandwich floor panels.

		δ_{Total} (mm)	
		SLS	ULS
Experimental	FP1	7.25	11.17
	FP2	7.73	11.22
	FP3	7.50	11.35
	FP4	7.45	11.20
	Average	7.48	11.23
Analytical	Flexural deflection	7.20	10.90
	Shear deflection	0.23	0.35
	Total deflection	7.48	11.21

Fig. 6.20 shows the influence of the number of U-shape GFRP profiles (n) on the midspan deflection of the sandwich panel, having been adopted values of n varying from 0 to 4. As can be observed, when deflection is computed for a panel without U-shape GFRP profile ($n = 0$) and for a panel with one U-shape GFRP profile ($n = 1$), a sudden decrease in the deflection of nearly 42% takes place. By using more than one U profile, the total deflection tends to decrease almost linearly with the increase of the number of GFRP profiles. Moreover, the relative contribution of bending (M) and shear (V) on the total deflection (indicated on the top right corner of **Fig. 6.20**) shows that the contribution of the shear deformation decreases with the increase of the number of GFRP profiles applied. When GFRP are not applied ($n=0$) the contribution of bending and shear for the total deformation is 60% and 40%, respectively, while when four GFRP profiles are adopted this relative contribution is 97% and 3%. Thus,

for the panel designed, the dominate deformation is flexural and not shear, since four U-shape GFRP profiles were used in each panel (two interior and two at edges) that are working as ribs, providing high shear stiffness (GA) to the panel.
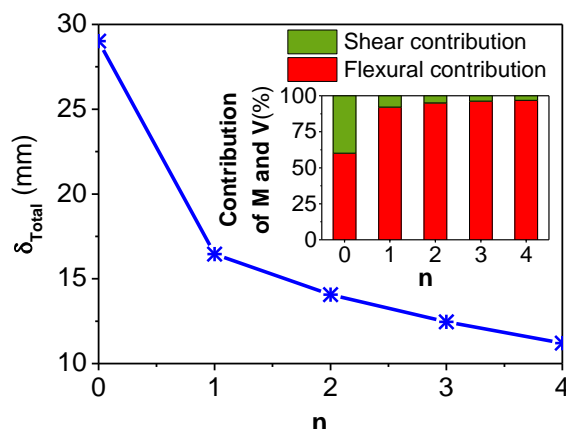
Fig. 6.20. Effect of the number of U-shape GFRP profiles on the total deflection of the sandwich panel.

The load-deflection behaviour of the tested single sandwich panel under four-point bending test configuration was also analytically determined by using FSDT and considering the same assumptions. Eq. (6.13) gives the total deflection for a four-point load configuration:

$$\delta_{Total-4PBT} = \frac{Pa}{(EI)_{eq}}\left(\frac{L_s^2}{8} - \frac{a^2}{6}\right) + \frac{Pa}{KGA} \tag{6.13}$$

where P is the applied line load, L_s is the span (equal to 2700 mm), a is the shear span (equal to 850 mm), $(EI)_{eq}$ is the equivalent flexural stiffness determined according to Eq. (6.12) (159.30 kN.m^2), and GA is the shear stiffness (6147.4 kN). By adopting these values, a midspan deflection of 62.01 mm was calculated, which is in good agreement with the experimental result, since the difference is 1.60 %.

6.4.5 Efficiency of the proposed connection system between panels

The Eqs. (6.12) and (6.13) were also applied to predict the midspan deflection of the jointed panels), and the results are presents in **Table 6.4** , which also include the flexural and shear stiffness values. Additionally, analytical results of a continuous slab (a slab formed by the same number of U-shape GFRP profiles as the jointed panels but assuming continuity between the panels) as depicted in the **Fig. 6.21,** with the same dimensions and configuration

of the jointed panels were obtained in order to evaluate the efficiency of the proposed connection.
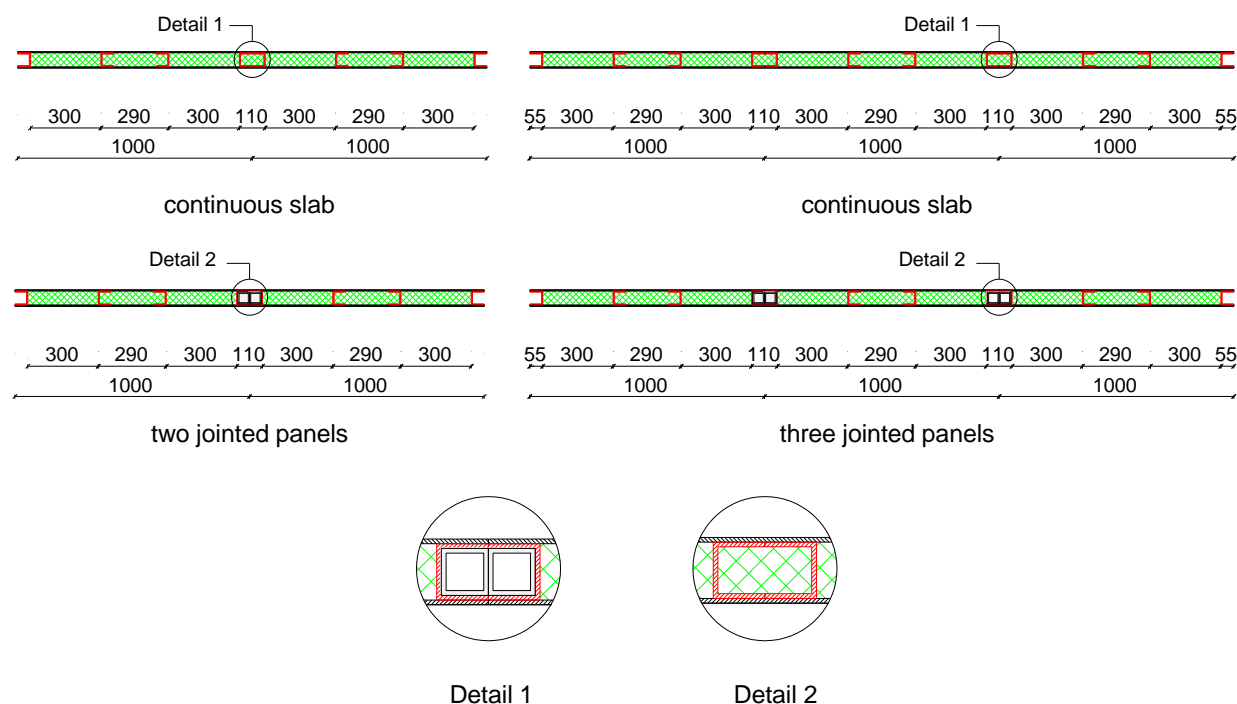
Fig. 6.21. Schematic of jointed panels and continuous slabs.

The results of **Table 6.4** indicate an acceptable predictive performance for the analytical expressions, since a relative difference of 2.15 % and 2.40 % for the, respectively, two and three jointed sandwich panels, was obtained. Comparison of analytical values between jointed panels and a continuous slab shows that using the proposed connection system results in decreasing the midspan deflection in 7.17% and 9.48% for two and three panels, respectively. This is the consequence of the influence of using the connector profile, which increases the flexural stiffness and shear stiffness of the jointed panels.

Table 6.4. Flexural response of jointed panels and continuous sandwich slab

	Jointed panels				Continuous slab		
	Panel's properties		Midspan deflection		Panel's properties		Midspan deflection
	EI (kN.m^2)	GA (kN)	Exp. (mm)	Anal. (mm)	EI (kN.m^2)	GA (kN)	Anal. (mm)
Two jointed panel	325.60	16494.80	9.79	10.88	305.90	12294.80	11.66
Three jointed panel	498.20	26842.30	9.25	10.65	458.90	18442.30	11.66

6.5   Numerical simulations

Nonlinear three-dimensional finite element (FE) models were developed to simulate the behaviour of a single panel, two jointed panels and three jointed panels. These models were developed considering all the geometrical and material information gathered in the physical models and the experimental tests described in the previous section. The FE simulations were developed using the commercial software ABAQUS v6.12 [92]. A nonlinear static analysis enabling geometric nonlinearities based on the direct Full Newton-Raphson Technique was used to run the simulations.

6.5.1   Finite element, mesh description, boundary condition and loading

All sandwich panel constituents, i.e. GFRP skins, PU foam core, GFRP U-shape profiles and GFRP connection profiles, as well as the frame components (GFRP beams and columns), were modelled using 3D hexahedral deformable solid elements, with 8 nodes and 3 degree of freedom per node (C3D8). After some preliminary analyses, it was found that elements with an approximate size of 50 mm of side were optimal in terms of accuracy, convergence and computational time of the simulation. A schematic representation of the developed finite elements models is represented in the **Fig. 6.22**.

Due to the symmetry of panels and loading conditions, and with the aim of reducing time of analysis, only one quarter of the structure was simulated in the case of the single panel and the jointed panels (see **Fig. 6.22**). Corresponding boundary conditions in the symmetry planes were applied, as well as a roller support condition at the end of the panels, under the bottom skin. In order to simulate the 4PBT configuration, a vertical displacement was imposed to the nodes positioned along a loading line located similarly to the experimental tests.

6.5.2   Constitutive models and interaction between the different panel components

Constitutive relations towards material behaviour of sandwich panel components were adopted according to the performed material characterization tests. The GFRP skins have a quasi-isotropic lay-up, so isotropic linear elastic material with an elastic modulus of 9.60 GPa, Poisson's ratio of 0.3 and ultimate stress of 117 MPa were used to represent the mechanical behaviour of the GFRP skin. The GFRP pultruted profiles were modelled assuming linear-elastic orthotropic material properties with an elastic modulus of 28 GPa and ultimate tensile stress of 415 MPa in the parallel to the fibre direction (longitudinal direction),

and elastic modulus of 13 GPa and ultimate tensile stress of 180 MPa in the perpendicular to the fibre direction (transversal).

Based on equations previously developed by other authors [93], the crushable foam core model was selected to represent the mechanical behaviour of the PU foam core by attributing to the shear modulus, the elastic modulus and the elastic-plastic constitutive relation with a compressive stress being of 3.15 MPa, 6.3 MPa and 0.30 MPa respectively.

Interaction between all adherent surfaces belonging to a panel (i.e. interfaces between PU and GFRP skins, PU and U-shape GFRP profiles, and GFRP skins and U-shape GFRP profiles) were modelled as cohesive [94]. The generalized cohesive-behaviour of ABAQUS package was used. This is a surface-based cohesive behaviour defined by a traction-separation law (**Fig. 6.23**a). The model considers linear-elastic behaviour until reaching a certain value of interface stresses (t) and surface separation (δ). Afterwards, initiation and evolution of damage occur.
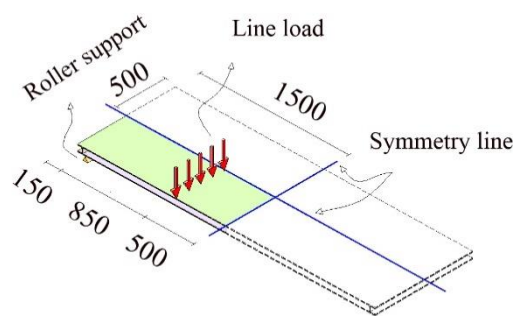
One-quarter single panel
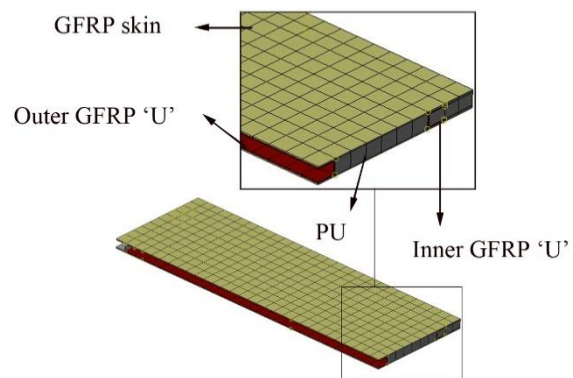
Single panel colse-up
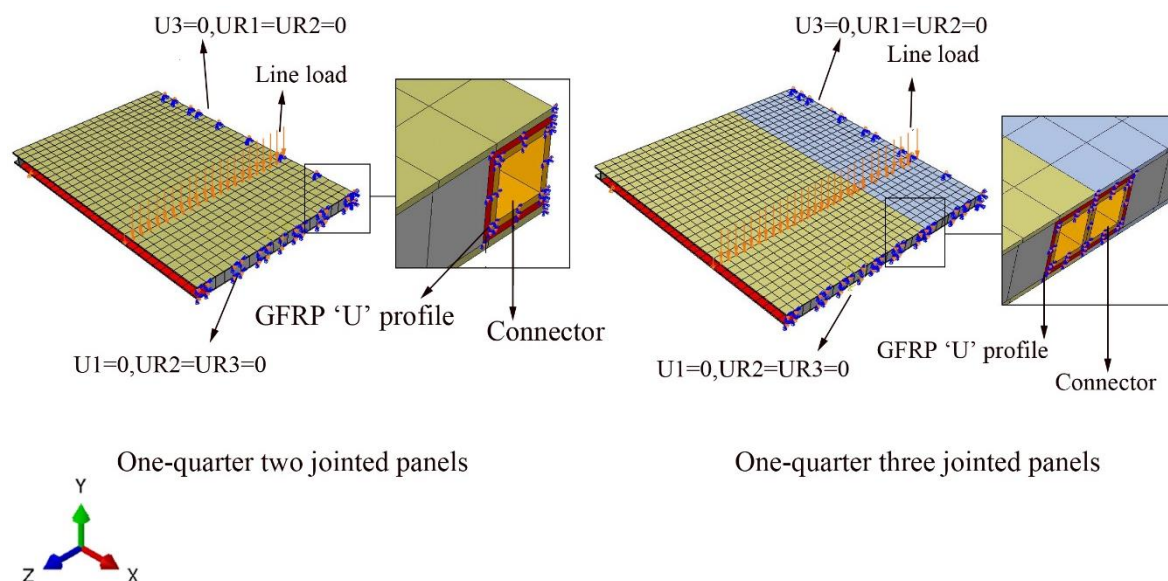
Fig. 6.22. FE models details.

The elastic behaviour of the model is written in terms of two components: $[k]$, an elastic constitutive matrix that relates normal and shear stresses to $[\delta]$, the normal and the shear separations across the interface. Thus, surface separation (δ) is computed by Eq. (6.14):

$$[t] = [k][\delta] \tag{6.14}$$

Associated cohesive elements contain three components (**Fig. 6.23**b): two shear forces parallel to the plan of interaction (s_1 and s_2) and a normal force (n) to the interaction plane. Accordingly, Eq. (6.14) could be written in the form of Eq. (6.15):

$$\begin{bmatrix} t_n \\ t_{s_1} \\ t_{s_2} \end{bmatrix} = \begin{bmatrix} k_{nn} & k_{ns} & k_{ns_2} \\ k_{ns_1} & k_{s_1 s_1} & k_{s_1 s_2} \\ k_{ns_2} & k_{s_1 s_2} & k_{s_2 s_2} \end{bmatrix} \begin{bmatrix} \delta_n \\ \delta_{s_1} \\ \delta_{s_2} \end{bmatrix} \tag{6.15}$$

In the simulation, an uncoupled behaviour was assumed between the tractions and separations. This means that the stress in the normal direction did not result in a separation in the shearing directions. Consequently, shear stress did not lead to any separation in the normal direction. Therefore, in the stiffness matrix $[k]$ the off-diagonal components (k_{nn}, k_{ss} and k_{tt}) were considered to be zero.
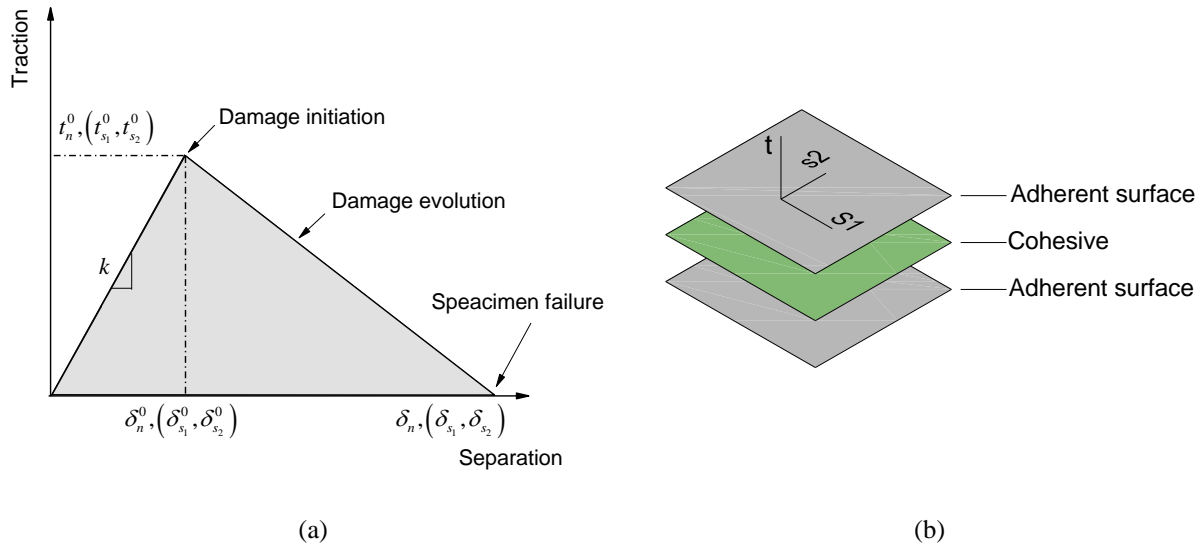
Fig. 6.23. Cohesive behaviour simulated: (a) traction-separation response; (b) cohesive element.

Degradation of bond between the two adherent surfaces is simulated with a damage model. Initiation of damage was defined by a stress based traction separation law, and it was assumed that failure mode corresponds to an "opening" (see **Fig. 6.24**), according Westergaard [95]. No mode-mixity was took into account for simplicity. Consequently, damage initiated in the model when the maximum contact stress ratio reached one of the maximum values presented [96] by Eq. (6.16):

$$\max\left[\frac{\langle t_n \rangle}{t_n^0}, \frac{t_{s_1}}{t_{s_1}^0}, \frac{t_{s_2}}{t_{s_2}^0}\right] = 1 \tag{6.16}$$

where t_n is the normal stress; t_{s_1} and t_{s_2} are the shear stresses (in planes s_1 and s_2); and t_n^0, $t_{s_1}^0$ and $t_{s_2}^0$ represent the peaks for normal stress and shear stresses (in planes s_1 and s_2), respectively. It must be mentioned that $\langle \rangle$ representing Macauluny bracket.
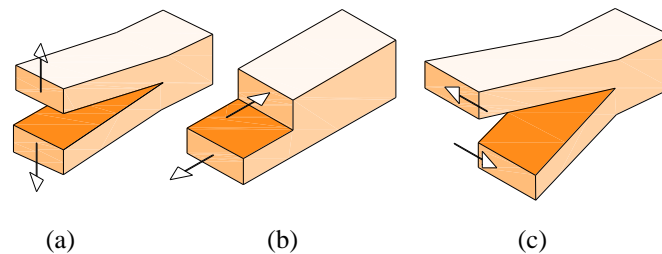
Fig. 6.24. Failure modes: (a) opening; (b) sliding; (c) shearing

Since direct pull-test in the material characterization test (Chapter 4-sec 4.5) showed that the stiffness degradation between GFRP skin and the PU foam core was due to failure of the foam itself, the peak values were substituted by the maximum tensile strength and shear strength of the foam core, as indicated in **Table 4.1.** It is worthwhile mentioning that, since the mode-mixity was not presumed in this simulation, hence defining the shear stress value did not have any influences on type of simulation (even though ABAQUS require those values [97]).

Finally, a damage evolution law was defined. For the evolution of the initiated damage, an energy based approach with a linear softening law was utilized. A fracture energy of 0.025 J/m^2 was adopted for the simulations.

Two types of failure criteria were taking into account to determine the failure of a panel: a stability failure based on skin outward or inward wrinkling, and the sandwich panel constituent materials failure. The first failure was identified when detected a sudden change in the stiffness due to the degradation of integrity between the sandwich panel components. The material failure was identified by controlling strain and stress in each component.

6.5.3   Panel-panel connections

Connections between panels and with panels and beams were modelled with interfaces, assuming a non-perfect connection. Behaviour in normal direction was modelled as "hard" contact in ABAQUS [92], meaning that no penetration was allowed between the two surfaces and there was no limit to the magnitude of contact pressure transmitted when the surfaces were in contact. Behaviour in tangential direction was modelled by the classical Coulomb friction law, but without any contact cohesion. A trial and error calibration of the model against the experimental results led to set the friction coefficient equal to 0.10.

6.5.4   FE results

6.5.4.1 Single panel up to failure

Fig. 6.25a shows the load-midspan deflection curve obtained from the FE simulation plotted against the experimental result, while the load-strain response in the GFRP skins, at the middle of the panel registered experimentally and numerically is showed in **Fig. 6.25**b. A very good match is observed between the numerical results obtained by the FE model and the experimental ones.

(a)

(b)
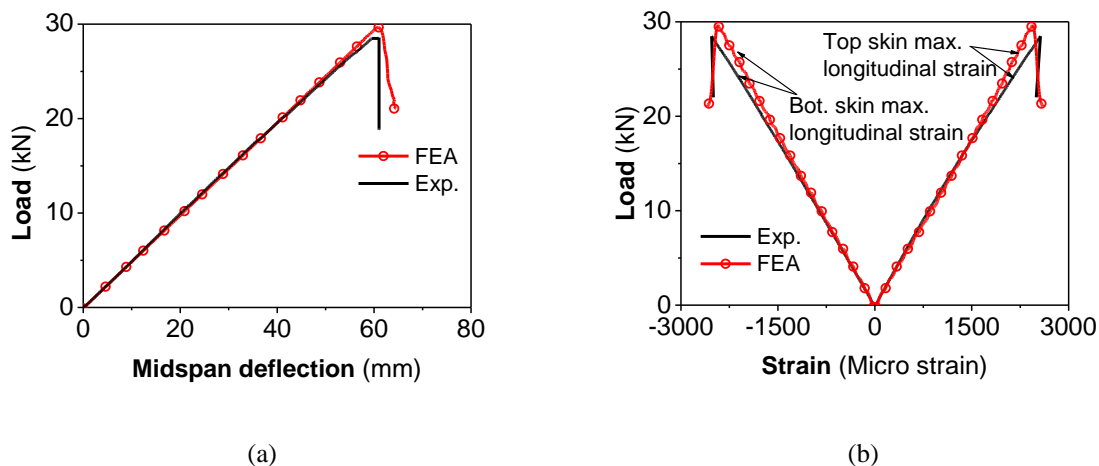
Fig. 6.25. Experimental *versus*. FE simulation of single sandwich panel: (a) load-midspan deflection; (b) load-strain.

From **Fig. 6.25**, it can be deduced that, the FE model accurately captured the single sandwich panel's flexural behaviour. The panel failed at a maximum load of 28.47 kN (29.66 kN in the FE model) registering a midspan deflection of 61.02 mm (60.83 mm in the FE model) with a linear behaviour prior to the abrupt failure. Experimentally, failure was caused by a localized debonding between the GFRP compression skin (top skin) and the PU foam core (**Fig. 6.26**a). The failure occurred in the region of maximum flexural moment, between the two line loads [50]. This phenomena known as local instability, or wrinkling failure mode of sandwich panel, leads to a sudden outward buckling of the GFRP skin in the compression side [28, 31, 88]. Similar failure mode was predicted by the FE model (**Fig. 6.26**b), and was the result of exceeding out-ward tensile strength at the interface between the GFRP skin and the PU foam core (i.e. failure criteria implemented in traction-separation law).

(a)

(b)
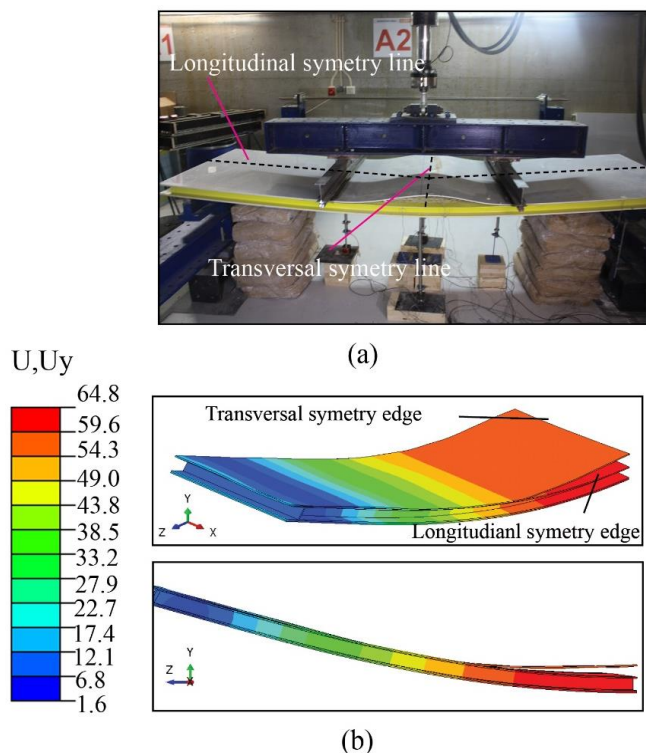
Fig. 6.26. Single panel failure mode: (a) experimental; (b) FE predicted (units in millimeters).

6.6   Parametric study and analysis

Parametric studies are carried out in this section by using the FE models developed and validated, to delve into the mechanical behaviour of single sandwich panel as well as jointed sandwich panels. In all simulations constitutive material models and properties were equal to those previously indicated in section 6.5. Besides, loading and boundary conditions were the same as those mentioned above for a single panel, two and three jointed panels.

(a)

(b)
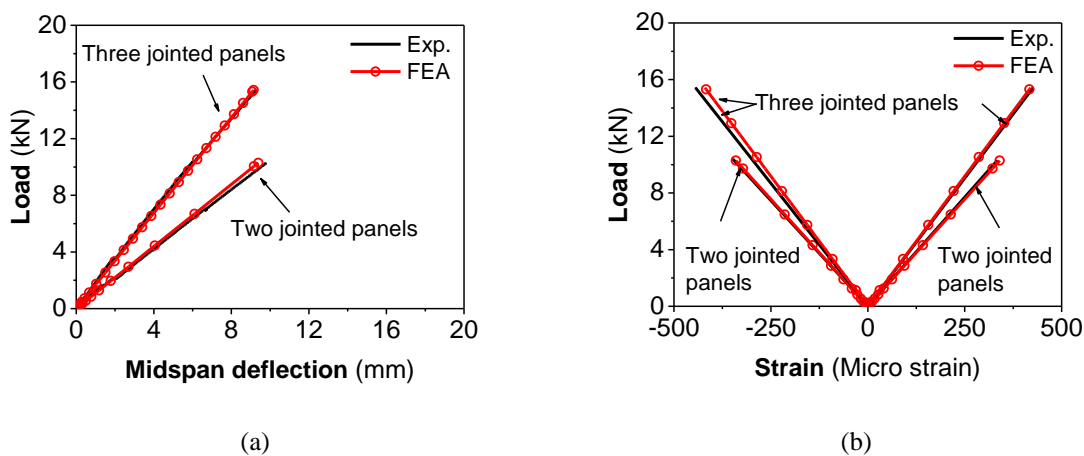
Fig. 6.27. Experimental *versus* numerical results of jointed panels subjected to ULS loading: (a) load versus midspan deflection ; (b) load versus strain.

6.6.1 Influence of the U-shape GFRP profiles

Considering a single sandwich panel with the same geometry as indicated previously, two new cross-sections were proposed according to **Fig. 6.28**: (i) "U_3" section, in which instead of four U-shape GFRP profiles, the panel was composed by the two outer U-shape profiles and one inner of U-shape profile; and (ii), "U_2" section, with only the two outer U-shape profiles.
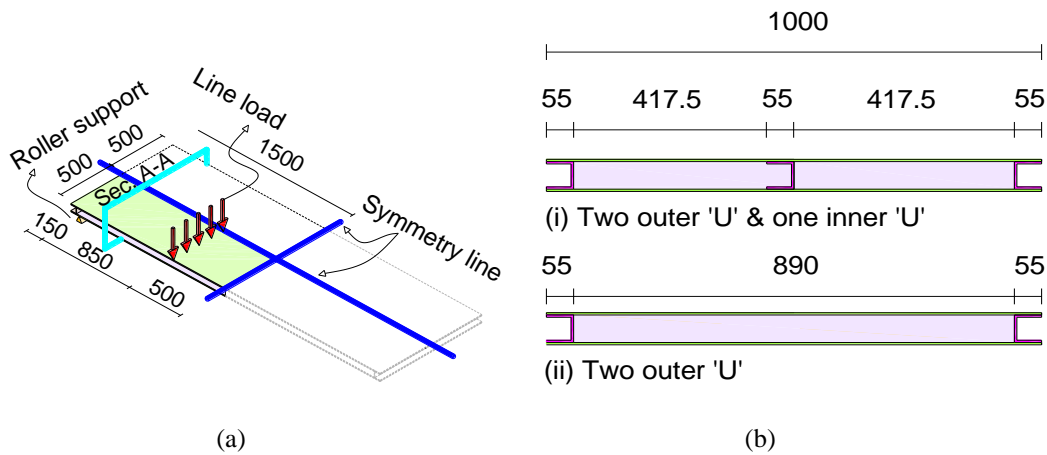
Fig. 6.28. Parametric study about flexural behaviour of single panel: (a) geometry and loading condition; (b) cross-section A-A.

Results of the new simulations for a single panel and jointed panels under a four-point bending test configuration in ULS loading are plotted in **Fig. 6.29** and expressed in terms of the maximum midspan deflection *versus* the numbers of U-shape profiles. A similar pattern was observed for the three considered cross sections (U_4, U_3 and U_2) in both the single panel and the jointed panels. It was noticed that, decreasing the numbers of U-shape profiles had a linear consequence in increasing maximum midspan deflection. In this case, decreasing the numbers of U-shape GFRP profiles from 4 to 3 and 2, leads to an increase in the maximum midspan deflection (thus decreasing stiffness) in about 10% and 20%, respectively.
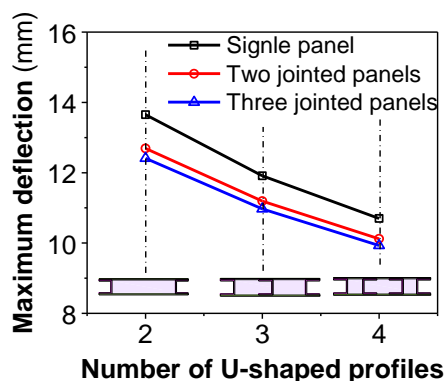
Fig. 6.29. Parametric study with U-shape profile variation in single panel and jointed panels.

6.6.2 Connection effectiveness

In order to interpret effectiveness of connection in increasing flexural stiffness of jointed panels, a continuous panel was simulated (without joints). The continuous panels were assumed having the same dimensions, loading conditions and U-shape profiles of the jointed panels. The unique difference of continuous and jointed panels is restricted to the presence of the joint in the jointed panels, since this joint does not exist in the continuous panel.

Linear-elastic relation between maximum midspan deflection and applied loads was found in both jointed and continuous panels. Based on that, the flexural stiffness was calculated as a slope of the load-deflection curve. The obtained flexural stiffness for the two and three jointed panels was 1095.84 N/mm and 1686.34 N/mm, while the flexural stiffness of the corresponding continuous panels was 1051.07 N/mm and 1568.09 N/mm, respectively. It is then possible to conclude that in the two jointed panels and three jointed panels the presence of the connector caused an increase of the flexural stiffness by a factor of 1.04 and 1.07, respectively.

6.7 Conclusions

Based on the experimental, analytical and numerical research carried out for different sandwich panels typologies, the following main concluding remarks can be drawn.

- In the small scale failure tests, fairly linear behaviour was observed for all specimens tested. In specimens with end U-shape GFRP profile, small reductions in the stiffness was noticed due to debonding of the lower GFRP skin. However, it was identified that

the presence of this GFRP profile had not significant effect in the flexural strength and stiffness;

- Shear failure of the core was the mechanism governing the behaviour of the specimens tested without end U-shape GFRP profile. On the other hand, the panels with end U-shape GFRP profile have failed due to the debonding between the bottom face of the GFRP profile and the GFRP bottom skin, followed by an abrupt formation of a tensile fracture surface on the core materials due to its low tensile strength;

- Long-term behaviour of proposed composite sandwich panels was studied with two support conditions: (i) with end GFRP 'U' profile, (ii) without that profile. Support conditions were found not have any influence for the creep behaviour of the panels since both panels presented the same viscoelastic behaviour. Findley power law was capable of fitting and predicting the maximum deformation of the panels after five years, which is 2.5 times higher than initial elastic deformation;

- For the load level considered, which is representative of a building structure, the sandwich panels presented an elastic linear behaviour. Their maximum deflection under service loads, taking into account the viscoelastic behaviour, fulfils the requirement established by the actual design standard;

- Ultimate carrying capacity of sandwich panels is substantially greater than the design demand levels. Failure occurs due to a local outward buckling known as wrinkling. The failure has started when outward tensile strength between skin and core has attained. The debonding propagates towards the centre of the panel leading to a loss of integrity between GFRP skin and PU foam core. A theoretical prediction employing Winkler hypothesis and utilizing mechanical properties of the constituent materials has shown that a critical wrinkling stress occur which leads panel to failure;

- Behaviour of jointed two and three sandwich panels exhibited adequate flexural performances and fulfilled the requirements in both SLS and ULS, in terms of deflection and strain. Moreover, the proposed connection system has demonstrated its effectiveness in transferring loads between the panels, guaranteeing deformation compatibility. Additionally, it was observed that using a connector in two and three jointed panels resulted in decreasing middle span deflection when compared to a continuous panel of equivalent dimensions;

- Experimental results and analytical predictions of the midspan deflection based on FSDT equations were compared. A very good agreement was observed, showing an

adequate precision of the FSDT in estimating the total deflection of the sandwich panels;

- The importance of using U-shape GFRP profiles inside the sandwich panels as ribs for increasing the flexural stiffness of the panel is clearly observed. In the panel without any rib, an analytical analysis showed that the contribution of flexural and shear deformation is about 60% and 40%, respectively. Conversely, when the number of ribs increased, the shear deformation contribution to the total deflection decreased. The amount of decreasing was obtained by a value of around 7% per rib.

- Nonlinear three-dimensional finite element models were developed to simulate the behaviour of a single panel up to failure. A very good agreement was observed between the numerical results and those obtained by the FE model. The model showed to be capable of predicting the behaviour of the sandwich panels under designed load;

- In the simulations of single panel, two jointed panels and three jointed panels with two, three and four U-shape GFRP profiles it was verified that, under ULS loading conditions, the midspan deflection has increased about 10% and 20% when the number of U-shape GFRP profiles has decreased from 4 to 3 and from 4 to 2, respectively;

- Effectiveness of connection in increasing flexural stiffness of jointed panels was investigated by comparing experimental results of jointed panels under ULS loading and by simulating continuous panels. It was concluded that in two and three jointed panels, the presence of connector caused an increase of the flexural stiffness by a factor of 1.04 and 1.07, respectively.

Chapter 7: Axial performance of jointed sandwich wall panels

7.1 Introduction

The investigations conducted pertain to individual sandwich panels submitted to axial loading. Joining composite sandwich wall panels introduce a different challenge level, and may lead to distinct behaviour. This chapter intends to assess the structural behaviour under concentric axial loads of both single and double composite sandwich wall panels, composed of GFRP skins and PU foam core, that are connected by an innovative system. Aspects related to assembly and disassembly, as well as ease of integration in the production line, were also considered. For this purpose, the structural performance of single sandwich wall panels, and two connected panels under concentric axial loading was experimentally investigated. Finally, an analytical investigation was performed to determine the axial capacity and stresses associated with various failure modes, both in single panels and two jointed panels.

7.2 Problem statement and technical considerations

Different techniques for connecting FRP panels in modular housing system applications are documented in the literature. Some of these techniques are depicted in **Fig. 7.1.** For instance, 'Z'-shape adhesively connected techniques (**Fig. 7.1**a) have been employed for connecting sandwich panels in the rehabilitation of building floors [74] and in bridge decks [75]. The main problem of this connection in modular systems is the need of adhesive for assembling the two components. Using adhesive requires time for curing and specific treatment, which increases the time of construction and requires suitable temperatures for the curing process. Additionally, it is fairly difficult to only replace one panel because all the panels are adhesively jointed. In this case, it might be necessary to replace the entire jointed panel, which can be a relatively expensive process. Scarfed and stepped overlap joints (**Fig. 7.1**b)

present the best performance among bonded joints [76]. However, this type of connection results in higher complexity in the production lines and, consequently, increases the price of the produced panels. Male-female connections (**Fig. 7.1**c) have been used in bridge applications [72, 77, 78]. In spite of providing integrity between panels and loading-transfer efficiency of the formed deck, these panels need to be placed horizontally by employing specific instruments, such as hydraulic jacks, which is a time consuming and expensive process. The use of this technique in building applications seems to be a more demanding procedure due to spatial limitation [74]. Tongue and groove mechanisms (**Fig. 7.1**d) are used in bridge deck applications [73]. The transportation of these panels must be undertaken very carefully. If a small part is damaged, the entire panel needs to be replaced. In addition, the integration of this system in production lines appears to be a major challenge.

GFRP rib | Adhesive
Stepped lap joint
Scarf joint

(a)   (b)

Mirrored unit
Dual cavity beam unit
Adhesive bond line

(c)   (d)
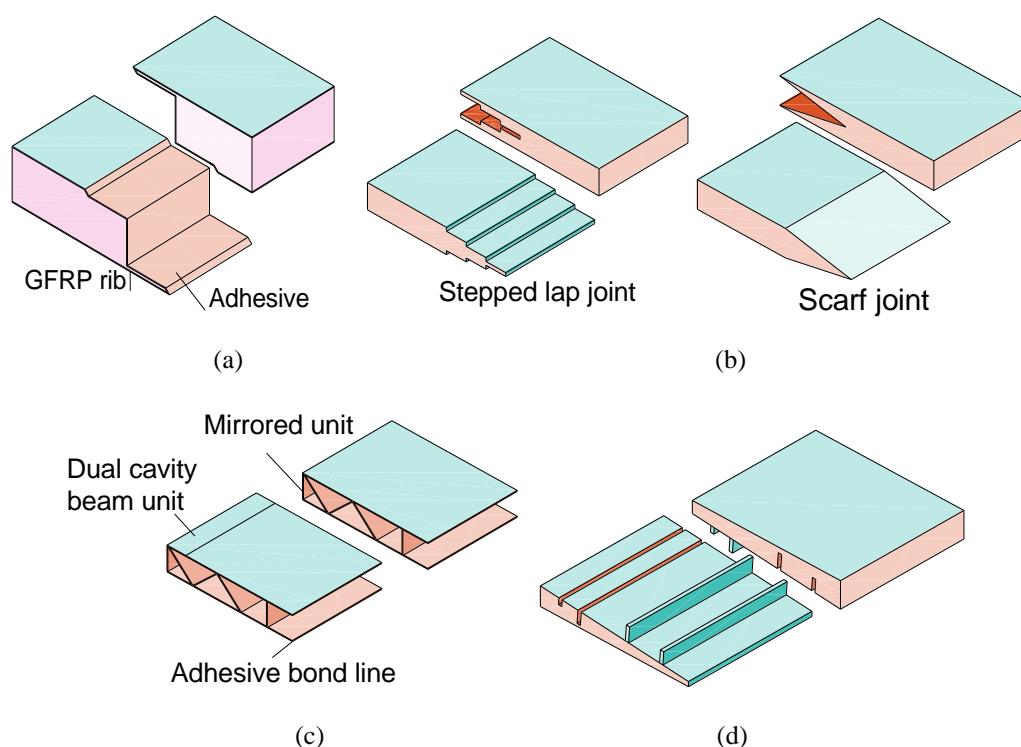
Fig. 7.1. Various types of the jointing sandwich panels techniques: (a) Z-shape; (b) stepped and scarf; (c) male-female; (d) tongue and groove.

In the present work, an interlocking technique is proposed for the connections. Different criteria were considered in the development of this system, namely: (i) to ensure adequate integrity and load transfer efficiency between jointed components; (ii) to guarantee practical assembly in confined spaces; (iii) to provide rapid installation of the panels with non-skilled manpower; (iv) to facilitate an easy integration in production lines; (v) to include a

disassembling system for repairing or replacing purposes and (vi) to provide functional and efficient connections by adjoining entire wall panels to roof elements.

A common sandwich panel made of two outer skins and an interior core (**Fig. 7.2**a) was adopted in the present work. Previous investigation indicated that using high strength material for the skin was not necessary [61] and that foam material exhibited good insulation characteristics [38], therefore, GFRP and PU foam core were chosen to form the main structure of the wall panels in this study.

The panels were designed to have the capability of joining together along their length and width (longitudinal and transversal directions, respectively) to other elements such as beams or columns, using two kinds of pultruded profiles: (i) GFRP pultruded 'U' profiles installed along the edges of the wall panels during the manufacturing process (see **Fig. 7.2**b); (ii) tubular pultruded GFRP profiles (designated as connectors) placed inside the GFRP 'U' profile during the assembly process (see **Fig. 7.3**c).

The sandwich wall panels were devised to be easily assembled in this system. After installing the first wall panel, the longitudinal connector is placed inside the corresponding GFRP 'U' profile, and, subsequently, another wall panel can be attached to this connector by sliding (**Fig. 7.3**d). The key manner to integrate the two wall panels is based on the mechanical interlocking of 'U' profiles with the tubular connector.

The connection between two wall panels and the beams form the main structural system of the construction, which is represented in **Fig. 7.3**e. In this respect, the first wall panel slides along the transversal GFRP tubular connector (that was previously attached to the beam or roof elements) up to its target position. After placing the first wall panel into position, a longitudinal GFRP tubular connector is placed into the corresponding GFRP 'U' profile. Finally, another panel slides along the transversal GFRP tubular connectors, being connected to the previous one.
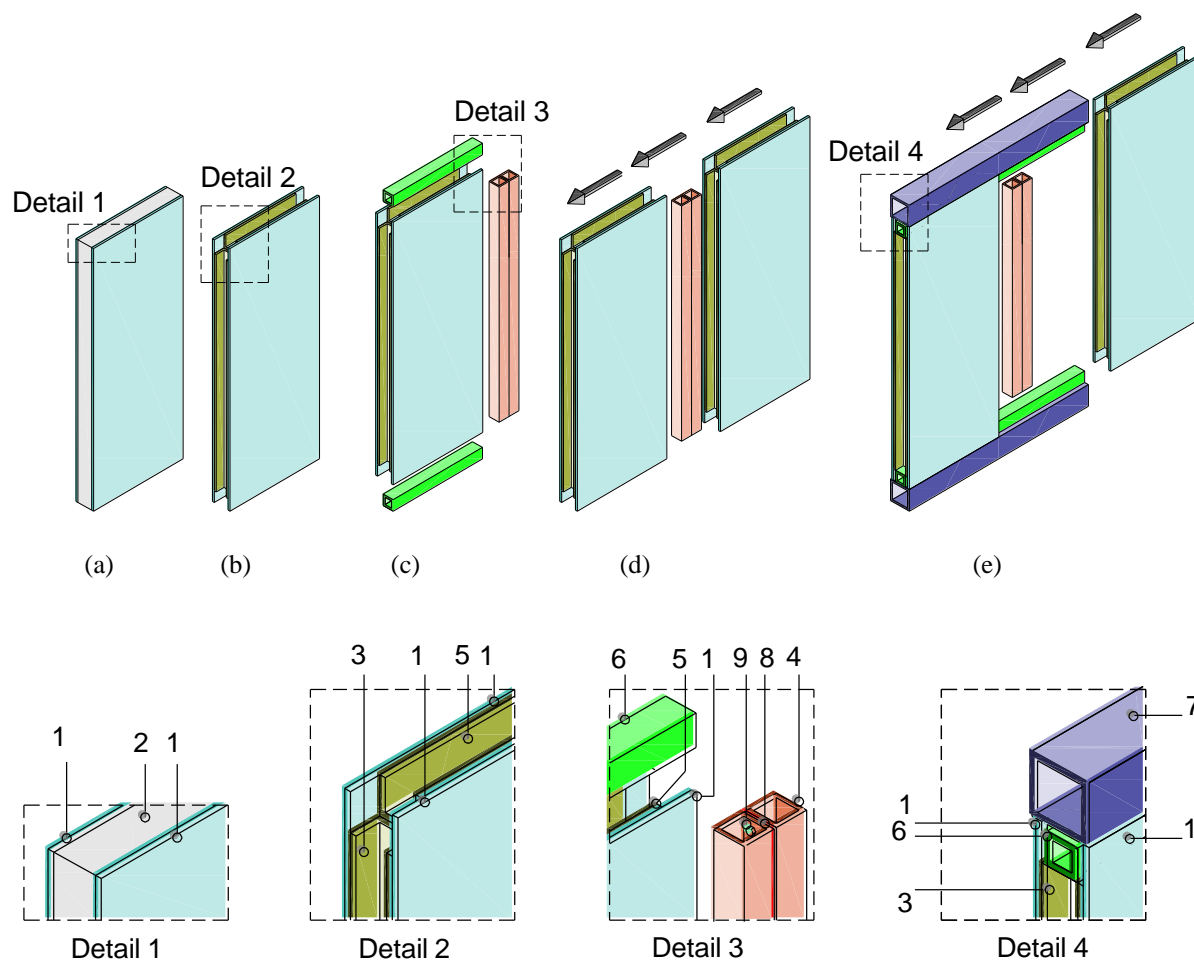
Legend: (1) GFRP skin; (2) foam core; (3) longitudinal GFRP U profile; (4) longitudinal GFRP tubular connector; (5) transversal GFRP U profile; (6) transversal GFRP tubular connector; (7) beam element; (8) adhesive layer; (9) M8 steel bolt.

Fig. 7.2. Schematic of sandwich wall panels: (a) common sandwich wall panel; (b) Sandwich wall panel with sub-connector GFRP U profiles; (c) sandwich wall panel with longitudinal and transversal GFRP U profile and GFRP tubular connector; (d) longitudinally connecting wall panels; (e) connecting panels together and into beam element.

7.3   Specimen description

Six sandwich wall panels, designated as WP1 through WP6, were manufactured using hand-layup technique. The GFRP skins have a thickness of 2 mm and were produced using dry glass fibres impregnated with an isophthalic polyester resin. PU foam blocks with a thickness of 60 mm and a nominal density of 48 kg/m^3 were used to form the sandwich panel core. These blocks were bonded to the skin with polyester resin. With these characteristics, the designed prototype fulfils thermal insulation performance demands for housing in terms of U-value [W/m^2 °C] which must be between 0.4 and 1.4 W/m^2 °C. Comprehensive information about manufacturing process and mechanical properties of utilized materials can be found in CHAPTER-3.

Sandwich wall panels present an overall thickness of 64 mm, a width of 960 mm and a height of 2880 mm. Each panel's weight was approximately 42±2 kg, making them easy to transport and install on-site. In this investigation, GFRP 'U' profiles with dimensions of $60\times55\times5$ mm^3 were adhesively bonded to the skins and PU foam core around the edges of the panels during the manufacturing process. The two GFRP pultruded tubular square profiles ($2Q50\times50\times5$ mm^3), with a length of 2700 mm, are considered as longitudinal connectors. These two profiles were bonded together with polyester resin and eight mechanical fasteners (M8 steel bolts), as shown in the Detail 3 of **Fig. 7.2**.

7.4 Experimental program

Four tests of both single and jointed wall panels were carried out, using WP1 and WP2 as single wall panels, and series WP3+WP4 and WP5+WP6 as jointed wall panels. These tests intend to identify the failure modes, evaluate the developed strains on the skins, assess the maximum axial loading capacity, and determine the maximum in-plane and out-of-plane deflection. Additionally, the tests with the jointed panels aim to verify the efficiency of the connector in facilitating integrity between two connected panels, as well as the connection's influence on the axial load capacity of the panel system.

7.4.1 Axial loading test setup and instrumentation

A self-balanced reaction axial loading frame was designed based on the estimated ultimate axial load of two jointed panels. Schematic view of this frame is shown in **Fig. 7.3**a. The frame comprised the following components: reaction beams, support system, high-strength steel DYWIDAG bars, and loading system (see **Fig. 7.3**b).

Two stiff HEB 200 steel profiles with a length of 2000 mm were designed as reaction beams in order to transfer axial loading to the panels. Each of these profiles was placed on the top and bottom of the specimens. The top beam was fixed to one existing steel frame with M20 steel bolts. The bottom HEB 200 profile was not fixed to any elements and was allowed to move in the axial direction of the panels (see **Fig. 7.3**b and **Fig. 7.3**c).

The specified supporting system was designed to act as a pined support at both ends of the panel (see **Fig. 7.3**d). This system comprised three segments: (i) two T-shape steel plates; (ii) a steel cylinder and; (iii) a steel UNP profile. The two 'T'-shape steel plates had a flange dimension of $200\times200\times10$ mm^3 and web dimension of $200\times150\times10$ mm^3, and were

connected together through steel cylinders with a diameter of 50 mm and length of 300 mm, allowing the rotation of these two 'T'-shape plates. One part of the 'T'-shape plate was attached to the HEB 200 beam profile with four M20 steel bolts, while the other part was welded to the UNP 120 steel profile, with a length of 2000 mm. To reduce misalignments and to distribute the load uniformly along the width of the sandwich wall panel, four of these pinned supporting systems were considered along the UNP profile at top and bottom of the wall panels (see **Fig. 7.3**c).

For applying the load from top HEB 200 beam to the bottom HEB 200 beam, four high strength steel DYWIDAG bars with a diameter of 16 mm were employed. These bars were locked to steel plates with dimension of $400 \times 200 \times 60$ mm^3 by using steel lock washers.

Two BVA hydraulic jacks with a maximum load capacity of 200 kN and including a through-hole load cell of the same capacity were used to apply and measure the load. The pressure on the jacks was controlled manually by using a hydraulic pump. Since during the loading the top steel plate is pushed by the hydraulic jacks, the produced tensile force in the DYWIDAG bars is transferred to the wall panel as a compression force. Additionally, different views of the test setup are presented in **Fig. 7.4**.

(a)

(b)   (c)

(d)
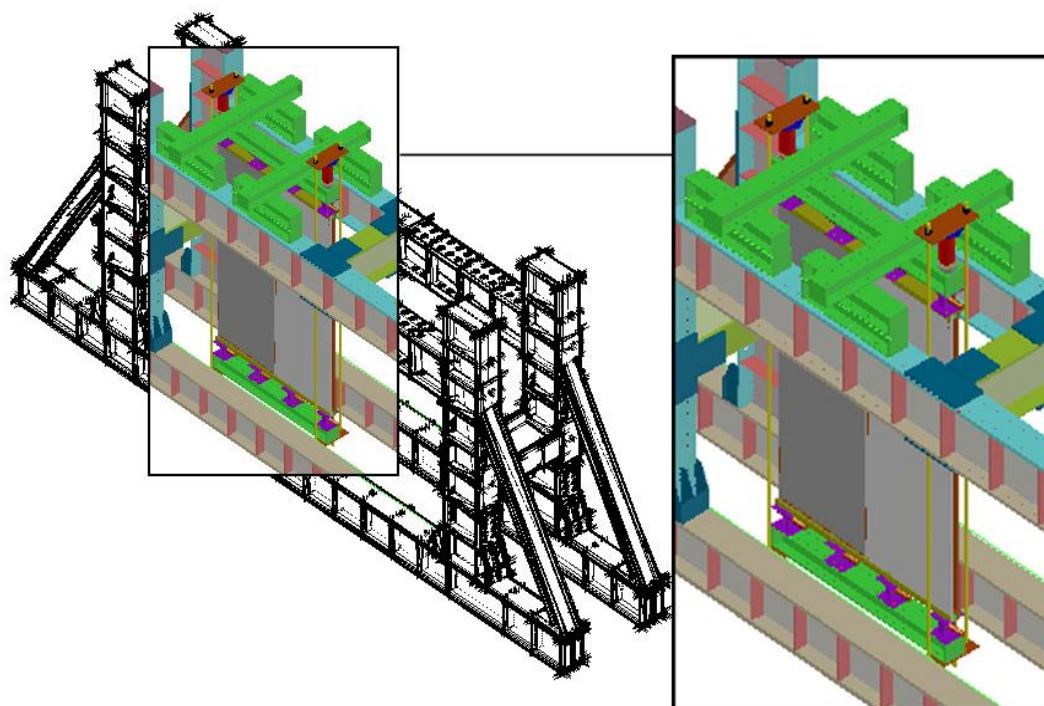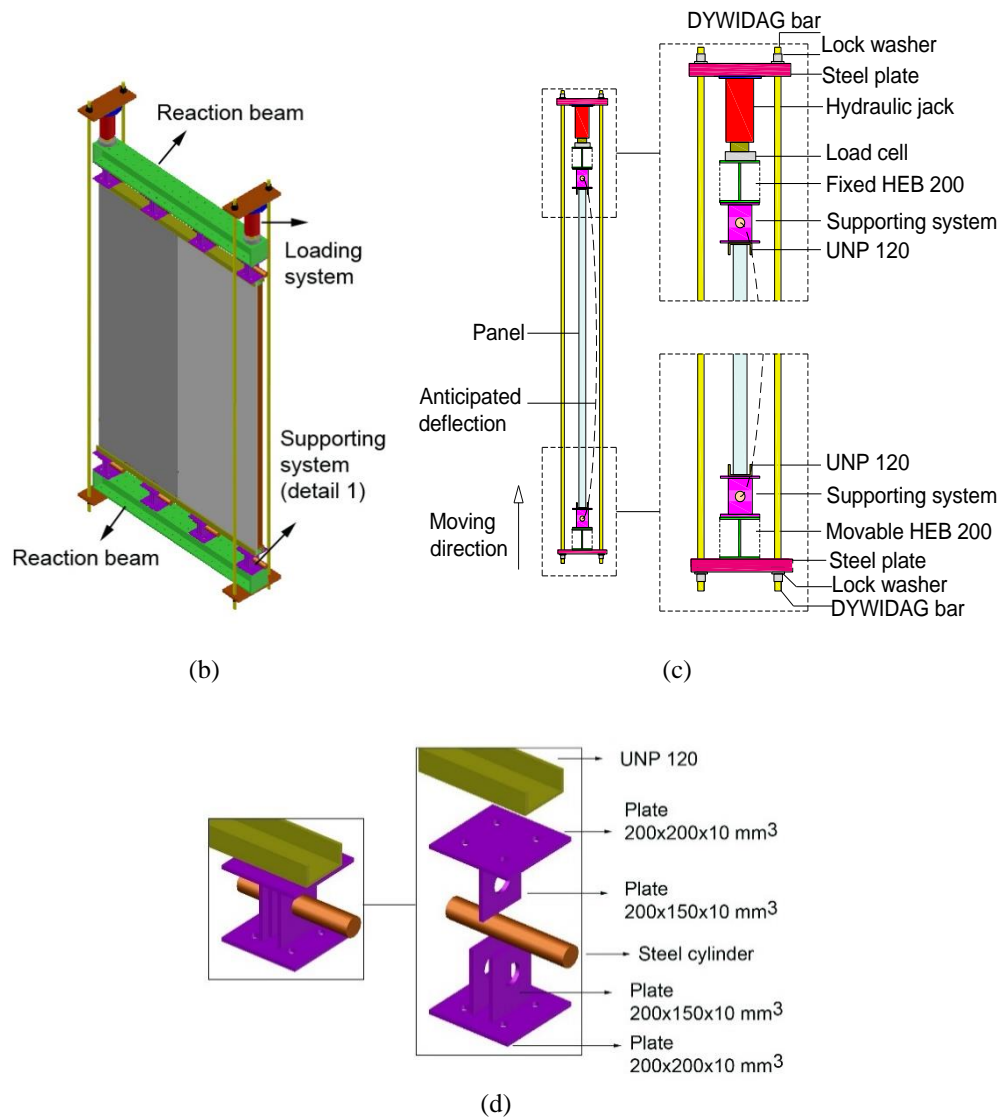
Fig. 7.3. Axial loading test setup: (a) overall test setup; (b) schematic representation; (c) detailing; (d) detail 1.
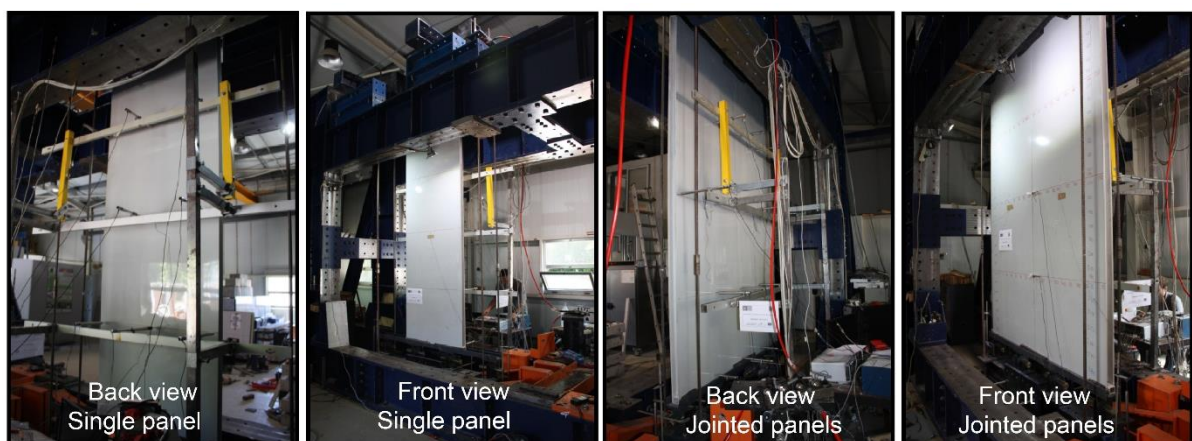
Fig. 7.4. Test setup for single panel and two jointed panels.

Single wall panels and jointed panels were instrumented with LVDTs (D) and strain gauges (S). LVDTs were placed at each quarter height of the wall panels for measuring the out-of-

plane deflection of the panels, D1 to D14 where used in single panel, while D1 to D18 were implemented in the jointed panels. Likewise, axial displacement of tested panels was measured by placing two LVDTs along the height of the panel at each end, D15 to D16 in single panel and D19 to D20 in jointed ones. Also, strain gauges were mounted along the centre lines of the panels for measuring longitudinal strains on both compression (C) and tension (T) skin sides. The monitoring arrangement in single panels and in two jointed panels is shown in **Fig. 7.5**

(a)   (b)
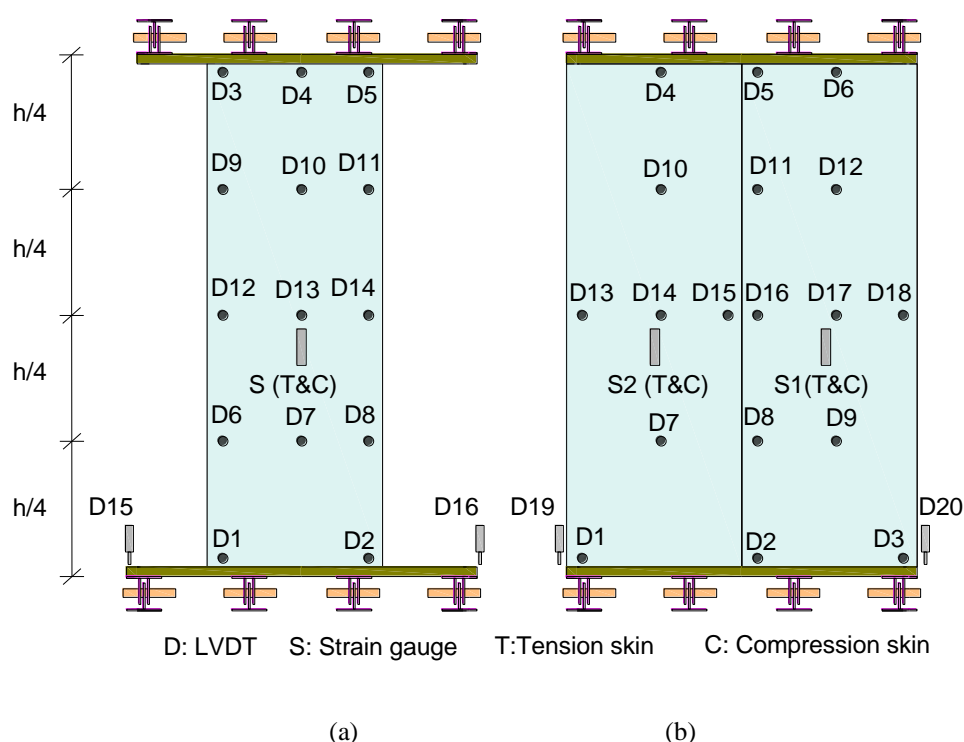
Fig. 7.5. Monitoring system: (a) single panel; (b) two jointed panels.

7.5   Results and analysis

7.5.1   Assembly functionality

The functionality of the proposed system for connecting sandwich wall panels was assessed during the practical assembling process. Since the installation process was done without using any chemical adhesive for joining sandwich wall panels, the total process was relatively quick to perform. From the assembly of the prefabricated segments in a confined space, it could be concluded that this system was much more efficient than conventional methods.

7.5.2 Axial loading test results

The axial load *versus* mid height deflection of the tested single wall panels and jointed wall panels are plotted in the **Fig. 7.6**a and **Fig. 7.6**b, respectively. For the single wall panels, lateral deflection was obtained based on the average deflection registered in the three LVDTs placed at mid height of the panels (D12-D14, **Fig. 7.5**a). In jointed panels, the lateral deflection was calculated based on the average measurement recorded by the six LVTDs installed at mid height of the panels (D13-D18, **Fig. 7.5**b).

Regarding the single wall panels, it is observed that the axial behaviour of both panels (WP1 and WP2) was similar until failure. Axial load capacity of these specimens increased almost linearly up to a load of 59.50 kN, at which a lateral deflection of 4.50 mm was registered. A nonlinear response was noticed after this loading stage. Inspection of panels showed that GFRP skin in the compression side initiated debonding from the PU foam core. This kind of localized failure mode is well known as outward wrinkling failure of the sandwich panel. Increasing the load resulted in the progression of this nonlinearity, which is correlated to the debonding process. This localized failure led to buckling at an average load of 66.75 kN, when the deflection was 11.76 mm.

Similar responses to the single wall panels were also observed in the case of the two jointed panels. The wall panels WP3+WP4 presented an axial load of 121.21 kN and mid height deflection of 18.09 mm when the panels experienced outward buckling of GFRP skin on one side. Thereafter, the jointed panels continued to carry out the load, and at the maximum axial load of 127.80 kN and mid height deflection of 35.61 mm the overall buckling has occurred. Regarding to the jointed panels WP5+WP6, the GFRP outward buckling and overall buckling failure modes seem to have occurred at nearly the same time. The jointed panel captured the maximum axial load and mid height deflection by the values of 168.47 kN and 3.01 mm respectively.

A slight disparity in axial load capacity and stiffness of the WP3+WP4 wall panels was triggered by an out-of-straightness geometric imperfection of the panels. Proposed imperfections of 3 and 5 mm were measured in WP3 and WP4, respectively, which have introduced initial eccentricities to the panels. This imperfection was produced by the misalignment of the PU core blocks during production process.

Through the analysis of **Fig. 7.6**b, it appears that the jointed panels WP5+WP6 failed due to global buckling instability since failure occurred rapidly after initiation of the localized debonding between GFRP compression skin and PU foam core. These panels presented insignificant nonlinear behaviour when compared to the WP3+WP4 jointed panels, which justifies the differences in the lateral displacement values at failure. During loading, jointed wall panels WP5+WP6 unexpectedly buckled out of the LVDTs stroke measuring range. After failure, all of the LVDTs were repositioned to measure the mid height deflection. Consequently, data was not recorded in this period of time (failure and rearranging).
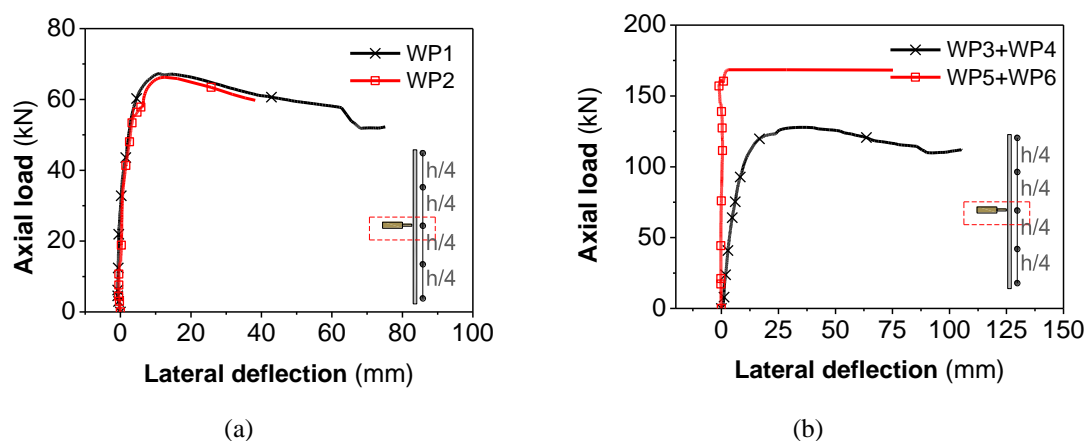
Fig. 7.6. Axial load *vs*. mid height lateral deflection: (a) single panel; (b) two jointed panels.

The axial displacements developed in each test for the buckling load are listed in **Table 7.1**. The axial displacements in all of the tested panels were calculated based on the average displacements of two LVDTs placed at the ends of the panels (D15-D16 for single panels and D19-D20 in jointed panels). Linear response was observed for load-axial displacements, and based on this response, axial stiffness of the panels was calculated as the slope of the curves. The results are indicated in **Table 7.1**. By comparing maximum axial load in the single wall panels with the jointed wall panels, it was observed that depending on the failure modes, axial capacity increased from 91% to 152 %.

Table 7.1. Main results from the axial loading tests.

Specimen	Maximum load (kN)	Lateral deflection at different levels (mm)					Axial displacement (mm)
		0	$h/4$	$h/2$	$3h/4$	h	
WP1	67.30	2.64	6.5	10.99	7.47	5.16	33.88
WP2	66.20	6.67	11.03	12.54	6.48	1.19	23.76
WP3+WP4	127.80	8.62	24.32	35.61	25.06	6.16	21.35
WP5+WP6	168.47	1.95	1.38	3.01	2.45	1.06	24.13

Fig. 7.7a and **Fig. 7.7**b show the axial load *versus* longitudinal strains for single wall panels and jointed wall panels. The strain gauge on the compressive skin of WP1 did not function

properly; however, for the remaining panels, the measured compression (C) and tension (T) strains are included. Regarding the jointed panels, the strain in the compression and tensile sides presented in **Fig. 7.7**b is the average of the values recorded in the two applied strain gauges. From the data recorded in the strain gauges, it was noticed that both skins start with approximately equal compressive strains just below the localized failure load. Thereafter, the strains diverged nonlinearly, indicating significant bending and eminent failure. Once failure occurred, strain gauges on the convex side of the deformed panel presented compression strains, while the strain gauges localized on the concave side of deformed panels registered tensile strains. After this nonlinear stage of the load *versus* strain evolution, both the compression and tensile strains increased suddenly due to the global failure of the panels.

The maximum registered strains on the tension side of the single wall panel and of the two jointed wall panels (0.0017 m/m and 0.0015 m/m, respectively) were significantly lower than the ultimate tensile strain measured in GFRP skins (0.0117 m/m) in skin material characterization. Thus, a direct conclusion could be drawn that during axial loading stage of composite sandwich wall panels at serviceability limit state conditions the material used in the GFRP skins was underutilized. Previously, Fam and Sharaf [42] observed the same situation in sandwich panels tested in bending.

(a)   (b)
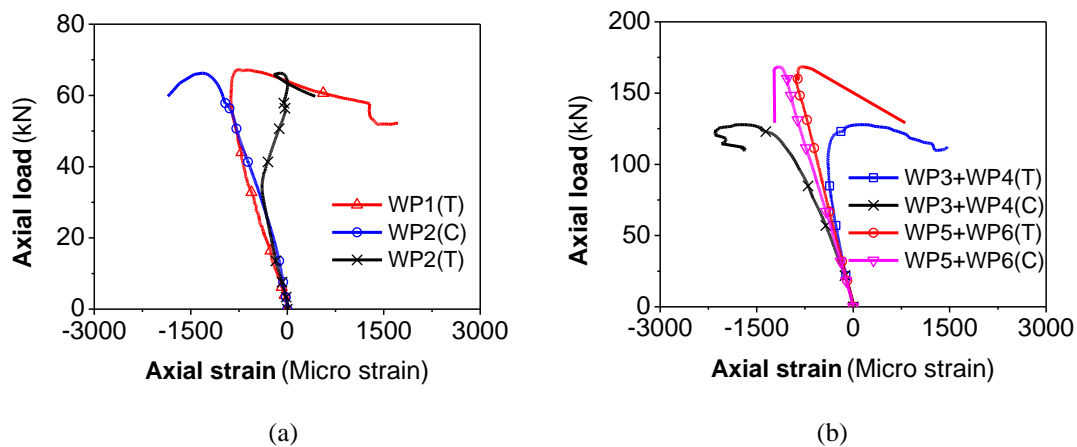
Fig. 7.7. Load vs. axial strain: (a) single panel compressive strain; (b) two adjusted panels.

7.5.3 Failure modes

Failure modes of all tested panels are depicted in **Fig. 7.8**. All tested panels primarily failed by the localized instability of the skins, in the form of outward wrinkling of the GFRP skin at the compression side (convex side of the deflected panels). This mechanism can be explained by the occurrence of interfacial tensile stresses between GFRP skin and PU foam core that

attained the ultimate tensile strength of PU foam core. This failure arose from the very soft nature of PU foam core and the relatively low tensile strength of the PU. Generally, a local failure was observed in the panel, localized at one-third of its height. Finally, localized failure mechanisms lead to an apparent overall buckling in all tested panels.
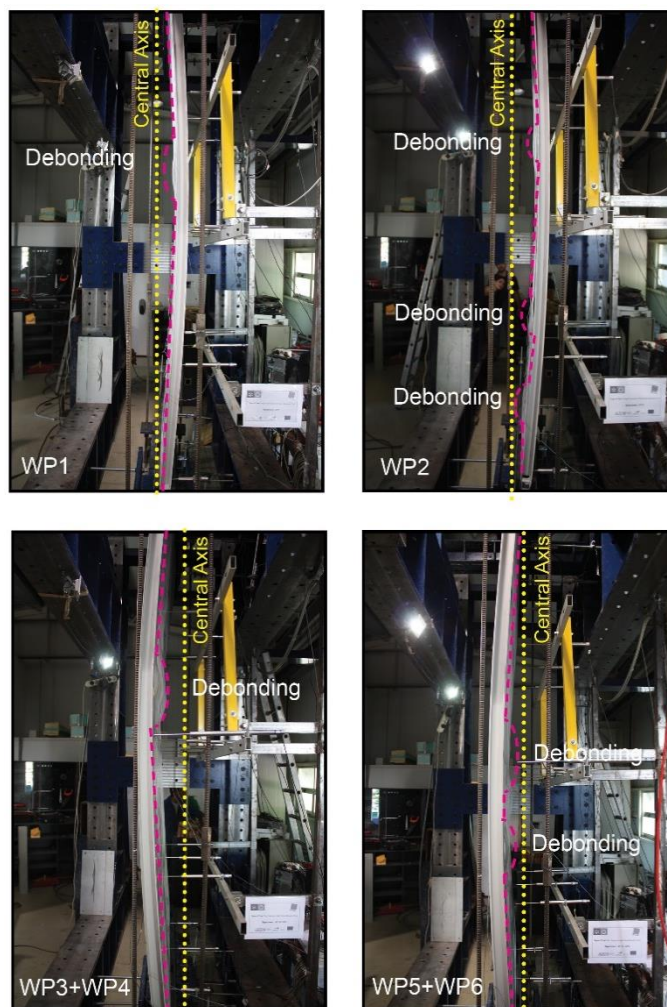
Fig. 7.8. Failure modes observed in axially loaded single panel and two jointed panels.

7.6 Analytical study

Consider a sandwich wall panel of height L, width b, and with simply supported boundary conditions at both ends (**Fig. 7.9**a) subjected to axial loading. The proposed panel has a skin thickness t_f, skin elastic modulus E_f, core thickness t_c, core elastic modulus and shear modulus, E_c and G_c, respectively.

A strut was selected to evaluate behaviour of the panel during the loading (**Fig. 7.9**b). It can be observed that sandwich wall panel started to buckle when the axial load acting on the

panel reaches the critical buckling load (P_{cr}). Due to this fact, significant lateral deflection in the panel occurred (**Fig. 7.9**c). At a cross section positioned far from y to the panel's extremity, two components could be considered for a resultant thrust, P. The first one is $P\sin(\theta)$ acting perpendicular to the middle surface of the panel representing a shear force, while the second one is $P\cos(\theta)$ that is tangent to this surface and imposes bending moments (**Fig. 7.9**d). Consequently, two superimposed lateral deflections Δ_1 and Δ_2 are developing during buckling. The first one results from additional displacement associated with the shear deformation, while the second one is ordinary bending displacement.

(a)   (b)   (c)   (d)
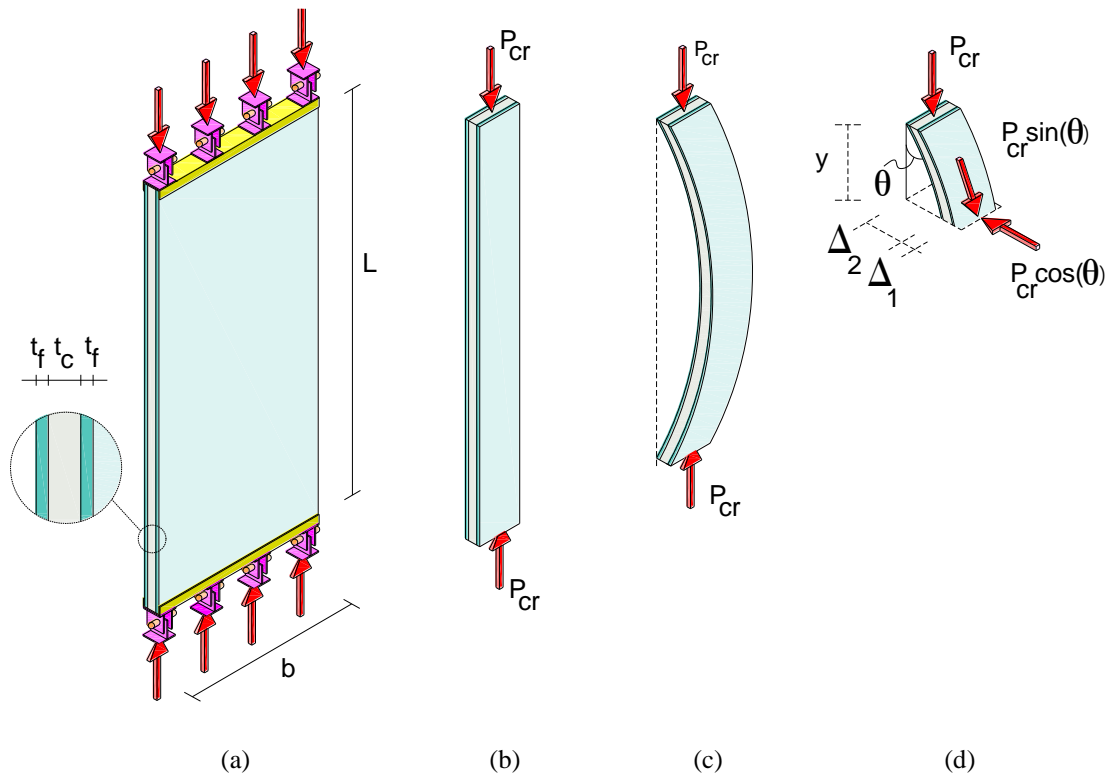
Fig. 7.9. Axially loaded wall panel: (a) schematic of axially loaded panels; (b) strut subjected to axial load; (c) deformed shape of strut and (d) free body diagram of the bucked strut.

7.6.1   Global buckling load

Based on those two deflections, Δ_1 and Δ_2, Allen [28] proposed a general equation for calculating the critical global buckling load (P_{cr}) in sandwich panels, as expressed by Eq. (7.1).

$$\frac{1}{P_{cr}} = \frac{1}{P_E} + \frac{1}{P_s} \tag{7.1}$$

where P_E is the Euler buckling load (based on bending moment), and P_s is the localized shear buckling load (based on shear force). Hence, in a sandwich panel with soft foam core, the critical buckling load is governed not only by the flexural stiffness of the panel but also by the shear stiffness of foam core. However, in panels with internal ribs, shear deformation of the core becomes negligible due to the relatively high shear stiffness ensured by GFRP ribs; thus, Euler load will be the dominant buckling load [28, 31, 49].

In this study, the Euler buckling load is considered the critical buckling load, since the two GFRP 'U' profiles placed in the longitudinal direction of the panel at its extremities act as ribs in wall panels.

$$P_E = \frac{\pi^2 \times (EI)_{eq.}}{L^2} \tag{7.2}$$

where $(EI)_{eq.}$ is the equivalent flexural stiffness of the panel. Since the cross section proposed in this study for the sandwich wall panel was symmetric, the neutral axis is placed at the middle-surface of the panel and then the equivalent flexural stiffness of the wall section is represented by Eq. (7.3)

$$(EI)_{eq.} = bE_f \left[\frac{t_f^{\,3}}{6} + 2t_f \left(\frac{t_f}{2} + \frac{t_c}{2} \right)^2 \right] + nE_U \frac{t_U t_c^{\,3}}{12} \tag{7.3}$$

where n, E_U and t_U are, respectively, the number, the elastic modulus and the thickness of the GFRP 'U' profiles.

Based on Eq. (7.3), a flexural stiffness of 63.0 kN·m^2 was obtained in the single wall panels. Substituting this result in Eq. (7.2) led to an Euler buckling load of 74.96 kN. It is clear that the analytical prediction differs from the experimental result (66.75 kN). This difference (about 12%) could be explained by the wall panel failure mode in axial loading, since both single panels failed due to local buckling instability, while the analytical Eq. (7.2) is only applicable when a global Euler instability occurs. Therefore, the loads corresponding to the interfacial tensile stress and critical wrinkling stress should be evaluated.

Concerning the jointed wall panels system, a flexural stiffness of 143.83 kN·m^2 was obtained from Eq. (7.3). Substituting this value in Eq. (7.2) led to a global buckling load of 171.15 kN. By comparing this value with the Euler buckling load obtained in the single wall panel (74.96

kN), it can be seen that these two values differ by a factor of 2.28. Since the total width of the jointed wall panels is twice that of the single wall panel, it is concluded that the presence of a connector led to an increase in the global buckling load by a factor of 1.28. Recalling the experimental axial loads of 127.80 kN (WP3+WP4) and 168.47 kN (WP5+WP6), it was observed that the load carrying capacity of the (WP3+WP4) connected jointed panels differed significantly from the analytically predicted ones, while this difference was less pronounced, as expected, in the second jointed panels (W5+W6). This fact can be explained by the observed failure modes. The dominant failure mode in the (WP3+WP4) was due to local buckling instability, while in the (WP5+WP6) the dominant failure mode was the global Euler buckling.

7.6.2 Skin wrinkling of sandwich wall panels

7.6.2.1 Interfacial tensile stress

During axial testing, local buckling failure occurred due to debonding of the GFRP skins in the compression side of the deflected sandwich wall panels. This particular instability of the GFRP skins corresponds to a wrinkling effect in which the GFRP skin buckled towards the outside in a sinusoidal shape, with half wave length (L_h) equal to the debonded part (see **Fig. 7.10**). It is worth mentioning that previous investigations [28, 98] demonstrated that L_h is of the same order of the thickness of PU foam core (t_c).
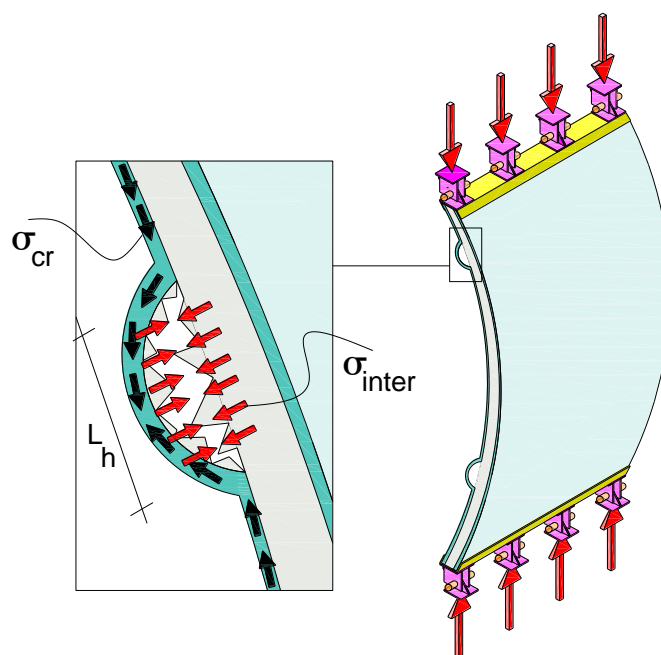
Fig. 7.10. GFRP skin wrinkling model and stresses.

Based on the Winkler Elastic Foundation (WEF) approach, Allen [28] assumed that the compressed GFRP skin could be modelled by a strut supported on an elastic foundation PU foam core. A set of closely-spaced springs was adopted to simulate the behaviour of an elastic foundation corresponding to the foam core. A fourth order differential equation was proposed in Eq. (7.4) and Eq. (7.5) to take into account the sinusoidal waves with half wavelength developed when the compression face skin buckles.

$$D\frac{d^4w}{dy^4} + P\frac{d^2w}{dy^2} = b(\sigma_{inter}) \tag{7.4}$$

$$w = w_m \sin\frac{\pi x}{L_h} \tag{7.5}$$

where D is the flexural stiffness of the strut, P is the axial thrust in the strut, w is the displacement, σ_{inter} is the interfacial stress and w_m is the maximum displacement. By substituting Eq. (7.5) in Eq. (7.4) and differentiating this latter equation, it was possible to obtain the interfacial stress, as defined by Eq. (7.6). The first part of this equation is the stiffness of the assumed springs in the WEF approach, as previously proposed by Mousa and Uddin [69], and the second part represents the sinusoidal displacement at the compressed GFRP skin.

$$\sigma_{inter} = \left[E_c t_c \left(\frac{\pi}{L_h}\right)^2 f(\theta) \right] \cdot \left[w_m \sin\frac{\pi x}{L_h} \right] \tag{7.6}$$

where L_h is the half wave length and $f(\theta)$ is the skin wrinkling mode shape. Three cases of skin wrinkling failure modes are defined in **Fig. 7.11**. Case I corresponds to rigid base or single sided, case II deals with antisymmetric wrinkling, and case III considers symmetric wrinkling. In this research, case I was considered the most appropriate since only one face skin was debonded. Accordingly, Eq. (7.7) was proposed to calculate the skin wrinkling shape mode [28].

$$f(\theta) = \left(\frac{2}{\theta}\right) \left(\frac{(3-\nu_c) \cdot \sinh\theta \cdot \cos h\theta + (1+\nu_c)\theta}{(1+\nu_c)(3-\nu_c)^2 \cdot \sinh^2\theta - (1+\nu_c)^3 \theta^2} \right) \tag{7.7}$$

where V_c is the Poisson's ratio of the PU foam core and θ is function of core thickness and half wave length, as given by Eq.(7.8).

$$\theta = \frac{\pi t_c}{L_h} \tag{7.8}$$

Interfacial tensile stress was calculated based on Eq. (7.6) and was used to compute the maximum out-of-plane tensile stress between the GFRP skin and the foam core, in order to evaluate the debonding between these two materials. The values of $f(\theta)$ and θ were determined based on Eq. (7.7) and Eq. (7.8), respectively, and the values of 0.18 and 3.14 were obtained. An interfacial stress value of 0.78 MPa was obtained by substituting these values into Eq. (7.6).
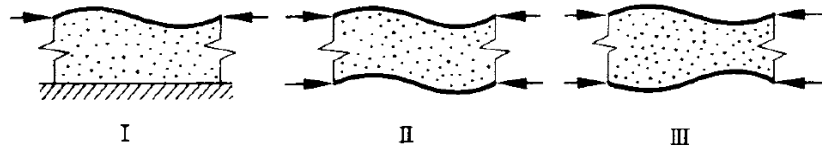
Fig. 7.11. Principal types of wrinkling instability [28].

Comparing this value with the maximum tensile strength of PU foam core suggests that the main reason for debonding failure mode could be explained by exceeding the interfacial tensile stress between GFRP skin and PU foam core from ultimate tensile strength of PU foam core. This was also observed in previous investigation work where the same failure mode was registered [69]. It is worth mentioning that interfacial tensile stress was independent of wall panel's geometry, therefore the same value is attained in the single panel and in the two jointed panels.

7.6.2.2 Critical wrinkling stress

The second stress associated with wrinkling failure modes in compressed GFRP skins is the critical in-plane compressive wrinkling stress (σ_{cr}), which can be obtained from Eq. (7.9). This stress is calculated based on the aforementioned Winkler Elastic Foundation (WEF) approach. Complementary information can be found elsewhere [28, 69]

$$\sigma_{cr} = \beta_1 E_f^{1/3} E_c^{2/3} \tag{7.9}$$

$$\beta_1 = \frac{\rho^2 \theta^2}{12} + \frac{f(\theta)}{\rho} \tag{7.10}$$

$$\rho = \frac{t_f}{t_c} \left[\frac{E_f}{E_c} \right]^{1/3} \tag{7.11}$$

where ρ is a coefficient depending on the elastic modulus and thickness of the GFRP skin and PU foam core. By comparing Eq. (7.9), used to calculate the critical wrinkling stress, with Eq. (7.6) adopted to determine interfacial tensile stress, it is noticed that critical wrinkling stress is evidently dependent on the material properties of GFRP skin and foam core, while interfacial tensile stress only depends on the foam core material properties.

Based on the critical wrinkling stress calculated on the compression GFRP face skin, an equation was suggested [69] to determine its corresponding critical buckling load:

$$P_{cr \rightarrow wrinkling} = \sigma_{cr} b t_f \tag{7.12}$$

Substituting Eq. (7.9) into Eq. (7.12) results in a general form of the critical buckling load:

$$P_{cr \rightarrow wrinkling} = \beta_1 \left(E_f^{1/3} E_c^{2/3} \right) b t_f \tag{7.13}$$

Eq. (7.13) was used to predict the critical load of both the single sandwich wall panels and the jointed wall panels. In this equation the variables E_f, E_c, t_f, t_c, b (in single wall panel) and b (in two jointed wall panels) were substituted by the values of 9600 MPa, 5 MPa, 2 mm, 60mm, 960 mm and 1920 mm, respectively. Coefficient β_1 was calculated according to the Eq. (7.10), having obtained a value of 0.59

Using Eq. (7.13) resulted in the values of 69.20 kN and 138.40 kN for the single wall panel and jointed wall panels, respectively. In the experimental program an average axial load of 66.75 kN for single panels (WP1 and WP2) and 127. 078 kN for jointed panels (WP3+WP4) was obtained. The comparison between these values and the analytical ones showed that Eq. (7.13) is quite precise in predicting the panels axial load capacity when a wrinkling failure mode occurs. Jointed wall panel WP5+WP6 was not taken into account in this comparison since this jointed panel developed a global buckling failure mode.

128

Additionally, by comparing the results experimentally obtained in single wall panels and in two jointed wall panels, it can be observed that these two values differ by a factor of 1.91. This result shows that connecting panels by the proposed techniques increased the critical wrinkling load nearly twice in comparison to single wall panels, demonstrating the high effectiveness of the proposed technique.

7.7   Conclusion

In this part of study, the possibility of employing sandwich wall elements in the ClickHouse project was studied. The capability of rapid on-site assembly/disassembly and ease of integration in the production line could be mentioned as advantages, achieved by the proposed wall system comprising GFRP skins, PU foam core and connectors. GFRP pultruded 'U' shape profiles were positioned along each edge of the panel and were considered as connectors. Some important conclusions can be drawn from the developed work:

- Using the proposed connection and the lightweight nature of structural members, the assembly of the wall panels was performed easily. As such, this system presents a high potential to be used as wall elements in prefabricated dwellings or in the building sector

- Linear elastic response of wall panels was observed, prior to failure, in all the tested wall panels, through the analysis of load–mid height deflection and load–axial displacement curves.

- Mounted strain gauges in both sides of the skins exhibited similar behaviour before failure, due to axial compression of the GFRP skins. After initiation of failure, the strain gauges positioned in the convex side and in the concave side of the deformed panels presented compressive and tensile behaviour, respectively. The maximum tensile strain registered in the GFRP skin was 14% of the ultimate tensile strain of this composite material. This represents that during axial loading of sandwich wall panels the material used for the GFRP skins is somewhat underutilized.

- Three modes of failure were observed in single wall panels and in two jointed wall panels. The panels first started to show a localized failure at GFRP skin in the compression side. This localized failure corresponds to the instability of the GFRP skin in a half wave length that is equal to the core thickness. The second failure mode was related to the propagation of this failure toward the GFRP skin and the PU core due to

the load increase. Finally, all the panels failed due to global instability of the system that resulted from the degradation of integrity between GFRP skins and foam core.

- In the jointed panels, disparities in ultimate load (of about 20%) and failure modes (local versus global) were triggered by initial eccentricity in one of the jointed panels during the loading process. The main reasons for this eccentricity are related to the actual geometry of the panels and the level of complexity of the test setup.

- Regarding to the theoretical study, a reasonable agreement between experimental results and theoretical predictions were observed in both failed panels due to global buckling and due to localized wrinkling buckling. It was concluded that in global buckling failure of jointed panels, axial load increased by a factor of 2.52 of the buckling failure load obtained in single wall panels. The presence of the connector was able to increase the global buckling load by a factor of 1.28. However, it was also verified that the axial load capacity of jointed panels that suffered localized GFRP skin wrinkling failure was nearly 2.0 times higher than the corresponding failure load measured in single wall panels.

- Finally, two kinds of stresses, namely interfacial out-of-plane stress and critical wrinkling stress were evaluated in this study. It was shown that high interfacial out-of-plane stresses between PU foam core and GFRP skins occur, and that these stress values were higher than the tensile strength of the PU foam, resulting in debonding in both single and jointed panels. The calculated critical wrinkling stresses were in good agreement with the experimental values measured in both single and jointed panels.

Chapter 8: Residential floor modular prototype

8.1 Introduction

In the chapter 6, the short and long-term behaviour of single sandwich floor panel flexural were comprehensively studied through experimental, analytical and numerical investigations. It was observed that, for the level of the load considered in designing residential floor modular system, sandwich panels performances with taking into account the viscoelastic behaviour, fulfil the requirements established by standards. Additionally, regarding to the connected two and three floor sandwich panels, it was deduced that the behaviour of jointed panels exhibited adequate flexural performance and fulfilled the requirements in both SLS and ULS conditions in terms of deflection and strain.

In this chapter the structural behaviour of two floor residential modular prototypes of 2.64 × 2.64 m^2 and 3.40 × 3.40 m^2 is investigated. The proposed prototypes are composed of GFRP profiles and sandwich panels. The floor panels are the same already studied in chapter 6. Experimental programs were conducted to evaluate the performance of the developed basic units floor prototypes as a structure designed to support serviceability and ultimate load conditions in residential houses. The performance included the feasibility of assembling and fulfilling the requirements by standards in short-term and long-term. Finally, some analytical and numerical studies were carried out to go further in depth in predicting the actual behaviour of the modular systems and connection effectiveness under designed load. In addition to that, parametric studies were carried out to explore the potentiality of the proposed materials and structural concept in floor residential building with different covered areas.

8.2   First prototype

8.2.1   Concept and geometry

For the sake of simplicity, effects of roof and walls were not taken into account in the current study. Thus, the study will be mainly focused on the floor slabs. The proposed prefabricated modular prototype is schematically represented in **Fig. 8.1.**

| (a) | (b) |
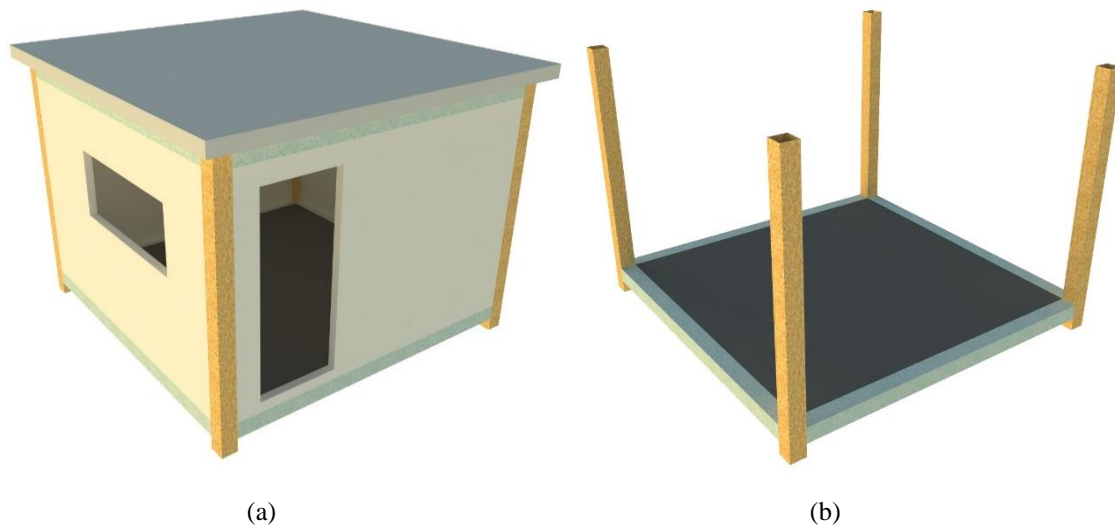
Fig. 8.1. Schematic representation of the modular prototype: (a) full prototype; (b) prototype without walls, roof and top beam elements.

The modular building floor prototype is comprised of two main components: the frame structure (columns and beams) and the slab that is composed of two sandwich panels. The sandwich panel contains an interior polyurethane (PU) foam core enclosed by two GFRP skins. The core and the skins have different functions: while skins bear the bending loads, the core deals with the shear loads, stabilizes the skins against buckling and wrinkling, and provides thermal and acoustic isolation.

Fig. 8.2 shows the frame structure of the prototype, which is constituted by four GFRP beams supported in four short columns. Tubular GFRP pultruded short elements with cross section of 120×120 mm^2 and a wall thickness of 8 mm are used as columns; for the sake of decreasing segments variation in the manufacturing process, the same profile was used for the beams disposed in the contour for the floor. In **Fig. 8.3**, a schematic view of the two floor sandwich panels is represented. Sandwich panels presented an overall cross section's depth of 70 mm, a width of 1200 mm and a length of 2400 mm. On the contour of the panel a GFRP

pultruded profile (U60×55×5) was adhesively bonded for its easy connection to the supporting elements (see **Fig. 8.3**– section CC).
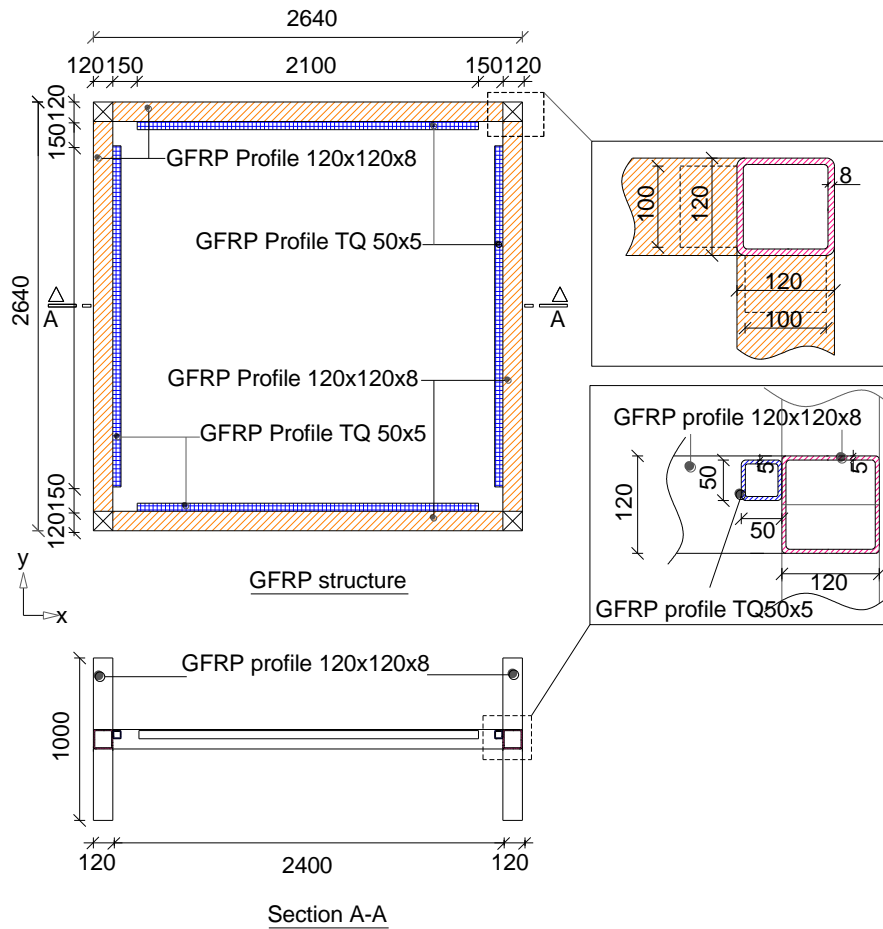
Fig. 8.2. Prototype frame structure (all units in millimetres).
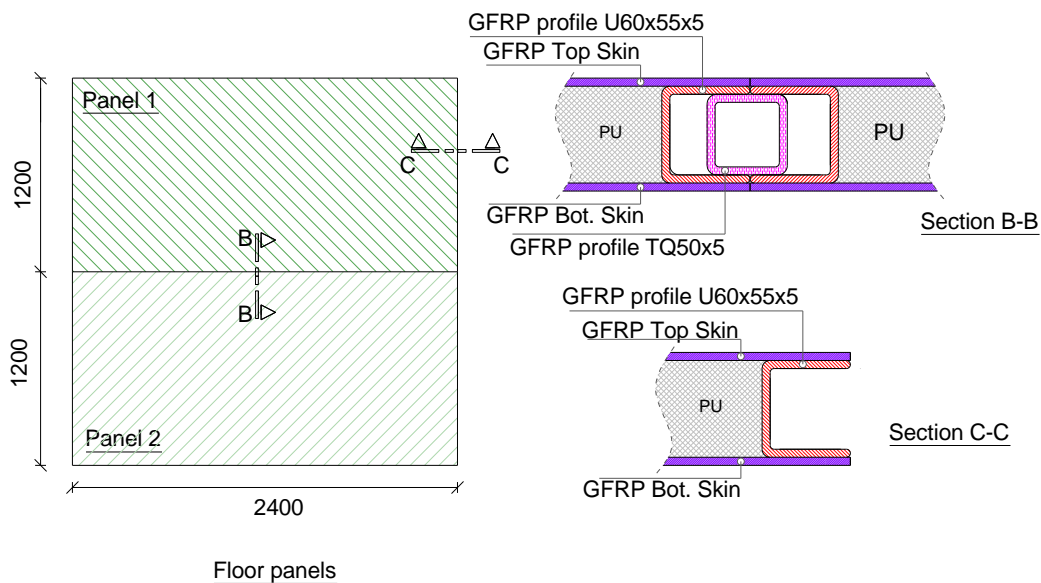
Fig. 8.3. Sandwich floor panel description (all units in millimetre).

133

There are three types of connections in the present prototype (**Fig. 8.4**): (i) beam-column, (ii) beam-panel and (iii) panel-panel. It should be mentioned that the resistance and the ability of an easy and fast assembling / disassembling of the prototype were taken into account in the design phase. Hence, for assuring disassembling with integral reuse of the prototype, adhesive connections were not used between the different elements. In the case of beam-column connections, steel tubular profiles of class S235 and cross section of 120×120 mm^2 were utilized to transfer the loads to the column; these steel profiles were directly connected to the GFRP columns with a series of M8 bolts (**Fig. 8.4**a). For beam-panel connection a GFRP square tubular profile of 50 mm edge and 5 mm of thickness was used; this profile was mechanically and adhesively bonded to the beam element as depicted in **Fig. 8.4**b, since it was assumed to be not disassembled from the corresponding supporting beam. Finally, the same GFRP square tubular profile used for beam-panel connection was employed for the panel-panel connection (**Fig. 8.4**c).

(a) (b) (c)
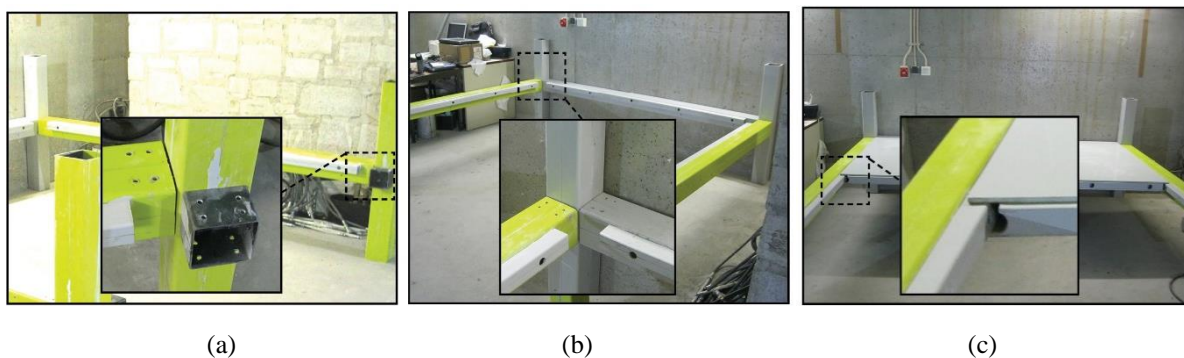
Fig. 8.4. Connections details: (a) beam-column; (b) beam-panel; (c) panel-panel.

8.2.2 Assembly process

The assembly process is expected to be conducted by non-experimented workers in disaster areas. In this context, an assessment of the prototype assembly was carried out to analyse the feasibility of the process. The assembly process is started by placing the four columns in their specified positions (**Fig. 8.5**a), and connecting them with three beams (**Fig. 8.5**b). The installation of the last beam is postponed to the end of assembly process in order to facilitate the introduction of the floor panels. Hence, the next stage of the assembly process is the installation of the first sandwich panel, by handling and mounting it along the beam-panel connections; as can be seen in **Fig. 8.5**c, panel is sliding along the tubular profiles fixed to the beams. Once the first panel is in its final position, and the panel-panel connector is mounted (**Fig. 8.5**d), the second panel is installed in a similar way (**Fig. 8.5**e). Finally, to complete the assembly process, the final beam is placed in its position (**Fig. 8.5**f). All this procedure is

performed in less than 2 hours by three persons without any special equipment, evidencing that the prefabricated prototype may be suitably assembled by non-experimented workers in a short period of time, and without the need of any special tool and equipment, which are normally scarce in a disaster area.

(a)   (b)   (c)

(d)   (e)   (f)
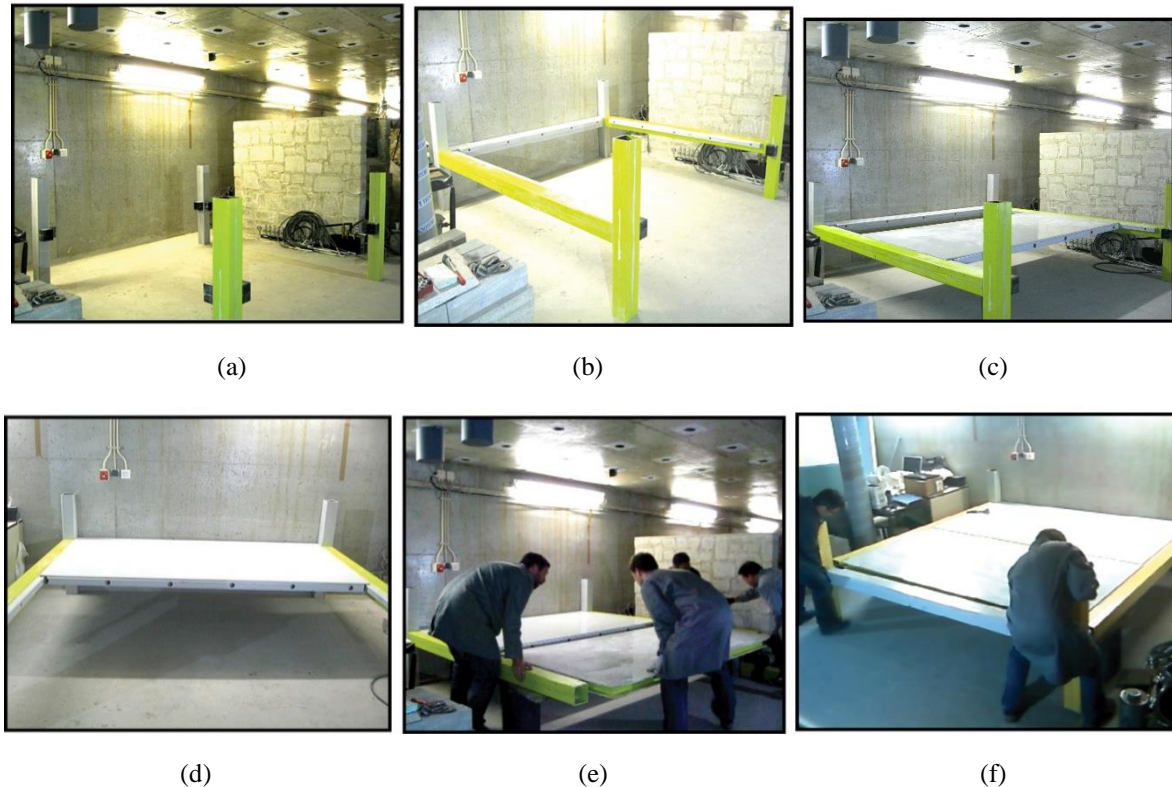
Fig. 8.5. Assembly process: (a) columns placement; (b) attaching the beams to the columns; (c) first panel mounting; (d) sliding the first panel to its correct position; (e) second panel installation; (f) installation of the final beam.

8.2.3   Experimental program

As previously referred, the lightweight prototype was designed to be the floor element of a residential house, and therefore it was necessary to analyse its performance when submitted to the serviceability vertical loads.

The response of the prototype under flexural loads was assessed by applying a uniform distributed load, representing a characteristic live load of 2 kN/m^2 in accordance with Eurocode 1 [85]. The structure was manually loaded and unloaded employing filler bags (20 kg of each) in two layers, each one of 12 bags, resulting in a uniform distributed load of 1 kN/m^2 per layer. Loading and unloading operations were performed fast to avoid any potential creep effect. **Table 8.1** schematically represents the loading and unloading sequences of the four tests. **Fig. 8.3** illustrates different phases of these tests.

Table 8.1. Loading/unloading phases schemes.

Phase	Test 1	Test 2	Test 3	Test 4
Phase 0				
Phase 1				
Phase 2				
Phase 3				
Phase 4				
Phase 5				
Phase 6				
Phase 7				
Phase 8				

Fig. 8.6. Distinct phases of the performed tests.

Monitoring arragement is shown in **Fig. 8.7**: seven LVDTs (D1 to D7) with a stroke ranging from 25 mm to 50 mm were placed at the bottom surface of the slabs's prototype, four in the beams (D1 to D4) and three in the panels (D5 to D7) to measure vertical deflections, while eight TML PFL-30-11-3L strain gauges (S1 to S8) were bonded to the beams (S7 and S8) and panels (S1 to S6) to register the longitudinal strains during the loading process.
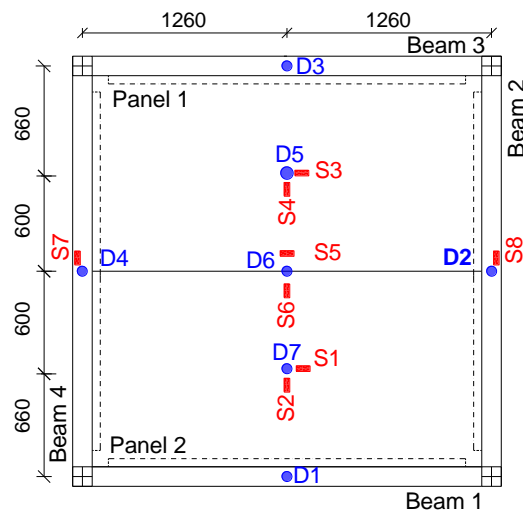
Fig. 8.7. Instrumentation layout for static tests in the assembled prototype: Positions of LVDTs (Di, i=1 to 7) and strain gauges (Sj, j=1 to 8).

8.2.3.1 Experimental results

The measured deflection-time and strain-time relationships in each carried out test are plotted in **Fig. 8.8**. The end of each loading/unloading operation is recognizable by the sudden change observed in the curves. In fact, the presence of small rate of deflections and strains at the end of each of the loading/unloading phases is the consequence of having three persons on the top of the panels during the loading/unloading procedures. Furthermore, it is interesting to mention that once all the load was applied, the four performed tests gave the same results in terms of deflections and strains; thus, all tests can be considered as equivalent, and differences between each one are mainly due to the loading/unloading scheme.

Based on the obtained deflections at the end of the loading process, four groups of LVDTs could be identified (see **Table 8.2**). The first group includes the LVDT placed at the middle of the two panels joint (D6 – see **Fig. 8.7**), which recorded a maximum value of about 16 mm. The second group are those LVDTs placed at the centre of the two panels (D5 and D7), which measured a value of around 12 mm. The third group corresponds to the LVDTs placed on longitudinal beams (D2 and D4), i.e. those beams placed perpendicularly to the panel-panel connection (beams 2 and 4), in which a deflection of approximately 7.5 mm was registered. Finally, the fourth group of LVDTs (D1 and D3) is related to those placed on transverse beams (beams 1 and 3), which recorded a value of 3 mm.
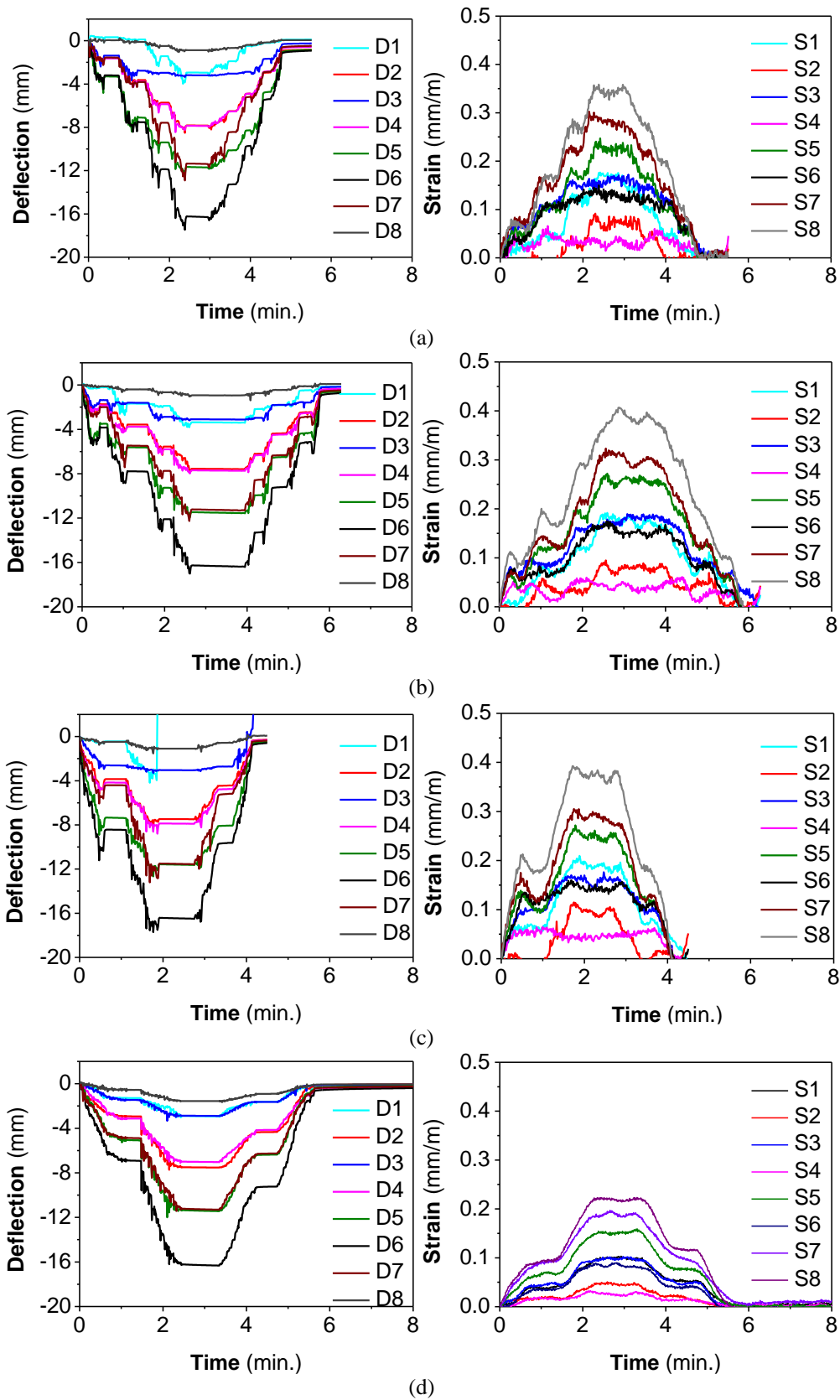
Fig. 8.8. Static test results on the assembled prototype: (a) Test 1; (b) Test 2; (c) Test 3; (d) Test 4.

Table 8.2. Maximum deflections (in mm) registered by the LVDTs in the assembled prototype subjected to a uniform load of 2 kN/m².

Test	Panels joint (D6)	Middle of panels (D5 and D7)	Longitudinal beams (D1 and D3)	Transverse beams (D2 and D4)
Test 1	-16.49	-11.93	-3.46	-7.91
Test 2	-16.29	-11.48	-3.09	-7.56
Test 3	-16.41	-11.56	-3.03	-7.47
Test 4	-16.21	-11.44	-2.87	-7.49

Similarly, the strain gauges may also be grouped in five groups. The first group involves the strain gauges bonded at the centre of the joint between the two panels in the longitudinal direction (S5), which measured a strain value of around 0.25 mm/m (positive value means a tensile strain). The second group corresponds to those gauges placed in the longitudinal direction in the middle of the panels (S1 and S3), which recorded a value of nearly 0.17 mm/m. The third group comprises the strain gauge located at the centre of the joint between the two panels in the transverse direction (S6), which registered a value of 0.15 mm/m. The fourth group consists of those gauges measuring transverse strains in the middle of the panels (S2 and S4), where a strain value of about 0.05 mm/m was recorded. Finally, the fifth group is comprised by those strain gauges placed in the middle of the two beams 4 and 2 (S7 and S8), where a maximum strain of 0.35 (mm/m) was registered. **Table 8.3** lists the maximum values of strains measured in the prototype.

Table 8.3. Maximum strains (in mm/m) registered by the strain gauges in the assembled prototype subjected to a uniform load of 2 kN/m².

Test	Group 1 (S5)	Group 2 (S1,S3)	Group 3 (S6)	Group 4 (S2,S4)	Group 5 (S7,S8)
Test 1	0.23	0.13	0.13	0.05	0.35
Test 2	0.26	0.17	0.16	0.05	0.37
Test 3	0.26	0.14	0.14	0.05	0.38
Test 4	0.15	0.09	0.08	0.04	0.22

From the analysis of the displacements and the strains some information can be extracted. Analysing the strains recorded in the first and second groups of gauges (S5, S1 and S3), and in the third and fourth groups (S6, S2 and S4) it is verified that the level of strains registered in the centre of each panel is significantly different from the level of strain recorded in the centre of the joint between the two panels. This indicates that the panels did not present one-way bending behaviour. Likewise, when compared the first and second groups of LVDTs (D6 against D5 and D7) it is revealed that floor panels presented a two-way bending behaviour, being the bending moments in longitudinal direction (i.e. where beams 2 and 4 work as support) higher than in the transverse direction. The response of the panels implies that beam-panel connection was tight, assuring a high degree of connectivity of the panel to

the supports. Regarding to the third and fourth group of LVDTs, their measurements show that beams 2 and 4 presented almost double deflection of beams 1 and 3, demonstrating the different load level transferred by the panels to these supporting beams. Furthermore, the largest strains were recorded in beams 2 and 4 (last group of gauges, S7 and S8). Finally, it should be referred, as expected, for the load levels applied the system behaved linearly, since after removing the loads negligible displacements and strains were registered.

8.2.4 Numerical simulation

8.2.4.1 General approach

The proposed modular prototype was numerically simulated by a nonlinear three-dimensional finite element (FE) analysis. Calibration of the model was performed based on the experimental results. The simulation enabled to assess the stress distributions in prototype components, such as beams and panels, as well as evaluate the global behaviour and load transfer mechanism of the connections, and assess their influence in load distribution.

8.2.4.2 Numerical model description

 The prototype was modelled by a 3-D finite element analysis with the same geometry of the experimentally tested elements. All prototype constituents, i.e. GFRP skins, PU foam core, GFRP beams and columns, were modelled using 3D hexahedral deformable solid elements with 8 nodes and 3 degrees of freedom per node. After have been conducted some preliminary analysis, an approximately size of the elements equal to 10 mm edge was found to be optimal in terms of both accuracy convergence and computational time of the simulation. The overall FE model for the tested modular floor building submitted to uniform static load is shown in **Fig. 8.9**. Loading and boundary conditions were applied in accordance with the particularities of the experimental test setup. In three of the columns, the displacement in the z direction of the nodes located in the surface in contact to the supporting pavement is prescribed, while in the other column all the displacement degrees of these nodes were prescribed. A uniform load of 2 kN/m^2 was applied on the top surface of the sandwich floor panels. Proper loading arrangement and boundary condition depicting the experimental setup is shown in **Fig. 8.9**. Nonlinear static analysis enabling geometric nonlinearity based on direct method 'Full Newton Solution Technique' was performed.

(a)

(b)

(c)
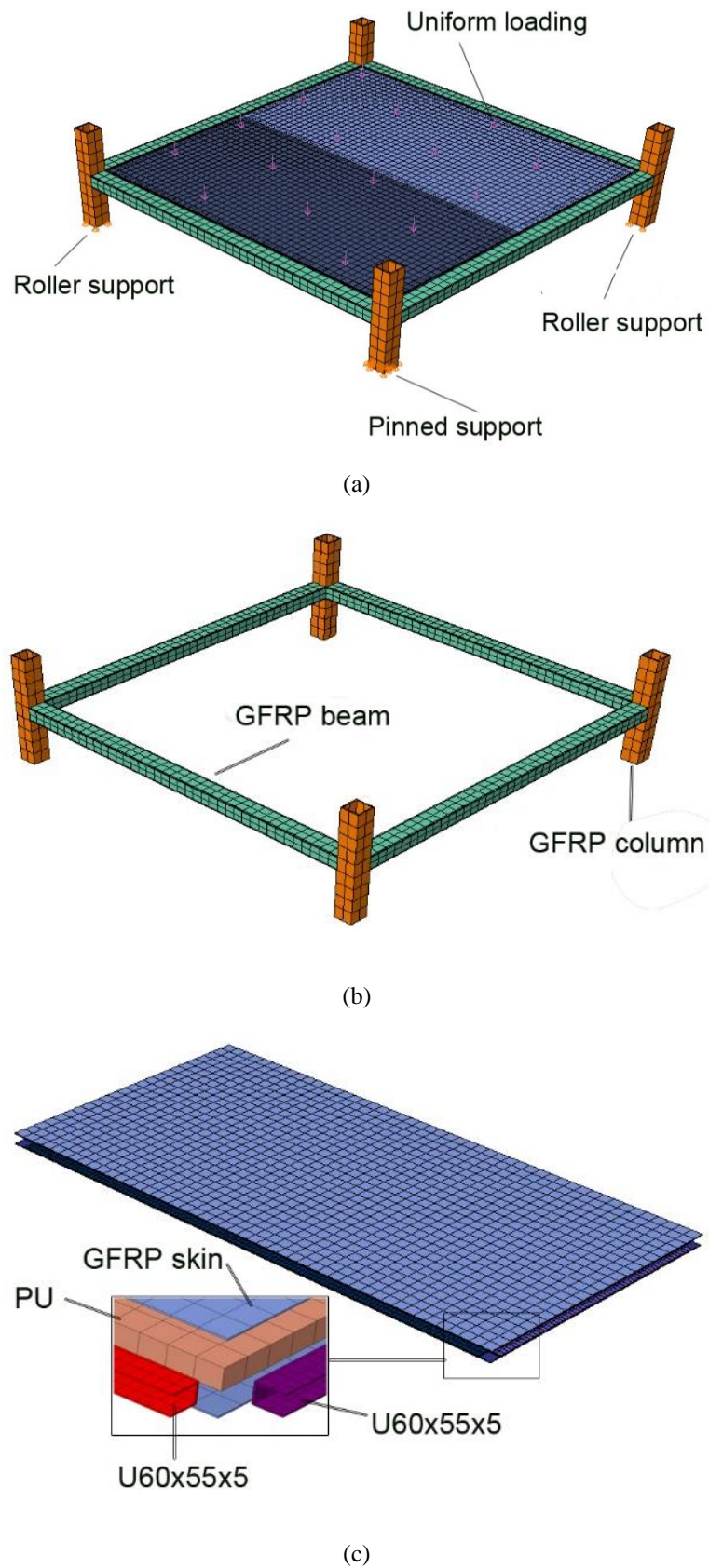
Fig. 8.9. FE model perspective of the tested panel: (a) overall view; (b) GFRP frame structure; (c) sandwich floor panels with constituent materials.

Constitutive relation towards material behaviour of sandwich panel components were adopted according to the performed material characterization tests. The GFRP skins have a quasi-isotropic lay-up, so isotropic linear elastic material with an elastic modulus of 9.60 GPa, Poisson's ratio of 0.3 and ultimate strength of 117 MPa were used to represent the GFRP skin mechanical behaviour. Based on equations previously developed by other authors [93], the crushable foam core was selected to represent mechanical behaviour of the PU foam core by allocating the shear modulus, the elastic modulus and the elastic-plastic constitutive relation with a compressive stress being of 3.15 MPa, 6.3 MPa and 0.30 MPa respectively. The GFRP pultruted profiles were modelled assuming linear-elastic orthotropic material properties with an elastic modulus of 28 GPa and ultimate tensile stress of 415 MPa in the parallel to the fibre direction (longitudinal direction), and elastic modulus of 13 GPa and ultimate tensile stress of 180 MPa in the perpendicular to the fibre direction (transversal).

Interaction between all adherent surfaces belonging to a panel (i.e. interfaces between PU and GFRP skins, PU and U-shape GFRP profiles, and GFRP skins and U-shape GFRP profiles) were modelled as cohesive. The generalized cohesive-behaviour model of ABAQUS [92] was used. Comprehensive information could be find in the numerical simulation of Chapter 6.

Contact connections between profiles and U-shape GFRP profiles of sandwich panels were modelled by a surface interaction: in the normal direction a ''hard'' contact is assumed, meaning that no penetration is allowed between the two surfaces, with no limit to the magnitude of contact pressure that can be transmitted when the surfaces are in contact. Behaviour in the tangential direction was modelled with Coulomb friction model, with a friction coefficient equal to 0.2 and with no adhesion.

8.2.4.3 FE model results

A comparison between the experimentally measured deflections and predicted ones by the FE simulation at different positions is provided in **Table 8.4**. Furthermore, experimentally obtained tensile strains are also compared with the predicted ones by the FE simulation. In general, a good agreement is observed between the results from the FE model and the ones measured experimentally in the prototype. This validates the developed model and enables its use for predicting the flexural behaviour of the proposed modular floor prototype.

Table 8.4. Comparison between experimental and numerical FEM results.

	Experimental	FEM
Deflection (mm)		
Panels joint (D6)	16.2	15.9
Middle of panels (D5 and D7)	11.4	11.04
Longitudinal beams (D1 and D3)	2.9	2.8
Transverse beams (D2 and D4)	7.5	6.5
Strain (mm/m)		
Group one (S5)	0.25	0.33
Group two (S1,S3)	0.17	0.18
Group three(S6)	0.15	0.12
Group four (S2,S4)	0.05	0.06
Group fifth(S7,S8)	0.35	0.48

The colour representation of the vertical displacement field (in y direction) obtained from the FE model is depicted in **Fig.8.10**. A maximum vertical deflection of 15.89 mm was registered in the central part of the pavement, in the join of the two sandwich panels. It is interesting to note that, the GFRP connector bridging internally the two panels while was not connected to the transversal beams. As a results, the contour plot resembles to the typical one as a continuous slab. However, a predominant longitudinal working direction can be observed. This is also confirmed by the deflection of the beams where one can notice that deflection in the frame beams placed orthogonal to the panels' length reach a slightly higher deflection than beams parallel to them.
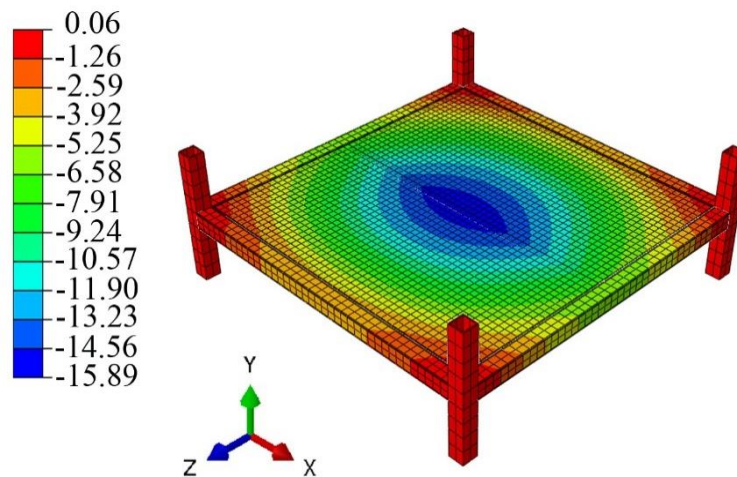
Fig. 8.10. Deflection representation of the prototype from the FE simulation (in millimetres).

Stresses developed in the longitudinal and transversal directions at the external face of bottom GFRP skins in the floor sandwich panels, due to the applied load (2 kN/m^2), are

143

shown in **Fig. 8.11**. Checking the level of stresses revealed that the maximum stresses were below the ultimate strength limit with adequate safety factor. A direct conclusion from this observation is that the proposed panels withstand the ULS load level as they are only 50% above the SLS limit according to Eurocode 1 [85]. The stress field installed in the middle of the panels and through their edges evidence that panels are working as a two-way slab, being the longitudinal the main working direction.

(a)   (b)
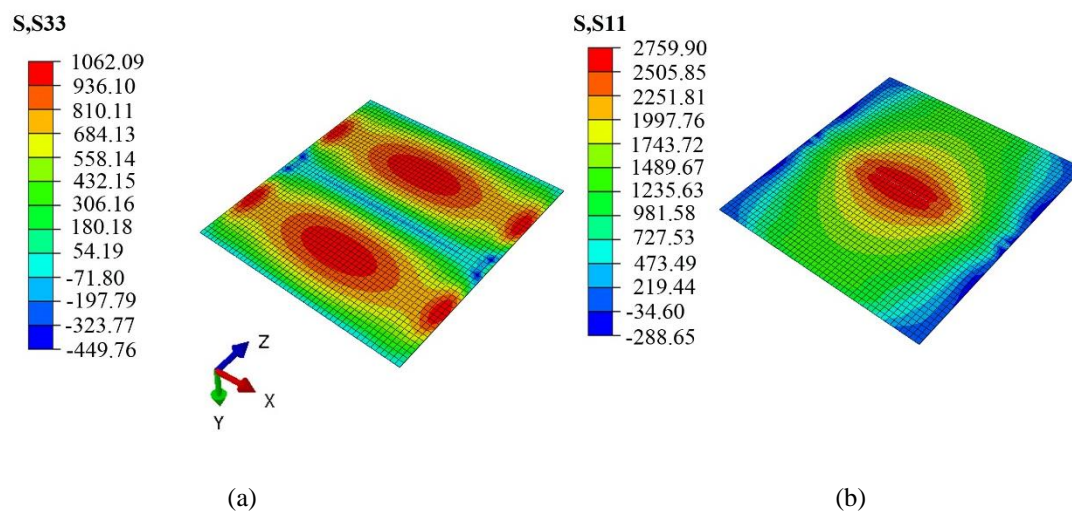
Fig. 8.11. Stress in the bottom surface of lower GFRP skin: (a) longitudinal direction; (b) transversal direction (stresses, in kPa).

From **Fig. 8.11** it can be observed that the presence of the connections provide some restriction along the support, thus contributing to reduce the overall floor sandwich panels flexibility. However, the amount of this restriction in reducing sandwich panel's deflection is not clear. It can be seen that the type of connection used does not act as a fully fixed support and thus, it would resemble to a semi-fixed connection. Hence, the proposed connection can be considered as a spring with a characteristics stiffness k_{sc}. Therefore the total deflection at panels midspan joint (δ) would be the sum of the deflection due to the fixed support (δ_c) and the connection flexibility (δ_θ), i.e, $\delta = \delta_c + \delta_\theta$.

To overcome that issue, a new simulation was carried out by considering fixed support condition between the floor panels and the GFRP beam elements. Fully composite action was assumed by using a tie interface between GFRP square profiles and GFRP 'U' profiles. **Fig. 8.12** shows the numerical load-midspan deflection obtained by considering fixed-support conditions compared with the deflection obtained by considering the real connections. Hence,

the difference between the two curves corresponds to the deflection caused by the connection flexibility (equal to 5.39 mm).
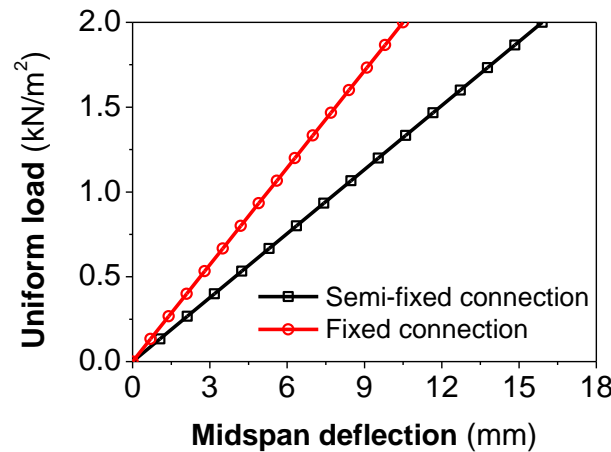
Fig. 8.12. Load-midspan deflection in fixed and semi-fixed connection.

Based on that figure, the proportion on stiffness, defined as the slope between load and deflection, may be expressed by Eq. (8.1):

$$\frac{k_c}{k_{sc}} = \frac{\delta_c + \delta_\theta}{\delta_c} \tag{8.1}$$

where k_c is the stiffness of panel in fixed support conditions and k_{sc} is the stiffness of panels in semi-fixed support conditions.

Eq. (8.1) could be modified in other term as Eq. 8.2, where Π is the stiffness reduction factor.

$$\frac{k_{sc} + \Pi \times k_{sc}}{k_{sc}} = \frac{\delta_c + \delta_\theta}{\delta_c} \tag{8.2}$$

Once computed, coefficient Π was calculated to be 0.51. Thus, a direct conclusion drawn from here is that, when using the proposed connection in the prototype, which acts as a semi-fixed support conditions, a stiffness reduction of a 51% respect to a fixed support condition can be expected.

8.2.4.4 Parametric analysis

The proposed FE model was shown to be an effective tool for investigating the flexural response of the residential floor modular system. A parametric study was then carried out to explore the potentiality of the proposed material and structural concept for pavements of higher span length in order to have more housing space and, consequently, to extend this concept for other markets.

The parametric study was addressed by changing the thickness of PU foam core (h_c) and span length of the sandwich floor panel (L), while keeping the thickness of the GFRP skin (h_f) and the width of the sandwich floor panel (w) equal to 5 mm and 1200 mm, respectively. Both parameters have significant impact on the stiffness of the sandwich floor panel. By changing h_c and maintaining h_f constant have the purpose of exploring the variation of panel's stiffness with the minimum cost, since foam is the less expensive constituent of this construction system. By varying L while w is keeping constant has a significant impact on the deformational response of the panel, due to its almost one way slab behavioural character. Maintaining w constant contributes for do not change significantly the transport conditions of these components, since by increasing both L and w above a certain limit the transport costs of these panels will increase. Additionally, the connection conditions between GFRP beams' elements and sandwich floor panels were evaluated for the following two scenarios: (i) semi-fixed (i.e. like the actual one on the experimentally tested prototype) with the designation of 'SC'; (ii) fixed connection with the nomination of 'FC'.

A total of 66 models were created and analysed under serviceability load conditions in residential houses by assuming a uniform distributed load of 2 kN/m^2 on the top surface of the sandwich floor panels. For deriving relevant conclusions some of the representative results indicated in **Table 8.5** were selected.

Table 8.5 shows that by increasing the panel's span length the maximum deflection increases in the longitudinal beams due to the more pronounced one-way slab character of the panel. This increase rate is reduced by the increase of the h_c / h_f ratio due to the larger contribution of the flexural stiffness of the panel. This observation can be seen in **Fig. 8.13**.

Table 8.5. Maximum predicted deflection in residential floor modular system components subjected to the serviceability load action.

$\dfrac{h_c}{h_f}$	$\dfrac{L}{w}$	Maximum deflection (mm)							
		Panels joint		Middle of panels		Longitudinal beams		Transverse beams	
		Sc	c	sc	c	sc	c	sc	c
12	1.5	9.51	6.41	6.60	5.50	1.11	1.10	5.53	3.85
	2.5	27.84	17.90	19.91	15.71	8.29	7.90	8.90	5.42
	3	44.54	28.71	33.48	26.11	17.35	16.13	10.68	6.13
	3.5	68.23	44.94	54.03	42.08	32.29	29.17	12.39	6.88
16	1.5	7.46	5.03	5.60	4.42	0.96	0.92	4.84	3.37
	2.5	21.10	13.66	15.53	12.09	7.22	6.77	8.45	4.69
	3	33.37	21.76	25.71	20.28	13.80	13.20	10.15	5.28
	3.5	51.11	34.98	41.35	33.20	25.45	23.87	11.80	6.02
20	1.5	6.76	4.03	4.80	3.60	0.82	0.73	4.77	2.82
	2.5	17.02	10.28	12.53	9.47	5.32	5.16	7.83	3.89
	3	26.18	16.88	21.53	16.15	12.14	10.97	8.21	4.56
	3.5	40.17	26.55	32.54	25.67	20.33	18.90	7.99	4.87

h_c : PU foam core thickness; h_f : skin thickness; L : length of the floor panel; w : width of the floor panel; sc: semi-fixed connection; c: fixed connection

By increasing h_c / h_f from 12 to 20 in the shorted panels (L=1800 mm) has provided a decrease in the maximum deflection that varied between 14% and 37% when the four considered components of the panel and the two connection conditions are analysed, having the highest decrease occurred in the panels with "FC" connection conditions. However, the range of values of the aforementioned decrease in the maximum deflection has decreased with the increase of the panel's length, having varied between 29% and 41% in the longer panels (L=4200 mm). In these longer panels, the higher decrease of the maximum deflection occurred in the panel's joint, regardless the connection conditions (about 41%).

The maximum deflection for quasi-permanent load conditions (i.e. 30% of the total live load) was computed for the mid-span of the floor modular system (δ_{qp}) in each analysis. The obtained deflections were subsequently manipulated by employing Eq. (4) to capture the long-term performance of the floor modular pavements (δ_{LT}). The results are shown in **Fig. 8.14**. It should be noticed that in this figure, the curves are named based on two characters. The first character is the h_c / h_f ratio, while the second character indicates the type of connection between GFRP beams' elements and sandwich floor panels.

h_c/h_f= 12, L=2400 mm h_c/h_f= 12, L=3000 mm h_c/h_f=12, L=4200 mm

h_c/h_f= 16, L=2400 mm h_c/h_f= 16, L=3000 mm h_c/h_f= 16, L=4200 mm
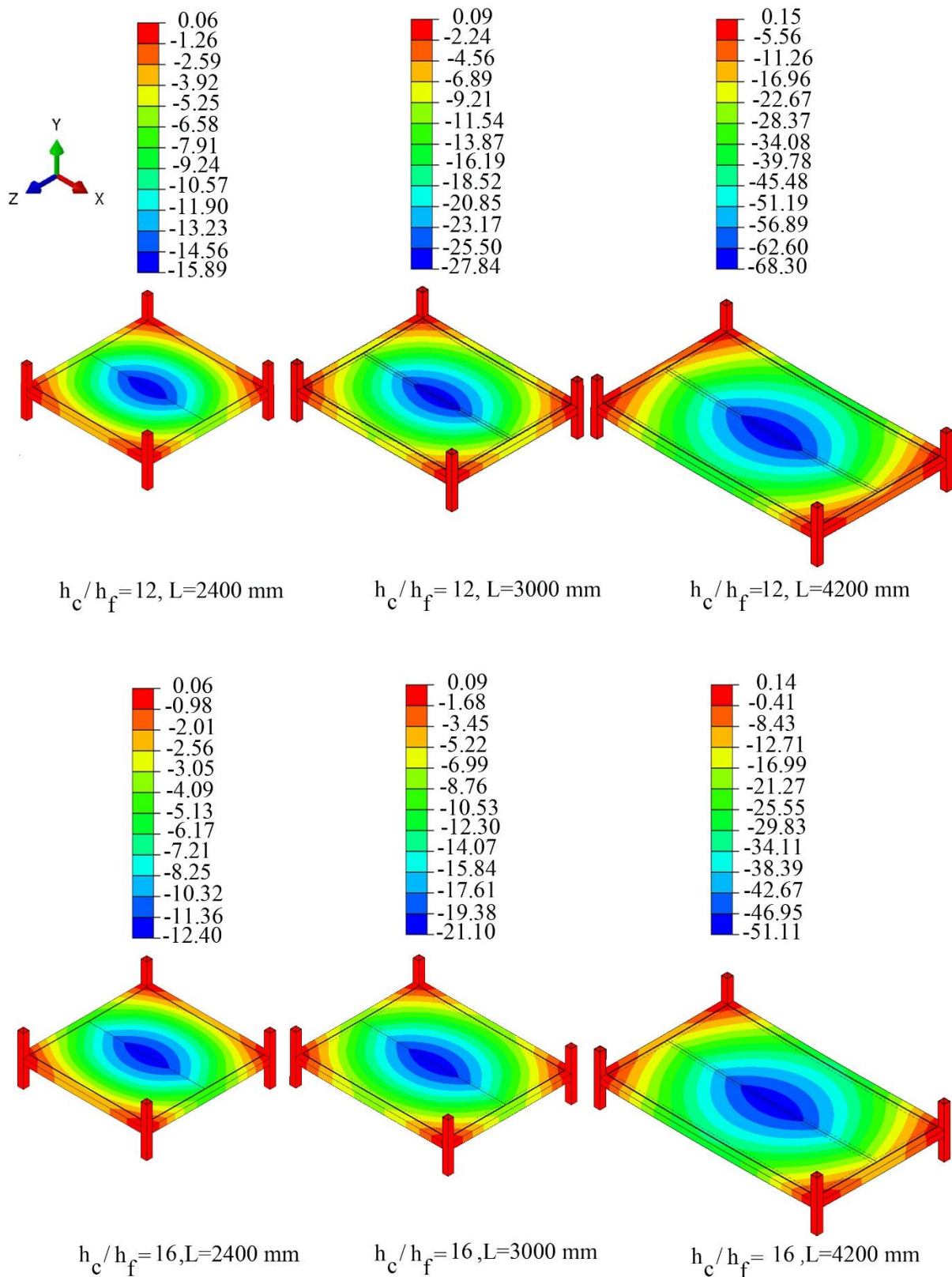
Fig. 8.13. Vertical deflection of the residential floor modular system under different h_c/h_f ratios and span lengths with 'SC' support condition (units in millimetres).

Graphics like the one represented in **Fig. 8.14** can be developed for assisting on the design of composite sandwich panels for residential building product applications. By taking the graphic of **Fig. 8.14** as an example of this pre-design approach, and assuming a span length

of 3000 mm for the composite floor panel (represented by a vertical dot line), and considering the maximum deflection criterion recommended by CNR [80] (plotted by a horizontal dot line), the panel '20-SC', and all the panels with 'FC' connection conditions are possible solutions, being the economic criterion critical for the final decision. For the other sandwich panels, do not fulfilling the requirement of maximum deflection, this can be overcome by increasing their flexural stiffness through adopting more internal GFRP ribs.
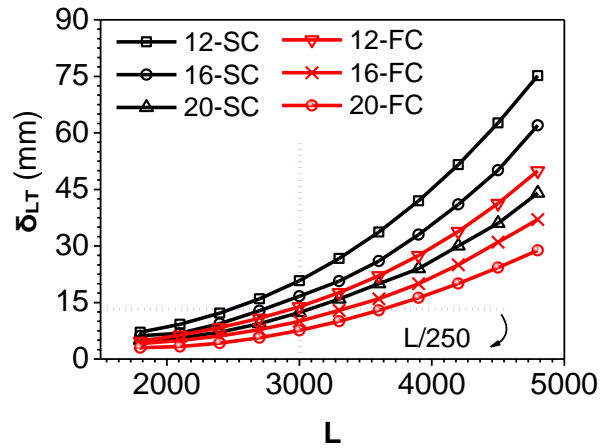
Fig. 8.14. Flexural response of the residential floor modular system at different conditions.

8.3 Second prototype

8.3.1 Concept and geometry

The designed temporary building house was composed of a single-story building with a rectangular plan of about $6.0 \times 3.0 \, \text{m}^2$, formed by connecting two blocks of about $3.0 \times 3.0 \, \text{m}^2$ and a height of about 3.0 m. **Fig. 8.15** shows a plan and three lateral views, as well as a photo of the built prototype. It is important to note that the capability of connecting blocks provides the possibility of erecting a pre-selected number of buildings by joining different blocks [59].

(a)   (b)

(c)   (d)
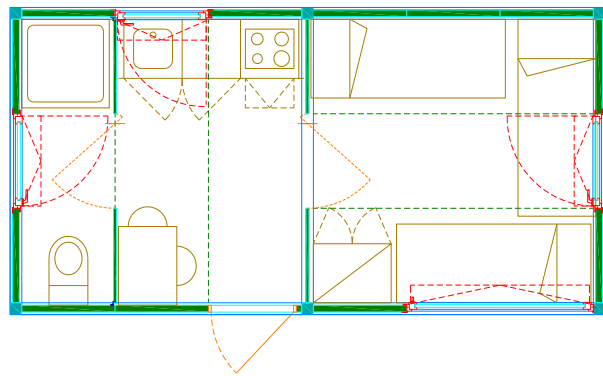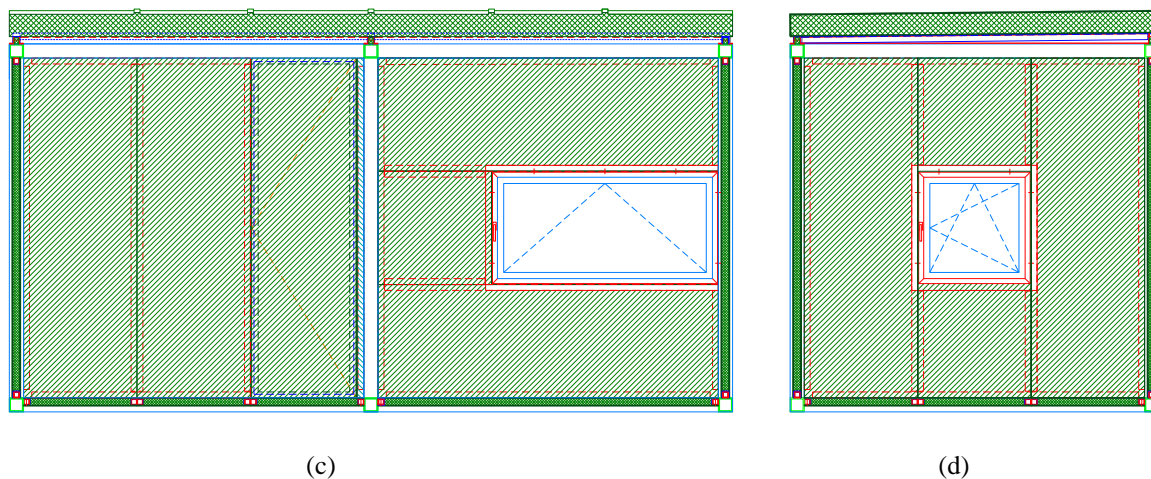
Fig. 8.15. Modular system schematic view: (a) Prototype built; (b) Plan view; (c) south view; (d) east view [59].

The floor module of the building is depicted in **Fig. 8.16** and was composed of two main components: (i) a frame formed by tubular GFRP pultruded profiles with a cross section of $120{\times}120$ mm^2 and a wall thickness of 8 mm (**Fig. 8.16**a), and (ii) the pavement constituted by three sandwich panels formed by two outer GFRP skins of 5 mm thickness and a core of PU foam (**Fig. 8.16**b). For the sake of decreasing segment's variation in the manufacturing process, the same profile was used in both beams and columns of the frame.

The panels presented an overall thickness of 70 mm, a width of 1000 mm and a length of 3000 mm. A U-shape GFRP pultruded profile with a cross section of $60{\times}55$ mm^2 and a wall thickness of 5 mm (U60$\times$55$\times$5) was adhesively bonded to the PU foam core during the manufacturing process, on the outer side of each panel, enabling the connection of each panel to the other elements of the prototype, such as beams and other panels (**Fig. 8.16**c) For increasing the flexural stiffness of the panel, two additional U60$\times$55$\times$5 profiles were installed in the interior of each panel. PU foam blocks with a thickness of 60 mm and nominal density of 48 kg/m^3 were used to form the sandwich panel core, providing the required thermal isolation. These blocks were bonded to the GFRP skins with a polyester resin.

The obtained panels resulted in a light system, each one weighting around 70 kg, taking into account every component, i.e. skins, core and the additional U-shape GFRP profiles, which facilitates its transportation and on-site installation.

The connections were designed for an easy and fast assembling / disassembling of the prototype, and assure continuity as much as possible between connected elements in order to mobilize efficiently their strength capacity (**Fig. 8.16**c). For beam-panel connections, the aforementioned U-shape GFRP profiles placed on the edges of the sandwich panels were

attached to a GFRP squared tubular profile of 50 mm edge and 5 mm of thickness that was mechanically and adhesively bonded to the GFRP beam. Finally, for panel to panel connection, a similar approach as that followed for beam-panel connection was used, by attaching the U-shape GFRP profiles to two GFRP squared tubular profiles (also of 50 mm edge and 5 mm of thickness) that were mechanically and adhesively connected together.
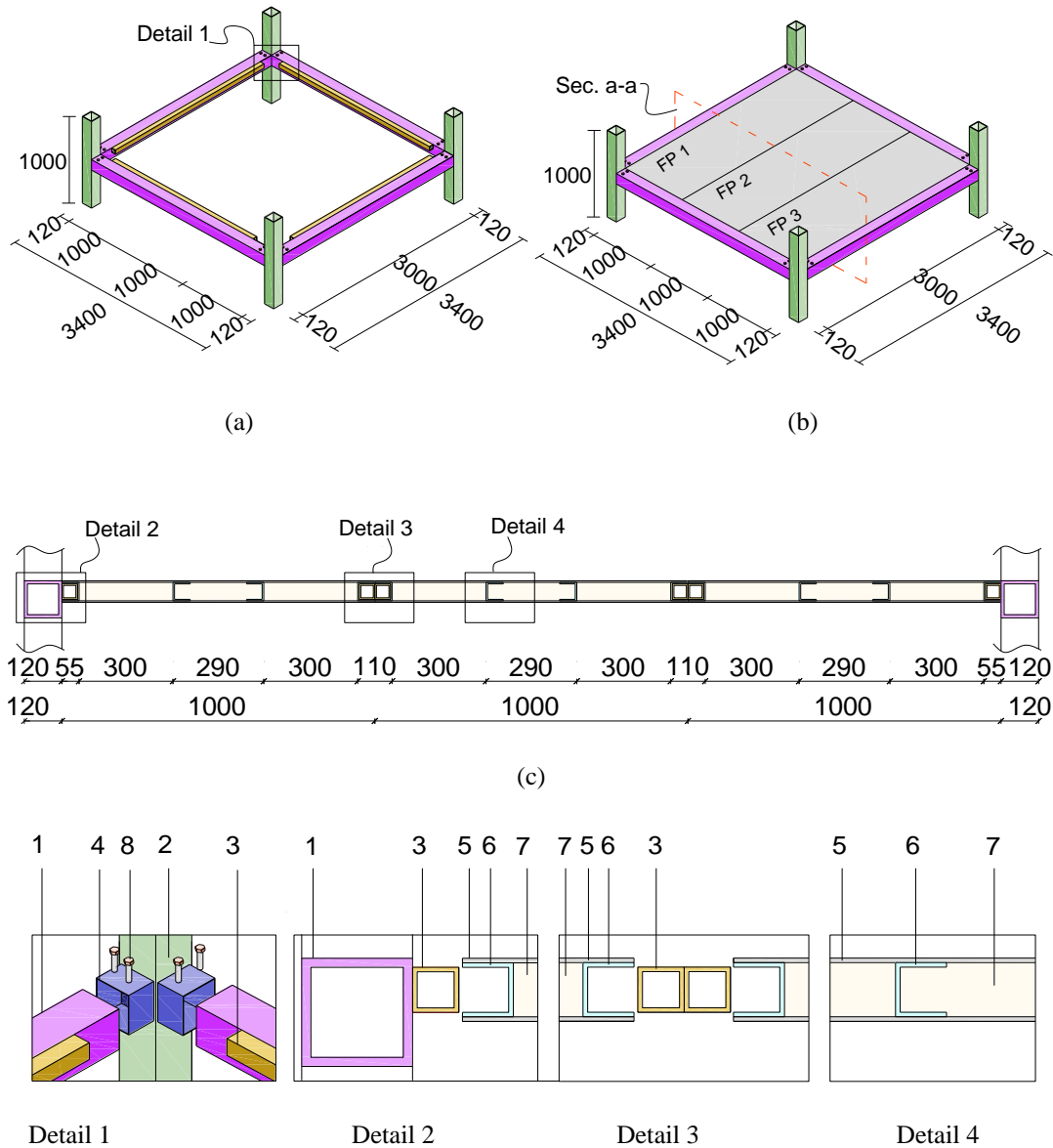
Legend: (1) GFRP beam; (2) GFRP column; (3) GFRP square profile; (4) steel profile; (5) GFRP skin; (6) GFRP U profile; (7) PU foam core; (8) steel bolt

Fig. 8.16. Schematic presentation of the floor prototype: (a) frame structure; (b) frame structure and sandwich floor panels; (c) cross section a-a (all units in millimeters).

8.3.2   Assembly process

The floor prototype was developed for disaster areas where special tools and equipment, as well as experimented workers, are scarce. Consequently, these issues were also considered in the design process of the prototype. **Fig. 8.17**.

Fig. 8.17 shows a general view of the process needed to assemble the floor of the developed prototype. The process starts by placing the four columns in their positions (note that for the floor test proposed in of this paper, short columns with approximately 1/3 of the real height were used), and then connecting three of them by beams (**Fig. 8.17**a and **Fig. 8.17**b). Afterwards, the three sandwich panels were installed. Panels were handled and mounted along the beam-panel connections (**Fig. 8.17**c), placing the panel to panel connectors after positioning the first and the second panels (**Fig. 8.17**d). After assembling the third panel, the last beam of the frame was installed and connected (**Fig. 8.17**e). Fixing ropes were used along the process for facilitating the adjustment of the panels. **Fig. 8.17**f shows the floor prototype after has been assembled, which required less than 2 hours and three people without any special equipment.

Fig. 8.17. Stages of the assembling process: (a) placing columns; (b) connecting beams to the columns; (c) mounting panels along beam-panel connection; (d) placing panel-panel connector; (e) installing the last beam; (f) final prototype.

8.3.3 Experimental program

The assembled floor modular prototype was evaluated under a uniform load. Following the UNHCR recommendation [86] for an emergency house, a uniform load of 1.6 kN/m^2 was selected as service load (SLS). That load was increased 1.5 times to evaluate ultimate limit state (ULS) of panels as traditionally defined in the Eurocodes. The structure was loaded using a swimming pool of circular area and 6.25 m^2 as illustrated in **Fig. 8.18**a. Volume for filling the pool was calculated based on the area of the three jointed sandwich panels. A total of 2160 litters was needed to reach the maximum value of 2.4 kN/m^2.

The monitoring system adopted for this test is displayed in **Fig. 8.18**b. Eleven LVDTs (D1 to D11) with a stroke ranging from 25 mm to 50 mm were placed at the bottom of the prototype to measure vertical deflection, while 15 strain gauges (S1 to S15) were positioned on the bottom surface of the beams and panels to register the strains during the loading process.

(a)

(b)
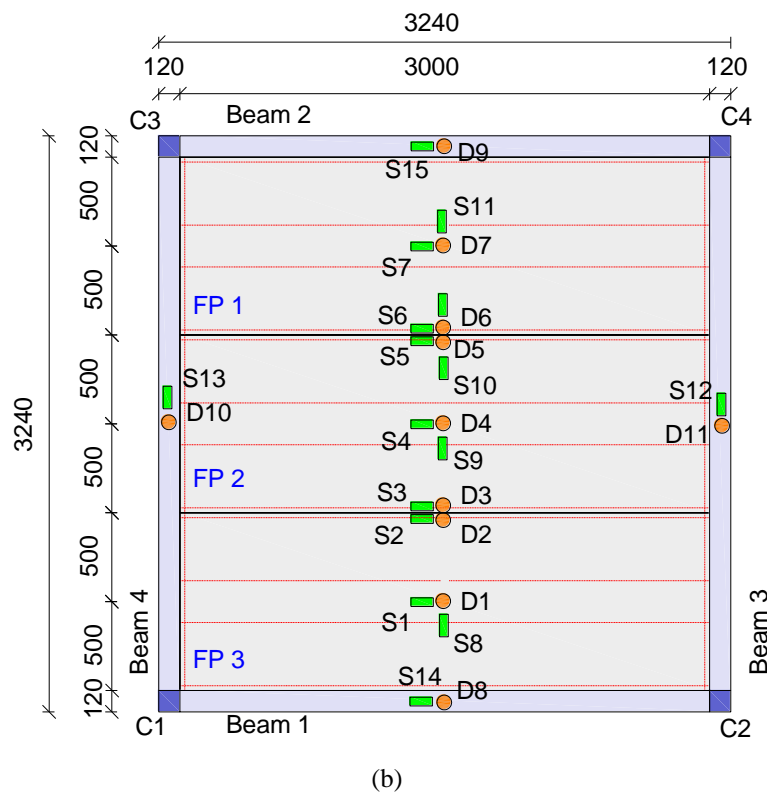
Fig. 8.18. Prototype test setup: (a) loading procedure; (b) monitoring system.

8.3.3.1 Experimental results

For a more comprehensive analysis of the results obtained in the test with the floor prototype, it was verified opportune to group the results measured in LVDTs and strain gauges. The arrangement of these groups takes into account the structural symmetry conditions in order to determine the average results in each group. Hence, regarding to LVDTs (all subsequent LVDTs names are related to **Fig. 8.18**b), Group DI corresponds to the LVDT placed at the centre of the middle panel (D4). Group D2 consists of the LVDTs placed at the middle of the interior edges of the panels (D2-D3 and D5-D6). Group DIII are composed of the LVDTs placed at the centre of the lateral panels (D1 and D7). Group DIV is formed by the LVDTs disposed in the transversal beams (D10 and D11). Group DV corresponds to the LVDTs placed on the longitudinal beams (D8 and D9). Similarly, for the case of strain gauges, the results were collected in the following seven groups (**Fig. 8.18**b): Group SI (S12 and S13), Group SII (S4), Group SIII (S2 and S6), Group SIV (S1 and S7), Group SV (S14 and S15), Group SVI (S9) and Group SVII (S8 and S11). **Table 8.6** lists the average values registered for each of the mentioned groups at the end of the test (i.e. for a load applied equal to the ULS conditions), while the registered deflection-time and strain-time relations are depicted in **Fig. 8.19**.

Table 8.6. Registered deflection and strain in the floor prototype.

	Group I	Group II	Group III	Group IV	Group V	Group VI	Group VI
Deflection (mm)	-33.37	-30.97	-21.63	-13.79	-4.6	---	---
Strain (µstrain)	786.19	637.53	569.27	420.08	235.72	101.39	27.33

The end of the loading operation corresponds to the instant when the measured entity remained almost constant. Both deflection-time and strain-time relationships revealed that the floor prototype developed a linear behaviour for the entire applied loading process. The higher deflection registered in the centre of the middle panel (LVDT of Group DI) was expected since this corresponds to the centre of the floor, in the panel that was mainly supported only by two edges. Conversely, since the lateral panels were supported along three edges, the deflection in the centre of these panels (Group DIII) were much smaller. The deflection in the groups DI and DIII indicates the floor panels presented a two-way bending behaviour, in longitudinal (parallel to the direction of the connection between panels) and transverse directions, being bending in the longitudinal direction more pronounced than in transverse direction. Confirmation of difference in the load transmission on the panels may be also seen by comparing results of the fourth and fifth groups of LVDTs, whose analysis showed that the load was not distributed equally by all beams: transversal beams registered nearly a triple deflection of that measured in longitudinal beams.

Furthermore, strains registered on the transverse beams (Group SI) were higher than other measured strains (Group SV). This demonstrates that the load was not uniformly distributed, but transversal beams carried out more load than longitudinal beams, in which the average strain recorded was 30% lower. Comparing the strain measured in the strain gauge located in the centre of the middle panel in longitudinal direction (Group SII), with those recorded in the strain gauge placed in the middle of the other two panels, also in longitudinal direction (Group SIV), a difference of nearly 65% was registered. This result is equivalent to what was observed with deflections, and is explained by the support conditions, since middle panel is supported on two opposite edges, while exterior ones behaved as panels mainly supported on three edges. Because of this, a similar result is obtained when comparing gauges in transverse direction (Strains - Group SVI and Strains - Group SVII).

(a)   (b)
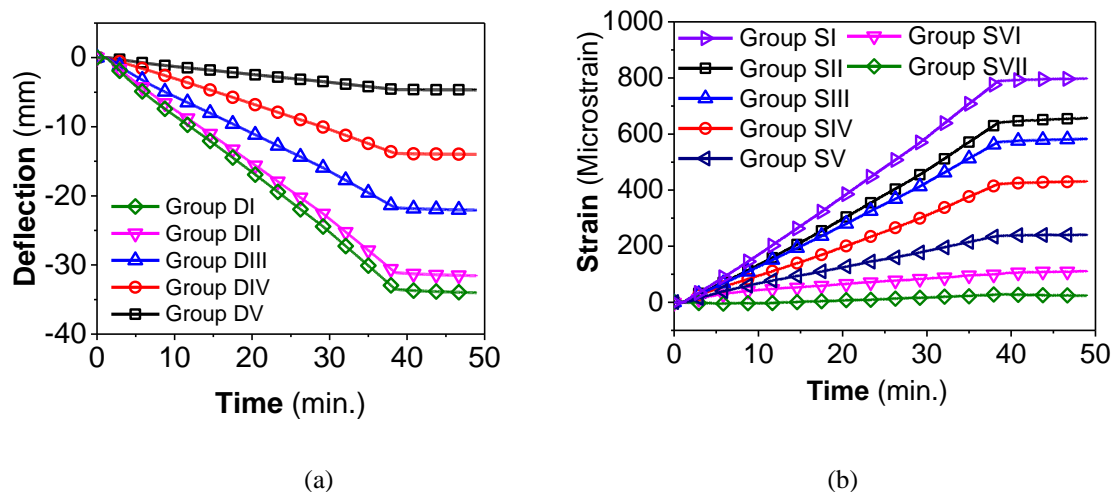
Fig. 8.19. Floor prototype flexural performance: (a) deflection *versus* time; (b) strain *versus* time.

Furthermore, strains registered on transversal beams (Group SI) were higher than other strains. This demonstrates that the load was not uniformly distributed, but transversal beams carried out more load than longitudinal beams, in which average strain computed was 30% lower.

The long-term maximum deflection of the prototype may be estimated considering the experimental results and using Eq. (6.4). For this purpose, and for the deflection corresponding to the ULS condition (2.4 kN/m^2), deflection registered on the transversal beams (13.79 mm) should be subtracted from the deflection registered in the middle panel (33.37 mm), resulting a value of 19.58 mm. Substituting this value in Eq. (6.4), an estimated long-term deflection of 9.86 mm is obtained. Taking into account that in the prototype the length of panels is equal to 3000 mm, the estimated value fulfils the deflection criterion recommended by CNR [80] ($\leq L/250=12$ mm). As in the other conducted tests, the GFRP strains were significantly lower than the ultimate strain measured in coupons of GFRP skins.

8.3.4   Analytical assessment

As demonstrated in Chapter 6, for the present solution of sandwich panels the contribution of shear deformation for the total deflection is marginal. Hence, neglecting shear effects in the evaluation of the total deflection of the modular prototype seems perfectly acceptable. Accordingly, the classical laminate plate theory (CLPT) can be used to analytically predict the floor prototype deformational behaviour.

The prototype was considered to be subjected to an uniform distributed load. In addition, it was considered that the sandwich panels were subjected to two kinds of support conditions:

(i) the exterior panels (FP1 and FP3) were considered as simply supported panels along three edges, while the other edge of these panels was assumed free of any displacement restriction, (ii) middle panel (FP2) was considered supported along only two edges, being the other two edges free of any displacement restriction.

Accordingly, Eqs. (11) and (12) are proposed for calculating the midspan deflection in panels FP1-FP3 (exterior panel) and FP2 (interior panel), respectively. Comprehensive information of the derivation methods can be consulted elsewhere [28, 31, 99].

$$w_{max} = 0.01302 \frac{qL^4}{(EI)_{eq}} \tag{8.3}$$

$$w_{max} = 0.0071 \frac{qL^4}{(EI)_{eq}} \tag{8.4}$$

where q is the uniform distributed load, L is the length of the panel and $(EI)_{eq}$ is the flexural stiffness of the panel obtained by Eq. (8.5).

$$(EI)_{eq} = bE_f \left[\frac{t_f^3}{6} + 2t_f \left(\frac{t_f}{2} + \frac{t_c}{2} \right)^2 \right] + \frac{nE_U}{12} \left[b_u t_c^3 - (b_u - t_u)(t_c - 2t_u)^3 \right] \tag{8.5}$$

where b is the width of the panel, E_f is the Young's modulus of the GFRP skin, t_f is the thickness of the GFRP skin, t_c is the thickness of the PU foam core, n is the number of the U-shape GFRP profiles (both located in the interior of the panel and at edges), and E_U, t_U, b_u are the Young's modulus, thickness and width of those profiles, respectively.

From Eq. (8.3) a deflection at midspan of the middle panel (maximum deflection) of 18.7 mm was computed for a uniform load of 2.4 kN/m^2 and a flexural stiffness determined from Eq. (8.5). This value is close to the maximum slab deflection of 19.6 mm which experimentally was obtained. In the case of exterior panels, the maximum deflection was occurred at the middle span of the free edge, and resulted in a value of 10.2 mm, calculated based on Eq. (8.4). Experimental observations showed a deflection of 12.6 mm. Therefore, experimental results obtained in the exterior panels are also coherent with the analytical ones. The differences found can be explained by the fact that the continuity between panels were neglected in this assessment.

Finally, load distribution factor (α_{LDF}) was evaluated to compute the working proportionality of the floor prototype in each longitudinal and transverse direction. This factor was assessed on the longitudinal and transverse GFRP beams according to Eq. (8.6).

$$\delta_{Lb} = \alpha_{LDF} \times (\delta_{Lb} + \delta_{Tb}) \tag{8.6}$$

where δ_{Lb} and δ_{Tb} are the experimentally measured beam deflection in ULS condition in the longitudinal and transversal direction directions respectively. Since deflection values experimentally measured on the transverse and longitudinal beams was 13.8 mm and 4.6 mm, respectively, the value of α_{LDF} was calculated as 0.75 and 0.25 in transverse and longitudinal beams, respectively.

8.3.5 Numerical simulation

The methodology herein adopted in the numerical simulation is the same implemented in the simulation of the first floor modular prototype. In order to simplify the model, only one-quarter of the structure was simulated. A uniform distributed load of 2.4 kN/m² was applied on the top surface of the sandwich floor panels to simulate effects of experimentally applied uniform loading. The simulation is depicted in the **Fig. 8.20**.

(a)   (b)
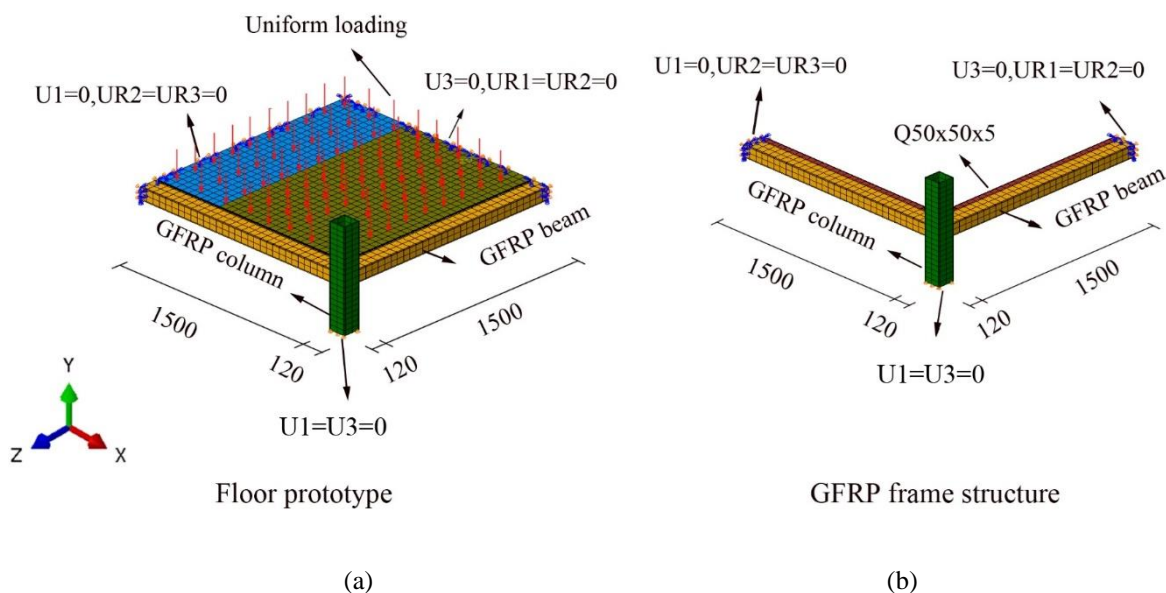
Fig. 8.20. Second floor modular simulation:(a) floor prototype; (b) frame GFRP structure (dimensions in mm).

8.3.5.1 Numerical simulation results

Table 8.7 presents the deflection and strain values experimentally measured in the floor prototype, at different monitoring positions, and compares them with the results extracted

from the FE simulations. There is a good agreement between the results obtained from FE model and the ones registered experimentally. Average difference in terms of vertical deflection is found to be 1.01, with a Coefficient of Variation (CoV) of 12.40 %, while in terms of deformation, average difference is less than 4% with a CoV of 13.00 %.

Table 8.7. Comparison between experimental and numerical FEM results in the floor prototype.

	Exp.	FE	Exp. / FE
Deflection (mm)			
Midspan of middle panel	33.46	31.01	1.08
Midspan of side panel	20.62	19.33	1.07
Midspan of longitudinal beams	4.60	5.59	0.82
Midspan of transversal beam	13.80	13.08	1.06
		Average	1.01
		CoV	12.40%
Strain (Micro strain)			
Midspan of middle panel	637.53	595.79	1.07
Midspan of side panel	420.08	435.06	0.97
Midspan of longitudinal beams	235.72	301.89	0.78
Midspan of transversal beam	786.19	781.67	1.01
		Average	0.96
		CoV	13.00%

The colour representing the vertical displacement field (in y direction) obtained from the FE model is depicted in **Fig. 8.21**. A maximum vertical deflection of 30.63 mm was registered in the central part of the pavement, at middle span of middle panel. It is interesting to note that the GFRP connector bridging internally the two panels while was not connected to the transversal beams.
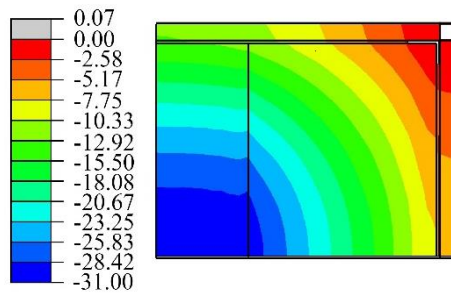
Fig. 8.21. Deformed shape for the modular FE models (deflections, in millimetres).

As a results, the contour plot could be classified into two dominates. The first one is related to the middle panel which contour related to the maximum deflection, localized in the middle of the span. This indicates that the middle panel is mainly working as a one-way slab. This is also confirmed by the deflection of the beams where one can notice that deflection in the frame beams placed orthogonal to the panels' length (13.08 mm) reach a higher deflection than beams parallel to them (5.59mm). The second dominate could be distinguished at the sides panels. Since these panels are supported along the beams, hence side panels working as

a panel supported along three-spans and showing the maximum deflection of 19.33 mm along the free edge (the edge which is contact with the middle panel).

Stresses developed at the external faces of bottom and top GFRP skins in the floor sandwich panels, due to the load applied (2.4 kN/m^2) in the longitudinal and transversal directions, are shown in **Fig. 8.22**. Checking the level of stresses revealed that all the stresses were below the ultimate strength limit with adequate safety factor. A direct conclusion from this observation is that the proposed panels withstand the ULS load level as they are only 50% above the SLS limit according to Eurocode 1 [85]. The stress field installed in the middle of the panels and through their edges evidence that panels are working as two-way slabs, being the longitudinal the main working direction.
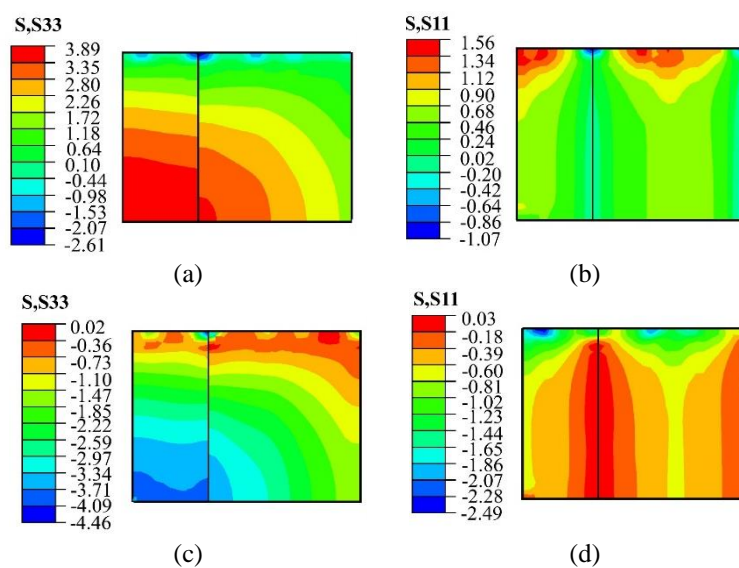
Fig. 8.22. Distribution of stress in the GFRP skins: (a) longitudinal direction-bottom skin; (b) transversal direction-bottom skin; (c) longitudinal direction-top skin; (d) transversal direction-top skin (stresses, in MPa).

8.3.5.2 Load distribution factor and beam-panel connection flexibility

Two new simulations were performed on the floor prototype in order to evaluate the influence of the panel-panel and the beam-panel connections. The first, named "full-connection" model, assumes perfect bond in the panel-beam connection (i.e. considers full composite action by using a tie interface between the squared GFRP profiles and the U-shape GFRP profiles); and the second, called "continuous-slab" model, defines a continuous slab with dimensions that correspond to the sum of the three jointed panels simulated in the floor prototype. In this last case, top and bottom skins, as well as PU foam, covered 3×3 m^2 without any interruption, U-shape profiles were placed inside the slab at the same positions

that were previously set for the three jointed panels, and since no connection existed, connection profiles between panels were not considered.

Fig. 8.23 compares the mechanical behaviour of the new simulations with the reference one (i.e. the original FE model) in terms of load *versus* deflection registered at the center of the slabs. All simulated cases follow a linear-elastic relationship between applied load and vertical deflection, but the maximum deflection is clearly different in each one. By estimating stiffness as the slope of the load vs deflection curves, it may be found that flexural stiffness is about 30% higher in the continuous slab and about 45% higher in the full-connection model, than in the reference slab.
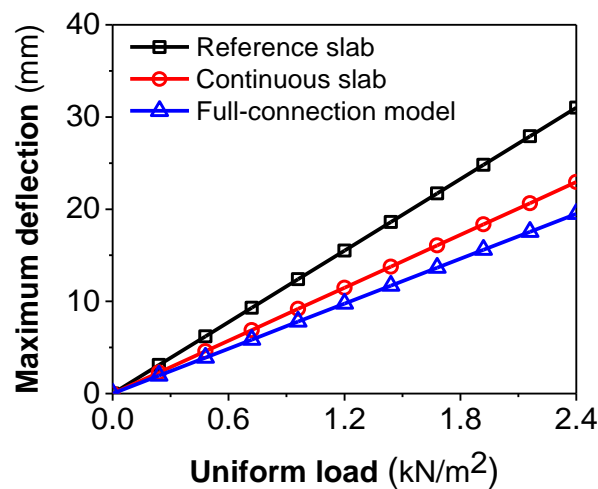
Fig. 8.23. Load *versus* maximum deflection in the different system proposed.

Accordingly, based on the Eq. (8.2) coefficient Π was calculated to be 0.57. Thus, a direct conclusion drawn from here is that, when using the proposed connection in the prototype, which acts as a semi-fixed support conditions, a stiffness reduction of a 57% respect to a fixed support condition can be expected.

The contour plot representing the vertical displacement (in *y* direction) obtained from FE models is presented in **Fig. 8.24.** In the case of the reference model, the deflection in the middle panel was 46% higher than the in the side panels. This represents that the middle panel was mainly working in one direction (parallel to panel-panel connections), which is confirmed by the deflection of the beams placed orthogonally to the panel's length: deflection of those beams reached 12.87 mm, while deflection of beams parallel to the panel's length had a deflection of only 6.78 mm. However, in the case of the continuous-slabs and full-connection model, the deflection of the middle panel is only 35% higher than the deflection in the side panels, and the flooring system showed a two-way slab behaviour. That confirms

the mentioned predominant behaviour of the prototype in one direction, which is explained by the existence of the U-shape profiles and by the type of the connection to the side panels.

<div align="center">(a)   (b)   (c)</div>
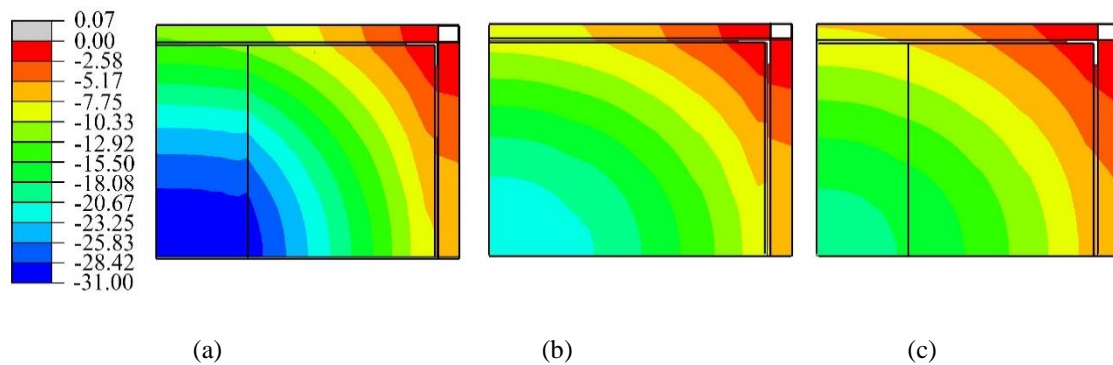
Fig. 8.24. Deflection contour plots (in mm) for: (a) reference slab composed by three jointed panels; (b) continuous-slab model; (c) full-connection model.

8.3.5.3 Influence of the aspect ratio and the slenderness ratio

Sandwich panel aspect ratio, r, is defined as L/w, where L and w are the panel's length and width, respectively. Slenderness ratio, r_s, is defined as h/w, being h the height of the sandwich panel. Both parameters have significant impact on the stiffness and on the deformability of the sandwich floor panel. They also have an impact on economic aspects of the floor prototype developed: changing the slenderness ratio enables exploring the variation of stiffness with a minimum cost, since PU foam is the less expensive constituent of the system. Aspect ratio variations relate the deformational response of the panels with their transport costs (due to dimensions).

New simulations, varying both the aspect ratio and the slenderness ratio, were conducted. In general, maintaining the width of the panels constant contributes to not changing significantly the transport conditions. Therefore, this dimension was kept constant and equal to 1 m in all simulations. The values considered for the panels span length were 1.0 m, 1.5 m, 2.0 m, 2.5 m, 3.0 m, 3.5 m and 4.0 m, which result in aspect ratio values of 1.0, 1.5, 2.0, 2.5, 3.0, 3.5 and 4.0, respectively. Similarly, the thickness of GFRP skins, was kept constant and equal to 5 mm in all simulations, because this material is significantly more expensive than PU foam core. Values considered for PU foam thickness were 60 mm, 80 mm and 100 mm, which leads to panels with a total height of 70 mm, 90 mm and 110 mm and results in slenderness ratio values of 0.07, 0.09 and 0.11, respectively.

Additionally, the connection conditions between GFRP beams elements and sandwich floor panels were evaluated for the following two scenarios: (i) semi-fixed (i.e. like the actual one

on the experimentally tested prototype) with the designation of 'SC'; (ii) fixed connection, called 'FC'.

A total of 42 models were created and analysed under ultimate load conditions in residential buildings by assuming a uniform distributed load of 2.4 kN/m^2 on the top surface of the sandwich floor panels. Selected representative results are indicated in **Table 8.8**.

Table 8.8. Maximum predicted longitudinal strain in residential floor system under ultimate uniform load of 2.4 kN/m^2.

| $r_s = h/w$ | $r = L/w$ | Longitudinal maximum strain (με) | | | | | | | |
| | | Middle of middle panel | | Middle of side panel | | Longitudinal beam | | Transversal beam | |
		SC	FC	SC	FC	SC	FC	SC	FC
0.07	1	92.4	91.8	71.8	84.9	19.8	16.9	274.0	228.8
	2	324.1	222.3	216.3	174.7	106.1	121.7	532.9	414.0
	3	595.8	353.6	435.1	280.7	301.9	307.3	781.7	555.5
	4	881.6	523.0	664.2	395.3	613.8	570.9	1043.0	644.6
0.09	1	71.3	59.1	57.0	66.0	20.4	13.1	259.7	207.9
	2	239.0	175.7	172.5	157.3	94.1	99.0	503.6	365.7
	3	458.5	305.8	368.9	283.5	255.1	256.6	722.2	479.5
	4	733.4	480.3	610.8	440.6	502.3	469.1	966.4	559.6
0.11	1	62.0	41.3	47.6	56.1	22.5	8.0	250.3	180.6
	2	200.4	144.4	148.8	141.5	77.3	76.8	493.2	309.3
	3	396.9	268.4	330.4	274.6	193.7	201.8	710.0	399.7
	4	662.1	448.7	571.5	459.6	388.5	372.5	967.9	459.0

h_c : PU foam core thickness; h_f : skin thickness; L : length of the floor panel; w : width of the floor panel; r_s : slenderness ratio; r : aspect ratio; SC: semi-fixed connection; FC: fixed connection.

Table 8.8 reveals that, in all cases, the maximum strain values in the residential floor system under ultimate uniform load are significantly below the ultimate strains obtained in the material characterization. It can be seen that the maximum strain is always occurring in the transversal beam. On the other hand, increasing the slenderness ratio leads to a reduction on the maximum strain in different components, due to contribution of the flexural stiffness of the panel.

Increasing the slenderness ratio from 0.07 to 0.11 in the shortest panels ($L = 1000mm$) provided a decrease in the maximum strain that varied between 45% and 65% when the four considered components of the panel and two connection conditions are analysed. In this case, the highest decrease occurred in the modular system with 'FC' connection. However, the range of the aforementioned values is altered with the increase of panel's aspect ratio, varying between 63% and 82% in the longest panels ($L = 4000mm$).

Predicted vertical deflection of the residential floor system under different slenderness and aspect ratios with 'SC' support conditions is depicted in **Fig. 8.25**. In all cases, the maximum

deflection occurred at the centre of the middle panel. Increasing geometric aspect ratio range from 1 to 4 leads to an increase in the maximum middle span deflection. Conversely, increasing slenderness ratio results in decreasing the maximum midspan deflection. In this case, the highest deflection occurred in the modular system with geometric aspect ratio and slenderness ratio of 4 and 0.07, respectively.
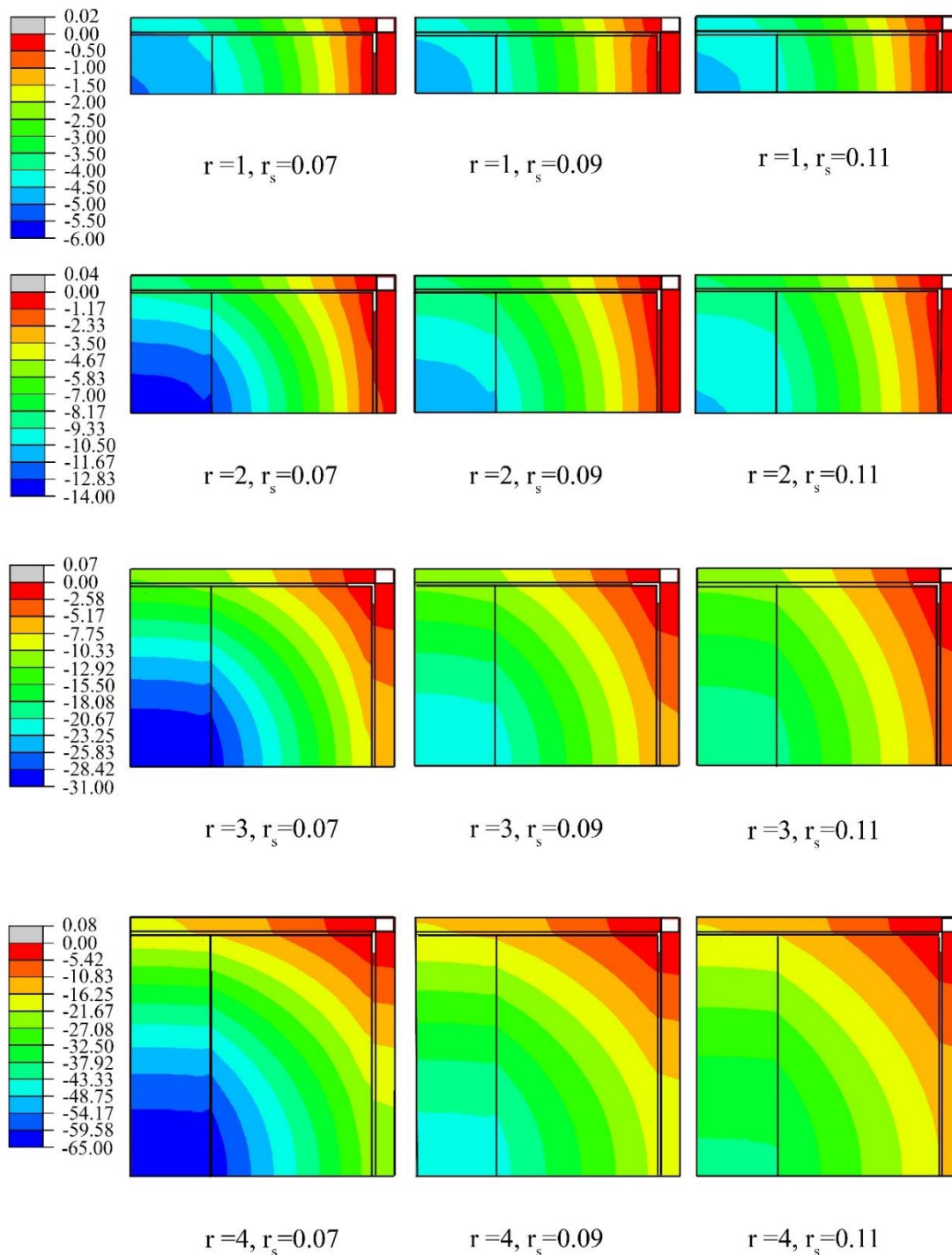
Fig. 8.25. Vertical deflection of the residential floor modular system, considering different slenderness and aspect ratios, with 'SC' support condition (values in millimeters).

The Italian standard CNR [80] is commonly used to verify the performance of composite sandwich panels under service conditions. Accordingly, the maximum deflection registered in long term for the quasi-permanent load (equal to 30% of the service load) should be less than *L/250*. Deflection in long term for a panel (δ_{LT}) can be estimated as:

$$\delta_{LT} = \alpha \times \delta_{SLS} \times \gamma_{Creep} \tag{8.9}$$

where, δ_{SLS} is the deflection corresponding to the service condition (in this case, for a uniform distributed load of 1.6 kN/m^2) , α is the proportion of the load in quasi-permanent load respect to load in service (i.e. 30%), and γ_{Creep} is an estimated coefficient due to effects of creep.

Computed results of a creep test previously developed on the studied sandwich panels yielded an increment of a 252% in the deflection of panels due to viscoelastic effects after the 5 years assumed to be the service life of the structure. Hence, value for coefficient γ_{Creep} can be set to 2.52 in this investigation.

For each of the 42 model studied, the deflection corresponding to long term can be computed based on Eq. (8.9). It should be mentioned that since floor sandwich panels are supported on exterior beams, comparison to the standard prescribed value should be done by subtracting deflection of those exterior beams. Obtained results are depicted in the **Fig. 8.26**. Results in this figure are based on: (i) the aspect ratio; (ii) the slenderness ratio; and (iii) the type of the connection between GFRP beam's elements and sandwich floor panels.
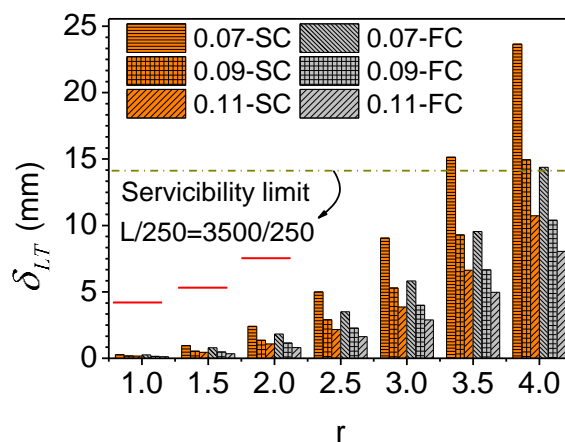
Fig. 8.26. Predicted long term deflection in floor panel modular system.

Fig. 8.26 could be utilized in the preliminary design of composite sandwich panels to be applied in residential buildings. In this figure, maximum deflection criterion recommended by CNR [80] is plotted by horizontal dotted lines. Accordingly, all of the proposed panels except than the panel designated by 0.07-SC could be selected.

Fig. 8.26 also shows that in some geometric aspect ratios, the predicted maximum long term deflection of the proposed residential pavement is much lower than the serviceability limit criteria. This shows a possible overdesign of the modular system, which may be put down. Thus, a study that indicates when to reduce the number of U-shape GFRP profiles from 4 profiles to 3 and from 3 to 2 profiles is interesting to carry out. Hence, in a similar way as indicated in the case of floor prototype with 4 U-shape profile, 84 models were studied for the floor prototypes with presence of 3 and 2 U-shape profiles. The deflections correspondent to the long term with respect to the aspect ratios and slenderness ratios are depicted in **Fig. 8.27**.

(a)   (b)
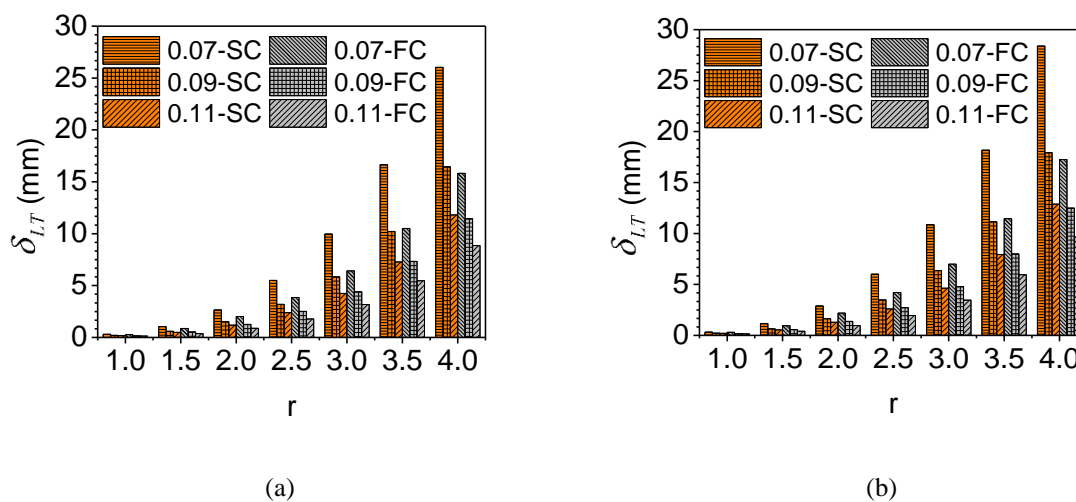
Fig. 8.27.Floor prototype with variation of U-shape profiles: (a) 3 U-shape profile; (b) 2 U-shape profile.

8.4   Conclusion

This chapter has presented two developed composite floor prototype modulus to be utilized as a part of a temporary houses. The prototypes consist of a skeleton of GFRP tubular pultruded profiles, and the slabs formed by two sandwich panels (first prototype) and three sandwich panels (second prototype). A fitting connection system is utilized to appropriately assemble the different components. The developed prototypes are capable of being prefabricated and easily transported to the site, and rapidly installed. This functionality illustrates the high potential of this system to be used in prefabricated emergency houses.

Experimental programs have been conducted, studying the behaviour of modular floor prototypes subjected to residential service loads. An analytical assessment has been developed to conduct a deeper study of the flexural behaviour of the prototype. Additionally, 3D finite element simulations have been proposed to assess behaviour of the prototypes and to evaluate types of the connection between sandwich panels and GFRP beams element. Some parametric studies have been carried out to explore the potentiality of the proposed material and structure concept for pavement of higher span length to extend this concept for other markets. The main concluding remarks drawn from this work can be listed:

- The GFRP composite sandwich panels and pultruted profiles were integrated in a floor modular prototypes. This made it possible to prefabricate a building that is easily transported to the site and rapidly installed;

- Using the proposed connections and thanks to the lightness of structure members, the assembly/disassembly process of the prototypes were performed in less than 2 hours by three persons without any special equipment. As such, this functionality illustrates the high potentiality of this system to be used as a prefabricated emergency house;

- The floor prototypes present a flexural behaviour more predominant in one direction. However, beam-panel and panel-panel connectors provided the floor panels to behave as a two-way spanning slab with load distribution factor of around 75% and 25%, for longitudinal and transverse direction, respectively. The excellent performance showed by the proposed prototype, along with the fulfilment of long-term behaviour requirements, highlighted the potential capacity of the proposed systems for being used as a temporary floor building.

- For the level of the load considered and typical of a building structure, floor modular systems present an elastic linear behaviour. Their maximum deflection under service loads, taking into account the viscoelastic behaviour, fulfil the requirement established by standard [80].

- An analytical expression using the classical laminate plate theory was utilized to predict maximum deflection in the interior and exterior sandwich panels of modular prototype. The predicted result by analytical expressions were also coherent with the experimental ones.

- A FE models were developed. The models showed to be capable of predicting the actual behaviour of the modular systems under designed loads. Accordingly, the models were used to assess the behaviour of proposed connection between sandwich panels and GFRP beam elements. It was noticed that employing the proposed connection provided some

degree of freedom in the support and acting this support as a semi-fixed. Stiffness reduction factors of 52% and 57% were computed in the case of the first and second modular prototype systems. That was meaning that reduction of around those values occur in the stiffness of systems respect to a fully fixed support condition, resulting in increments in the floor panel flexibilities.

- Some graphics were developed for assisting on pre-design of composite sandwich panels for residential building product applications with different ratios of span/width and thickness/ width.

- Flexural performance of the floor modular prototype with variation of internal GFRP 'U' profiles was assessed numerically. It was noticed that, by decreasing the number of profile from 4 to 3 and 2 resulted in increasing deflection due to decreasing flexural stiffness of the panels. It was concluded that removing one U-shape profile had an effect in 10% increasing maximum deflection of the prototype.

Chapter 9: Conclusion and future developments

Building industrialization through prefabrication lead to a reduction in the cost of buildings and to the improvement of the manufacturing quality. Moreover, after a natural disaster, accessibility to the roads is limited, so low weight of the prefabricated dwellings components is a very convenient requisite for their transport. Recently, composite sandwich panels have been increasingly used in structural applications due to some main features such as its high strength and stiffness to weight ratio, its immunity to corrosion, and a low thermal and acoustic conductivity. In the past, efficiency of using sandwich panels has been proved in several structural applications such as cladding, facades, roofing and walls.

Settling down surviving communities in shelters or temporary houses is one of the major concerns after a natural disaster. This issue remains difficult to manage despite decades of experience. Availability of temporary housing is crucial since it allows people to quickly commence their daily activities such as school, working and cooking. Even though there are different sorts of temporary buildings made of steel, wood and plastic, many of these temporary dwellings do not offer a basic level of security and protection for its occupants, and/or result in very complex and expensive solutions. Nowadays, a clear trend is observed in the temporary buildings trade towards industrial manufacturing and prefabrication. Not only did the proportion of factory production increase, compared to on-site manufacturing, but the degree of prefabrication also, increased leading to higher quality control and increasing potential for a better production economy.

The composite solution herein proposed uses GFRP profiles and sandwich panels and fits very well into this trend, as it is capable of being prefabricated, transported to the disaster area and easily assembled. Likewise, pultruded GFRP composite profiles show a series of promising advantages such as low production costs, low maintenance, high durability and immunity to corrosion and high strength.

The present study was motivated by introducing a residential modular temporary building in the scope of the ClickHouse R&D Project for accommodating dislocated families in urgent situations such as occurrence of natural disasters. Proposed building is composed of a frame structure, panels and a tailored connection system. The frame structure and connection are composed of glass fiber reinforced polymer (GFRP) pultruded tubular profiles. While for the panels, composite sandwich panels made of polyurethane foam (PU) core and GFRP skins, are utilized. A new connection system is defined for connecting adjacent members.

The main characteristics for designing 'ClickHouse' which took into account could be cited as: (i) light weight; (ii) ease of transport; (iii) the speed and ease of assembly and disassembly; (iv) compliance with regulatory requirements, including structural safety and thermal performance, and the latest international recommendations for this type of housing system; (v) sel-sufficient with regard to energy supply requirement and water; and (vi) competitive cost compared with conventional solutions such as metal and wood.

This chapter presents all the summaries and concluding remarks from the presented thesis and presented in the same logical order depicted from chapters 3-8.

9.1   Temporary residential building

The designed temporary house was composed of a single-story building with a rectangular plan of 6.12×3.12 m^2, formed by connecting two blocks of 3.12×3.12 m^2 and a height of 3.12 m for accommodating a family of 4-5 members. All of the house's components including walls, floors and roofs were designed in somehow to incorporate all the for water supply, drainage, sewage, and electricity. The proposed building is composed by three main components namely as: framed members, panels and connection.

The framed members including beams and columns are selected by using tubular GFRP pultruded profiles. However, the panels are composed of a PU foam core sandwiched between two layers of GFRP skins, adhered using epoxy resin. Accordingly, three types of slabs are proposed to be used in this thesis as:

(i) floor panels consisted of a sandwich panel of 3.0 m of length, 1.0 m of width and 0.07 m of height with GFRP skins of 5 mm thickness, a foam core of 60 mm, and two interior GFRP ribs made of pultruded U60×55×5 profiles for increasing flexural stiffness of the panels and two exterior ribs made of the same profiles used on

each side of the panels for allowing connection of the panels to the other elements. The roof panel's weighted around 70±2 kg.

(ii) roof panels, with a dimension of 3.0 m of length, 1.0 m of width and 0.19 m of height, with GFRP skins of 5 mm thickness, and a PU foam core of 180 mm. To allow the connection of panels with other panels, three U-shape GFRP pultruded profiles (U60×55×5) were place and adhesively bonded on each of the longitudinal outer faces of the sandwich panel. The roof panel's weighted around 100±2 kg.

(iii) wall panels, have a dimension of 2.88 m of height, 0.96 m of width and 0.64 m of thickness, with GFRP skins of 2 mm thickness, and a PU foam core of 60 mm. U-shape GFRP profile (U60×55×5) were adhesively bonded to the skins and PU foam core around the edges of the panels during the manufacturing process in order to facilitate the connecting of wall elements to the other elements such as wall panel, GFRP beams and GFRP columns. Each panel's weight was approximately 42±2 kg, making them easy to transport and install on-site.

Regarding to the connection system, three types of the connection are proposed as: (i) beam-column, (ii) beam-panel and (iii) panel-panel. The beam-column connection is proposed by tighten GFRP beams to GFRP columns with a series of M8 bolts and short steel tubular profiles. The beam/column-panel connection system is solved by adjusting U-shape profile around the panel to a squared tubular profile (this profile is mechanically and adhesively bonded to the column and beam). Finally, the panel- panel connection system is proposed by a similar approach as in the case of beam/column-panel connection system by adjusting the U-shape GFRP profiles around the panel to the two connected GFRP squared tubular profiles as a connector.

9.2 Connection system

The efficiency of the proposed fitting connection system in jointing sandwich panel experimentally assessed by friction and hybrid techniques in both longitudinal and transversal directions. In the friction technique a connector (two connected GFRP tubular profiles) is placed inside the U-shape GFRP profiles. Likewise, in hybrid technique mechanical fastener used for connecting the connector to U-shape profile in the friction technique.

The main concluding remarks drawn from this experience can be listed as:

1- Regarding to the longitudinal direction, both friction and hybrid techniques represented the same amount of the ultimate load and using mechanical fastener in hybrid technique did not have any influence in increasing flexural capacity of the specimens.

2- In the transversal direction, connected panels with hybrid techniques represented higher load than friction technique.

3- In the longitudinally jointed panels in both friction and hybrid techniques, the same failure mode was observed. The failure mechanism started by debonding of PU foam core from GFRP skin and eventually progressed by failure of U-shape profile in the sandwich panels.

4- In the transversally connected panels, in the friction technique the failure initiates in the GFRP U-shape profiles while in the hybrid technique the failure occurred in the connector.

9.3 Single and jointed floor sandwich panels

The experimental, analytical and numerical investigations addressed flexural performance of single sandwich panels and jointed sandwich panels. The following conclusions may be drawn as:

1- Carried out experimental program on the small scale sandwich panels in the failure test showed that, the presence of the end U-shape GFRP profiles have not significant effects in flexural strength and stiffness of the panel. In the panel without end U-shape profile, the dominate failure is reported as a shear failure while in the panel with that profile, the debonding between the bottom face of the GFRP profile and the GFRP bottom skin is the dominate failure mechanism.

2- Long-term behaviour of the small scale panels with two support conditions namely without end U-shape GFRP profile and with that profile was studied. It was observed that, the support conditions have not any influence for the creep behaviour of the panels.

3- Considering 5 years as a service life for the temporary building, maximum deflection is predicted as 2.5 times higher than initial elastic deformation of the panel.

4- In the full scale tested panels, it is noticed that, ultimate carrying capacity of the sandwich panels is substantially greater than the design demand level of the load.

Additionally, full scale experimental failure test showed that the failure occurs due to a local outward buckling known as wrinkling.

5- Regarding to the jointed panels, adequate flexural performances in fulfilling the requirement standards in both SLS and ULS loading conditions observed. Moreover, the proposed connection system demonstrated its effectiveness in transferring loads between the panels and guaranteeing deformation compatibility of the panels.

6- Capability of FSDT in estimating flexural performance of the single sandwich panels and jointed panels was observed. Analytical study showed that, in the panel without any ribs, the contribution of flexural and shear deformation is about 60% and 40 % respectively. However, by increasing the numbers of the ribs, shear contribution is decreased by a value of around 7% per each rib.

7- Nonlinear three-dimensional finite element simulation showed that, under ULS loading conditions, the midspan deflection has increased about 10% and 20% when the number of ribs has decreased from 4 to 3 and from 4 to 2. Furthermore, effectiveness of the connection in increasing flexural stiffness in jointing panels was noticed. It was concluded that the connector caused an increase of flexural stiffness by a factor of 1.04 and 1.07 respectively.

9.4   Axial performance of jointed sandwich wall panels

A new system for jointing sandwich wall panels was proposed. The behaviour of the single panels as well as jointed panels experimentally studied by a self-balanced reaction axial loading frame. Experimental results were compared using some analytical equations. The following conclusion drawn as:

1- Linear elastic responses of the single wall panels and jointed wall panels were observed prior to the failure. In both single and jointed panels, the failure initiate as a localized failure at compression side of GFRP skin. The localized failure propagates towards the GFRP skin and PU foam core due to the load increase. Finally, all the panels failed due to global instability of the system.

2- It was concluded that in global buckling failure of jointed panels, axial load increased by a factor of 2.52 of the buckling failure load obtained in single wall panels. The presence of the connector increased the global buckling load by a factor of 1.28. However, in the jointed panels that suffered localized GFRP skin wrinkling failure

was nearly 2.0 times higher than the corresponding failure load measured in single wall panels.

1. Two kinds of stresses, namely interfacial out-of-plane stress and critical wrinkling stress were developed. Interfacial out-of-plane stresses between PU foam core and GFRP skins occur, and that these stress values were higher than the tensile strength of the PU foam, resulting in debonding in both single and jointed panels. However, the calculated critical wrinkling stresses were in good agreement with the experimental values measured in both single and jointed panels.

9.5 Residential floor modular prototype

Two residential floor modular prototypes are introduced. Experimental programs were conducted to evaluate the performances of the developed basic units floor prototypes as a structure designed to support serviceability and ultimate load conditions in residential houses. The performances included the feasibility of assemblage and fulfilling the requirements by standards in short-term and long-terms.

Some analytical and numerical assessments were undertaken to predict the actual behaviour of the modular systems and connection effectiveness under designed load. The main conclusion drawn as:

1- The high potentiality of proposed systems to be used as an emergency house in disaster areas was observed due to quick assembly/disassembly process without using any special equipment.

2- For the level of the load considered, the floor modular prototype presented an elastic linear behaviour. The maximum deflection under service load tacking into account the viscoelastic behaviour, fulfilled the standard requirement.

3- Nonlinear finite element simulations showed that the proposed fitting connection system used for jointing different components of the floor modular prototype, working as a semi-fixed connection. It is worth mentioning that, the stiffness reduction factor was computed by a value of nearly 50%.

4- Some graphics were represented in for assisting on pre-design of composite sandwich panels for residential building product applications with different ratios of span/width and thickness/ width.

5- Flexural performance of the floor modular prototype with variation of internal U-shape GFRP profiles was simulated. It was noticed that, decreasing the number of profile from 4 to 3 and 2 resulted in increasing deflection with the value of 10% per each profile.

9.6 Recommendation for Future Work

The present study proposing a residential floor modular prototype to be used in urgent situations for accommodating dislocated families due to natural disasters. A number of major achievements have been accomplished in terms of through understanding of flexural behaviour, failure modes, axial behaviour and numerical modeling. To further promote application of this system in the field of temporary dwellings, the following areas need further investigations:

1- Behaviour of more than two jointed wall panels under axial loading test.

2- Behaviour of the single wall panels and jointed wall panels under combined bending and axial compression loads. The study may investigate slenderness effects and overall buckling behaviour of the panels.

3- Regarding to the wind effects on the jointed wall panels, the high-cycle fatigue simulation can be studied.

4- Investigate the long-term performance of the sandwich wall panel under sustained axial loading and different environmental conditions.

5- Developing design guides and optimizing techniques for residential modular buildings.

10 References

[1] Studzinski R, Pozorski Z, Garstecki A. Failure maps of sandwich panels with soft core. 10th International Conference Modern Building Materials, Structures and Techniques2010. p. 1060-5.

[2] Lawson RM, Ogden RG. 'Hybrid' light steel panel and modular systems. Thin-Walled Structures. 2008;46:720-30.

[3] Veljkovic M, Johansson B. Light steel framing for residential buildings. Thin-Walled Structures. 2006;44:1272-9.

[4] Sousa JM, Correia JR, Cabral-Fonseca S, Diogo AC. Effects of thermal cycles on the mechanical response of pultruded GFRP profiles used in civil engineering applications. Composite Structures. 2014;116:720-31.

[5] Correia JR, Cabral-Fonseca S, Branco FA, Ferreira JG, Eusébio MI, Rodrigues MP. Durability of pultruded glass-fiber-reinforced polyester profiles for structural applications. Mechanics of Composite Materials. 2006;42:325-38.

[6] Rizkalla S, Lucier G, Dawood M. Innovative use of FRP for the precast concrete industry. Advances in Structural Engineering. 2012;15:565-74.

[7] Oppe MW, Knippers J. Application of bolted connections in fibre-reinforced polymers. Proceedings of the Institution of Civil Engineers: Structures and Buildings. 2011;164:321-32.

[8] Zenkert D. An intoduction to sandwich construction. Stockholm: Cradley Heath, Warley:Engineering Materials Advisory Services., 1995.

[9] Vinson JR. The behavior of sandwich structures of isotropic and composite materials. United States of America: Technomic publishing company,Inc, 1999.

[10] Kootsookos A, Burchill PJ. The effect of the degree of cure on the corrosion resistance of vinyl ester/glass fibre composites. Composites Part A: Applied Science and Manufacturing. 2004;35:501-8.

[11] Nguyen CH, Chandrashekhara K, Birman V. Multifunctional thermal barrier coating in aerospace sandwich panels. Mechanics Research Communications. 2012;39:35-43.

[12] Allard JF, Atalla N. Propagation of Sound in Porous Media: Modelling Sound Absorbing Materials2009.

[13] Johnson C. Impacts of prefabricated temporary housing after disasters: 1999 earthquakes in Turkey. Habitat International. 2007;31:36-52.

[14] Arslan H, Cosgun N. Reuse and recycle potentials of the temporary houses after occupancy: Example of Duzce, Turkey. Building and Environment. 2008;43:702-9.

[15] Barakat S. Housing reconstruction after conflict and disaster.: London: Overseas Development Institute., 2003.

[16] Dodoo A, Gustavsson L. Life cycle primary energy use and carbon footprint of wood-frame conventional and passive houses with biomass-based energy supply. Applied Energy. 2013;112:834-42.

[17] Datin PL, Prevatt DO. Using instrumented small-scale models to study structural load paths in wood-framed buildings. Engineering Structures. 2013;54:47-56.

[18] Imperadori M, Salvalai G, Pusceddu C. Air Shelter House Technology and its Application to Shelter Units: the Case of Scaffold House and Cardboard Shelter Installations. Procedia Economics and Finance. 2014;18:552-9.

[19] Ljunggren F, Ågren A. Potential solutions to improved sound performance of volume based lightweight multi-storey timber buildings. Applied Acoustics. 2011;72:231-40.

[20] Winandy JE, Hunt JF, Turk C, Anderson JR. Emergency housing systems from three-dimensional engineered fiberboard : temporary building systems for lightweight, portable, easy-to-assemble, reusable, recyclable, and biodegradable structures. General Technical Report FPL-GTR-166. Madison, WI: U.S. Department of Agriculture, Forest Service, Forest Products Laboratory2006.

[21] Davies JM. Lightweight Sandwich Construction. . Wiley-Blackwell; 2001.

[22] Zenkert Dan. An intoduction to sandwich construction. Stockholm: Cradley Heath, Warley:Engineering Materials Advisory Services, 1995.

[23] Vinson J.R. The behavior of sandwich structures of isotropic and composite materials. United States of America Technomic publishing company,Inc., 1999.

[24] D'Alessandro V, Petrone G, Franco F, De Rosa S. A review of the vibroacoustics of sandwich panels: Models and experiments. Journal of Sandwich Structures and Materials. 2013;15:541-82.

[25] Davies J.M. Lightweight Sandwich Construction. Wiley-Blackwell; 2001.

[26] Adams DF. Sandwich panel test methods. High Performance Composites, no. 5: 4-6; 2006.

[27] Naji B. FLEXURAL ANALYSIS AND COMPOSITE BEHAVIOR OF PRECAST CONCRETE SANDWICH PANEL: UNIVERSITY OF DAYTON, 2012.

[28] Allen GH. Analysis and Design of Structural Sandwich Panels. . London: Pergmon Press, 1969.

[29] Taylor EM. Two-Way Behavior and Fatigue Performance of 3-D GFRP Sandwich Panels North Carolina State University 2009.

[30] Bitzer T. Honeycomb Technology. London: Chapman and Hall, 1997.

[31] Carlsson LA, Kardomateas GA. Structural and Failure Mechanics of Sandwich Composites. New York Springer, 2011.

[32] Ashby MF. Materials Selection in Mechanical Design. Burlington, USA: Butterworth-Heinemann, 2011.

[33] Daniel IM, Ishai O. Engineering Mechanics of Composite Materials. New York: Offord University Press, 1994.

[34] Gere JM. Mechanics of Materials. Bemont: Books/Cole, 2004.

[35] Gibson LJ, Ashby MF. Cellular solids: structure and properties: Cambridge University Press, 1999.

[36] Boh JW, Louca LA, Choo YS, Mouring SE. Damage modelling of SCRIMP woven roving laminated beams subjected to transverse shear. Composites Part B: Engineering. 2005;36:427-38.

[37] Kim J, Swanson SR. Design of sandwich structures for concentrated loading. Composite Structures. 2001;52:365-73.

[38] Sharaf T, Shawkat W, Fam A. Structural performance of sandwich wall panels with different foam core densities in one-way bending. Journal of Composite Materials. 2010;44:2249-63.

[39] Manalo AC, Aravinthan T, Karunasena W, Islam MM. Flexural behaviour of structural fibre composite sandwich beams in flatwise and edgewise positions. Composite Structures. 2010;92:984-95.

[40] HERRANEN H, PABUT O, EERME M, MAJAK J, POHLAK M, KERS J, et al. Design and Testing of Sandwich Structures with Different Core Materials. MATERIALS SCIENCE. 2012;18.

[41] Kim DJ, Park SH, Ryu GS, Koh KT. Comparative flexural behavior of Hybrid Ultra High Performance Fiber Reinforced Concrete with different macro fibers. Construction and Building Materials. 2011;25:4144-55.

[42] Fam A, Sharaf T. Flexural performance of sandwich panels comprising polyurethane core and GFRP skins and ribs of various configurations. Composite Structures. 2010;92:2927-35.

[43] Dawood M, Taylor E, Ballew W, Rizkalla S. Static and fatigue bending behavior of pultruded GFRP sandwich panels with through-thickness fiber insertions. Composites Part B: Engineering. 2010;41:363-74.

[44] Correia JR, Garrido M, Gonilha JA, Branco FA, Reis LG. GFRP sandwich panels with PU foam and PP honeycomb cores for civil engineering structural applications: Effects of introducing strengthening ribs. International Journal of Structural Integrity. 2012;3:127-47.

[45] Corigliano A, Rizzi E, Papa E. Experimental characterization and numerical simulations of a syntactic-foam/glass-fibre composite sandwich. Composites Science and Technology. 2000;60:2169-80.

[46] Manalo AC, Aravinthan T, Karunasena W. Shear behaviour of glued structural fibre composite sandwich beams. Construction and Building Materials. 2013;47:1317-27.

[47] Reis EM, Rizkalla SH. Material characteristics of 3-D FRP sandwich panels. Construction and Building Materials. 2008;22:1009-18.

[48] Norton TM. 3d Orthogonal Woven Glass Fiber Reinforced Polymeric Bridge Deck: Fabrication and Experimental Investigation: North Carolina State University, 2014.

[49] Mathieson H, Fam A. Axial Loading Tests and Simplified Modeling of Sandwich Panels with GFRP Skins and Soft Core at Various Slenderness Ratios. J Compos Constr. 2015;19:04014040.

[50] Mousa MA, Uddin N. Flexural behavior of full-scale composite structural insulated floor panels. Advanced Composite Materials. 2011a;20:547-67.

[51] Mousa MA, Uddin N. Global buckling of composite structural insulated wall panels. Materials & Design. 2011b;32:766-72.

[52] Engesser F. Die Knickfestigkeit gerader Stäbe. Zeitschrift des Architekten und Ingenieure Vereines zu Hannove. 1981;35:455.

[53] Haringx JA. On Highly Compressible Helical Springs and Rubber Rods, and Their Application for Vibration-Free Mountings, I. Phillips Research Reports,Eindhoven, the Netherlands. 1948;3:401-49.

[54] Frostig Y. Buckling of sandwich panels with a flexible core—high-order theory. International Journal of Solids and Structures. 1998;35:183-204.

[55] Frostig Y, Barnch M. High-order buckling analysis of sandwich beams with transversely flexible core. Journal of Engineering Mechanics. 1993;119:476-95.

[56] Félix D, Branco JM, Feio A. Temporary housing after disasters: A state of the art survey. Habitat International. 2013;40:136-41.

[57] Memari AM, Huelman PH, Iulo LD, Laquatra J, Martin C, McCoy A, et al. Residential Building Construction: State-of-the-Art Review. Journal of Architectural Engineering. 2014;20:B4014005.

[58] Arlikatti S, Andrew SA, Kendra JM, Prater CS. Temporary Sheltering, Psychological Stress Symptoms, and Perceptions of Recovery. Natural Hazards Review. 2015;16:04014028.

[59] Ginjeira do Nascimento J. Transitional architecture in emergency scenarios. Clickhouse case study: modular shelter made of advanced composite materials. Portugal: Técnico Lisboa, 2015.

[60] Afonso A, Neves e Sousa A. Clickhouse Task 2.5. Design of Water Supply and Sewerage Systems ICIST: Lisboa: Instituto Superior Técnico; 2015.

[61] Shawkat W, Honickman H, Fam A. Investigation of a novel composite cladding wall panel in flexure. Journal of Composite Materials. 2008;42:315-30.

[62] American Society for Testing and Materials. ASTM D3039/D3039M-14, Standard Test Method for Tensile Properties of Polymer Matrix Composite Materials. West Conshohocken, PA 19428-2959, United States2000.

[63] ASTM. Standard Test Method for Flatwise Tensile Strength of Sandwich Constructions. ASTM C297-04. United States: West Conshohocken, PA 19428-2959; 2010.

[64] ASTM. Standard Test Method for Flatwise Compressive Properties of Sandwich Cores. ASTM C365. United States: West Conshohocken, PA 19428-2959; 2005a.

[65] Borsellino C, Calabrese L, Valenza A. Experimental and numerical evaluation of sandwich composite structures. Composites Science and Technology. 2004;64:1709-15.

[66] Garrido M. Composite sandwich panel floors for building rehabilitation. UNIVERSIDADE DE LISBOA: INSTITUTO SUPERIOR TÉCNICO; 2015.

[67] ASTM. Standard Test Method for Tensile Properties of Plastics. ASTM D638. United States: West Conshohocken, Pennsylvania 19428-2959; 2004.

[68] ASTM. Standard Test Method for Tensile Strength of Concrete Surfaces and the Bond Strength or Tensile Strength of Concrete Repair and Overlay Materials by Direct Tension (Pull-off Method) ASTM C1583. United States: West Conshohocken, PA 19428-2959; 2005b.

[69] Mousa MA, Uddin N. Structural behavior and modeling of full-scale composite structural insulated wall panels. Engineering Structures. 2012;41:320-34.

[70] ASTM. Standard test method for bearing strength of plastics. ASTM D953-95. United States,West Conshohocken, PA 19428-2959,1982.

[71] Girão Coelho AM, Mottram JT. A review of the behaviour and analysis of bolted connections and joints in pultruded fibre reinforced polymers. Materials & Design. 2015;74:86-107.

[72] Zhou A, Keller T. Joining techniques for fiber reinforced polymer composite bridge deck systems. Composite Structures. 2005;69:336-45.

[73] Mara V, Al-Emrani M, Haghani R. A novel connection for fibre reinforced polymer bridge decks: Conceptual design and experimental investigation. Composite Structures. 2014;117:83-97.

[74] Garrido M, Correia JR, Keller T, Branco FA. Adhesively bonded connections between composite sandwich floor panels for building rehabilitation. Composite Structures. 2015;134:255-68.

[75] Keller T, Rothe J, de Castro J, Osei-Antwi M. GFRP-Balsa Sandwich Bridge Deck: Concept, Design, and Experimental Validation. J Compos Constr. 2014;18:04013043.

[76] Hart-Smith LJ. Adhesively Bonded Joints for Fibrous Composite Structures. In: Tong L, Soutis C, editors. Recent Advances in Structural Joints and Repairs for Composite Materials. Dordrecht, Netherlands: Springer Science & Business Media; 2003. p. 173-210.

[77] Turner MK, Harries KA, Petrou MF, Rizos D. In situ structural evaluation of a GFRP bridge deck system. Composite Structures. 2004;65:157-65.

[78] Liu Z, Majumdar P, Cousins T, Lesko J. Development and Evaluation of an Adhesively Bonded Panel-to-Panel Joint for a FRP Bridge Deck System. J Compos Constr. 2008;12:224–33.

[79] ASTM C393. Standard Test Method for Flexural Properties of Sandwich Constructions,. West Conshohocken, PA 19428-2959, United States,American Society for Testing and Materials, 2000.

[80] Council INR. CNR, Guide for the Design and Construction of Structures made of FRP Pultruded Elements. ROME2008.

[81] Zenkert D, Shipsha A, Persson K. Static indentation and unloading response of sandwich beams. Composites Part B: Engineering. 2004;35:511-22.

[82] Petras A, Sutcliffe MPF. Indentation resistance of sandwich beams. Composite Structures. 1999;46:413-24.

[83] Rizov V, Shipsha A, Zenkert D. Indentation study of foam core sandwich composite panels. Composite Structures. 2005;69:95-102.

[84] Petras A, Sutcliffe MPF. Indentation failure analysis of sandwich beams. Composite Structures. 2000;50:311-8.

[85] European Committee for Standardization (CEN). Eurocode 1: Actions on structures – Part 1-1: General actions – Densities, self-weight, imposed loads for buildings Technical Committee CEN/TC 250, Brussels2002.

[86] UNHCR. United Nations High Commissioner for Refugees Supply Management Service HQSF00. Budapest, Hungary2010.

[87] ASTM. Standard Test Method for Flexural Properties of Sandwich Constructions. ASTM C393. United States,West Conshohocken, PA 19428-2959,2000.

[88] Zenkert D. The Handbook of Sandwich Construction. London, United Kingdom: Chameleon Press Ltd., 1997.

[89] The Buckling of Sandwich-Type Panels. Journal of the Aeronautical Sciences. 1945;12:285-97.

[90] Mousa MA, Uddin N. Debonding of composites structural insulated sandwich panels. Journal of Reinforced Plastics and Composites. 2010.

[91] Eskandari H. The effect of shear deformation on material selection for bending components. Materials & Design. 2003;24:143-9.

[92] ABAQUS. The numerical model was performed in collaboration with the Department of Construction Engineering of the Universitat Politècnica de València . 6.12 ed.

[93] Deshpande VS, Fleck NA. Isotropic constitutive models for metallic foams. Journal of the Mechanics and Physics of Solids. 2000;48:1253-83.

[94] Wang W. Cohesive Zone Model for Facesheet-Core Interface Delamination in Honeycomb FRP Sandwich Panels: Morgantown, West Virginia, 2004.

[95] Westergaard HM. Bearing pressures and cracks. Transactions of the American Society of Mechanical Engineers. 1939;61:A49-A53.

[96] Awad ZK, Aravinthan T, Zhuge Y. Experimental and numerical analysis of an innovative GFRP sandwich floor panel under point load. Engineering Structures. 2012;41:126-35.

[97] Mitra N, Raja BR. Improving delamination resistance capacity of sandwich composite columns with initial face/core debond. Composites Part B: Engineering. 2012;43:1604-12.

[98] Southward T, Mallinson GD, Jayaraman K, Horrigan D. Buckling of Disbonds in Honeycomb-core Sandwich Beams. Journal of Sandwich Structures and Materials. 2008;10:195-216.

[99] Timoshinko S. Theory of plates and shells. New York: McGRAW-HILL Book company, 1989.